CONDITIONING DENDRITIC CELL RESPONSES USING ENGINEERED BIOMATERIALS FOR IMMUNOTHERAPY

A Dissertation
Presented to
The Academic Faculty

by

Sangeetha Srinivasan

In Partial Fulfillment
of the Requirements for the Degree
Doctor of Philosophy in Bioengineering
in the
Department of Biomedical Engineering

Georgia Institute of Technology
December 2016

CONDITIONING DENDRITIC CELL RESPONSES USING ENGINEERED BIOMATERIALS FOR IMMUNOTHERAPY

Approved by:

Dr. Julia E. Babensee, Advisor
Wallace H. Coulter Department of Biomedical Engineering
Georgia Institute of Technology

Dr. Julie A. Champion
School of Chemical and Biomolecular Engineering
Georgia Institute of Technology

Dr. Edward A. Botchwey
Wallace H. Coulter Department of Biomedical Engineering
Georgia Institute of Technology

Dr. Susan N. Thomas
George W. Woodruff School of Mechanical Engineering
Georgia Institute of Technology

Dr. Krishnendu Roy
Wallace H. Coulter Department of Biomedical Engineering
Georgia Institute of Technology

Date Approved: November 02, 2016

To my family: your immense love and support keeps me going

ACKNOWLEDGEMENTS

My graduate student years at Georgia Tech have taken me on a journey of scientific as well as self-discovery during which several people have encouraged and supported me – I take this opportunity to express my gratitude to all of them. First, I would like to sincerely thank my graduate thesis advisor, Dr. Julia E. Babensee for her persistent support, enthusiasm for research and remarkable knowledge – your immense faith in my abilities as a researcher has helped me harness confidence even during the most trying times. I would also like to thank my committee members Dr. Julie Champion, Dr. Susan Thomas, Dr. Edward Botchwey and Dr. Krish Roy, for their patience and guidance during this work. I would like to convey my special thanks to the Bioengineering program, mainly Dr. Andrés Garcia, Laura Paige and Chris Ruffin R.I.P., as well as Shannon Sullivan at the Department of Biomedical Engineering, for their generous advice and support. Further, I would like acknowledge the Georgia Tech Counseling Center as well as my therapist, Dr. Jill Silbiger for not only patiently listening to my woes for countless hours and more, but also taking the time out of her busy schedule to be present during my dissertation defense – your friendly face provided me with enormous comfort and strength.

I would like to acknowledge the funding resources for this work: National Institute of Health, the Georgia Tech/Emory Center: Individual Investigator Initiated Seed Grant in Regenerative Medicine and the Georgia Tech and Petit Institute: Investigator-Initiated Collaborative Seed Grant in Immuno Engineering. Next, I would like to extend my gratitude to: our collaborators at Dr. Brian Evavold's laboratory at

Emory University for their assistance with the *in vitro* multiple sclerosis model; Dr. John Copeland at Dr. Carsten Sievers' laboratory for assisting with infrared spectroscopy; Dr. Laura O'Farrell and Kim Benjamin at the Physiological Research Laboratory at Georgia Tech for their training and assistance with animal studies; the phlebotomists at the Georgia Tech Health Center for their skill at blood collection and to all the blood donors who made our human studies possible. I would also like to recognize the technical and logistical support of the staff at Petit Institute of Bioengineering and Biosciences (IBB), particularly, Steve Woodard, Andrew Shaw, Nadia Boguslavsky and Allen Echols.

Furthermore, I would like to express my sincere gratitude towards current and former members of the Babensee laboratory: Dr. Todd Rogers, Dr. Peng Meng Kou, Dr. Nathan Hotaling, Rishi Patel for training me during my initial years in the lab; Dr. Aline Thomas for helping me with my thesis proposal; undergraduate students – Gopi Patel, Gargi Mukherjee and Jenny Goh for assisting and pilot-testing numerous experiments; Christi Koutrelakos, Stella Wang and Nicholas Beskid for your continued enthusiasm in our lab's research.

I would like to thank my near and dear friends, from Georgia Tech and elsewhere; Catherine Rivet, Hajira Ahmed and Gaurav Dwivedi, for providing countless hours of company during late night haunts in the IBB 1-D lab wing; Sonal and John Phan, for being my pizza buddies and my perpetual ride before I learnt to drive; Karthik Reddy, for unaccounted hours of ridiculous conversations; Ranjani Murali and Shokhi Shah, for always being there when I needed someone despite being so incredibly far away; Janani Kutti, and Chitra Omprakash, my friends via Isha Yoga, for their whole-hearted friendship that has been a positive influence on me in the recent years. Finally, to my

roommate of four years and perhaps the closest thing I have to a sister, Lakshmipriya Palamadai, I find no words but these four to express my affection, “Nitwit! Blubber! Oddment! and Tweak!”

I would like to thank my boyfriend of eight years who also happens to be husband of nine months, Ravishankar Arivazhagan, for being loving, patient and endlessly supportive during these years whether being near or far away – I know we’ve missed being there for each other’s milestones in recent times but I can’t wait to start our life together as a married couple. I would also like to acknowledge my in-laws Shanti, Arivazhagan and Venkatesh for their support during my PhD.

Saving the best for last, there are not enough words in the English vocabulary to express my love and gratitude to my parents, Shyamala and GS Srinivasan, for being my pillars of strength, for teaching me to pursue my passion and for not once raising me, their only child and daughter, any differently than a son – I am because of you, I am nothing without you.

TABLE OF CONTENTS

ACKNOWLEDGEMENTS ..... **iv**

LIST OF TABLES ..... **xiv**

LIST OF FIGURES ..... **xv**

LIST OF SYMBOLS AND ABBREVIATIONS ..... **xix**

SUMMARY ..... **xxii**

CHAPTER 1 INTRODUCTION **1**

CHAPTER 2 SPECIFIC AIMS **5**

2.1 Specific Aim1: 5

2.1.1 Significance and Approach 5

2.2 Specific Aim 2: 8

2.2.1 Significance and Approach 8

2.3 Specific Aim 3: 9

2.3.1 Significance and Approach 9

CHAPTER 3 LITERATURE REVIEW **11**

3.1 Innate and Adaptive Immunity 11

3.1.1 Innate Immunity 11

3.1.2 Adaptive Immunity 12

3.2 Dendritic Cells (DCs) 13

3.2.1 Endogenous DC Populations 16

3.2.2 Experimental and Induced Tolerogenic DCs 19

3.3 Biomaterial Strategies to Influence Adaptive Immune Responses 21

3.3.1 Biomaterials Influence DC Phenotype 22

3.3.2 DC-Mediated Biomaterial Adjuvant Effect 24

3.4 Autoimmunity 24

3.4.1 Mechanisms of Immune Tolerance 24

3.4.2 DCs and Autoimmunity 25

3.4.3 Current Strategies for Autoimmunity Amelioration and Future of DCs 26

CHAPTER 4 DENDRITIC CELL INVOLVEMENT IN SUPPORTING ANTIGEN PRESENTATION FOR A PROLIFERATIVE ANTIGEN-SPECIFIC T CELL RESPONSE IN THE PRESENCE OF PLGA 29

4.1 Overview 29

4.2 Materials and Methods 33

4.2.1 Animals: 33

4.2.2 Characterization of CD11c+ Cells Depletion in CD11c-DTR Model on Multiple Diphtheria Toxin (DT) Doses: 34

4.2.3 Preparation PLGA/OVA Scaffold: 35

4.2.4 Adoptive Transfer of CFSE-Labeled T-Cells: 36

4.2.5 In vivo effect of PLGA on Co-Delivered Antigen-Specific Clonal Expansion Of T Cells in the Absence of Dendritic Cells in CD11c-DTR mice: 38

4.2.6 Tracking In Vivo T-cell proliferation: 39

4.3 Results 40

4.3.1 Effect of Repeated DT Treatments on CD11c-DTR Mouse Model 40

4.3.2 CD4+ T-Cell Response to Antigen-Loaded PLGA in the Absence of DCs 45

4.3.3 CD8+ T-Cell Response to Antigen-Loaded PLGA in the Absence of DCs 48

4.4 Discussion 51

CHAPTER 5 DESIGN AND DEVELOPMENT OF A SCAFFOLD WITH THE ABILITY OF TEMPORAL DELIVERY OF MULTIPLE IMMUNOMODULATORS 58

5.1 Overview 58

5.2 Methods 63

5.2.1 Gelatin Microparticle (MP) Formulation: 63

5.2.2 Microparticle Size and Zeta Potential Measurements: 64

5.2.3 Microparticle Loading, Incorporation Analysis and Release Profile Characterization: 65

5.2.4 Fourier Transform Infrared (FTIR) Spectroscopy: 66

5.2.5 Preparation of MP-Embedded Agarose Cryogel Scaffold: 67

5.2.6 Imaging 68

5.2.7 Overall Experimental Approach 68

5.2.8 Statistical Analysis 69

5.2.9 Model and Fitting Analysis 69

5.3 Results 70

5.3.1 Characterization of Gelatin Microparticles 70

5.3.2 Effect of Crosslinking on Chemical Composition of Gelatin MPs (IR spectroscopy) 73

5.3.3 Effect of Crosslinking on Release Profile of Microparticles Loaded with Model Biomolecules of Varying Sizes 75

5.3.4 Embedding Gelatin MPs in Agarose Cryogel Scaffold 78

5.3.5 Release Profiles of Model Biomolecule-Loaded Gelatin MPs Embedded in Agarose Scaffold 79

5.3.6 Mathematical modeling of release profile data to determine the optimal scaffold design for the delivery of 2 or more immunomodulating biomolecules of varying sizes from the scaffold 81

5.3.7 Predicting Rate of Release Required From Scaffold Containing MPs Loaded with Immunomodulators. 94

5.4 Discussion 97

5.4.1 Gelatin and Agarose as Carriers 97

5.4.2 IR Spectrograph 98

5.4.3 Bayesian Approach 100

5.4.4 Weibull Equation, Physical Significance of Parameters and Limitations 101

5.4.5 Charge, Scaffold Design and Applicabiltiy 105

CHAPTER 6 EFFECTIVENSS OF THE MULTIFUNCTIONAL IMMUNOMODULATORY SCAFFOLD IN GENERATING FUNCTIONAL ALTERNATIVELY ACTIVATED DENDRITIC CELLS 108

6.1 Overview 108

6.2 Methods 111

6.2.1 Animals: 111

6.2.2 Mixed Lymphocyte Reaction of Human DCs with Allogeneic Naïve T-Cells 114

6.2.3 Murine Bone Marrow-Derived DC (BMDC) Culture and MI Scaffold Treatment: 115

6.2.4 Murine MOG Antigen Presentation Assay: 117

6.2.5 Flow Cytometry with Intracellular Cytokine Staining for BMDCs 118

6.2.6 CCR7-Induced BMDC Migration Assay 119

6.2.7 Statistical Analysis 119

6.3 Results 120

6.3.1 Treatment of Human PBMC-Derived DCs with MI Scaffold Lowered the Expression of Maturation Markers While Increasing that of Tolerogenic Markers 120

6.3.2 Treatment of Human PBMC-Derived DCs with MI Scaffold Increased the Secretion of IL-10 126

6.3.3 Treatment of Human PBMC-Derived DCs with MI Scaffold Suppressed Proliferation of Allogeneic T-cells in a Mixed Lymphocyte Reaction (MLR) 132

6.3.4 Treatment of Murine BMDCs with MI Scaffold Lowered the Expression of Maturation Markers While Increasing that of Tolerogenic Markers 135

6.3.5 Treatment of Murine BMDCs with MI Scaffold induces Increased Intracellular Expression of Interleukin (IL-10) 138

6.3.6 Treatment of Murine BMDCs with MI Scaffold MI Scaffold Increased their Secretion of IL-10 140

6.3.7 Multiple Sclerosis Antigen-Loaded Murine BMDCs Cultured in the Presence of MI Scaffold Lowered Antigen-Specific T-Cell Responses – Lowering T-Cell Autoimmune Response in an Antigen-Presentation Assay 145

6.3.8 Murine BMDCs Treated with MI Scaffold Were More Migratory Towards CCL-19 Gradient Due to Their Surface Expression of CCR7.. 147

6.4 Discussion 149

6.4.1 Induction of Tolerogenic Human PBMC-Derived DCs Upon MI Scaffold Treatment Based on Surface Marker Expression and Cytokine Secretion. 150

6.4.2 Suppression of Allogeneic T-Cell Responses by Human DCs Treated with MI Scaffold 155

6.4.3 Induction of Tolerogenic Murine BMDCs Upon MI Scaffold Treatment Based on Surface Marker Expression and Cytokine Secretion 156

6.4.4 Murine BMDC Multiple Sclerosis-Specific in vitro Antigen Presentation Assay 157

6.4.5 Murine BMDC CCR7-Specific Chemotactic Migration 158

6.4.6 Future Directions: 161

CHAPTER 7 CONCLUSIONS AND FUTURE DIRECTIONS.....165

7.1 Conclusions 165

7.2 Significance of Findings 169

7.3 Future Directions 171

7.3.1 Efficacy of MI Scaffold in Re-Educating Multiple Sclerosis Patient-Derived DCs to Obtain an Antigen-Specific Alternatively Activated Phenotype. 172

7.3.2 Therapeutic Application of the MI Scaffold in Alleviating Disease Severity in an Experimental Autoimmune Encephalitis (EAE) Model in Mice 174

7.3.3 Therapeutic Application of the MI Scaffold in Alleviating Disease Severity in an a Spontaneous Type 1 Autoimmune Diabetes Model in Mice 177

APPENDIX A. 179

A.1. Supplemental to Aim 1 179

A.1.1. Confirmation of in vitro OT-II T-Cell proliferation 179

A.1.2. Confirmation of Adoptive Transfer via intravenous injection 180

A.1.3. Assessing in vivo OT-II T-Cell Proliferation in Response to Intraperitoneally Delivered Model Antigen OVA 181

A.2. Supplemental to Aim 2 183

A.3. Supplemental to Aim 3 185

A.3.1. Optimizing Bone Marrow-Derived DC Culture 185

A.4. Determine the differential effects of biomaterials co-delivering a model cellular antigen on the humoral immune response in an *in vivo* mouse model 193

A.4.1. Overview 193

A.4.2. Methods 194

A.4.3. Results 195

A.4.4. Discussion 198

REFERENCES 201

LIST OF TABLES

Table 5.1 Biotin release - Parameter values obtained from non-linear regression using Weibull Equation 85

Table 5.2 OVA Release - Parameter values obtained from non-linear regression using Weibull Equation. 86

Table 5.3 Biotin release from scaffold-embedded gelatin MPs – parameter values obtained from non-linear regression using Weibull Equation. 89

Table 5.4 OVA release from scaffold-embedded gelatin MPs- Parameter values obtained from non-linear regression using Weibull Equation 90

Table 5.5 Uncoupled values of βand η due to N_{MP} alone corresponding to Figure 5.14 92

Table 5.6 Configuration of MI scaffold required in Human DC cultures at different time-points. 95

LIST OF FIGURES

Figure 3.1 Dendritic cells exhibit functional plasticity 17

Figure 4.1 Timeline of repeated Diphtheria Toxin injections 35

Figure 4.2 Timeline incorporating PLGA/OVA scaffold implantation 38

Figure 4.3 Effect of three DT injections on mouse body weight 41

Figure 4.4 Surface marker expression of CD11c-DTR murine splenocytes after repeated DT injections. 44

Figure 4.5 Proliferation profile of OVA-specific CD4+ T-cells in the absence of CD11c+ cells 45

Figure 4.6 Statistical comparison of DT treatments on OVA-specific CD4+ T-cell proliferation: 2-way ANOVA followed by Sidak's post-test. 46

Figure 4.7 Proliferation profile of OVA-specific CD8+ T-cells in the absence of CD11c+ cells 50

Figure 4.8 Statistical comparison of DT treatments on OVA-specific CD8+ T-cell proliferation. 2-way ANOVA followed by Holm-Sidak's post-test. 50

Figure 5.1 *In vitro* culture to alternatively activated DC (aaDC) phenotype from human DCs 60

Figure 5.2 Schematic of MI scaffold preparation work flow 68

Figure 5.3 Size distribution histogram of un-crosslinked gelatin MPs. 72

Figure 5.4 Zeta potentials of gelatin MPs. 72

Figure 5.5 Analysis by Fourier Transform InfraRed Spectroscopy: 74

Figure 5.6 Incorporation efficiency of gelatin MPs: 76

Figure 5.7 Varying crosslinking concentration of GA to regulate release. 77

Figure 5.8 Embedding gelatin MPs in agarose cryogel. 79

Figure 5.9 Varying MP number density in agarose cryogel scaffold to regulate biomolecule release. 81

Figure 5.10 Non-linear regression of %fractional release of biotin from crosslinked standalone MPs over time (in seconds) using the Weibull equation (Eq.5.1). 82

Figure 5.11 Non-linear regression of %fractional release of OVA from crosslinked standalone MPs over time (in seconds) using the Weibull equation (Eq.5.1). 84

Figure 5.13 Non-linear regression of %fractional release over time (in seconds) using the Weibull equation (Eq.5.1) 88

Figure 5.16 Schiff's base formation by GA crosslinking of gelatin 99

Figure 5.17 An Alternative Mechanism of GA crosslinking of gelatin (based on [172]) 99

Figure 6.1 Dendritic cells cultured with MI scaffold increase expression of inhibitory marker while decreasing MHC II and co-stimulatory molecules. 121

Figure 6.2 Fold change of geometric Mean Fluorescence Intensity (gMFI) of human MI scaffold-treated DCs over iDCs. 122

Figure 6.3 Surface marker expression on MI Scaffold-treated human DCs. 124

Figure 6.4 MI scaffold treatment induced human PBMC-derived DCs to produce IL-10. 130

Figure 6.5 MI scaffold treatment induced human PBMC-derived DCs to lower secretion of pro-inflammatory cytokine 132

Figure 6.6 Mixed lymphocyte reaction with allogeneic T-cells: MI-scaffold treated human PBMC-derived DCs lowered T-cell proliferation compared to mDC control, in a dose-dependent manne. 134

Figure 6.7 Predicted release profiles of mGM-CSF, DEX and PGN loaded into the optimized MI scaffold designed for mouse DC culture. 136

Figure 6.8 Surface marker expression of MI scaffold-treated murine DCs. 137

Figure 6.9 Intracellular cytokine expression of MI scaffold-treated murine DCs. 139

Figure 6.10 Secreted IL-10 Quantification of MI scaffold-treated murine DCs. 142

Figure 6.11 Secreted IFN-γ Quantification of MI scaffold-treated murine DCs. 145
Figure 6.12 Antigen presentation assay – MOG-treated murine DCs were co-cultured with MOG-specific 2D2 T-cells and the extent of T-cell proliferation was determined. 146
Figure 6.13 Migration assay – Extent of CCR7 expressed on murine DCs after treatment with the MI scaffold. 148
Figure 7.1 Schematic of assessing the efficacy of MI scaffold as an *ex vivo* treatment in reconditioning DCs from MS patients (human or mice) 173
Figure 7.2 Schematic of assessing efficacy of MI scaffold in alleviating disease in EAE mouse model 175
Figure 7.3 Schematic of testing MI scaffold in an autoimmune diabetes model 177

Figure A 1 OT-II T-cells proliferated in vitro in response to OVA peptide (323-339). 179
Figure A 2 Confirmation of adoptive transfer of T-cells 181
Figure A 3 OT-II T-cells proliferated *in vivo* in response to OVA in PBS (top) or CFA(bottom). 182
Figure A 4 Light microscopic images of crosslinked gelatin MPs (left)10mM, (right) 25mM of glutaraldehyde crosslinker 183
Figure A 5 Gelatin MP exhibit autofluorescence at 360nm that increases with crosslinking density 184
Figure A 6 Light microscopic images of swollen agarose cryogel scaffold at 4x magnification. 185
Figure A 7 CD11c surface expression on BMDCs derived with GM-CSF (20ng/ml) and IL-4 (20ng/ml) added every other day over an 8 day period. TNF-α (5ng/ml) or LPS (1μg/ml) was added on day 6 and cells were assessed with flow cytometry on day 8. shown 186
Figure A 8 I-A (MHC-II) surface expression on BMDCs stimulated with a maturation agent 187

Figure A 9 CD80 surface expression on BMDCs stimulated with a maturation agent 188
Figure A 10 CD86 surface expression on BMDCs stimulated with a maturation agent 189
Figure A 11 PirB surface expression on BMDCs stimulated with a maturation agent 190
Figure A 12 Qa-1 (MHC-I) surface expression on BMDCs stimulated with a maturation agent 191
Figure A 13 CD80 vs. CD86 surface expression on BMDCs stimulated with a maturation agent 191
Figure A 14 Comparison of non-adherent and adherent murine BM-derived DCs displayed strong DC characteristics in terms of surface marker expression. iDC – immature or untreated DC, mDC – mature DCs stimulated by LPS or TNF-α, DC10s – IL-10-treated DCs. NA –non- oe loosely adherent, Adh – adherent. (top) GMFI fold change of unstained or (middle) iDCs. (Bottom) Expression of PirB, a tolerogenic marker. (For specific concentrations of treatments and timings please refer to the Methods section on BMDC culture in Chapter 6). Data is averaged over n=2 mice. 192
Figure A 15 Standard curve of serially diluted OVA for anti-OVA ELISA 196
Figure A 16 Viability of scaffold-encapsulated OVA. 197
Figure A 17 PLGA adjuvant effect *in vivo*. OVA/PLGA Scaffold-implanted mice were monitored over a 12-week period (top – timeline) during which orbital blood was collected and assessed with an ELISA against OVA-specific antibodies such as IgG, IgG1, IgG2a 198
Figure A 18 Timeline for determining biomaterial adjuvant effect to encapsulated OVA-secreting cells 199

LIST OF SYMBOLS AND ABBREVIATIONS

aaDCs - alternatively activated DCs, 4

AARDA - American Autoimmune Related Disease Association, 2

APC - antigen presenting cell, 12

CCL - CCL-chemokine ligand, 15

CCR1-10 - CC-chemokine receptor, 14

C_{GA} - glutaraldehyde crosslinking concentration, 73

CLR - C-type Lectin receptor, 14

CTL - cytotoxic T-cell, 13

DC - dendritic cells, 1

DC10 - IL-10-treated DC, 117

DCM - dichloromethane, 36

Dex or DEX - dexamethasone, 3

DEX+PGN-DCs - DCs treated with soluble dexamethasone and peptidoglycan, 114

DT - diphtheria toxin, 6

DTR - diphtheria toxin receptor, 6

EAE - experimental autoimmune encephalomyelitis, 157

GA - glycolic acid, 30

GFP - green fluorescence protein, 6

GILZ - glucocorticoid-induced leucine zipper, 20

GM-CSF - granulocyte monocyte-colony stimulating factor, 8

iDC - immature DC, 14

IL-10 - Interleukin 10, 3

ILT-2,3,4 - Immunoglobulin-like transcript 2, 3 or 4, 19

LA - lactic acid, 30

LN - lymph node, 8

LPS - lipopolysaccharide, 18

MAC - membrane attack complex, 12

mDC - mature DC, 14

MHC - Major Histocompatibility Complex, 12

MI - multifunctional immunomodulatory, 9

MI DC - MI scaffold-induced DCs or MI scaffold-treated DCs, 114

MM - metallophilic macrophages, 54

MOG - myelin oligodendrocyte glycoprotein, available as MOG_{35-55} peptide, 157

mTOR - mammalian target of rapamycin, 20

MZM - Marginal zone macrophages, 54

МФ - Macrophage, 11

NLR - Nod-like receptor, 14

N_{MP} - number of MPs, 61

OT-I mouse - C57BL/6-Tg(TcraTcrb)1100Mjb/J, 33

OT-II mouse [B6.Cg-Tg(TcraTcrb)425Cbn/J, 34

OVA - Ovalbumin or chicken egg albumin, 3

PBMC - peripheral blood mononuclear cells, 112

pDC - plasmacytoid DC, 18

PDL1,2 - programmed death ligand 1 or 2, 19

PGN - peptidoglycan, 3

PLGA - poly(lactic-co-glycolic acid), 3

PRR - pattern recognition receptor, 14

RLR - retinoic acid-inducible gene-I (RIG-I)-like receptor, 14

TCR - T-cell receptor, 157

tDC - tolerogenic DCs, 114

tDCs - tolerogenic DCs, 3

TGF-β - transforming growth factor β, 3

T_H - Helper T-cell, 12

TLRs - Toll-like receptors, 1

TNF-α - Tumor Necrosis Factor α, 17, 158

Tr1 - FoxP3$^-$ regulatory T-cells, 16

Tregs - regulatory T cells, generally refers to Fox3+ Tregs, 18

SUMMARY

Pivotal discoveries in the field of immunology over the last five decades have changed the way new therapies are designed for applications as varied as organ transplantation, autoimmune diseases or even cancer. In this regard, dendritic cells (DCs) were identified as crucial immune cells linking the innate and adaptive immunity, playing an important role in the orchestration of the adaptive immune response. Notably, the phenotype of DCs is a powerful indicator of their downstream effector functions. In the recent years, parallel advancements made in biomaterial design and biocompatibility considerations are being directly translated into developing improved immunotherapies. Interestingly, biomaterials also elicit differential effects on the host immune response as well as on the phenotypic state of DCs. For example, poly (lactic-co-glycolic acid) (PLGA), an FDA-approved biodegradable synthetic polymer, was able to enhance the *in vivo* immunogenicity of a co-delivered model antigen such as ovalbumin (OVA) through an adjuvant effect which correlated with the *in vitro* finding that PLGA induced a mature phenotype in DCs. On the other hand, agarose, a naturally available, neutrally charged polysaccharide, was able to maintain DCs in an immature state while also inducing autologous regulatory T-cells towards co-delivered OVA in a co-culture. In this dissertation, we explore the inherent differences in behavior of these two materials on DCs in understanding and enabling new design of biomaterial-based immunotherapies.

The objective of this work is explored in two parts of which the first is to validate the role of DCs in supporting antigen presentation for a proliferative antigen-specific T

cell response in the presence of PLGA, consistent with the previously observed adjuvant effect of PLGA. As noted above, PLGA was able to boost the humoral immune response against co-delivered OVA as well as modify DCs to express a mature phenotype; although these findings correlated with each other, the direct dependence of PLGA adjuvancy on DCs was only speculated and not proved until now. Herein, CD11c+ DCs were conditionally ablated *in vivo* by delivering diphtheria toxin to CD11c-DTR transgenic mice while simultaneously implanting PLGA scaffolds with incorporated OVA for its controlled release. As a read-out of induced OVA-specific T cell proliferation, fluorescently labeled OVA-reactive OT-II or OT-I cells were adoptively transferred and loss of fluorescence determined. Upon adoptive transfer of OT-II, CD4+ T-cells into DC-depleted mice failed to undergo full-fledged proliferation in comparison to those in DC-non-depleted control mice. The reduced clonal expansion of T-cells *in vivo* was likely due to the loss of antigen presentation in the absence PLGA-dependent DC maturation. Additionally, the CD8+ T-cell response was also affected by DC depletion, indicating that PLGA may be important for boosting the antigen cross-presentation response of DCs as well. Thus, the work described in Chapter 4 conclusively established that the effect of PLGA *in vivo* on the antigen-specific proliferative T-cell response, a likely early precursor to antibody response, was indeed due to its effects on DC presence and phenotype. This result is highly relevant in the context of designing improved vaccines using materials such as PLGA can boost antigen-specific adaptive immunity against infectious diseases or even cancer.

The second objective of this doctoral work was to address the feasibility of designing an agarose-based controlled delivery system that can deliver small-molecule as well as protein-based drugs at distinct times (perhaps mimicking culture doses and times) to condition DCs to acquire a tolerogenic phenotype that can subsequently be applied in immunotherapies for autoimmunity or to alleviate allograft rejection. For this purpose, we synthesized crosslinked gelatin MPs and characterized the release profiles of loaded 'model' molecules such as Biotin-Alexa Fluor 647 (~1000 Da) or OVA-Alexa Fluor 647 (~45,000 Da) from the MPs either when they were embedded in a macroporous layer of agarose cryogel scaffold or as standalone MPs. From this data, we developed an empirical model using the Weibull equation and determined correlations between experimentally variable parameters such as crosslinker concentration or MP number density per scaffold with Weibull equation parameters as means of enabling predictions of future formulations of a multicomponent, multifunctional immunomodulatory (MI) scaffold. In order to mimic tolerogenic human DC culture, we proposed that the MI scaffold should contain granulocyte monocyte colony-stimulating factor (GM-CSF; delivered within 0-3 days) to induce differentiation of monocyte precursors into DCs after dexamethasone (DEX, delivered within 3-6 days) addition would induce regulatory properties to these cells. Additionally, we decided to incorporate peptidoglycan (PGN, delivered on days 5-6) to induce a semi-mature phenotype in DCs strongly correlated with functional migratory properties necessary for success in future in vivo therapies. Based on the model, predictions for the scaffold formulation were defined and experimentally tested with these immunomodulators and any differences measured between predicted and measured release profile was used to optimize the model for future

predictions. Importantly, the model design was made such that it would be amenable to designing delivery of any set of biomolecules as long as they share the criteria of charge and size to Biotin or OVA and the delivery time frames of 1-2 weeks.

Subsequently, it was necessary to establish the effectiveness of the multifunctional immunomodulatory (MI) scaffold (delivering DEX and PGN only) design in inducing tolerogenic properties in human and murine DCs. First, the cellular surface markers of DCs generated from human blood monocytes upon treatment with the MI scaffold revealed a decrease in expression of the maturation marker CD86/DC-SIGN with and concomitant decrease of the tolerogenic marker ILT-3/CD86. Second, the secreted cytokines from these MI DCs showed an increase in the immunosuppressive cytokine IL-10 along with a decrease in the pro-inflammatory cytokine IFN-γ compared to mDCs (DCs matured using LPS). Third, MI DCs were able to diminish the allostimulatory T-cell response when co-cultures with allogeneic naïve T-cells. Collectively, these results indicated that the MI scaffold was able to induce a functional tolerogenic phenotype in DCs derived from human blood monocytes. Importantly, the ability of human MI DCs to lower the allostimulatory T-cell response is highly relevant in clinical scenarios of alleviating allograft rejection.

Similar to the human studies, when the optimized MI scaffold was tested with murine bone marrow-derived DCs to establish a tolerogenic phenotype, the cell surface marker expression profile showed a lowering of maturation markers such as MHC II, primary co-stimulatory marker CD86 and secondary co-stimulatory molecule ICAM-1

along with an elevation in tolerogenic marker PirB (analogous to human ILT-3). Additionally, murine MI DCs increased secreted IL-10 while decreasing IFN-γ, results that we corroborated by the intracellular expression profile of the same cytokines. Furthermore, these murine MI DCs, when pre-treated with a Multiple Sclerosis-specific antigen, namely MOG_{35-55}, were co-cultured with MOG-reactive T-cells, were able to alleviate the MOG-reactive T-cell response. The addition of PGN to the MI scaffold was done to ensure that immunosuppressants it released would not render the treated DCs incapable of migrating to LNs, a response that is essential in determining the successful outcome of using these DCs in immunotherapies. A late-stage release of a TLR ligand, such as PGN, to DEX-treated DCs would likely endow the DCs with migratory properties similar to endogenous populations of circulating tolerogenic DCs by upregulating LN-homing related chemokine receptor, CCR7. In order to determine the efficacy of the MI scaffold (containing DEX and PGN) in inducing functional CCR7 expression in murine DCs, the ability of murine MI DCs to migrate towards a CCR7-specific ligand, namely CCL19, was analyzed in a CCR7-chemotactic assay. The results from this assay showed that MI DCs as well as DCs treated with soluble DEX and PGN, were able to migrate towards CCL19, separated by a 5μm mesh barrier, at a significantly higher rate than untreated iDCs suggesting the importance of incorporating PGN along with immunosuppressive treatments in the future. Taken together, the MI scaffold design proposed was successfully able to induce tolerogenic properties in treated DCs, for human studies and optimized for murine studies. In addition, PGN release from the MI scaffold was able to bestow CCR7-dependent migratory properties on to murine DCs and hence can be considered ‘alternatively activated’ or aaDCs.

Overall, in this thesis, the importance of DC phenotype in determining its functional downstream outcome while using biomaterials to condition the response has been reiterated, first in the context of using PLGA (known to induce a mature phenotype in DCs) in the absence of DCs to diminish the immunogenicity of OVA in vivo and second, by delivering temporally differential immunomodulators from a DC-non-stimulatory biomaterial such as agarose, to induce functional DCs with tolerogenic and migratory properties that are highly relevant in designing future immunotherapies targeting autoimmune diseases as well as in alleviating allograft rejection.

CHAPTER 1 INTRODUCTION

Dendritic cells (DCs) play a central role in the host immune response and act as the link between the innate and the adaptive immune system. They express a variety of specialized pattern recognition receptors including toll-like receptors (TLRs) that can identify foreign, danger and self-associated molecular patterns. Circulating DCs in the periphery are maintained in a relatively immature state and constantly sample their environment for such patterns and process them to present to naïve lymphocytes. While responding to such environmental cues, DCs may undergo a change in their morphology and phenotype to become relevant to the required downstream function. Thus, in the presence of pro-inflammatory cytokines or TLR agonists they may transform from their immature, rounded state to a mature dendritic phenotype to drive active immunity towards associated antigen, or, alternatively acquire a tolerogenic phenotype to regulate immune tolerance when exposed to immunosuppressants or anti-inflammatory cytokines. Many a time, however, they express a phenotypic plasticity between the two, in a semi-mature state, that directs either downstream response depending on the cellular microenvironment. The introduction of biomaterial scaffolds as a means to direct such phenotypic preference of DCs can change the face of traditional immunotherapies. As such, the potential of biomaterials to modulate specific immune responses has only been recently explored in the context of antigens associated with biological component (as in a vaccine or tissue engineered construct); an adjuvant effect is possible if there is an enhancement of the immune response to a co-delivered antigen. This necessitates a deeper understanding of the involvement of DCs in such an adjuvant effect. Additionally,

differential expression of DC phenotype can be exploited favorably to drive tolerance or suppression of over-active immune aberrations in a myriad of autoimmune diseases. By using biomaterials to regulate and re-educate DCs, we can develop a variety of immunoengineering strategies that can assist the immune system in controlling diseases.

1.1 Research Significance and Innovation:

The American Autoimmune Related Disease Association (AARDA) estimates close to 50 million[1] Americans suffer from approximately 80 different conditions classified as autoimmune related disorders while the National Institute of Health suggests a total for 23.5 million[2] from epidemiology studies of 24 autoimmune diseases. Autoimmune disorders occur in individuals whose adaptive immune systems malfunction to generate immune responses against self or harmless antigen[3,4]. Professional antigen presenting cells, such as dendritic cells (DCs), are vital mediators of several downstream adaptive responses that lead to immunity or tolerance under normal conditions, and to autoimmunity under aberrant conditions[5]. Commonly prescribed treatments for such ailments require the long-term oral consumption of immunosuppressive drugs that although effective cause severe side effects due to the systemic nature of their delivery within the body[2]. Hence there is a widespread interest among researchers in developing targeted treatments of which biomaterial delivery systems are extensively being explored.

Biomaterial research over the last several decades has revealed the capability of materials eliciting distinct host responses as a function of their physical and chemical characteristics[6]. Relatedly, it has been observed that immune cells, specifically DCs,

respond differentially across a wide range of materials[7-10]; materials such as poly(lactic-co-glycolic acid) (PLGA) induce a phenotype in DCs that appears more activated than that induced by agarose[7,11], which maintains DCs in a rather immature phenotype. These findings were corroborated by *in vivo* studies, in which PLGA elicited an adjuvant effect [12] and also a differential humoral immune response to a co-delivered model antigen such chicken egg albumin or ovalbumin (OVA) compared to agarose[12,13]. Collectively, these studies suggest that materials themselves may have underlying mechanisms by which they interact with immune cells to alter their phenotype and thereby their function. We are interested in understanding the role DCs play in enhancing adaptive immune outcomes induced by PLGA and also in exploring the idea of developing solely material-based immunomodulation by exploiting the differential nature or DC responses to PLGA versus agarose in an *in vivo* setting.

Interestingly, the phenotype of DCs that engender regulatory immune responses have been artificially developed and studied in culture studies using anti-inflammatory cytokines such as interleukin-10 (IL-10)[14,15], transforming growth factor - β (TGF-β)[16] or with glucocorticoids[17] such as cortisone or dexamethasone. Although rendered tolerogenic, these artificially induced tolerogenic DCs may not perform their function effectively in an *in vivo* model where they would not only require regulatory properties but also features that enhance their peripheral lymphoid circulation and antigen-presentation. It has been shown that some toll-like receptor agonists of DCs such as bacterial peptidoglycan[17] can induce the upregulation of necessary chemotactic factors in these regulatory DCs to improve their homing in to peripheral lymphoid structures –

hence they were termed alternatively activated DCs (aaDCs). While we are interested in investigating solely biomaterial-based mechanisms of immunomodulation therapies, we are also attracted to the possibility of developing a targeted immunomodulator delivery system using a biomaterial device whose properties can be experimentally designed and controlled. It would be of great potential therapeutic value to develop a technique of recruiting endogenous DCs in an individual afflicted with an autoimmune disease, in a site-specific manner. For instance, a single implantable biomaterial niche that can locally release immunomodulators and specific molecular or cellular antigen simultaneously would be able to prime endogenous DCs to express an antigen-specific regulatory phenotype perhaps in an effort to mimic the generated phenotype of aaDCs.

CHAPTER 2 SPECIFIC AIMS

2.1 Specific Aim1:

Demonstrate that DCs (CD11c+ cells) play a significant role in supporting antigen presentation for a proliferative antigen-specific T cell response in the presence of PLGA, consistent with the previously observed adjuvant effect of PLGA.

2.1.1 Significance and Approach

The Babensee lab has previously shown that PLGA elicits an *in vivo* adjuvant effect towards co-delivered model antigen ovalbumin (OVA) as evidenced by higher levels of OVA-specific antibody titers in peripheral blood in mice, as compared to OVA delivered in PBS (negative control)[12,13,18]. These results were shown to be independent of biomaterial form– microparticle, film or scaffold. Interestingly, these findings correlated with *in vitro* data showing that PLGA influenced DCs to express a mature phenotype[19]. Maturation of DCs following or concomitant with antigen uptake is known to be necessary for effective T cell stimulation due to stable, high levels of expression of MHC molecules and costimulatory molecules. It would thus be expected that such effective presentation of OVA antigen, associated with PLGA implants, would occur, for the observed adjuvant effect. However, the direct association between the *in vivo* influence of PLGA on the supported humoral immune response to co-delivered antigen and the *in vitro* PLGA-induced DC maturation has not been established. As DCs are thought to be important target cells for immunomodulation in a biomaterial context. we are interested in understanding the functional role DCs play in vivo as far as supporting

or enhancing a humoral immune response to co-delivered antigen. A first step for the eventual humoral immune is efficient antigen presentation, particularly by DCs, which can be detected by clonal expansion (proliferation) of antigen specific T cells. To demonstrate the contribution/need for DCs to support the PLGA adjuvant effect, the analysis of T cell proliferation, an early event for the generation of a humoral immune response to delivered antigen, was undertaken in mice with conditional ablation of endogenous DCs.

CD11c-DTR transgenic mice (henceforth referred to as DTR mice) express a simian diphtheria toxin receptor coupled with green fluorescence protein (GFP) under the control of CD11c-expressing cells[20]. CD11c is ubiquitously expressed on all murine myeloid DC populations. As the simian diphtheria toxin receptor (DTR) is highly sensitive to its agonist, diphtheria toxin (DT), the genetically modified DTR mice, when treated with DT, would undergo targeted ablation of CD11c+ cells. Loss of GFP fluorescence in specific immune compartments in these mice can be used to determine the effectiveness of DT treatment on CD11c+ cell ablation. Such a conditional ablation model serves as a powerful tool to study the significance of a particular cell population *in vivo* on an observed phenomena[21].

The CD11c-DTR model allows DC depletion only during short time spans without causing mouse lethality. Assessing the humoral immune response to OVA in the presence of PLGA would require several (up to to 12) weeks of mouse survival. As it would not be possible to measure the antibody response using the DTR mouse model, we

instead assessed the effects of DC depletion in early T-cell response, namely clonal expansion of antigen-specific T cells. DC antigen presentation is known to be an early step involved in the adaptive immune response that would initiate a T-cell response and later an antibody response against associated antigen. Therefore, we used the OVA-OT-II/I model to investigate if the conditionally-ablated depletion of DCs *in vivo* would influence the proliferative response of adoptively transferred OVA-reactive T-cells in mice that were pre-implanted with an OVA-loaded PLGA scaffold. Upon exposure to a model antigen such as OVA, healthy wild-type mice would elicit a cellular immune response mediated by T-cells specific for OVA, resulting in antibody generation against OVA that would take a minimum of two weeks reach detectable levels[22]. An earlier alternative read-out of the immune response is to follow the proliferation of adoptively transferred fluorescently-labeled OVA-specific T-cells from OT-I/OT-II transgenic mice[22]. As these fluorescently-labeled cells proliferate, the intracellular label is divided into daughter cells, resulting in lower fluorescence levels. We *hypothesize* that conditional ablation of CD11c+ DCs in DT-treated DTR mice that are implanted with a PLGA scaffold delivering OVA would exhibit a lower extent of proliferation of adoptively transferred OVA-specific T-cells. This system can be an effective readout of a diminished immune response in the absence of DCs and thereby establish a correlation of DC significance in the adjuvant effect previously seen for PLGA[13].

2.2 Specific Aim 2:

Develop a microparticle-embedded scaffold system for temporal controlled release of multiple immunomodulators as predicted based on a mathematical model of release profile data as would be required to generate aaDCs.

2.2.1 Significance and Approach

We are interested in developing a biomaterial-based system that can promote endogenous recruitment and phenotypic control of DCs to render them tolerant towards co-delivered antigen and thereby serve as a potent treatment method in applications such as localized transplantation tolerance or targeted tolerance to autoimmune diseases. Alternatively activated dendritic cells [23] have been previously derived in culture from murine bone marrow cells or human PBMCs with the addition of specific immunomodulators such as granulocyte monocyte-colony stimulating factor (GM-CSF), dexamethasone (DEX)[17] and peptidoglycan (PGN)[17,24], each given at different time points within a seven-day period. GM-CSF is an essential growth factor for the development of cells of the monocyte lineage primarily conventional dendritic cells[22]; DEX is a molecule of the corticosteroid family, known to have anti-inflammatory effects[17] and, peptidoglycan is a pattern recognition receptor (PRR) agonist, a maturation factor, that has been shown to enhance lymph node (LN) migration[17] of tolerogenic DCs. We *hypothesize* that we would be able to reproduce the culture conditions (doses and timing) for generation of aaDCs using a biomaterial-based controlled release strategy. In order to ensure that the released biomolecules do not have off-target effects, we plan to localize and deliver them from a single biomaterial scaffold. However, to achieve temporally distinct release profiles for each biomolecule, we would need an additional

layer of control, which we *hypothesize*, is possible by using distinct microparticles with differential crosslinking to deliver each biomolecule yet tethered or embedded in a single defined scaffold.

In order to develop a biomaterial-based module that can deliver three or more biomolecules of varying molecular weights and release characteristics from a single scaffold niche, in Specific Aim 2, we propose to use a low-melting temperature ultrapure agarose cryogel scaffold, which by itself is non-stimulatory towards DCs[7,25], along with embedded gelatin microparticles, whose crosslinking densities can be tailored to suitably control the delivery times of appropriate immunomodulators.

2.3 Specific Aim 3:

Assess the *in vitro* ability of the multifunctional immunomodulatory (MI) scaffold in generating functional aaDCs and demonstrate their effectiveness in alleviating the T-cell response in a Multiple Sclerosis antigen-specific manner.

2.3.1 Significance and Approach

As mentioned in the research strategy of Specific Aim 2, we aimed to develop a multicomponent and multifunctional (MI) scaffold to induce alternative activated phenotype in DCs in a manner similar to aaDC generation in the culture procedure where the immunomodulators are added solubly at distinct time-points. The ability of the MI scaffold thus prepared with embedded gelatin MPs of varying crosslinking densities loaded with GM-CSF, DEX and PGN, to induce alternative activation of DCs can be

evaluated in several ways. The simplest method would be to culture peripheral blood mononuclear cells from human blood or murine bone-marrow derived myeloid precursors *in vitro* in the presence of the scaffold and compare it to the standard culture by evaluating the surface and intracellular cytokine markers of the ensuing DC fraction, whereas a more functional method would be to apply the scaffold-treated DCs in a mixed lymphocyte reaction to determine the suppression of allogeneic T-cell responses by the DCs. Yet another method would be to use the scaffold-treated DCs pre-pulsed with a disease model-specific antigen in an *in vitro* antigen presentation assay to determine the reduction or suppression of antigen-specific T-cell response. This would bolster the possible antigen specificity that can be achieved with the MI scaffold-treated DCs hence deriving a system more suitable for disease-specific applications. We, additionally, hypothesize that *in vivo* implantation of the scaffold, in a site-specific manner, would cause surgery-associated trauma and recruit endogenous monocyte precursors from the blood to the surgery site; the release of the loaded immunomodulators from the scaffold would then give rise to an alternatively activated phenotype in differentiating monocytes to give aaDCs. Further, these DCs would likely possess upregulated chemokine receptors that would enhance their migration to draining LNs, a scheme typically subdued in pure tolerogenic DCs, and potentially improve presentation of any co-delivered antigen.

CHAPTER 3 LITERATURE REVIEW

3.1 Innate and Adaptive Immunity

3.1.1 Innate Immunity

Innate Immunity is the first line of host defense against foreign entities in a non-specific, rapid manner. It has the ability to respond to microbes, foreign cells, and/ or products of injured cells. These responses are non-specific and initiated molecular structures that are common to pathogens and not found on eukaryotic cells. They actively clear foreign antigen, materials or apoptotic cells, and influence repair of damaged host tissue[26].

The innate immune system, first, provides physical and chemical barriers in the form of epithelia and epithelial surface-bound antimicrobials respectively. Second, phagocytic cells such as macrophages (MΦs) resident in the sub-epithelial tissue offer protection. Recognition of pathogens by these phagocytes results in the secretion of cytokines and chemokines that initiate the recruitment and activation of leukocytes such as neutrophils and monocytes/MΦs from circulation at the site of infected tissue. These leukocytes subsequently recognize and destroy pathogens[26].

Conserved effector mechanisms specifically, the complement system, serve to enhance the innate immune response. The complement system comprises of a set of plasma proteins that can bind to pathogen surfaces resulting in their activation to generate proteolytic degradation fragments[49]. These cleavage products coat foreign antigen

surfaces (opsonin) for leukocyte recognition and clearance, release of soluble chemotactic mediators for leukocyte recruitment and activation with the terminal product of the complement activation cascade being the membrane attack complex (MAC) that lyses the targeted cell[27].

3.1.2 Adaptive Immunity

An adaptive immune follows the innate response and being antigen-specific, it is greatly effective compared to it in eliminating antigens as it is antigen-specific. It is achieved via three broad strategies[28-30]:

1. B cells take up antigen, process them and subsequently differentiate into antigen-specific antibody (Ab)-secreting plasma cells. Secreted Abs recognize and bind to extracellular antigens, marking (or opsonizing) them for clearance by phagocytes. Antigen-Ab complexes also initiate the complement cascade via the classical pathway.
2. Phagocytosis of antigen is achieved by antigen presenting cells (APCs) such as DCs and MΦs. Antigen presenting cells process antigen, load it and present it in the context of major histocompatibility complex (MHC) molecules on their surface. Activated DCs are unique in their ability to present MHC-bound antigen to naïve T-cells to stimulate their clonal expansion and elicit appropriate effector functions. Engagement of MHC-II molecules on APCs are CD4 restricted presenting their bound antigenic peptides to CD4+ cells such as Helper T (T_H) cells to stimulate cytokine release that provides help for activation of APCs and lymphocyte function.
3. Exogenous antigens can be cross presented for loading into MHC-I molecules on APCs that are CD8 restricted presenting their bound antigenic peptides to CD8+ cytotoxic T cells (CTLs) for targeted cell cytotoxicity[95]. Foreign cells or cells expressing

foreign proteins (e.g. upon viral infection) present these antigenic peptides loaded on the MHC-I molecules to effect CTL responses.

3.2 Dendritic Cells (DCs)

In 1973, Ralph Steinman identified 'accessory' cells that were necessary to generate primary antibody response in culture, and coined them dendritic cells due to their morphology[31]. These cells had dendritic-like projections, moderate phagocytic ability and limited numbers of lysosomes while expressing high levels of MHC molecules necessary for presenting extracellular antigens[32]. Since then DCs have been characterized as distinct from MΦs and lymphocytes due to their predominant function as APCs are thus known to play a central role in the host immune response to self[33] and foreign antigen[34,35].

Generally, DCs express MHC I and MHC II molecules and occasionally, CD14 (associated with monocyte / MΦs) and CD16 (of neutrophils), while lacking CD3 (of T-cell), CD19 (of B-cell) and CD56 (of NK cell) [36]. They also express a variety of adhesion molecules including CD11a (LFA-1), CD50 (ICAM-2), CD54 (ICAM-1), CD58 (LFA-3), and CD102 (ICAM-3); and co-stimulatory molecules namely, CD80 (B7.1), and CD86 (B7.2) - expressions of which are upregulated during DC maturation[37,38]. The co-stimulatory molecule, CD86 tends to be a marker of early DC maturation, while CD80 expression increases in fully mature DCs.[37] Hematopoietic bone marrow progenitors differentiate into circulating DC progenitors (myeloid or plasmacytoid subsets) [39,40] that infiltrate peripheral tissues as immature DCs (iDCs)[41]. These cells possess the specialized

ability of responding to environmental cues using their wide array of PRRs such as TLRs, Nod-like receptors (NLRs), C-type lectin receptors (CLRs), retinoic acid-inducible gene-I (RIG-I)-like receptors (RLRs), scavenger receptors [26,42] and other inflammatory mediators such as chemokines [43] and cytokines [44]. As such, a myriad of environmental triggers can cause the variety of available DC subsets to differentiate extensively, thus rendering DCs highly immunocompetent cells and the essential link between innate and adaptive immunity.

As iDCs, these cells constantly sample their surroundings and uptake antigen by phagocytosis, receptor-mediate endocytosis or micropinocytosis[45] and as such the route of uptake influences presentation[46]. Soon after, there occurs an increase in their antigen presentation machinery that results in the upregulation of antigen-loaded surface MHC I and II molecules[47]. As maturation occurs (resulting in mature DCs or mDCs), these cells downregulate their ability to further phagocytose local signals (ex. CC-chemokine receptor-5 (CCR5) ↓ , CCR6 ↓[41,48]), hence losing their ability to process new peptides while expressing co-stimulatory molecules (ex. B7 family[49]) and chemokine receptors such as CCR7[48] that improve homing to nearby draining LNs. At the LNs, mDCs polarize naïve T-cells [50,51](via a highly complex structure known as the DC-T-cell synapse[52]) to downstream effectors by presenting processed antigen in the context of MHC molecules (signal 1), co-stimulatory and adhesive molecules (which bind to cognate receptors on T-cells; signal 2) and T-cell-priming cytokine signals (ex. IL-12; signal 3). Naïve CD4+ T-cells differentiate into effectors of Th1, Th2 or Th17 subtypes. Typically, exogenous antigen peptides are expressed on MHC II molecules and prime

naïve $CD4^+$ T-cells. While, in most mammalian cells endogenous antigen bound to MHC I molecules to stimulate CTL responses, only DCs have the unique ability of presenting exogenous antigen with MHC I molecules that can prime naïve CD8+ T-cells in CTL effectors; this mechanism is known cross-presentation[53]. We can perhaps also describe a fourth type of signal occurring in the DC-T-cell synapse that enables direct trafficking of the effectors T-cells. For example, in gut-associated LNs, transforming growth factor (TGF-β) and retinoic acid induced by DCs cause $CD4^+$ T-cells to express α4β7 and CCR9 that act as gut-homing receptors[54]. Analogously, in skin-associated draining LNs, vitamin D metabolites from DCs induce T-cells to express CCR10 that bind their cognate ligand CC-chemokine ligand 27 (CCL27), allowing them to home back to the skin[55]. In another example, antigen-loaded (OVA[56] or myelin-peptide[57]) DCs injected intracerebrally in mice, migrated to cervical LNs using high CCR7[56,57] and initiated antigen (OVA) -specific T-cells responses; a fraction of the T-cells migrated out in to the central nervous system[56]. Although, the specific homing mediators of these T-cells are as yet unknown, it is sufficient to conjecture that a similar fourth signal is involved. Collectively, these studies indicate the potential usefulness of effector T-cell-homing signals induced by DCs in specialized and targeted therapeutic applications.

Alternatively, tissue-resident DCs that obtain harmless environmental or self-antigens, in the absence of inflammatory mediators, may migrate to their respective draining LN. As relatively immature or unstimulated cells they may express overall lower levels of MHC-II, co-stimulatory molecules, secreted IL-2 and instead secrete IL-10, retinoic acid[58,59] that can act as tolerogenic primers. DCs expressing processed innocuous, self-antigen

activate one of several types of regulatory T-cells (Treg, Tr1, Th3) that reinforce immune tolerance.

3.2.1 Endogenous DC Populations

A plethora of DC subtypes have been currently discovered in different organ systems and animals and it is highly likely that more will be in the future. Many of these have tolerogenic properties in their steady state (such as myeloid or plasmacytoid); however due to their phenotypic plasticity (Figure 3.1), their surrounding environmental pro-inflammatory signals supersede native tolerogenicity and convert them into immunostimulatory DCs[60].

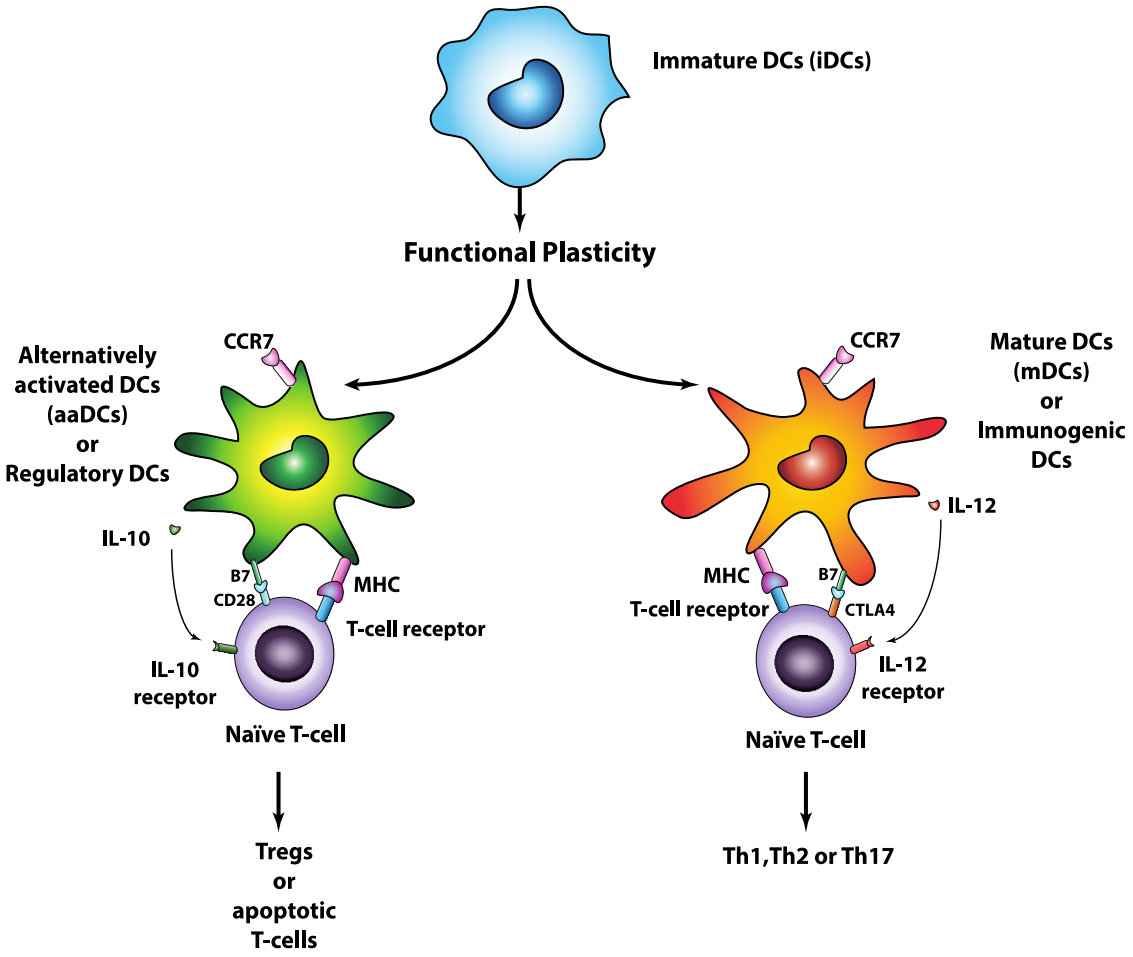

Figure 3.1 Dendritic cells exhibit functional plasticity

Three distinct subsets of myeloid DCs (MDCs) based on their surface molecule expression exist in peripheral human blood; $CD1c^+$ or blood dendritic cells antigen (BDCA)-1^+ Lin^- $CD123^{lo}$ MHC-II^+ HLA-DR^+ $CD11c^+$ form the major subset while CD141/BDCA-3^+ Lin^- HLA-DR^+ $CD11c^+$ comprise the minor subset[61]. BDCA-3^+ DCs expresses CLEC9A, an endocytosis mediating C-type lectin with a cytoplasmic immune receptor tyrosine-based activation-like motif[62]. The third and final subset was more recently recognized to present a carbohydrate variation P-selectin glycoprotein ligand-1 (PSGL-1), called 6-sulfo-LacNac. These DCs have been shown to produce TNF-α more strongly than BDCA$^+$ DCs in response to bacterial cell membrane lipopolysaccharide

(LPS) stimulation[63]. Plasmacytoid DCs (pDCs) on the other hand are MHC-II^{+} CD1^{-} CD123^{hi} and also express BDCA-2, BDCA-4, IL-3RA and ILT-7. BDCA-1^{+} DC subset possess superior allostimulatory ability and secrete abundant IL-12[64] while BDCA-3+ MDCs and BDCA-2+ pDCs secrete interferons (ex. IFN-γ, IFN-α respectively). Recently, a small tolerogenic subset of DCs expressing IL-10 and that are CD1c- CD303- CD14+ have been isolated from peripheral human blood; however, their regulatory properties have occurred in combination with an *in vitro* counterpart.[65]

Tissue-resident DCs population especially of the gut or liver, during steady state, largely maintain a regulatory state. Intestinal DCs such CD11c^{+} CD11b^{+} CD103^{+} cells (for example) in their unperturbed state constitutively express retinaldehyde dehydrogenase-2 (RALDH2), TGF-β and indoleamine-2,3-deoxygenase (IDO) so as to direct antigen-specific (commensal flora or other food-related harmless antigen) responses towards tolerogenic effects except during inflammatory events in the intestine when these signals (TGF-β and RALDH2) are considerably downregulated[58,66-68]. Similarly, liver is another organ system where constant tolerance is required to be maintained; human hepatic DCs, predominantly BDCA1+, unlike their circulating blood counterparts, secrete copious amounts of IL-10 upon TLR-associated stimulation and directing strong regulatory response via CD4+ CD25+ Foxp3 regulatory T cells (Tregs)[36].

3.2.2 Experimental and Induced Tolerogenic DCs

In vitro, a variety of tolerogenic DCs have been generated with the aid immunosuppressive agents such as corticosteroids[17,69-73], vitamin D3[74-77], immunosuppressive cytokines such as IL-10[78-82] and others, rapamycin[83-85], neuropeptides[86,87] and many more[88-93], either alone or in combination with others treatments. Among them, IL-10-, vitamin D3-, dexamethasone-, and rapamycin-induced tolerogenic DCs are most prominent groups, well-studied in mouse and/or human systems. The immunosuppressive cytokine, IL-10, was one of the first mediators shown to induce a tolerogenic phenotype in human DCs[78,79], collectively indicating that IL-10-treated monocyte-derived DCs displayed lowered expression of MHCII and co-stimulatory molecules and could induce effector T-cell anergy. Interleukin-10 induced semi-mature CD14+ monocyte-derived DCs from atopic asthmatic individuals were able to suppress specific allergen-driven proliferative and Th2 cytokine response of autologous peripheral blood CD4+CD25- FoxP3- effector T-cells and irreversibly convert effector T-cells into Tregs[94]. Semi-maturation of DCs due to cocktail of IL-1β, TNF-α, IL-6 and PGE-2 rendered them resistant to further LPS-induced maturation. These induced tolerogenic DCs exhibited, in addition to low MHC and co-stimulatory molecules, low expression of 4-IBB, OX40L and increased expression of DEC205, IFN-α1, CCR7, immunoglobulin-like transcript 2 (ILT2) and IL-10. They thereby induced IL-10-secreting CD25+ FoxP3+LAG3+CTLA4+ Tregs. Another study, also using a similar model of IL-10 and semi-mature DCs revealed increased expression of inhibitory markers such as ILT-3, ILT-4, programmed death ligand 1 (PDL1) and PDL2, were able to strongly respond to LN-homing chemokine CCL19[14]. They also induced Tregs that

were capable of suppressing allogeneic T-cell responses in a contact-dependent but IL-10 and TGF-β-independent manner[95]. These DCs have also been correlated with the expression of glucocorticoid-induced leucine zipper (GILZ), which is both necessary precursor to expressing ILT-3, PDL1 and IL-10, such that silencing of GILZ results in the loss of their tolerogenic properties[96,97].

Rapamycin, unlike IL-10, is a macrolide immunosuppressive agent that restricts DC maturation through binding serine/threonine protein kinase mammalian target of rapamycin (mTOR). Antigen activation by naïve CD4+ and CD8+ T-cells activates mTOR and thereby engenders cellular differentiation to FoxP3- effector T-cells; whereas a suppression of mTOR signal results in inducing functional CD4+ CD25+ FoxP3+ Tregs[98]. Clinically, rapamycin has been shown to prevent allograft rejection in renal transplants[99] although associated with limiting side effects such as adverse cutaneous manifestations[100]. Rapamycin, however, is unique in its ability to affect T-cells and DCs, although it displays albeit exhibiting opposing effects on myeloid and monocyte-derived DCs; it supplements the allostimulatory ability of myeloid DCs and suppresses the immunogenic nature of monocyte-derived DCs. Rapamycin-treated DCs have shown to increase FoxP3+ Tregs in murine heart transplant recipients and is correlated with long-term organ allograft survival[101].

Glucocorticoids, unlike rapamycin, may have very complex effects on DCs: when supplied as a single treatment of as part of a combination, glucocorticoids such as DEX are known to reduce MHCII, co-stimulatory molecules and IL-12 secretion[72,102]; increase IL-10 while also upregulating ILT2, ILT3[97] and GILZ[103]. More importantly, DEX-

treated DCs were capable of retaining the tolerogenic properties despite stimulation with LPS[17,71]. Further DEX-DCs induce FoxP3+ Tregs and lowered graft-associated inflammatory cell infiltrates and prolonged graft survival in the case of experimental corneal allografts.[104]. It is evident from wide research in 'inducing' tolerance in DCs that countless methods are available for *in vitro* generation of tolerogenic DCs, however there needs to be a mechanism to translate this growing knowledge into clinically applicable models of therapeutic benefit. Also, it is apparent that the type of immunosuppressant chosen may entirely depend on expected application; for example, when dual modes of immunosuppression may be required i.e. when T-cells and DCs need to be induced with tolerance, rapamycin may be used as the immunosuppressant while when strong Treg responses are required, IL-10-based or DEX-based treatments may be applied. Another group has used only GM-CSF at low continuous doses, in the absence of IL-4, to develop maturation-resistant regulatory DCs, inducing T-cell unresponsiveness both *in vitro* and *in vivo* as well as efficacy in a cardiac allograft survival model[105]. Irrespective of the application of induced tolerance, it is important to note than the use of a late-stage maturation stimulus is applied for improved efficacy not only due to the possibility of generating enhance migratory capabilities of these DCs but also with the deeper understanding that semi-mature DCs may be more functionally similar endogenous circulating populations of regulatory DCs[60].

3.3 Biomaterial Strategies to Influence Adaptive Immune Responses

With a growing understanding of intrinsic biological pathways of immune responses, biomaterial scientists aim to develop strategies to engineer appropriate interactions with the immune system using biomimetic strategies, controlled release or

biomaterial design as required by the context – vaccines for infectious disease or cancer, tissue engineered constructs, cell/tissue transplants, and autoimmune disorders. The adaptive immune response in any given scenario is vastly influenced by the phenotypic state of DCs which direct immune responses. Hence, an attempt to successfully modulate DC phenotype through biomaterial strategies can be a way that potentially leads to need-based tailoring of the body's immune response.

3.3.1 Biomaterials Influence DC Phenotype

Dendritic cells have been previously elucidated by the Babensee laboratory in the context of biomaterial contact. Dendritic cells, both human monocyte-derived and murine bone marrow-derived, have to ability to respond differentially to a variety of biomaterials[7,9,25] – particularly, iDCs when in contact with materials such as agarose displayed no maturation or activation whereas iDCs in contact with PLGA undergo activation and display a phenotypic similarities with mDCs; PLGA-treated DCs expressed enhanced levels of co-stimulatory molecules (CD40, CD80 and CD86), MHC II (HLA-DQ and DR) and DC maturation marker (CD83) in comparison to untreated iDC controls[7]. Not only did these PLGA-treated DCs exhibit dendritic processes similar to mDCs they also displayed improved allostimulatory capabilities to induce T-cell clonal expansion in a mixed lymphocyte reaction (MLR).[7] As noted above, biomaterials elicited similar responses in murine bone-marrow derived DCs and in addition provided evidence for PLGA-treated DCs secreting higher levels of TNF-α, IL-8, IL-6 and IL-10 compared to those secreted by agarose DCs[11]. In addition, the structural form of the material either as films, scaffolds of microparticles[7] as well as varying surface contact[11] have indicated

an influence on DC response. Furthermore, a differential effect of DC maturation was induced by different biomaterials. More specifically, PLGA or chitosan films induced DC maturation while alginate and agarose did not; hyaluronic acid film exhibited suppressed DC maturation[106]. An MLR showed that DCs treated with PLGA and chitosan films supported higher levels of T-cell proliferation than iDCs; DC treated with hyaluronic acid films induced lower levels of T-cell proliferation, and DCs treated with agarose and alginate films did not differ from iDCs in allostimulatory capacity[25]. Interestingly, both PLGA and alginate induced higher NFκB activation than iDCs, and the activation level is much higher in the DCs treated with agarose[11,106]. In characterizing the vastly different aspect of PLGA and agarose of DC phenotypes, DCs treated with agarose not only supported an immature or 'non-stimulatory' phenotype, these DCs also promoted the priming autologous T-cells (in a co-culture of DC and autologous T-cells) to regulatory FoxP3+ phenotype.[107]. Furthermore, in this co-culture, agarose treatment induced release of IL-12p70 and IL-10 at higher levels as compared with DC treatment with other biomaterial films/OVA, suggesting Th1 and Th2 polarization, respectively. Dendritic cells treated with PLGA film/OVA treatment induced release of IFN-γ at higher levels than that of co-cultures with iDCs or DCs treated with all other biomaterial films. From these results, it is evident that biomaterial composition and form can influence DC phenotype and in turn their downstream immune responses providing a potential tool for immunomodulation by directing autologous T-cell responses.

3.3.2 DC-Mediated Biomaterial Adjuvant Effect

In the case of combination products, constructs that consist of both non-immunogenic biomaterial and biologics, the differential biomaterial effect results in model antigen OVA-specific differential humoral responses when OVA was co-delivered with the respective biomaterial *in vivo*[12,13,18]; a likely downstream consequence of DC maturation. Mainly, PLGA was found to support a moderate humoral immune response that was predominantly Th2 as suggested by IgG1 antibody titers.[18] and the PLGA scaffold was able to maintain longer duration of immune response than MPs[12]. The enhanced humoral response was likely due to the implantation-associated potent danger signals such as HMGB1 found at higher concentration in exudates from subcutaneously implanted PLGA SCs in comparison to naïve controls[10], suggesting a possible role of danger signal biomaterial-induced adjuvant effect. While DC were shown *in vitro* to mature upon contact, the actual connection of DCs in mediating the observed PLGA adjuvant effect observed, was one of the subjects of this investigation.

3.4 Autoimmunity

3.4.1 Mechanisms of Immune Tolerance

Immunologic tolerance or regulation is the fundamental approach that prevents immune reactions against harmless or self antigen. Two primary modes of tolerance are achieved by the immune system. First, primary or central tolerance occurs by deletion of T-cells and B-cells with receptors extremely sensitive to self antigen : In the developmental stage, B and T-cells are comprised of BCRs and TCRs respectively that have the ability to spontaneously recombine with existing gene segments in a process

known as V(D)J recombination to give rise to a theoretical 10^8-fold increase over in possible number of antigens the adaptive system can respond to, simply based of genetic information[22]. However, arbitrary recombinations may elicit TCRs that are highly reactive to self-antigens. Normally, T-cells bearing these TCRs are marked for elimination, thereby achieving central tolerance. Secondary or peripheral tolerance is associated with the extra-thymic cellular signaling experienced by T-cells in response to APCs: Self-reactive T-cells that escaped thymic screening come into contact with APCs presenting self-antigen in the absence of co-stimulatory molecules, can induce T-cell anergy. Alternatively, when these self-antigen expressing APCs also co-express co-inhibitory molecules such as CTLA-4[108] or PD-1[109] along with immunosuppresive cytokine microenvironment, the responding self-specific T-cells may become Tregs. These Tregs can actively suppress other effector T-cells mechanism as well as immunogenic DCs. Recently, a subset of CD4+ T-cells with regulatory properties have been defined as adaptive Tregs[110] or IL-10-producing Tr1 cells, distinguished by the co-expression of surface molecules such as CD49b and LAG-3[111]. Interestingly, considerable research in the field of regulatory T and B-cells shows the possibility of existence of CD8+ Tregs[112,113] as well as regulatory B-cells[114].

3.4.2 DCs and Autoimmunity

Autoimmunity can occur due to a multi-level dysfunction of checkpoints associated with tolerance towards self-antigen. Evidently, failure of either central or pepheriral tolerance or both can result in the occurrence of highly self-specific T-cells that are recruited during the onset of an autoimmune disease[4]. Ddendritic cells, the only known APCs capable of triggering an autoimmune response have been closely linked

with the pathogenesis of autoimmune diseases[115,116]. *In vitro* culture in the presence of strong maturation stimuli and myelin basic protein, of bone maroow-derived DCs from wild type mice donors, generated Th1 response that ultimately developing into experimental autoimmune encephalitis[117]. Also, chronic maturation of tissue-resident DCs within their native microenvironment can engender critical organ-specific autoimmune disease as well as systemic autoimmunity[118].

3.4.3 Current Strategies for Autoimmunity Amelioration and Future of DCs

Two types of approaches have been traditionally applied in treating autoimmune and allergy disorders. First approach is the administration of immunosuppressive drugs that can diminish immune responses and alleviate the severity of self-reactive immune mechanisms. However, systemic immunosuppression is associated with deleterious long-term health issue of patients making them vulnerable for severe infections. In the case of renal transplantation, the administration of cyclosporine has long been associated with decreased episodes of graft rejection, however, long-term effects of cyclosporine resulted in an increased rate of malignant disorders[119]. In the same vein, a study done on the effects of chronic corticosteroid therapy in transplant patients (not restricted one a particular type of transplant) revealed the acute incidence of diverticulitis which resulted in 25% overall mortality of these patients. In such cases targeted approaches to delivering immunosuppressive agents may improve the disease-associated patient outcomes.

Second approach is based on the idea that if self-antigens targeted by the immune system in various autoimmune disorders are identified, then it should theoretically be

feasible to deliver these antigens to patients under the control of mechanism that are non-stimulatory than promote autoimmune responses. In the context of clinical applications to treat allergies, a proof of this concept has been practiced for several years for instance allergen-specific immunotherapy.

Mechanisms likely combining both approaches are being extensively explored in the context of autoimmune diseases[120] as well as (most importantly) in cancer[121,122]. The rationale for such a combination is that DCs, as noted previously, are a crucial cell type involved in active autoimmune disease onset and progression however these cells simultaneously have the capability to undergo re-education of phenotype under the tight conditioning of their microenvironment to espouse auto-antigen-specific tolerance. In the context of DCs, Sipuleucel-T[123] continues to be the only FDA-approved DC-based vaccine albeit for treating prostate cancer by *ex-vivo* manipulation of patient-derived blood DCs which is stimulated with a fusion protein GM-CSF and antigen prostatic phosphatase (PAP) (present in 95% of prostate cancer cells). The combination promotes maturation of DCs in the context of PAP and the DCs are converted from quiescent or suppressive DCs to active immunogenic DCs. A reversal of this mechanism, that is delivery of autoimmune-associated protein along with tolerogenic factors to self-immunogenic DCs ,would give rise to auto-antigen-specific tolerogenic DCs and subsequently tolerance in the autoimmune disorder. Although the goal of most strategies is to develop a deliverable *in vivo* therapy, the sheer complexity of interplay of signals of host response may require years and years of research, there is a an open market for developing *ex-vivo* based therapies as well due to the decreased system complexity and

likely shorter turnaround time. These types of strategies serve as primary motivation for developing a multifunctional immunomodulatory scaffold to induce tolerogenic DCs in the context of human and murine cells, and although this thesis currently focusses on understanding the *in vitro* implications for the system, we have also kept in the mind its subsequent application in *in vivo* therapeutic models of autoimmune disease.

CHAPTER 4 DENDRITIC CELL INVOLVEMENT IN SUPPORTING ANTIGEN PRESENTATION FOR A PROLIFERATIVE ANTIGEN-SPECIFIC T CELL RESPONSE IN THE PRESENCE OF PLGA

4.1 Overview

Dendritic cells function as the most proficient antigen presenting cells in the mammalian immune system. While originally thought to be indistinct from monocyte/macrophages, collective research on DCs over the last 3 decades suggest conclusively that they are a unique group of cells, derived from hematopoietic progenitors, that can process antigen in their microenvironment and present them on their surface for identification by naïve T-cells. By expressing a wide variety of PRRs, DCs can respond differentially to "antigen – motif" associated molecular patterns. While similar to macrophages is origin and shared functions such phagocytosis, the antigen presentation mechanism in DCs is 40x better than MΦs. In addition, DCs are also known to function as regulators of the immune system, by inducing peripheral anergy to self-reactive T-cells or by inducing antigen-specific regulatory T-cells. Due to their combined ability of phagocytosis and antigen presentation, the role of DCs in the host response to biomaterials used in combination products is crucial to understand. In association, it has been shown previously that biomaterials produce a differential adjuvant effect on phenotype of DCs and in turn their function.

Poly(lactic-co-glycolic acid) is a biodegradable copolymer of lactic acid (LA) and glycolic acid (GA) that has been extensively applied in the field of biomolecule delivery. It is often selected as the most suitable material for therapeutic applications in diseases such as cancer, and many others, that want to be fast-tracked to clinical trials primarily because it is approved by the FDA for medical use and not particularly due to its ability to modify an immune response with its adjuvant effect. The polymer as such is highly modifiable in composition to control rate of degradation as well as in geometry (films, scaffolds and matrices, microparticles, nanoparticles) to suit the needs of the considered application. Unlike commonly available synthetic polymers, PLGA exhibits a high extent of biocompatibility and reduced toxicity since the degradation products are identical to body metabolites. Other factors influencing commercial development such as cost and ease of synthesizing are also favorable for PLGA. Due to these attractive features, PLGA was and is being used in therapeutic applications in several of clinical trials recently[124]. A select set of these completed trials failed to show any significant benefits over controls either due to a non-ideal experimental setup or due to insufficient understanding of the host interaction[125,126]. This necessitates a deeper insight in to the host response PLGA carriers or combination products (PLGA and biologic) may engender *in vivo*. In general, PLGA alone (surface modality, geometry, degradation products) may trigger a non-specific immune/inflammatory response while biologics added to it may result in an adaptive immune response. The ability of biomaterials to modify the overall host response in such a setting is important – they may produce an adjuvant / immunostimulatory effect or an immunosuppressive / tolerogenic one. Particularly their ability to influence the immune outcome, requires that they be studied in depth in

conjunction with key immune-fate determining cells such as APCs. As PLGA is the most widely used FDA-approved material synthetic material in tissue engineering and regenerative medicine, it is important to understand its effect on the immune system with and without APCs.

Poly(lactic-co-glycolic acid) has been shown to elicit an adjuvant effect *in vivo* by inducing the Th2 response to co-delivered model antigen OVA. In conjunction, its effects on DCs *in vitro* have been analyzed for human-derived and non-human mammalian cells (murine) and together, they indicate that PLGA has a maturation-like stimulatory effect on DCs; PLGA induces a shift in the phenotype of DCs to render them more immunogenic than immature/untreated/quiescent DCs. Although this level of DC maturation was less than the standard maturation agent (TLR agonists such LPS, etc.), it could certainly aid in bolstering the immune response induced by the DCs – could be used in vaccine delivery as an adjuvant. Although not uptaken into DCs by the same route as PRR-agonists, it is likely the strong acidic environments inside phagosomes/endosomes results in increased degradation of endocytosed PLGA which may result in altering internal sensitivity of associated antigen-peptides to downstream cellular processing in the DC antigen-presentation machinery. As noted (in the DC description section), a change in DC phenotype is a crucial indicator of a potential change in DC function and the downstream variety of the adaptive response (stimulatory or regulatory). By connecting the dots between *in vitro* and *in vivo* immune response data for antigen-carrying PLGA, it is rather straightforward to hypothesize that the adjuvant effect induced by PLGA to co-delivered antigen *in vivo* is likely due to its effect on

immune-fate determining DCs. Such a level understanding of cellular influences of PLGA could result in designing improved delivery products likely targeted for locations of quiescent and hence programmable DCs within the body, that would have a higher chance of being successful as a therapeutic vehicle for human immune-associated disorders.

In this study we wanted to revisit our hypothesis that the *in vivo* adjuvant effect of PLGA to model co-delivered antigen OVA is due to the role of DCs in mediating such an immune response. As mouse models are highly customizable while maintaining the integrity of functioning as a self-sustaining mammalian organism, we used a previously designed model derived from C57BL/6 wild-type mouse, in which CD11c+ cells within the animal could be conditionally ablated. CD11c gene in these mice was modified by attaching a simian diphtheria toxin receptor (DTR) so that all CD11c expression occurred along with DTR. As the major group of cells expressing CD11c+ in mice were DCs, treating these mice diphtheria toxin (DT) was able to conditionally deplete DCs. The depletion of DCs was maintained as long as there was circulating DT in the periphery. (DT has a relatively short half-life). Thus we used this model (henceforth termed CD11c-DTR or simply DTR mouse) to study the effect of PLGA on the immune outcome targeting co-delivered model antigen OVA in the artificially-induced (immunocompromising) depletion of DCs.

The CD11c-DTR model allows DC depletion only during short time spans without causing mouse lethality. Assessing the humoral immune response to OVA in the

presence of PLGA would require several (up to to 12) weeks of mouse survival. As it would not be possible to measure the antibody response using the DTR mouse model, we instead decided to study the effects of DC depletion in early T-cell response such as proliferation. DC antigen presentation is known to be an early step involved in the adaptive immune response that would initiate a T-cell response and later an antibody response against associated antigen. Therefore, we used the OVA-OT-II/I model to investigate if the conditionally-ablated depletion of DCs *in vivo* would influence the proliferative response of adoptively transferred OVA-reactive T-cells in mice that were pre-implanted with an OVA-loaded PLGA scaffold. As a readout of the adaptive response to OVA, fluorescently-labeled OVA-specific CD8+ or CD4+ T-cells (isolated from commercially available genetically-modified mice, OT-I or OT-II, respectively) were adoptively transferred into DC-depleted mice cotemporaneous with subcutaneous surgical implantation of OVA-laden PLGA scaffold and their extent of proliferation (clonal expansion) *in vivo* was assessed. Using a quicker readout of the OVA-specific response than before allowed us to use the CD11c-DTR model. Expected outcome was a mitigated clonal expansion of OVA-specific T-cells in CD11c+ cell-depleted mice.

4.2 Materials and Methods

4.2.1 Animals:

Animal care and treatment were in compliance with the Institution Animal Care and Use Committee at Georgia Institute of Technology. Male C57BL/6 mice, CD11c-DTR [B6.FVB-Tg(Itgax-DTR/EGFP)57Lan/J], OT-I^{127} [C57BL/6-

Tg(TcraTcrb)1100Mjb/J] and OT-II[128] [B6.Cg-Tg(TcraTcrb)425Cbn/J] of 8-12 weeks old were purchased from Jackson Labs, Bar Harbor, ME. Mice were housed at 6 or less per cage and allowed to acclimate for 1 week prior to receiving experimental treatments.

4.2.2 Characterization of CD11c+ Cells Depletion in CD11c-DTR Model on Multiple Diphtheria Toxin (DT) Doses:

To determine the effect of repeated DT injections on CD11c-DTR model, the time-points for injections and analysis were setup according to Figure 4.1. On day 0, mice either received adoptive transfer of carboxyfluorescein diacetate succinimidyl ester (CFSE)-labeled OT-II T-cells ($2x10^7$ cells/ 300µl of sterile phosphate buffered saline(PBS)) via I.V. tail vein or penile injection or not. Group 1 mice received 1 DT injection on day 1; group 2 mice received 2 DT injections on days 1 and 3, whereas Group 3 mice received 3 DT injections on days 1, 3 and 5.

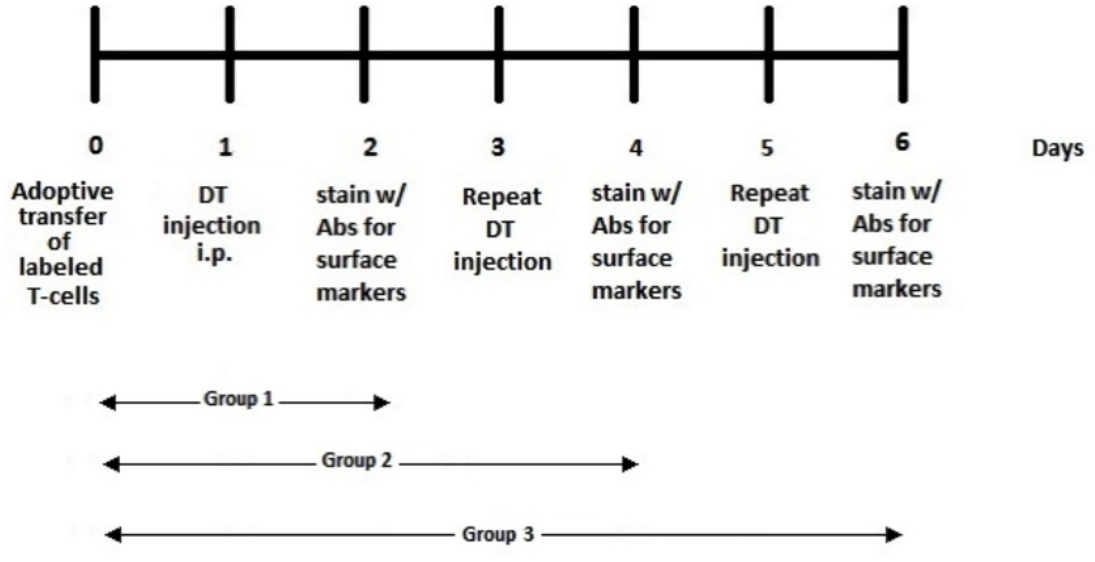

Figure 4.1 Timeline of repeated Diphtheria Toxin injections

Each DT injection was at 4ng/g body weight diluted in sterile PBS at a volume of 100µl. Mice in Groups 1, 2 and 3 were sacrificed on day 2, 4 and 6 respectively. Their spleens were harvested and splenocytes were washed and suspended in a single-cell suspension of 2-5x10^6 cells/ml in FACS buffer (100ml D-PBS(Invitrogen), 1% Bovine Serum Albumin (BSA) (Sigma-Aldrich), 0.1% Sodium Azide (Sigma-Aldrich), pH 7.4). Subsequently cells were stained with fluorescently labeled antibodies against CD11c (Clone HL3, BD Pharmingen), CD3 (Clone 1452CII, BioLegend), CD8α (Clone 53-6.7, BioLegend), CD4 (RM4-4, BioLegend), F4/80 (Clone BM8, BioLegend), 33D1 or DC marker (Clone 33D1, BioLegend) for 40 minutes at 4°C and analyzed by flow cytometry (BD LSR II). Percentage stained above respective isotype was gated and the gMFIs of each marker were calculated body weight of each mouse was measured just before each DT injection and 24 hours after. Each group consisted of 3 or 4 of the following subgroups of mice – (i) C57BL/6 treated with DT (wild-type negative control), (ii) CD11c-DTR mice untreated by DT (transgenic negative control), (iii) CD11c-DTR mice treated with DT along with adoptively transferred T-cells and (iv) CD11c-DTR mice treated with DT without adoptively transferred T-cells. Each subgroup consisted of 4-6 mice.

4.2.3 Preparation PLGA/OVA Scaffold:

All biomaterial scaffolds were freshly prepared for each experimental procedure. The PLGA SCs were prepared using the solvent casting, particulate leaching method with minor modifications[12]. Briefly, 1.25g of 75:25 poly(DL-lactide-co-glycoside) or PLGA

(intrinsic viscosity = 0.55 – 0.75 dL/g, LACTEL Corporation, Cupertino CA) was dissolved in 15ml of 20% dichloromethane (DCM; Sigma-Aldrich) at 83.3 mg/ml. For preparing PLGA SC with co-delivered OVA, OVA was added to the PLGA-DCM solution at 166 mg/ml and poured on to two, porogen (sodium chloride 90-125μm; 0.3 g NaCl/mL PLGA solution)-packed Teflon dishes; after rapid mixing, the suspension was allowed to dry overnight. While the DCM gradually evaporated, the scaffold was washed thoroughly in water until all the porogen was leached out over several days. Dried PLGA SCs (0.8 cm in diameter) were cut, stored and endotoxin content determined by Limulus Amebocyte Assay (Lonza, Walkersville, MD) according to manufacturer's instructions, with scaffolds in the presence of the reagents until the addition of the stop reagent.

4.2.4 Adoptive Transfer of CFSE-Labeled T-Cells:

T-cells were obtained from splenocytes using a negative selection magnetic bead isolation kit (CD4+ or CD8+ or Pan T-cells) (Miltenyi Biotech Inc., Auburn, CA) according to manufacturer's protocol with appropriate modifications[129]. Briefly, spleens were isolated from OT-I or OT-II mice by either antemortem or postmortem splenectomy, washed and processed through 40μm nylon cell strainers. Red blood cells were then lysed from the suspension and the remaining splenocytes were treated with a buffer containing PBS (Invitrogen), 0.5% bovine serum Albumin (BSA) (Sigma-Aldrich) and 2mM ethylenediaminetetraacetic acid (EDTA) (Sigma-Aldrich) at 40μl/10^7cells, biotin-bound antibody cocktail (Miltenyi Biotec) at 10μl/10^7cells and after a short while followed by 20μl/10^7cells of anti-biotin magnetic beads (Miltenyi Biotec). Tagged cells

are run through a magnetic LS column (Miltenyi) and the effluent contains the unlabeled fraction of the respective enriched T-cells. For fluorescent labeling, the cells were diluted to 10^6/ml, passed through a 40μm strainer to obtain a single-cell suspension and stained with CFSE; Molecular Probes, Inc.) solution (dissolved in dimethylsulfoxide) at a final working concentration of 10μM. Upon repeated washing (3x) with ice cold water, the cells were prepared at $2x10^7$/300μl for adoptive transfer into recipient mice (C57BL/6 or CD11c-DTR) via either tail or penile vein.[130] One OT-I/OT-II mouse provided T-cells sufficient for 2-3 adoptive transfers.

4.2.5 In vivo effect of PLGA on Co-Delivered Antigen-Specific Clonal Expansion Of T Cells in the Absence of Dendritic Cells in CD11c-DTR mice:

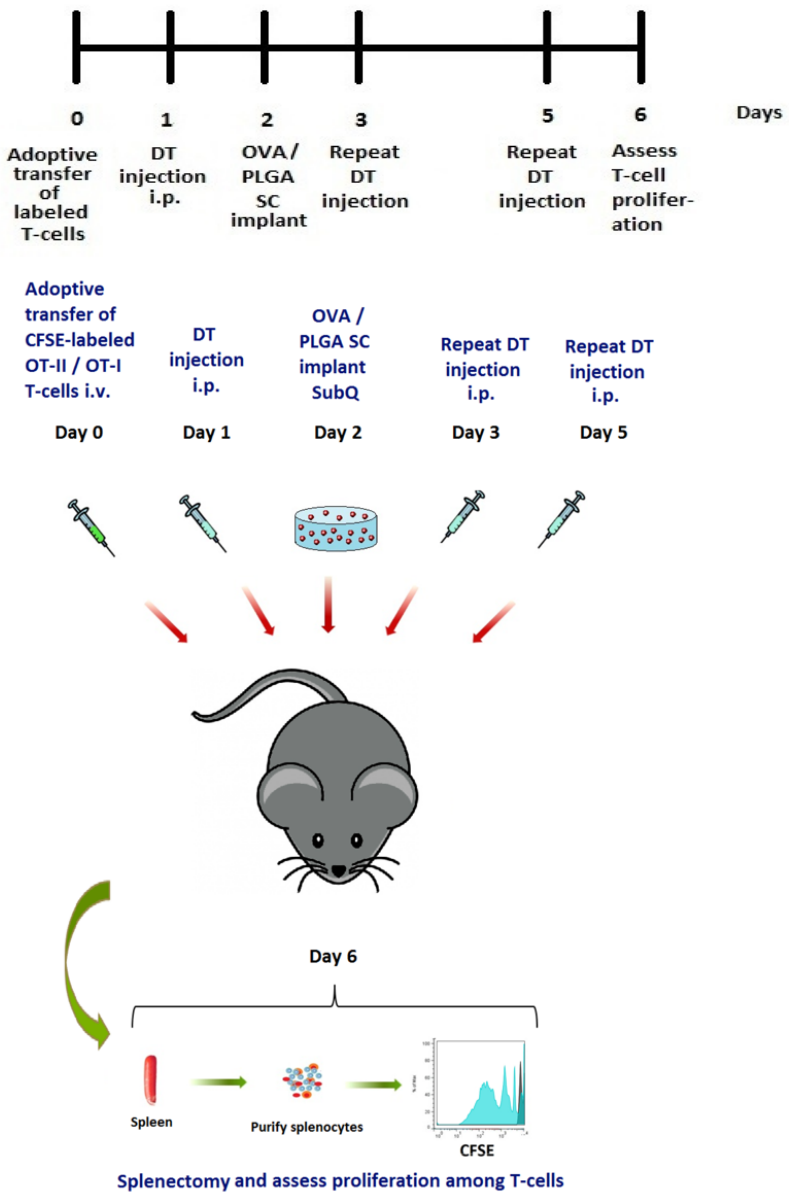

Figure 4.2 Timeline incorporating PLGA/OVA scaffold implantation

To determine the outcome of DT-mediated depletion DC cells in CD11c-DTR mice, the time-points for injections, implantation and analyses were setup according to

Figure 4.2. On day 0, mice either received adoptive transfer of CFSE-labeled OT-II or OT-I T-cells ($2x10^7$ cells/ 300µl of sterile phosphate buffered saline(PBS)) via intravenous tail or penile vein injection. On days 1, 3 and 5, a DT injection in the intraperitoneal cavity. was given at 4ng/g body weight diluted in sterile PBS at a volume of 100µl. On day 2, an 8mm diameter scaffold of 0.016g PLGA containing 0.0128g OVA was introduced into the mice as a dorsal subcutaneous implantation or a subcutaneous injection of equivalent quantity of OVA emulsified in Complete Freund's Adjuvant (positive control) as previously described[13]. On day 6, the mice were sacrificed and their spleens were harvested for T-cells that were subsequently analyzed by flow cytometry.

4.2.6 Tracking In Vivo T-cell proliferation:

The method was adapted from a previously published protocol[131]. CFSE-labeled T-cells were prepared in a single-cell suspension of $5x10^6$ cells/ml for detection by a flow cytometer (using a 488nm excitation laser) prior to the adoptive transfer. This group served as the unproliferated control. According to Figure 4.2, on day 6 T-cells were harvested from splenocytes of sacrificed mice using a magnetic sorting kit (Miltenyi Biotec). Additional antibody stains against T-cell antigen CD3, CD4 and/or CD8αβ, compatible (non-overlapping in fluorescent emission profile) with CFSE was added and the cells were screened by a flow cytometer. To assess cell death, 1µl / 200 µl of cells of propidium iodide was added prior to flow cytometer analysis. Using FlowJo software '%Divided cells' defined as the percentage of cells from the original sample that have divided (assuming no cell death) was calculated. In addition, the fluorescence intensity

(FI) histograms were gated into 6 FI-distinct populations that were compared across treatments groups by statistical analysis of n=6.

4.3 Results

4.3.1 Effect of Repeated DT Treatments on CD11c-DTR Mouse Model

It is evident from literature that the magnitude of T-cell response depends on the duration of antigen availability *in vivo*[132]. Also, a minimum 24-48h is necessary for T-cells to undergo detectable levels of proliferation[133]. To accommodate for sufficient antigen and T-cell contact we designed a timeline of 6 days for the experiment (Figure 4.2). A single DT injection was known to maintain depletion of CD11c+ cells for up to 48h after which the numbers of circulating CD11c+ cells began increasing[20]. As it was necessary to achieve DC depletion throughout the period of T-cell antigen contact, we required three consecutive injections of DT (Figure 4.1 and 4.2). To determine the effect of three DT injections spaced at two days apart each on the CD11c-DTR mouse model, we measured the body weights of mice before after each DT injection. Figure 4.3 shows that the weights of mice treated with one, two or three DT injections did not undergo significant changes in weight compared to the untreated control group. Secondly, the introduction of adoptively transferred OT-II T-cells did not influence any changes in weight either. Since body weight is a reliable indicator of immediate health status in animals[134], these results indicated that the administration of three DT injections to CD11c-DTR mice did not adversely affect their health and could be deemed safe for use in subsequent experiments.

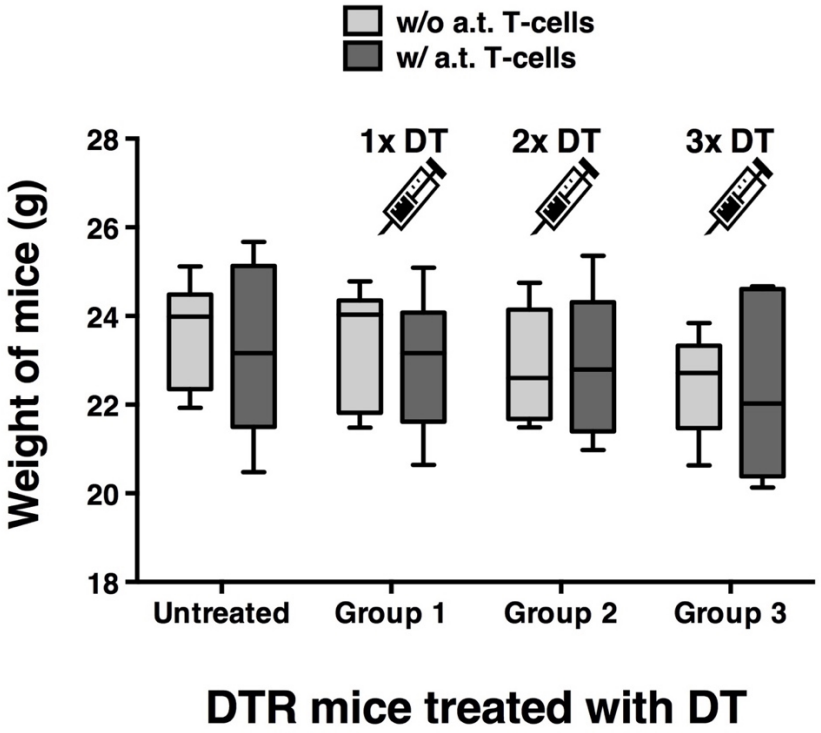

Figure 4.3 Effect of three DT injections on mouse body weight

Along with assessing body weights, we determined the effect of repeated DT injections on immune system of CD11c-DTR mice by analyzing cell surface markers of their splenocytes with or without the presence of adoptively transferred T-cells. Figure 4.4 shows that the total CD11c content was significantly lowered upon one, two or three DT doses and the magnitude of CD11c loss increased with more injections. Murine lymphoid-circulating conventional DCs are primarily composed of CD11c+ CD8α+ and CD11c+ CD8α-; the CD8α+ subset is largely associated with the expression of DEC205 (CD205) while the CD8α- subset expressed 33D1 (DCIR2)[135-137]. The decrease in CD11c was coupled with significant loss of 33D1 (a DC marker) as well as DEC205 suggesting that different DC subsets were depleted in response to DT injections.

Importantly, the magnitude of decrease in expression of these markers in group 3 indicated that the mice were, in part, losing immunocompetency with each repeated dosage of DT. Contrary to previously published work[21,138], we noticed a change in the expression profile of CD4 and F4/80 in addition to the typical set of DC-associated markers. The presence of adoptively transferred T-cells prior to DT administration showed a noticeable effect of the surface marker profile especially during the early stages of DC depletion, i.e. for groups 1 and 2. Collectively, these results indicated that CD11c+ cells, predominantly DCs, were significantly lowered in numbers in CD11c-DTR mice during the 6-day period due to the three DT injections and presence of adoptively transferred T-cells minimally aided in the general immunocompetency of the animals.

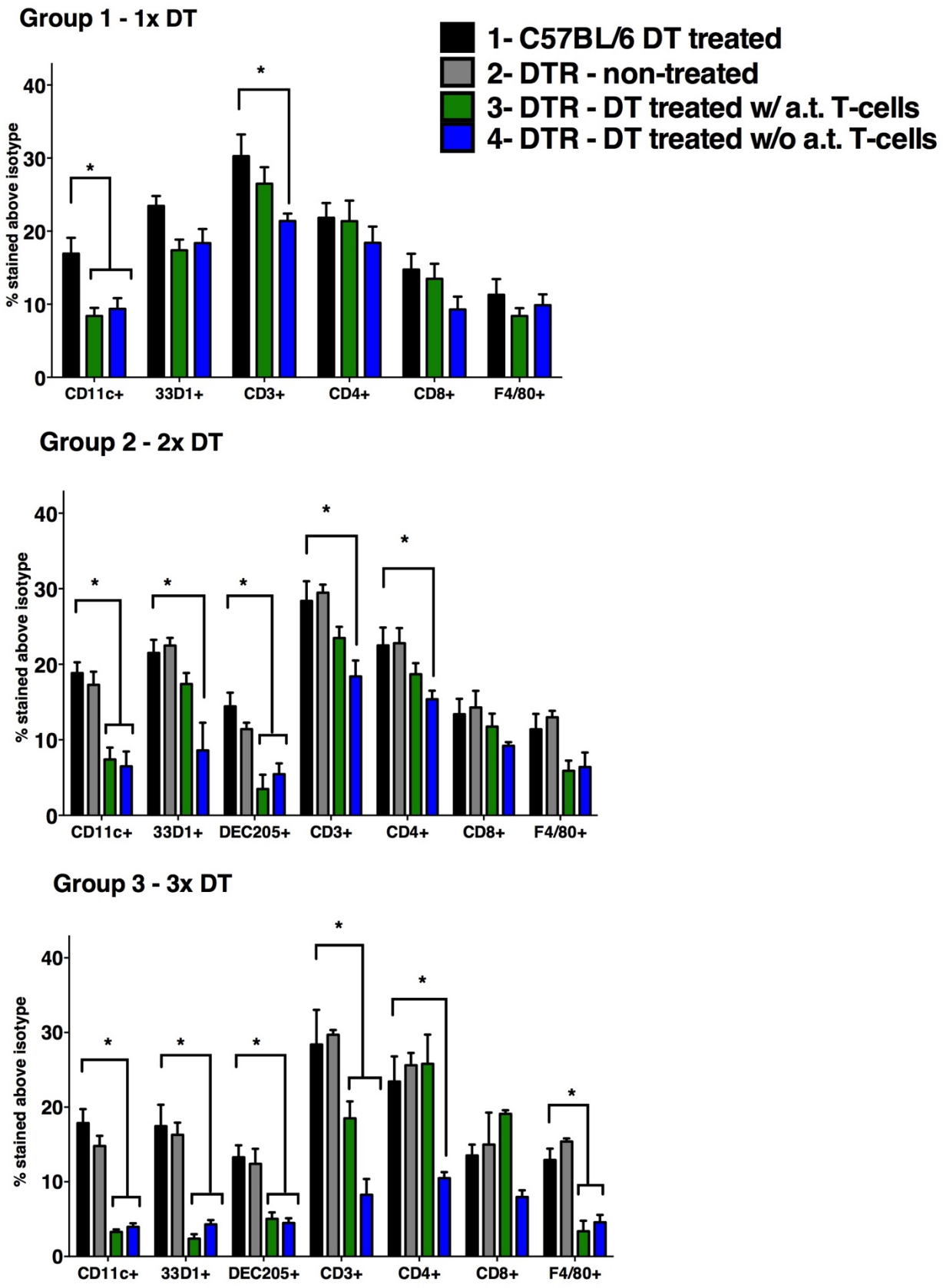
Group 1 - 1x DT
1- C57BL/6 DT treated
2- DTR - non-treated
3- DTR - DT treated w/ a.t. T-cells
4- DTR - DT treated w/o a.t. T-cells
% stained above isotype
0
10
20
30
40
CD11c+
33D1+
CD3+
CD4+
CD8+
F4/80+
Group 2 - 2x DT
% stained above isotype
0
10
20
30
40
CD11c+
33D1+
DEC205+
CD3+
CD4+
CD8+
F4/80+
Group 3 - 3x DT
% stained above isotype
0
10
20
30
40
CD11c+
33D1+
DEC205+
CD3+
CD4+
CD8+
F4/80+

Figure 4.4 Surface marker expression of CD11c-DTR murine splenocytes after repeated DT injections.

Group 1 received 1x DT injection, group 2 – 2x DT and group 3 – 3x DT. Statistical analysis was done using 2-way ANOVA followed by Sidak's post-test and differences within 95% confidence intervals were accepted as significant (* = $p < 0.05$). Error bars represent standard error of mean values of n=5 or 6 mice.

4.3.2 CD4+ T-Cell Response to Antigen-Loaded PLGA in the Absence of DCs

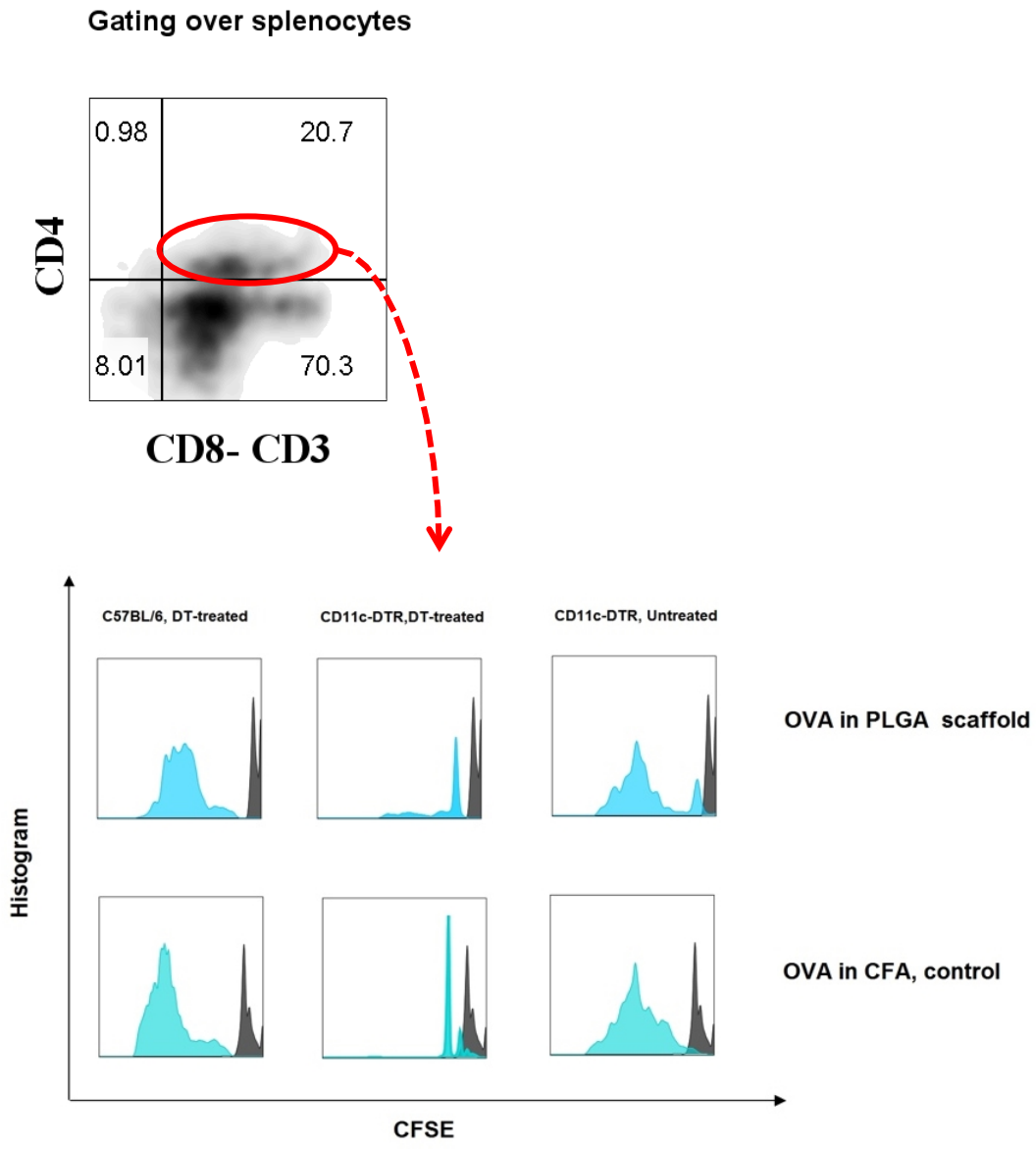

Figure 4.5 Proliferation profile of OVA-specific CD4+ T-cells in the absence of CD11c+ cells

Splenocytes obtained from mice were stained with antibodies against CD3, CD4 and CD8 and assessed by flow cytometry. Gated region (representative of all groups)

marked in red (top) was analyzed for CFSE fluorescence (bottom). Data representative of n=6 mice per group

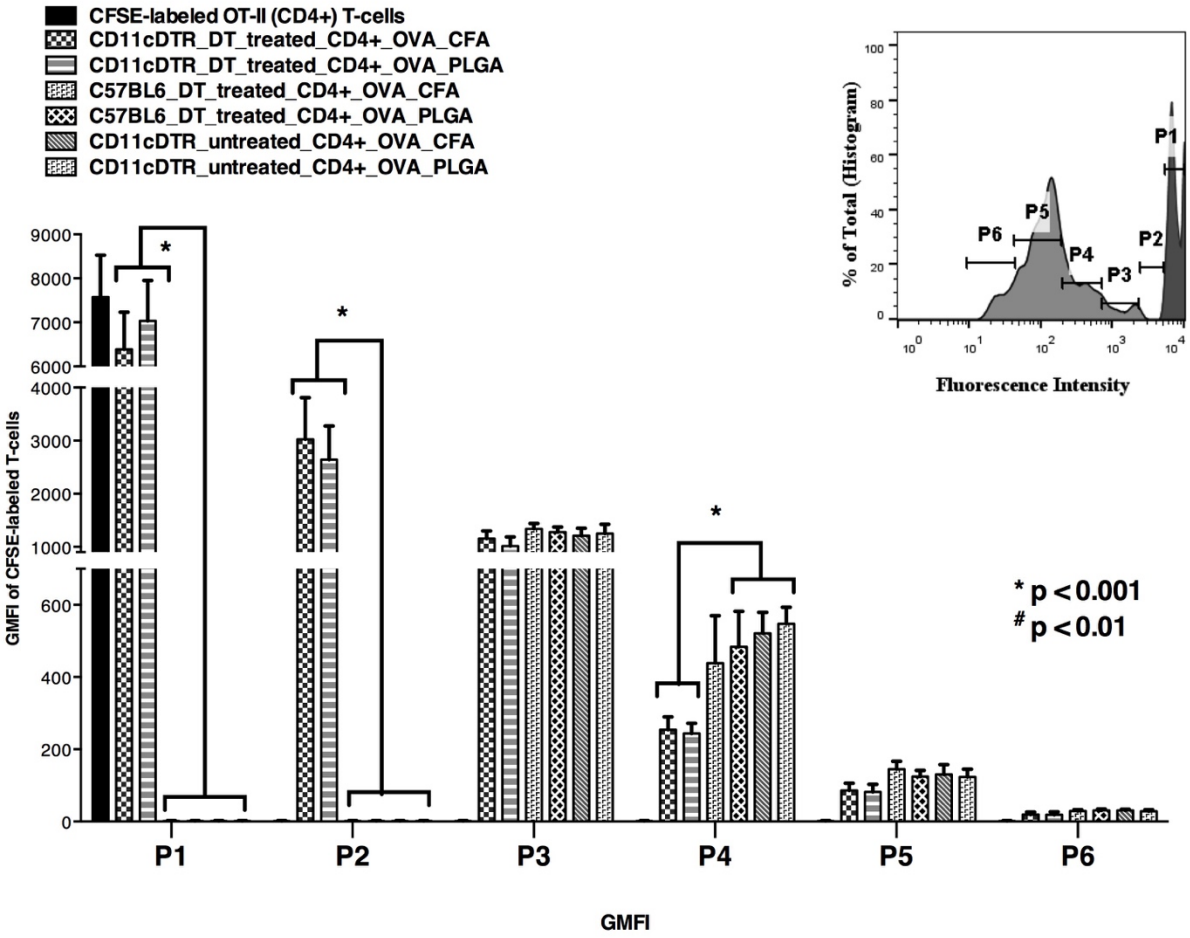

Figure 4.6 Statistical comparison of DT treatments on OVA-specific CD4+ T-cell proliferation.

Statistics were performed using 2-way ANOVA followed by Holm-Sidak's post-test. Error bars indicate standard error over mean of n=6 mice per treatment or control group

To assess the effect of the depleted DC environment on the effect of PLGA on the antigen-specific T cell proliferation outcome, we introduced a dorsal subcutaneous

implant of a PLGA scaffold co-delivering model antigen OVA and the proliferation profile of the adoptively transferred CFSE-labeled OVA-specific OT-II cells were assessed on day 6 (Figure 4.2). In a DC-unmodified environment, a dilution of CFSE fluorescence signal was to be expected with each subsequent cell division such that up to 8 consecutive FI peaks would be visible until the fluorescence of CFSE was lowered to background levels[131]. Accordingly, (Figure 4.5) we observed such a pattern for control groups where there was no DT-mediated depletion on DCs. On the other hand, in DT-treated CD11c-DTR mice, the CFSE fluorescence intensity of CD3+ CD4+ CD8- splenocytes, on the end of day 6, was nearly as high as the originally injected CFSE-labeled T-cells for both OVA/PLGA and OVA/CFA administered mice. Only 1 or 2 visible peaks of FI from these mice indicated that despite allowing 4 days (from day 2 – day 6) of antigen contact, the adoptively transferred T-cells likely underwent 1-2 rounds of cell division, indicating that the T-cell response was greatly diminished in the absence of sufficient numbers of DCs.

In order to better understand the distribution of divided cells in fluorescence intensities, we allotted the CFSE fluorescence profile to 6 consecutive gates of decreasing intensities and compared the same across all treatment and control groups. Figure 4.6 shows that cells gated in P1 and P2 (early division) of CD11c-DTR mice exposed to OVA either in the presence of PLGA or CFA as adjuvant, exhibited high FI and were significantly different from the other groups that showed negligible FI. While cells in P4 (mid-stage) from DC-unmodified mice showed higher FI than DC-depleted mice, suggesting that DC-depleted mice underwent minimal or no mid-stage cell division or

rather their cell division was still in the early phases. Collectively these results indicate that administration of DT to CD11c-DTR receiving OVA with PLGA or CFA led to an altered proliferation profile of OVA-specific OT-II T-cells. Since OT-II T-cells are primarily CD4+, the significant loss of DCs *in vivo* likely diminished the otherwise strong MHC-II – CD4+ T-cell antigen recognition involved in such models of antigen-specific responses.

4.3.3 CD8+ T-Cell Response to Antigen-Loaded PLGA in the Absence of DCs

To assess the effect of PLGA in a DC-depleted environment on the cross-presentation of antigen to CD8+ T-cells, we used a similar setup as before and replaced OT-II T-cells with OT-I T-cells. CD3+ CD8+ CD4- splenocytes from DT-treated CD11c-DTR mice, analyzed for their CFSE fluorescence on day 6, showed an altered T-cell proliferation profile compared to control groups. Multiple, albeit, short peaks shown for these mice in Figure 4.7 suggest that minimal amount of OT-I T-cell division occurred that was visibly higher that of their OT-II counterparts from the above section. The histograms were gated as before from P1 to P6 in decreasing order of fluorescence intensity. Comparison of P1 and P2 (early division) across groups showed that minimal dilution of CFSE signal had occurred in the DC-depleted environments than the respective controls. Interestingly in P3 (mid stage), the CFSE intensity from DC-depleted mice was higher than controls likely due to associated early stage cell divisions. Conversely in P5 (late stage), the CFSE signal for DT-treated CD11c-DTR mouse with OVA/CFA was significantly lower than DC-unmodified controls. Together, these results indicate that the mechanism of cross presentation of OVA to OT-I CD8+ T-cells in the

presence of co-delivered PLGA was affected when the DC numbers *in vivo* were greatly diminished.

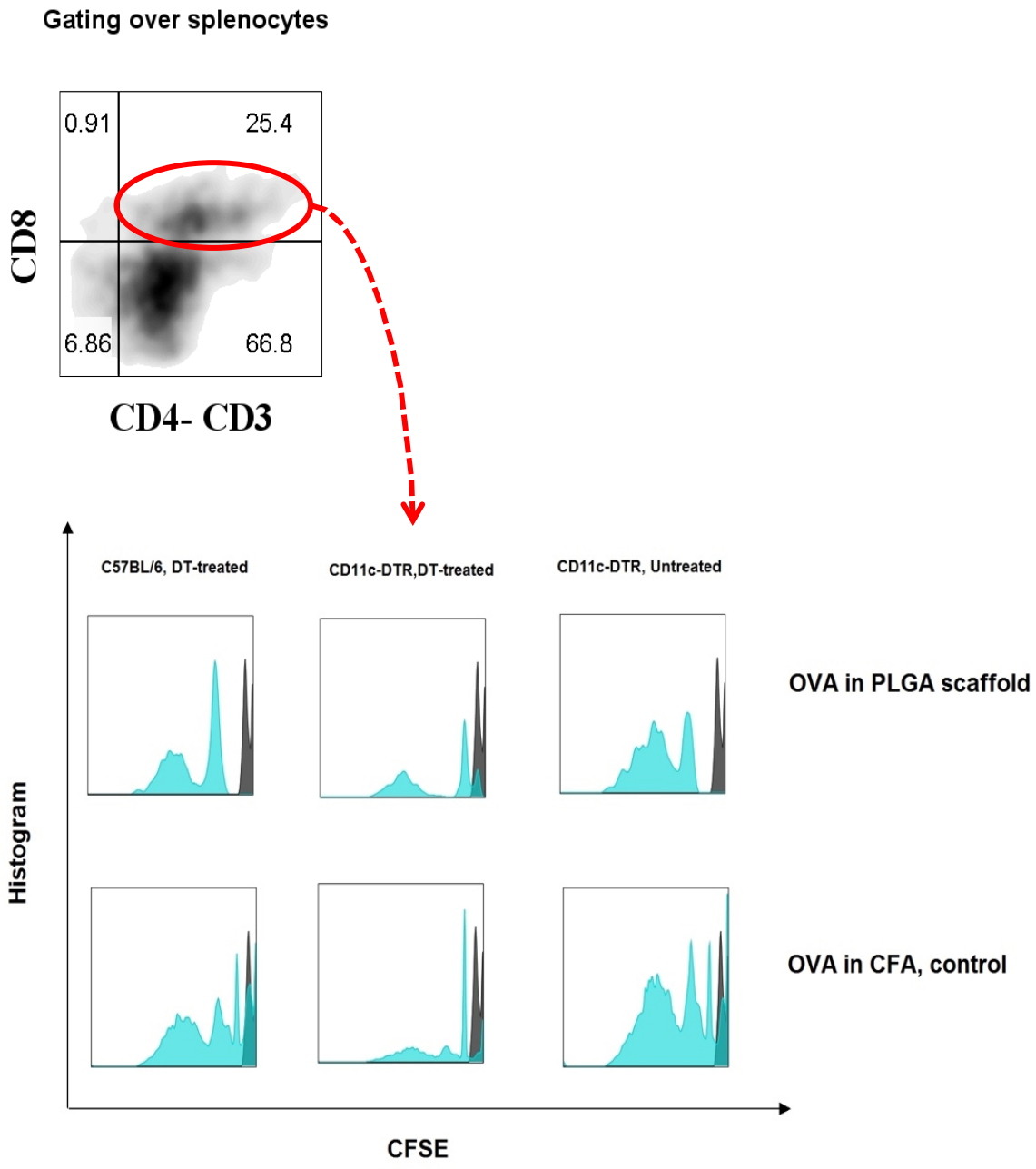

Figure 4.7 Proliferation profile of OVA-specific CD8+ T-cells in the absence of CD11c+ cells.

Splenocytes obtained from mice were stained with antibodies against CD3, CD4 and CD8 and assessed by flow cytometry. Gated region (representative of all groups) marked in red (top) was analyzed for CFSE fluorescence (bottom). Data representative of n=6 mice per group

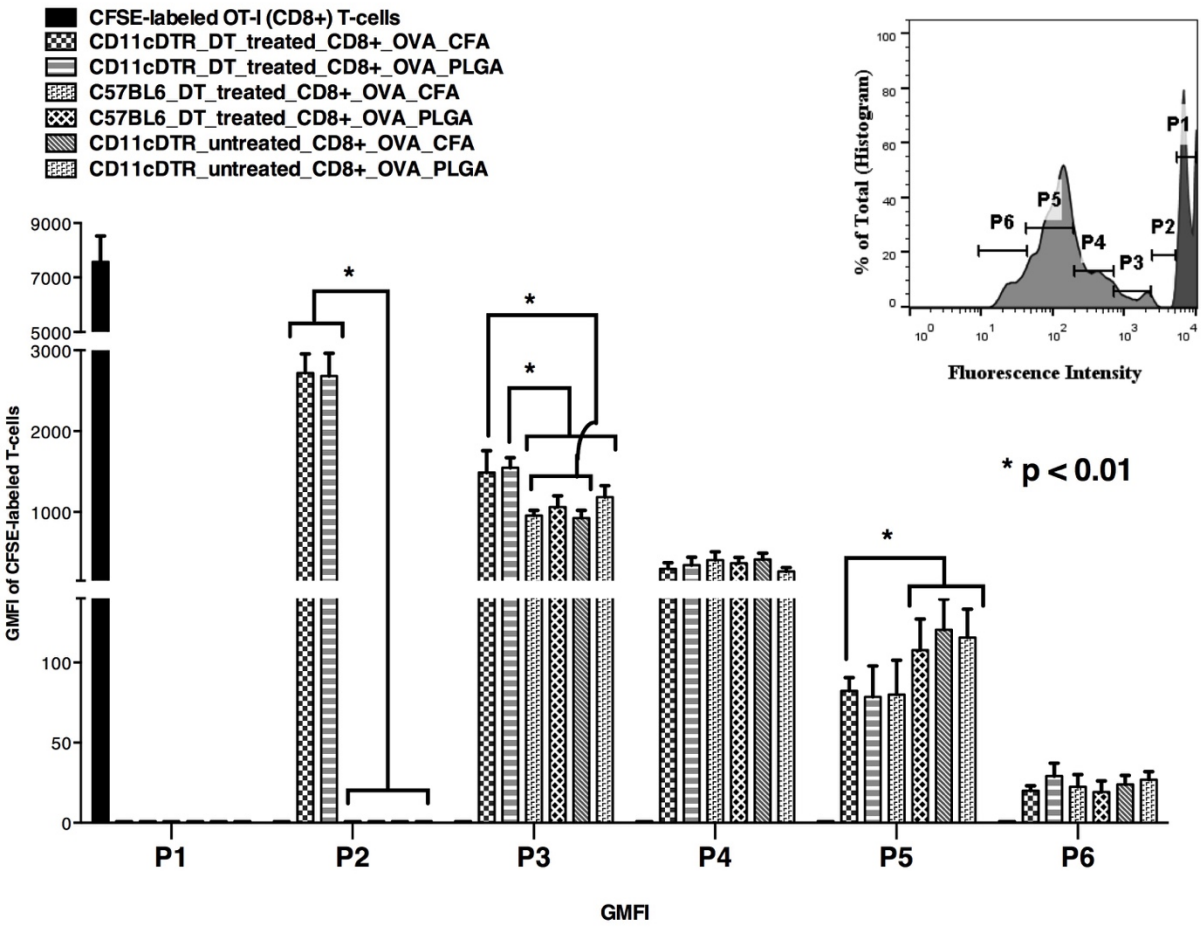

Figure 4.8 Statistical comparison of DT treatments on OVA-specific CD8+ T-cell proliferation.

Statistics were performed using 2-way ANOVA followed by Holm-Sidak's post-test. Error bars indicate standard error over mean of n=6 mice per treatment or control group.

4.4 Discussion

The PLGA adjuvant effect was previously identified in mice in the context of co-delivered model antigen OVA, in which the humoral OVA-specific immune response was enhanced in the presence of the biomaterial, PLGA, compared to adjuvant-free controls[13]. *In vitro*, treatment of human or murine primary culture DCs with PLGA films induced maturation of DCs, such that they demonstrated enhanced ability to stimulate antigen-specific T cell responses[7]. However, to connect the significance of these two studies, we needed to observe the resultant biomaterial effect on co-delivered antigen-specific T cell proliferation, in a mouse model where DCs were reliably depleted. Through this study, we were able to demonstrate that in support of the PLGA adjuvant effect to co-delivered antigen, antigen-specific T cell proliferation, an early event for the generation of a humoral immune response to delivered antigen, depended on the presence of $CD11c^+$ DCs.

In this study, we investigated the intensity of the ability of PLGA in enhancing antigen-specific T-cell proliferation — a cellular immune response rather than a humoral immune response studied previously — to co-delivered model antigen OVA concomitant with DC depletion. Herein, we use the OVA-specific T-cell proliferation model as an

early read-out known to be consistent with and necessary for subsequent humoral immune responses.

Antigen presentation by DCs is a crucial first step in bringing about an OVA-reactive immune response, and is dependent on the state of DC phenotype[37]. Antigen (OVA) processed and presented by DCs stimulate naïve or OVA-specific T-cells to clonally expand. Clonal expansion is another important step required to initiate strong T-cell responses. In the presence of DC along with OVA-laden PLGA scaffold acting as a maturation stimulus, we expected OVA-T-cells to proliferate excessively. On the contrary, during an absence of DCs, we expected that the antigen presentation to T-cells *in vivo* would be considerably diminished and thereby hinder T-cell proliferation. We use the extent of proliferation of OVA-reactive T-cells in the context of PLGA as a measure consistent with its adjuvant effect.

In order to deplete DCs *in vivo* for the period of the study we used the CD11c-DTR model, in which, a single DT-administered at 4ng (per g of mouse body weight) is known to deplete CD11c+ cells for up to 48h[20]. Since a DC-depleted environment was required for 5-6 days, we employed the use of three DT of 4 ng (per g body weight) each. By pre-delivering CFSE-labeled OVA-specific T-cells to these mice, we were able to circumvent any severe immunodeficiencies caused by repetitive DT doses. A OVA-loaded PLGA scaffold was implanted 24h after the administration of the 1st DT dose since CD11c+ cell depletion is known to be maximal around this time-point[21]. Upon analysis of surface markers and CFSE fluorescence of the resultant splenocytes of DT-

treated DTR mice at the end of the experimental duration of 6 days, we determined that in a CD11c, DC-depleted environment led to a significantly delayed/lowered antigen-specific CD4+ T-cell proliferative response and a slightly less affected CD8+ T-cell proliferative response. Classic presentation of exogenous antigen through MHC-II molecules as well as cross-presentation of antigen through MHC-I mechanisms were likely diminished due to a DC-deficient environment. Collectively these results indicate that the *in vivo* effect of PLGA in enhancing an antigen-specific proliferative T-cell response — a cellular adaptive immune response — to co-delivered model antigen OVA is mediated largely via DCs.

Although the scheme of T-cell response was affected in this study, we did see some proliferation of OVA-specific T-cells indicating that we were not able to completely eliminate *in vivo* antigen presentation with CD11c depletion. In the CD11c-DTR model, numbers of CD11c+ cells are lowered but they are not fully eradicated – as shown in Figure 4.4 small percentages of CD11c+ cells remained even after three consecutive injections – meaning some conventional DCs were still in circulation. In addition, CD11c- DCs, albeit a minority, were likely unaffected by DT treatments. There are documented inherent limitations of this CD11c-DTR mouse model that restrict its use beyond a short testing period (<1 week[20]). Repeated injections of DT over several weeks are known to cause lethality of the CD11c-DTR mice and require the use bone marrow chimeras to reverse DT-induced immunodeficiency. An alternative model known as CD11c-DOG could be used, in which the simian DTR of CD11c-DTR model was replaced by a human DTR. This change eliminates lethality of the repeated DT delivery

in study mice even when administered repeatedly for over two weeks. However, both models are capable of achieving only incomplete DC depletion and improved models of DC depletion are yet to be developed. A potential need for using a model that allows for prolonged DC depletion would be for the assessment of the humoral response to OVA-loaded PLGA; the endpoint that was used in the original study to document the humoral immune response to OVA as previously studied[13]. Herein, since we required DC depletion for only 5-6 days, we used the commercially available CD11c-DTR mouse model which was known to be safe (non-lethal) to repeated DT treatments within this study duration.

Another reason for the incomplete elimination of antigen presentation (i.e. low levels of proliferation of T-cells in DT-treated DTR mice) may have been due to the presence of macrophages and B-cells that are capable of antigen presentation although not to the same extent as DCs. Although previously unreported in literature[20,21,138], our results showed an overall decrease in the expression of surface CD4+ and F4/80 cells. F4/80 loss in cell surface markers is associated with the loss of red pulp splenic MΦs[139]. Relatedly, histological analysis on the spleens of DT-treated DTR mice indicated a loss of marginal zone MΦs (MZM) and metallophillic MΦs (MM)[138]. Although MZMs and MMs are predominantly F4/80–, the loss of F4/80 in our results is, in part, associated with an overall loss of specific MΦs. DT treatments, therefore resulted in depleting cells other than simply CD11c+ cells. However, for our specific goal of understanding the effect of PLGA on the adaptive immune response in the absence of antigen presentation, such a system was still relative suitable for use..

To further abate the antigen presentation system, we could potentially combine CD11c-DTR-based DC depletion with *in vivo* ablation of MΦs using clodronate liposome microspheres[140]. It may valuable to understand the effect of PLGA on the host immune response in the absence of antigen presentation due to DCs and macrophages (or macrophages alone for comparison).

Using an adoptive transfer of CFSE-labeled OT-II or OT-I T-cells allowed us to determine the antigen-specific immune response within a shorter time frame (1 week). Although several published works have shown distinct consecutive peaks on FI plots, corresponding to successive T-cell divisions, for our control groups with DC-depletion we only observed a collected pooling of FIs (shown in Figures 4.5 and 4.7). The lack of distinct peaks may have been due to excessive T-cell division in response to OVA, i.e. the OVA delivering medium CFA or PLGA acted as an extremely potent adjuvant *in vivo*. Further, CFSE and CFDA-SE dyes are known to be vulnerable to photocobleaching[141] (occurred during adoptive transfer) also resulting in lowered fluorescence and lack of distinct peaks in *in vivo* proliferated T-cells.

Adjuvant effect of PLGA in the context of tissue engineering has been previously assessed[13,19,106]; delivery of PLGA microparticles (MPs) or scaffolds by injection or implantation, respectively, with a model shed antigen has resulted in increased production of antigen-specific antibody[18] and this increased humoral response was dependent on the form of PLGA[12]. Furthermore, this humoral response was distinct for

the material in use; PLGA and not agarose induced an increased response to the model shed antigen[13], as predicted based on their *in vitro* effects on DC maturation[7].

In exploring the interactions of PLGA with the immune system, its effect on crucial immune cells such as DCs has also been characterized along with other materials such as agarose, alginate, chitosan etc. PLGA induced DC maturation similar to that of standard TLR agonist (like LPS) resulting in a phenotype associated with promoting antigen-specific adaptive immune response; whereas agarose maintained DCs in a rather immature phenotype[7,25], that were capable of priming co-cultured autologous T-cells into Tregs[107].

As such, biodegradable materials such as PLGA are being studied for both vaccine delivery and tissue engineering applications in preclinical and clinical studies where adjuvant effect and associated increase in immunity may or may not be desirable, respectively. To more closely mimic a clinically relevant autoimmune disease situation, the model antigen, could be replaced with a Multiple Sclerosis-relevant antigen, myelin MOG peptide and cognate 2D2 T-cells for tracking induced extent of proliferation. It would also be of interest to confirm the observed differential adjuvant effect (mirroring their *in vitro* effects on DC maturation) for antigen delivered with agarose scaffolds. Taken together, these suggest a complex interaction of biomaterials with immune cells for which a deeper understanding of the immunomodulatory ability of biomaterials through effects on DCs is important to the development of materials for use in combination products.

CHAPTER 5 DESIGN AND DEVELOPMENT OF A SCAFFOLD WITH THE ABILITY OF TEMPORAL DELIVERY OF MULTIPLE IMMUNOMODULATORS

5.1 Overview

The mammalian immune system unlike other organ systems is diversely distributed across the body and is composed of a multitude of organ types such as the thymus, bone marrow, spleen, peripheral draining LNs and various cell types of the innate and adaptive subsets that collectively orchestrate the immune response against a variety of invaders. Dendritic cells are professional antigen presentation cells that serve as a link between innate and adaptive immune systems to direct T and B-cell responses.

The application of biomaterial technology offers distinct advantages over traditional routes of drug delivery; it enables access to specific compartments of the immune system, either to locally delivery small-molecule or protein-based drugs. Biomaterials can also serve as excellent scaffolds for cell and tissue regeneration due to their highly tunable physical properties such as surface modality, porosity, surface and bulk charge and many others. Not only in *in vivo* therapies, biomaterials have also been used in transdermal drug delivery, wound healing and *ex vivo* cellular therapies.

The function of DCs is complex: they not only trigger classical immune responses, they are also responsible for maintaining immune homeostasis and hence form a crucial part of the establishing peripheral tolerance to harmless or self-antigen. The

absence of DCs' regulatory function is associated with aberrant responses as in the case of autoimmune diseases, allergies and transplant rejection. By constantly sampling and processing components from their environment, DCs restructure their surface and cytokine profiles to respond appropriately to pathogens or auto-reactive T-cells. Altering the characteristics of their microenvironment can induce a change in the characteristic of the downstream response of DCs. In this context, here we discuss the design and characterization of a biomaterial-based system that can deliver up to three immunomodulators in a temporally differential manner to DCs to render them tolerogenic in phenotype and function.

Tolerogenic DCs have been generated *in vitro* using a variety of immunomodulators, the prominent ones being IL-10[78-82], DEX[17,69-73], vitamin D3[74-77] and rapamycin[83-85]. Additionally, alternative activation with a TLR ligand after immunosuppressant treatment is correlated with improved *in vivo* performance due to the likely enhancement of LN homing in capabilities[60]. Here, we suggest a biomaterial design to generate aaDCs *in vitro* from human peripheral blood mononuclear cells using GM-CSF, DEX[17] and PGN [17,24], each given at different time points within a seven-day period (Figure 5.1). GM-CSF is an essential growth factor for the development of cells of the monocyte lineage primarily conventional DCs[22]; DEX on the other hand is a molecule of the corticosteroid family, known to have anti-inflammatory effects[17] whereas, PGN is a PRR agonist that has been shown to enhance LN migration[17] of tolerogenic DCs. We *hypothesize* that we would be able to reproduce the culture

conditions (doses and timing) for generation of aaDCs using a biomaterial-based controlled release strategy.

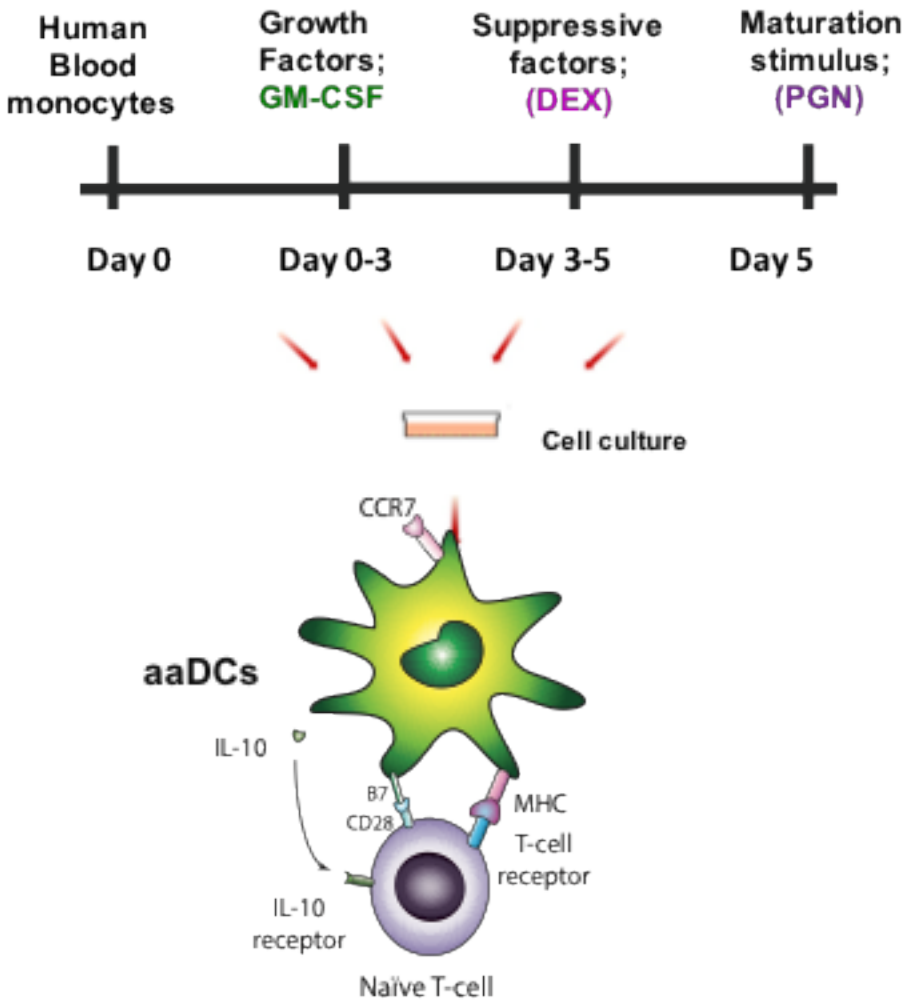

Figure 5.1 *In vitro* culture to alternatively activated DC (aaDC) phenotype from human DCs

The design for such a biomaterial system uses differentially crosslinked gelatin microparticles (MP) that can be incorporated with GM-CSF, DEX or PGN. The crosslinking of the MPs would be used as a primary factor in regulating the release of the immunomodulators. In order to ensure that the released biomolecules do not have off-target effects, the MPs will be localized and deliver them from a single biomaterial

scaffold. The number of MPs (N_{MP}) embedded in each scaffold may serve as an additional layer of control for the differential release. Traditionally, gelatin MPs have been used to deliver charged biomolecules such as bone morphogenetic protein 2 (BMP-2)[142], vascular endothelial growth factor (VEGF)[143] and many others, and as such have been well characterized for their size, morphology and synthesis. In this study, gelatin was selected due to its safety of use, being recognized by the FDA as Generally Recognized As Safe (GRAS) as well as its known physical properties and crosslinking customizability. These MPs are to be embedded in a scaffold of macroporous agarose cryogel specifically chosen because agarose is known to maintain DCs in a relatively immature environment[7,25] and is capable of inducing autologous regulatory T-cell recruitment in a mixed lymphocyte reaction with DCs[107].

Since the exploratory development of such a scaffold would require the use of expensive cytokines, we propose an alternative method of release characterization using 'model' molecules similar in size to the required immunomodulators. Fluorescently tagged Ovalbumin or Biotin were used to investigate the changes in release profiles while varying either the crosslinking density of the MPs or the number of MPs in the scaffolds. Modeling of release profiles from biomaterial carriers is a method commonly used for controlled drug delivery studies allowing the researcher to appropriately design tailored biomaterials for the respective drug while providing insight about the dominant mechanism controlling delivery. Several mathematical models have been used by researchers over the last few decades that sufficiently model release profiles within a fixed set of constraints, such as the Higuchi equation[144], Peppas[145] equation. A more

recent model used for such delivery analyses is the Weibull function[146,147] that incorporates the stretched exponential function of the Peppas equation. Weibull function is a more robust equation that can account for Fickian, non-Fickian and intermediate diffusion profiles[147] and we hence used the 3-paramter Weibull function[148,149] to depict fractional drug release from our standalone gelatin MPs as well from scaffold-embedded gelatin MPs. In this manner, it formed the basis for predicting scaffold configurations for required differential delivery of immunomodulators.

In this chapter, we describe the development and characterization of a multi-component time-differential release system using crosslinked gelatin MPs embedded in a macroporous agarose scaffold. Using 'model' biomolecules, an empirical model was defined to obtain correlations between model-associated parameters and experimentally variable conditions such as crosslinking density and number of MPs per scaffold. From known conditions such as required time of delivery of immunomodulators, the necessary values for experimentally variable parameters were interpolated and a scaffold design for delivering three immunomodulators namely GM-CSF (0-3 days), DEX (3-5 days) and PGN (5-6 days) was determined. The predicted release profiles of these immunomodulators were compared with experimentally measured values and differences between measured and predicted values was used to optimize the model for future predictions. Since the MP-laden scaffold system could potentially be applied in *in vitro* and *in vivo* immunotherapeutic applications, it was named multifunctional immunomodulatory (MI) scaffold. The ability of the MI scaffold to generate aaDCs with tolerogenic properties will be discussed in the following chapter.

5.2 Methods

5.2.1 Gelatin Microparticle (MP) Formulation:

Gelatin MPs were synthesized according to a previously published study with minor modifications[150]. Briefly, a 10% w/w solution of gelatin type B (Sigma-Aldrich) in distilled deionized (dd) H2O was heated to 60°C, of which 5ml was added drop-wise to 150 mL of corn oil. Upon homogenizing at 7000 RPM for 5 min this water-in-oil emulsion was chilled for 10min at 4°C without mixing. After sonicating the emulsion to reduce particle size, 35 mL of cold (4-8°C) acetone was added to it. The solution was cooled at 4°C for 10 min and the MPs were retrieved through centrifugation at 200 X g followed by 3 washes in 25 mL of acetone. The MPs were then crosslinked at room temperature with 1.25 – 25 mM glutaraldehyde, 0.1% w/w Tween 20 (Sigma-Aldrich) solution in dd H2O at 4°C under stirred conditions. After 15 h of crosslinking, the MPs were retrieved by centrifugation and treated with 25 mL of 25 mM glycine in dd H2O to block residual aldehyde groups from reacting. MPs were washed 3 times in 25 mL dd H2O, counted, aliquoted, lyophilized and stored at -80°C until further use.

Some MPs were prepared for confocal imaging by labeling with fluorescein isothiocyanate (FITC) in a 0.1 M sodium bicarbonate solution at a pH of 8.3 for 1 h at room temperature. Fluorescently-labeled MPs were washed three times in 25 mL of di H2O to remove un-conjugated dye.

5.2.2 Microparticle Size and Zeta Potential Measurements:

The average size of the MP populations was assayed using a Multisizer III (Beckman Coulter, Fullerton, CA) equipped with a 100 mm aperture with a lower detection limit of 2 mm. MPs were suspended in Isoton II diluent (Beckman Coulter) at a dilution which resulted in the counting of at least 2000 events in a sample size of 0.5 mL. Alternative size measurements and zeta potential measurements were performed using tunable resistive pulse sensing with qNano Gold (iZON Science, Christchurch, New Zealand) with 'nanopore' of size 1.6-16μm (NP4000, iZON) after calibrating with standard polystyrene beads (CPC4000, iZON) according to a previously published protocol[151] and manufacturer's instructions, and data was analyzed using the accompanying data acquisition software (iZON). Briefly, lower and upper fluid cells were the set into place, and 50μL of standard buffer (consisting of 0.1 M aqueous KCl, 0.01 M tris(hydroxymethyl)aminomethane (Tris, pH 8, 0.01% of Triton X-100 and 3 mM EDTA) were added to each without air bubbles. 3. The nanopore was primed with a drop of buffer on both the cis and the trans side, then set onto the mechanical stretching jaws to remain in place, prior to setting the upper cell. Pore width was controlled by adjusting the jaw width, pressure was controlled with an external pump connected to the upper fluid cell), and voltage was maintained at 0.3V for all experiments using the connected computer. Bead suspensions were made by diluting a stock solution of particles in standard buffer and were sonicated for at least 5 minutes. The beads were run through the equipment first. After washing with buffer, un-crosslinked or crosslinked MPs, previously swollen in PBS (pH 7.2), were re-suspended at roughly 10^5/ml concentration in the standard buffer and run through.

5.2.3 Microparticle Loading, Incorporation Analysis and Release Profile Characterization:

Freeze-dried gelatin MPs were diffusionally loaded by swelling in solutions of Alexa Fluor (AF) 647-biotin 5mg (Invitrogen), AF 647 -ovalbumin OVA) 200µg (Invitrogen), recombinant human GM-CSF 200µg (PeproTech, 14.6 kDa), Dexamethasone (DEX) 4mg (Sigma-Aldrich) or peptidoglycan (PGN) 50µg (Sigma-Aldrich). Briefly, 20µl of loading solution was added drop-wise onto aliquoted MPs of 20mg and agitated continuously for 16h at 4°C. For MPs that were to be incorporated into scaffolds, the MPs were aliquoted and freeze-dried by number (10^8, 10^9 or 10^{10}) rather than by weight, before loading, and the loading solution volumes were adjusted accordingly such that they were less than that theoretically impregnated into the each MP[152].

After 12h of loading, the MPs were washed in 500µl of dd H2O three times for 5 min and total liquid from the washes was collected and analyzed for the respectively loaded molecules (methods described below). Some loaded MPs were frozen at -80°C for 24h prior to addition in scaffolds with or without freeze-drying.

Loaded MPs were placed in 1ml sterile PBS in 12 well-plates (Corning) and incubated at 37°C for up to 14 days. At every time point 0.3 ml of supernatant was withdrawn for sampling and replaced with fresh buffer. The amount of AF-biotin or OVA

in each withdrawn sample was determined by measuring the fluorescent intensity at wavelengths 650nm (Tecan Infinite F500) and comparing them to a standard dilution curve derived from AF-biotin or AF-OVA, respectively.

GM-CSF and PGN release were assessed using an enzyme-linked immunosorbent assay (ELISA) kit (Beckton Dickinson) and a silk-larvae protein (SLP) reagent assay (Wako Chemicals Inc.) respectively, according to manufacturers' instructions. DEX was measured with high performance liquid chromatography (HPLC) system (VP series, Shimazdu) using a previously published protocol[13]. Briefly, samples were filtered with a 0.45 μm nylon filter prior to injection. The isocratic mobile phase consisted of acetonitrile and water (42:58). The samples were injected onto an OmniSpher C18 column (150×4.6 mm) with 5 μm particle packing (Agilent Inc.) and detected at 246 nm with the UV detector. Retention time of DEX was 4.1 min. DEX concentration was determined by constructing a standard curve, ranging from 1ng/ml to 100 μg/ml, relating concentration to peak height.

5.2.4 Fourier Transform Infrared (FTIR) Spectroscopy:

All spectra were collected with a Nicolet 8700 FT-IR spectrometer with an MCT/A detector and a single bounce ATR attachment. For each spectrum, 64 scans were recorded from 4000 to 400 cm^{-1} with a resolution of 4 cm^{-1} [153]. Each sample of lyophilized and differentially crosslinked gelatin was pressed into a self-supported wafer. The wafer, in turn, was placed into the sample holder, which was then inserted into the

transmission cell, and a spectrum was collected at room temperature and ambient pressure by utilizing a background that contained ambient air in the empty cell.

5.2.5 Preparation of MP-Embedded Agarose Cryogel Scaffold:

Cryogel scaffolds were made from low melting temperature agarose (Invitrogen) by freezing and controlled rate thawing as previously described[154]. Briefly, a 1.5% agarose solution in dd H2O was prepared by heating at 70°C in a water bath. The bath temperature was lowered to 37°C at which biomolecule-loaded or blank gelatin MPs or FITC-gelatin MPs (that were swollen or freeze dried) were rapidly dispersed by vortexing for 30s agarose solution until the temperature reaches 31°C. Cast the solution at 31°C into stainless steel molds of dimensions 15mm x 15mm x 5mm (VWR) and cool for 1hr at room temperature until gels are formed. Freeze in a cryostat (Leica) to -30°C for 1hr and at a controlled rate of 0.3°C/min thaw the gels until they reach -5°C. Retain at 5°C in the cryostat for 24 hours and then lyophilize and store at -80°C or use for further experiments.

Composite scaffolds consisting of loaded gelatin MPs were placed in 6-well plates (Corning) or in petri dishes (Beckton Dickinson) in 3 or 10ml of PBS and sampled (1/3rd the volume extracted and replaced with fresh buffer) at specific time points over a 2-week period. Samples were serially diluted and analyzed to determine the amount of released biomolecules as done before for standalone gelatin MPs. Note: when the

scaffold contained immunomodulators such as GM-CSF, DEX and/or PGN, the scaffold specifically identified as MI scaffold.

Note: Gelatin MPs with or without loaded biomolecules, with crosslinking used/analyzed on their own without being incorporated into the agarose cryogel scaffold are also referred to as standalone MPs or standalone gelatin MPs, while embedded MPs are explicitly specified whenever used.

5.2.6 Imaging

Free MPs or MP-embedded scaffolds were imaged using fluorescence (Zeiss) or confocal microscopy (LSM 510, Zeiss) to determine MP sphericity and spatial arrangement in the scaffold. Cryogel scaffolds were frozen at -20°C and sectioned into 1mm slices prior to imaging. Images were obtained at a minimum depth of 30 mm (significantly greater than MP diameters) and analyzed using ImageJ software (NIH).

5.2.7 Overall Experimental Approach

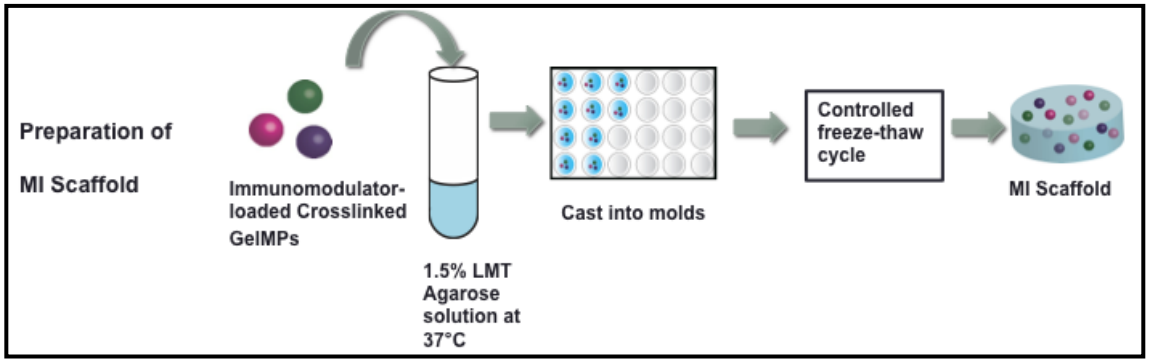

Figure 5.2 Schematic of MI scaffold preparation work flow

5.2.8 Statistical Analysis

Experimental values are reported as mean and standard error for n=3 for all samples unless explicitly mentioned. Statistical analysis was determined using one or two-way ANOVA coupled with Sidak's post-test analysis using GraphPad (Prism Inc., La Jolla, CA). p-values <0.05 were considered statistically significant.

5.2.9 Model and Fitting Analysis

The Weibull cumulative density function is given by

$$\boldsymbol{F(t) = 1 - \exp\left[-\left(\frac{t-\gamma}{\eta}\right)^{\beta}\right]} \qquad \textbf{Equation 5.1}$$

where,

'F' is the fractional drug released, a stretched exponential function of time 't'

'γ'<'t' is the location parameter, or 'lag' with units of time (second)

'η'>0 is the scale parameter, or time constant with units of time (second) and corresponds to the time taken for F ≈ 0.632 or when 63.2% of the loaded molecule is released. (see discussion of this chapter for explanation)

'β'>0' is the shape parameter, a dimensionless constant that determines the shape of the F(t) vs. t curve. (i) β=1, curve is exponential (ii) β>1, the curve is a sigmoid, S-shaped, with upward curvature followed by a turning point (iii) β<1 the curve is parabolic, with a higher initial slope and after that becomes consistent with the exponential.

Release profile measurements were analyzed using a non-linear regression model with hierarchically assigned priors for some parameters, fitting data to the Weibull equation, using WinBUGS[155], a Bayesian statistics software (The BUGS project, MRC, Cambridge, UK) and results were reported as median and confidence intervals at 2.5% and 97.5% instead of p-value. Markov chain Monte Carlo iterations of 10000 were first run and discarded before running 100,000 iterations to obtain results.

Priors for Weibull parameters, when not assigned as hierarchical, were derived by linearizing the experimental data as previously described[156]. Briefly, the double logarithm was applied onto the Weibull equation as in

$$\boldsymbol{log}\,(-\boldsymbol{ln}\,(\mathbf{1}-\boldsymbol{F}(\boldsymbol{t}))=\beta\,\boldsymbol{log}\,(\boldsymbol{t}-\gamma)-\beta\boldsymbol{log}\,\eta \qquad \textbf{Equation 5.2}$$

such that, graphing ***log(-ln(1-F))*** and ***log t***, assuming γ=0 would result in $\boldsymbol{\beta}$ and $\boldsymbol{\beta\,log\eta}$ being the slope and the intercept of the plot, respectively. The estimates for β and η obtained from these linearized plots was used to select suitable prior distributions in Bayesian modeling. γ was assigned as 0 for all samples except when the release was from 10^8 MPs in scaffold for which γ was obtained visually from plotted non-linearized graphs as the x-intercept.

5.3 Results

5.3.1 Characterization of Gelatin Microparticles

In order to determine the size and sphericity of un-crosslinked versus crosslinked MPs, we analyzed multiple samples of MPs. Fluorescent micrographs of gelatin microparticles

(gelatin MPs) indicated a relative spherical structure in their hydrated state. Un-crosslinked MPs exhibited a minimal amount of autofluorescence while crosslinking with glutaraldehyde (GA) increased fluorescence intensity (data not shown). (Figure 5.3) Earlier exploratory release studies used un-crosslinked MPs of 5.5 ± 3.8µm while subsequent studies of both standalone and agarose scaffold-incorporated MPs involved slightly larger particles 9.0 ± 4.2 µm. This increase was likely due to increase in temperature of dehydrating solvent (acetone)[157] used during MP synthesis from 0-4°C to 4-8°C. Gelatin MPs showed gradual decrease in mean size as the concentration of GA crosslinker was increased. Zeta potential (Figure 5.4), on the other hand, increased in magnitude with an increase in crosslinking.

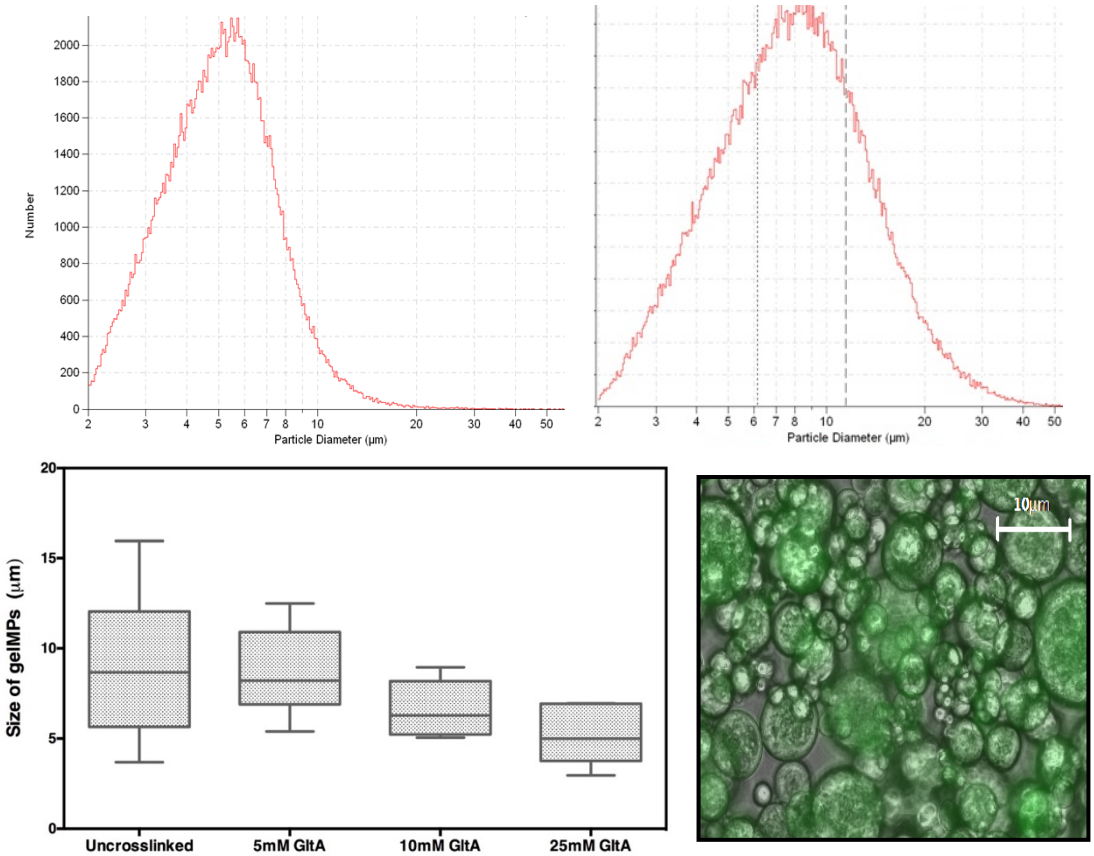

Figure 5.3 Size distribution histogram of un-crosslinked gelatin MPs.

During MP synthesis chilled acetone of (upper left) 0-4°C or (upper right) 4-8°C used resulted altering mean particle size. The latter group was MPs were crosslinked and (lower left) the box plot shows variation of MP size with crosslinking. Error bars represent SD of n=6 samples. The lower left panel shows a fluorescent micrograph of un-crosslinked gelatin MPs

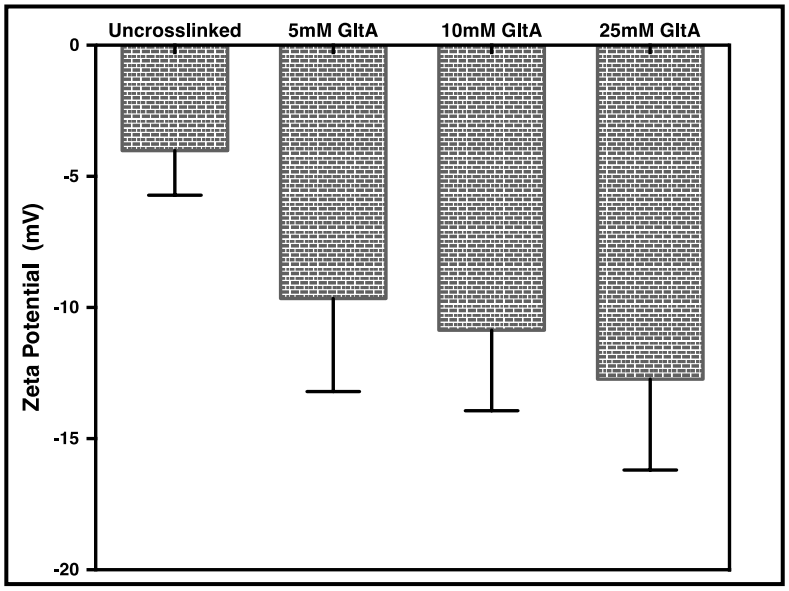

Figure 5.4 Zeta potentials of gelatin MPs.

Zeta potentials increased in magnitude with the increase GA crosslinking concentration (C_{GA}). Error bars represent SD of n=6 sample.

5.3.2 Effect of Crosslinking on Chemical Composition of Gelatin MPs (IR spectroscopy)

In order to assess whether chemical crosslinking with glutaraldehyde had altered the molecular composition or configuration of gelatin MPs, were performed infrared spectroscopic analyses. (Figure 5.5) FTIR spectrographs of gelatin MPs crosslinked differentially by GA of concentration from 1.25mM to 25mM showed that 3 distinct region of the IR plots varied gradually in heights. Region 1 from 3010-3310 cm^{-1} indicates a relative decrease in peaks with respect to single bonds of N-H, C-H and O-H with increasing glutaraldehyde crosslinking concentration (C_{GA})[158] suggesting a change in single bonds to double bonds. Region 2 from 1700 – 2000 cm^{-1} shows a decrease in C=O bond stretching that likely occurs due to a change in the absorption of in amide I band, possibly due to a modification in the secondary structure [159,160]. Region 3 from 1400 to 1200-cm^{-1} represents the amide III mode which in a simple amino acid derivative such as N-methylacetamide is the in-phase combination of the N-H bending and the C-N stretching vibration with small contributions from the C=O in plane bending and the C-C stretching vibration. Taken together, it is evident that gradual changes in C_{GA} resulted in gradual changes in 3 different regions in the spectrograph, supporting that the chemical composition of gelatin MPs underwent modification due to GA crosslinking.

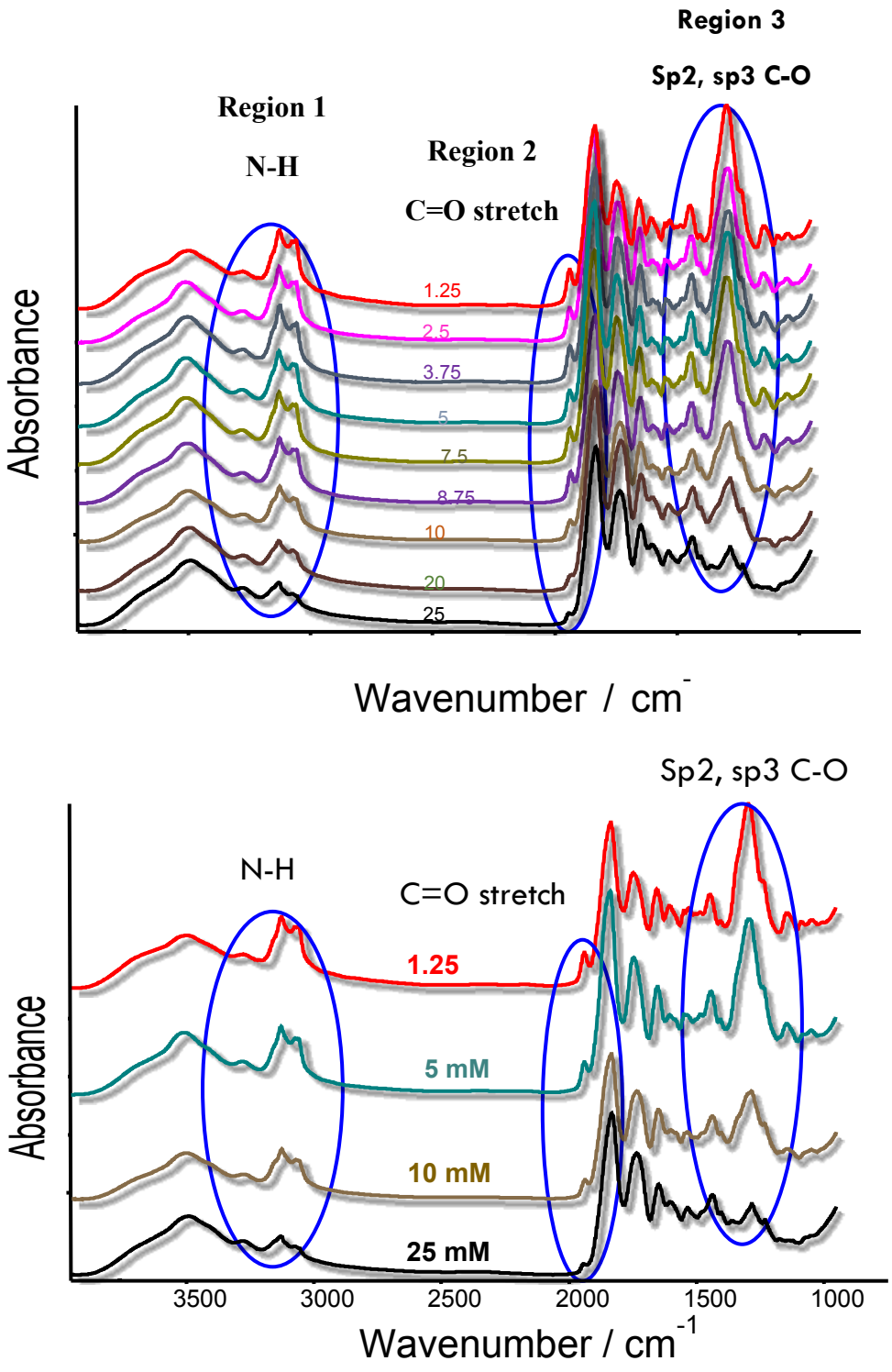

Figure 5.5 Analysis by Fourier Transform InfraRed Spectroscopy:

Absorbance profiles of gelatin MPs crosslinked with GA of 1.25 – 25mM were analyzed using FTIR. Top panel shows all spectrographs overlaid in order to visualize trend on absorbance while the bottom panel shows a subset of the same consisting of only four values spread across the range of crosslinking concentration. Circled region indicate the wavenumbers at which clear changes in absorbance are seen.

5.3.3 Effect of Crosslinking on Release Profile of Microparticles Loaded with Model Biomolecules of Varying Sizes

From the previous experiment, it was sufficiently determined that crosslinking was indeed capable of altering the chemical composition of the gelatin MPs and it is expected to be the primary factor in constricting the porosity and thereby release properties of the gelatin MPs. In the final scaffold for modulating DC phenotype, it is required to incorporate both a small molecule namely DEX[17] (~400kDa) as well as large molecules like GM-CSF (recombinant human (14.6 kDa) and PGN (25-100kDa). As development and optimization of release studies with these molecules would be expensive and extremely time consuming, model molecules such as biotin or OVA tagged with a fluorophore were considered as suitable alternatives. These model molecules were chosen due to their size similarity between the required immunomodulators such as DEX (small, <1000 Da) or GM-CSF or PGN. (large >10 kDa) respectively.

Incorporation efficiency of biotin or OVA into gelatin MPs decreased as the crosslinking extent increased for identical conditions during loading, however there was no significant difference between those of OVA and biotin-loaded gelatin MP (Figure 5.6). Release profiles of these molecules characterized the effectiveness in sustaining release of small and large biomolecules over a defined time period with a significant reduction in the initial burst release (Figure 5.7). Smaller changes in the crosslinking concentration showed minimal differences (data not shown) in the release profiles, especially for small molecules suggesting that in the spectrum of tested C_{GA}, specific groups can be chosen for delivery of particular small or large molecules and that it would be sufficient to work with four groups with distinct crosslinking extent differences (as shown in Figure 5.7) for the remainder of release experiments with OVA or Biotin, 'model' molecules.

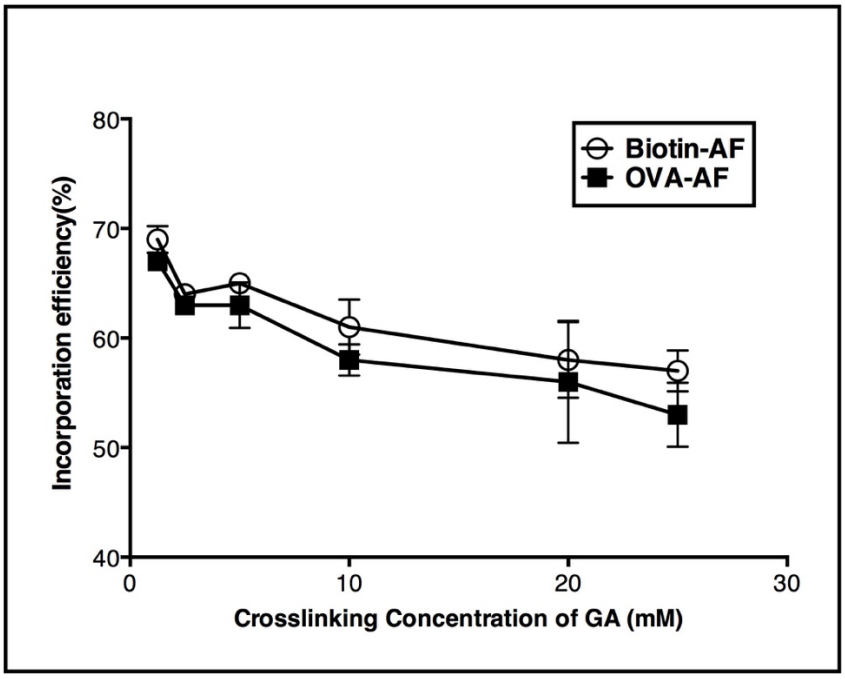

Figure 5.6 Incorporation efficiency of gelatin MPs:

Plots indicate the trend in the incorporation efficiencies of gelatin MPs loaded with either Biotin-AF or OVA-AF with changing crosslinking concentration of GA. Error bars represent the standard deviation with n=3 samples.

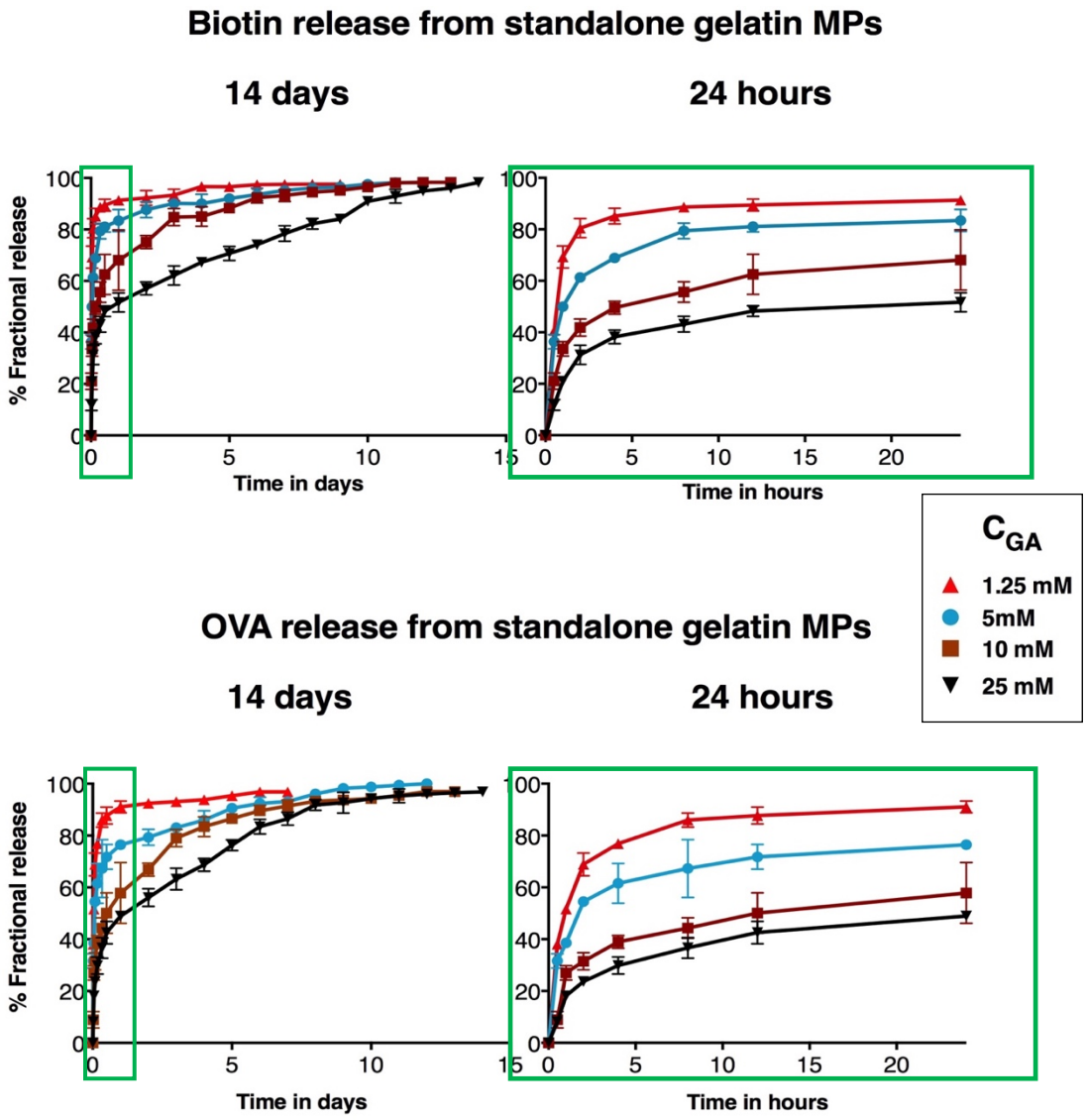

Figure 5.7 Varying crosslinking concentration of GA to regulate release.

Increasing GA concentration during crosslinking shows a graded sustains prolonged release over 2 weeks (left panels), and also decreases the burst release within the first 24 hours (right panels) for both large molecule OVA and small molecule,

biotin, tagged with AlexaFluor-647. Four representative C_{GA} are shown from the entire set of serial dilutions of GA

5.3.4 Embedding Gelatin MPs in Agarose Cryogel Scaffold

While optimizing the method of addition of biomolecule-loaded gelatin MPs to the agarose solution prior to cryogelation, we experimented with swollen MPs versus freeze-dried MPs and learnt that the latter were better at dispersing evenly in the agarose solution while the former tended to aggregate and due to their water content modified the true composition percentage of the agarose. We also worked with a range of temperatures from 21-40°C for this procedure and concluded that 37°C was the optimal incorporation temperature. At 37ºC, both swollen and freeze-dried gelatin MPs dispersed reasonably well while minimizing any unwanted biomolecule release from the gelatin MPs into the agarose solution. Importantly, the higher temperature was maintained only for 5 min to obtain an even dispersion of MPs after which the suspension was immediately transferred into molds for to cryogelation. For confocal imaging experiments gelatin MPs were tagged with FITC prior to incorporation into agarose solution to improve the visibility of the MPs in the embedded system. The confocal micrograph in Figure 5.8 shows that FITC gelatin MPs were embedded within the depths of the agarose scaffold while being largely proximal to the pores. Initially, this caused concern as the gelatin MPs were design to remain embedded in the scaffold and were not meant to elute out. However, upon repeatedly washing the scaffold in deionized water, we were unable to find any trace of eluted gelatin MPs. Interestingly, the gelatin MPs associated to scaffold near the pores while not actually inside them. Gelatin MPs likely rearranged themselves within the agarose during cryogelation with their water molecules aggregated to some parts of

the MP surface. Upon controlled thawing the ice crystals network of the agarose ablated[154] while likely maintaining gelatin MPs proximal to agarose's internal porous network. Also, it is evident from Figure 5.8 that the process of freeze-thawing did not destroy the integrity of the gelatin MPs in the scaffold.

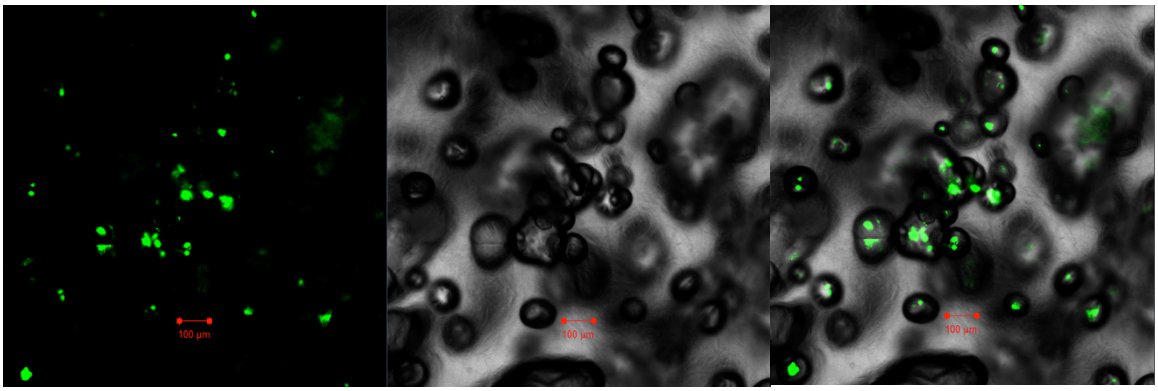

Figure 5.8 Embedding gelatin MPs in agarose cryogel.

Gelatin MPs were found within the scaffold closely allocated to the porous regions although they are not eluted after scaffold formation. Confocal microscopic images of scaffold containing cross-linked gelatin MPs tagged with FITC to enhance fluorescent. Scale bars represent 100µm

5.3.5 Release Profiles of Model Biomolecule-Loaded Gelatin MPs Embedded in Agarose Scaffold

As noted previously, characterization of release profiles from standalone gelatin MPs provides only partial information about how the loaded particles would release their agents when embedded in a layer of an additional diffusion barrier. Accordingly, it was imperative to characterize their release from the MP-embedded scaffold. Release profiles

of these embedded crosslinked MPs were similar in trend to their standalone counterparts however, the scaffold alone did not particularly affect the release profile (data not shown). Interestingly though, the release profile from the embedded gelatin MPs seemed to mimic standalone MP behavior only when the total MPs per scaffold (MP number density) were maintained at 10^{10} per scaffold while lower MP number densities resulted in loss of burst release and a change in shape of the release curve (Figure 5.9). Both biotin and OVA, though vastly different in molecular size, displayed a similar behavior for embedded MPs and the shape of the curve visually seemed to depend on number of microparticles carrying a particular biomolecule rather than the actual biomolecule size or the scaffold-induced diffusional barrier. Hence MP number density was selected as another variable (to customize scaffolds for immunomodulatory delivery) rather than altering the agarose composition, as it required less time-consuming optimization of the release characteristics.

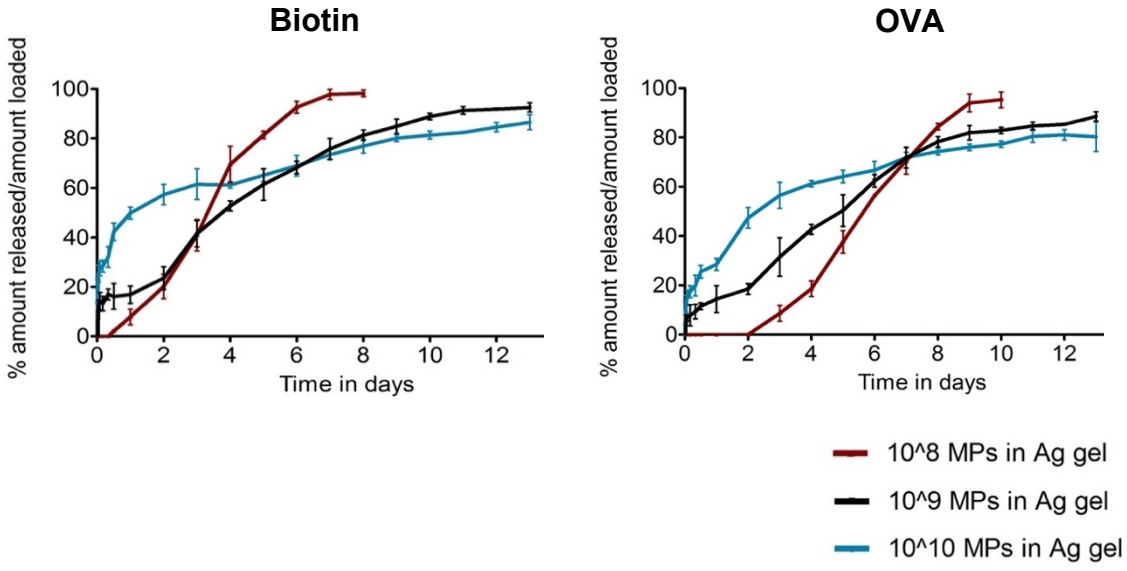

Figure 5.9 Varying MP number density in agarose cryogel scaffold to regulate biomolecule release.

Release profiles shown of AlexaFluor-647 labeled OVA (left) or Biotin (right) loaded onto gelatin MPs were cross-linked with 10mM GA and incorporated into agarose cryogel scaffold. Data was obtained by averaging over 3 individual experiments.

5.3.6 Mathematical modeling of release profile data to determine the optimal scaffold design for the delivery of 2 or more immunomodulating biomolecules of varying sizes from the scaffold

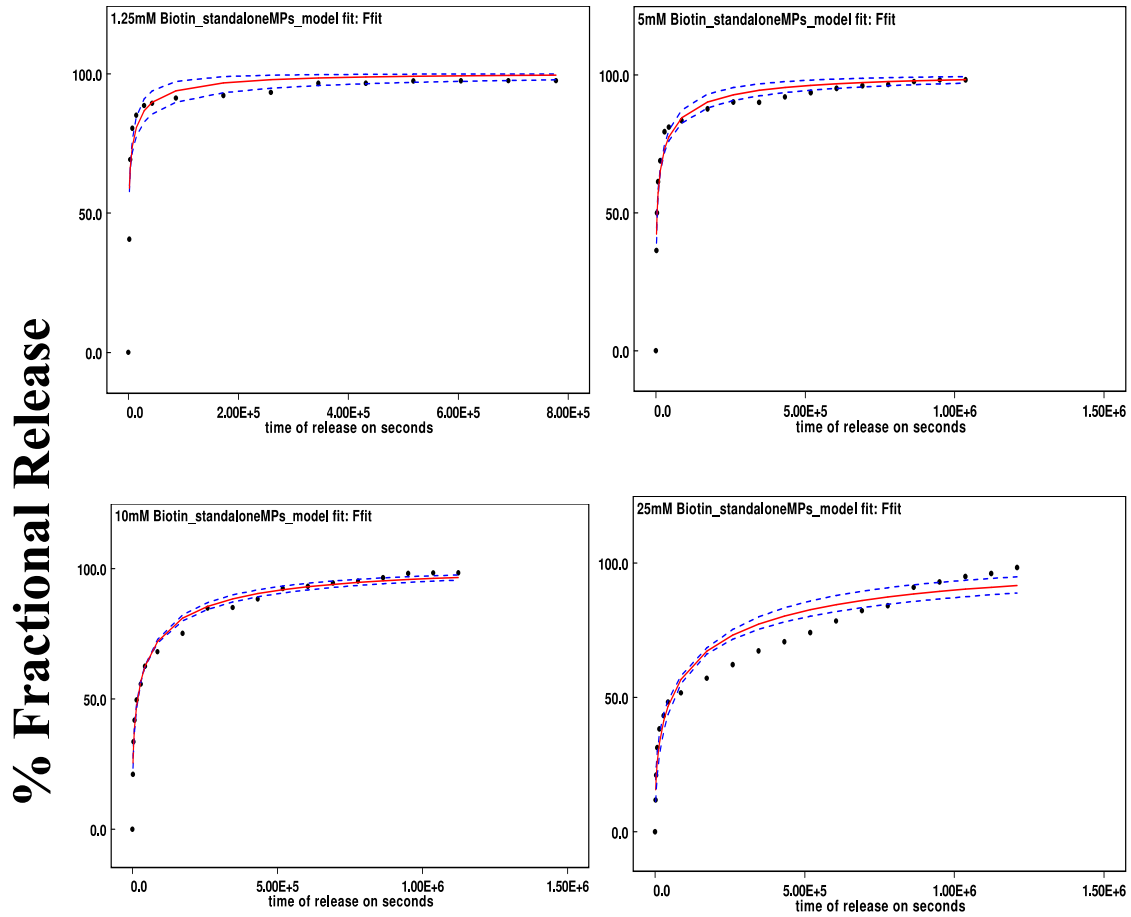

Figure 5.10 Non-linear regression of %fractional release of biotin from crosslinked standalone MPs over time (in seconds) using the Weibull equation (Eq.5.1).
Dots represent the experimentally measured release, smooth curve and dashed lines indicate the median fitted release along with standard deviation. Data was obtained by averaging over 3 individual experiments.

In order to derive a quatitative understanding of the MP release system, the release profiles of biotin and OVA were fitted to the Weibull model as shown in Figure 5.10 and 5.11. The fitted profile of fractional release (identical to "% Amount Release/ Amount Loaded" in Figures 5.6) closely corresponded to the measured values and as noted before, the reduction in burst release with an increase in crosslinking concentration is evident. From tables 5.1 and 5.2, we note that the fitted value for γ for standalone MP release of biotin or OVA varied from 0 to 2s. Due to the really large times (>24h) involved in the study, the (t-γ) term in Equation 5.1 would be largely unaffected by γ, and hence for standalone MP release systems the effect of γ becomes negligible or zero, thereby reducing to the Weibull 2-parameter equation with all other parameters described in Eq. 5.1.

$$\boldsymbol{F(t) = 1 - \exp\left[-\left(\frac{t}{\eta}\right)^{\beta}\right]} \qquad \textbf{Equation 5.3}$$

The time constant, 'η', widely varies with changing crosslinking concentrations as evident from Tables 5.1 and 5.2 for both Biotin and OVA respectively. The fitted η_{OVA} was higher than η_{biotin} at all values of C_{GA} with the differences increasing at higher

concentrations shown in tables 5.1, 5.2 and Figure 5.11. Further, fitted values of β increased with C_{GA}, and varied from 0.2 to 0.6 for standalone MPs with negligible differences between biotin and OVA, suggesting that the biomolecule size only minimally influenced β. According to an in-depth analysis of Weibull paramters for drug release by Papadopoulou and colleages[161], $\beta < 0.75$ is an indication of release that is primarily due to Fickian transport. Another important takeaway from these results is that,

Subsequently, in order to correlate the variation in Weibull parameters with differential crosslinking, we applied a one-phase association exponential equation to model the consolidated release data from all standalone MPs. Figure 5.12 shows the association of C_{GA} with β and η. The R^2 for β versus C_{GA}, for biotin and OVA release, was 0.9516 and 0.9424 respectively, while that for log η versus C_{GA} was 0.9991 and 0.9895 respectively. Due to high R^2 values (> 0.9), we accepted these equations (tables in Figure 5.12) to be representative of correlating varying crosslinking densities with Weibull parameters.

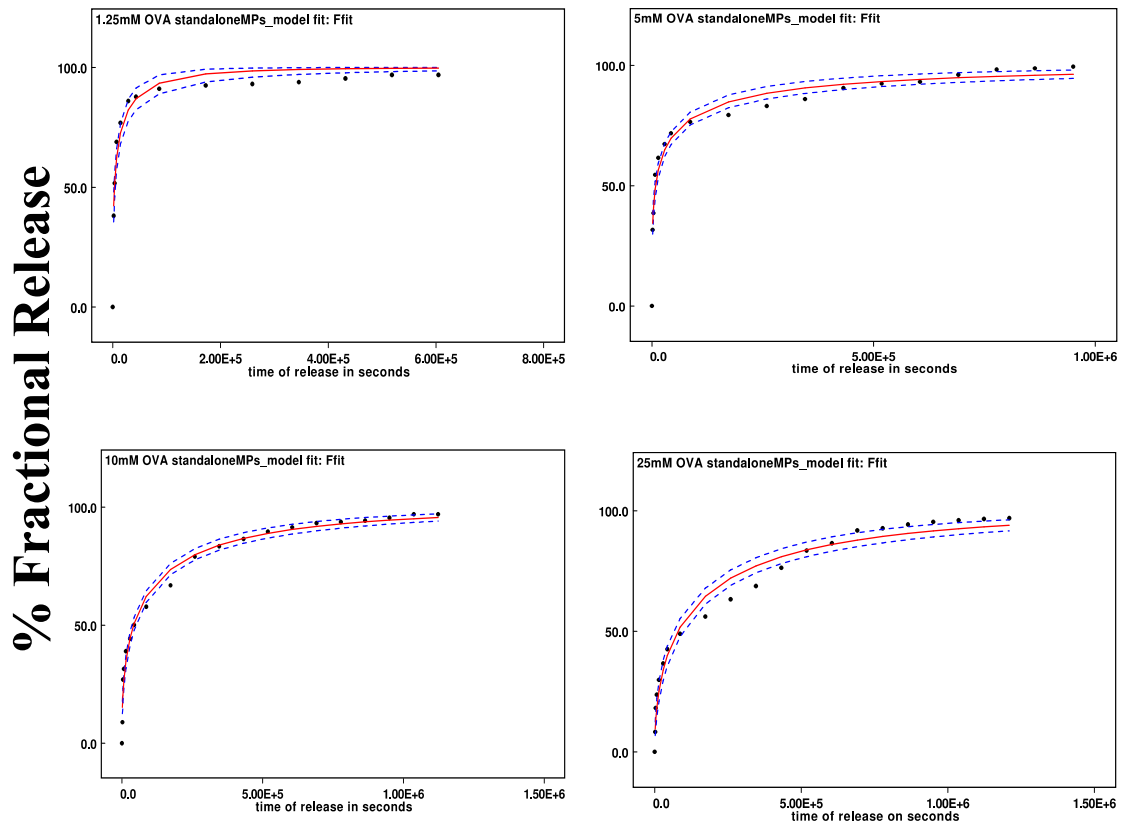

Figure 5.11 Non-linear regression of %fractional release of OVA from crosslinked standalone MPs over time (in seconds) using the Weibull equation (Eq.5.1).

Dots represent the experimentally measured release, smooth curve and dashed lines indicate the median fitted release along with standard deviation. Data was obtained by averaging over 3 individual experiments.

Table 5.1 Biotin release - Parameter values obtained from non-linear regression using Weibull Equation. β,η,γ are parameters described by Eq.5.1, while σ is the standard deviation of the fit, as plotted in Figure 5.12 by dashed lines.

C_{GA} mM	Statistic	β	η	γ	σ
1.25	**2.50%**	0.2376	2579	0.1998	0.04232
	median	0.2962	2666	1.709	0.05873
	97.50%	0.3693	2753	2.279	0.08924
5	**2.50%**	0.2825	11180	0.2031	0.02366
	median	0.3154	12010	1.709	0.03252
	97.50%	0.3678	12840	2.279	0.04933
10	**2.50%**	0.3549	44620	0.2031	0.01917
	median	0.379	45500	1.705	0.02595
	97.50%	0.4092	46370	2.279	0.03796
25	**2.50%**	0.3565	124500	0.204	0.04736
	median	0.4112	133200	1.706	0.0646
	97.50%	0.4911	141600	2.28	0.09628

Table 5.2 OVA Release - Parameter values obtained from non-linear regression using Weibull Equation. β,η,γ are parameters described by Eq.5.1, while σ is the standard deviation of the fit, as plotted in Figure 5.12 by dashed lines.

C_{GA} mM	Statistic	β	η	γ	σ
1.25	**2.50%**	0.2587	5848	0.2069	0.03059
	median	0.2915	7643	1.707	0.04453
	97.50%	0.2997	10380	2.279	0.07404
5	**2.50%**	0.294	19910	0.2069	0.02646
	median	0.3281	25020	1.706	0.03711
	97.50%	0.3779	31560	2.28	0.058
10	**2.50%**	0.4203	79240	0.2021	0.02564
	median	0.457	92090	1.706	0.03489
	97.50%	0.5037	106200	2.281	0.05213
25	**2.50%**	0.4567	134300	0.2041	0.03645
	median	0.5122	161300	1.708	0.04938
	97.50%	0.583	190800	2.28	0.07276

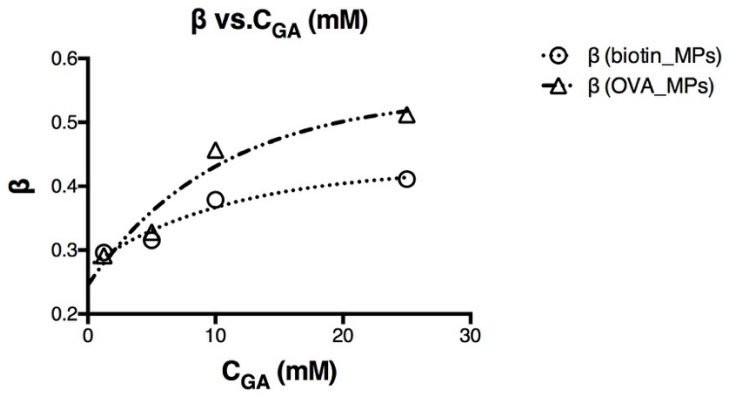

Best-fit values	Y=Y0 + (Plateau-Y0)*(1-exp(-K*x))			
Xlinked MPs	Y0	Plateau	K	R square
Biotin	0.2737	0.4297	0.09102	0.9516
OVA	0.2455	0.5442	0.09703	0.9424
x = Crosslinking concentration	Y = β			

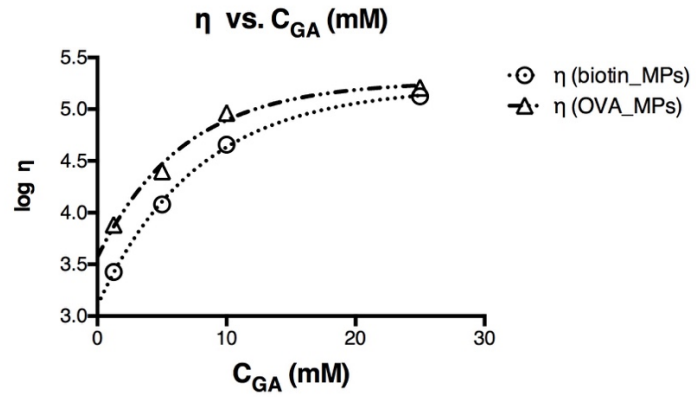

Best-fit values	Y=Y0 + (Plateau-Y0)*(1-exp(-K*x))			
Xlinked MPs	Y0	Plateau	K	R square
Biotin	3.102	5.215	0.129	0.9991
OVA	3.569	5.269	0.151	0.9895
x = Crosslinking concentration	Y = log η			

Figure 5.12 Correlation of Weibull parameters with C_{GA} (mM) using a one-phase association equation model of biomolecule release from standalone gelatin MPs. Circle represents model-derived parameters of biotin release while triangles represent that of OVA release.

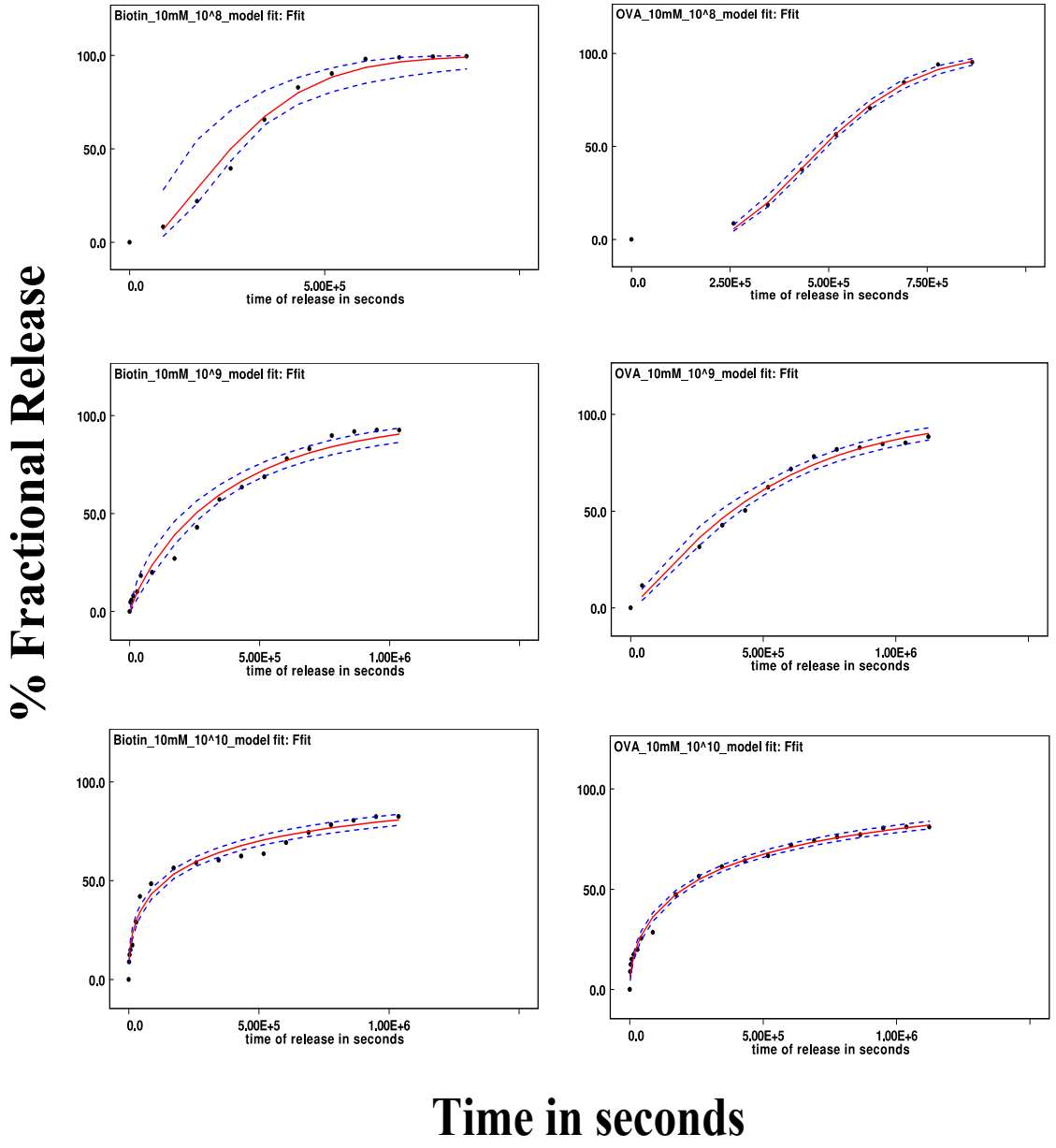

Figure 5.13 Non-linear regression of %fractional release over time (in seconds) using the Weibull equation (Eq.5.1)

Biotin (left) or OVA(right) from crosslinked (C_{GA} = 10mM) MPs embedded at N_{MP} = 10^8 (top), 10^9(middle) or 10^{10} (bottom) per scaffold. Dots represent the experimentally measured release, smooth curve and dashed lines indicate the

median fitted release along with standard deviation. Data was obtained by averaging over 3 individual experiments.

Table 5.3 Biotin release from scaffold-embedded gelatin MPs – parameter values obtained from non-linear regression using Weibull Equation. β,η,γ are parameters described by Eq.5.1, while σ is the standard deviation of the fit, as plotted in Figure 5.14 (left panel) by dashed lines.

N_{MP}	Statistic	β	η	γ	σ
10^8	**2.50%**	0.7593	171900	43150	0.02147
	median	1.412	280300	43200	0.05235
	97.50%	1.792	305500	43250	0.19740
10^9	**2.50%**	0.7931	327050	14751	0.03479
	median	0.9647	385400	14800	0.05188
	97.50%	1.112	427800	14849	0.08988
10^{10}	**2.50%**	0.3871	275700	1.264	0.03002
	median	0.4313	324700	50.42	0.04123
	97.50%	0.4828	376800	98.64	0.06153

Table 5.4 OVA release from scaffold-embedded gelatin MPs- Parameter values obtained from non-linear regression using Weibull Equation. β,η,γ are parameters described by Eq.5.1, while σ is the standard deviation of the fit, as plotted in Figure 5.14 (right panel) by dashed lines

N_{MP}	Statistic	β	η	□γ	σ
10^8	**2.50%**	1.698	364600	172800	0.01196
	median	1.916	379400	172800	0.02002
	97.50%	2.078	391400	172800	0.04543
10^9	**2.50%**	0.8357	438400	28750	0.02923
	median	1.058	494900	28800	0.04421
	97.50%	1.25	535500	28850	0.07878
10^{10}	**2.50%**	0.4823	367400	0	0.01988
	median	0.5219	400800	24.14	0.02703
	97.50%	0.5659	434700	48.02	0.03982

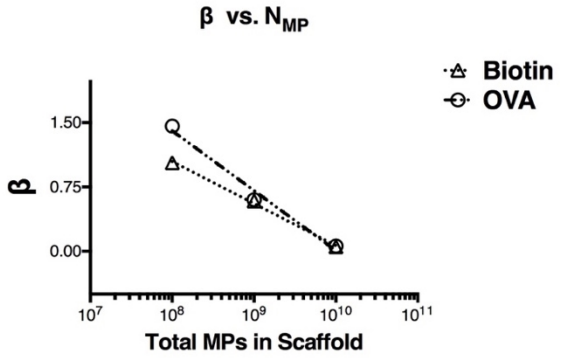

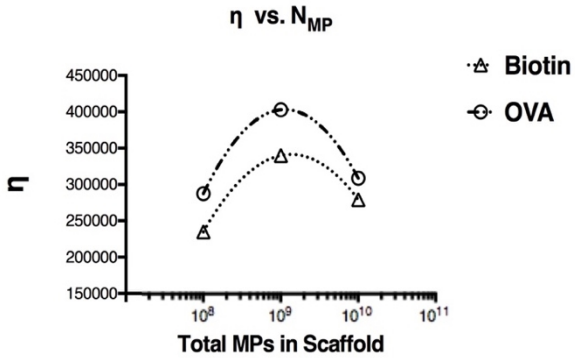

Best -fit values	Y = Yintercept + Slope*log(X)		
Scaffold + Crosslinked MPs	Yintercept	Slope	R square
Biotin	339900	22200	0.9974
OVA	402810	10700	0.9829
X = NMP		Y = β	

Best -fit values	Y = B0 + B1*XC + B2*XC^2			XC = log (X) - log (Xmean)	
Scaffold + Crosslinked MPs	B0	B1	log (Xmean)	B2	R square
Biotin	339900	22200	9	-82900	1
OVA	402810	10700	9	-104800	1
X = NMP		Y = η			

Figure 5.14 Correlation of Weibull parameters with N_{MP} using biomolecule release from agarose scaffold-embedded gelatin MPs uncoupled from the effects of C_{GA}. Circle represents model-derived parameters of OVA release, while triangle denotes that of biotin release.

Table 5.5 Uncoupled values of βand η due to N_{MP} alone corresponding to Figure 5.14

		Biotin		OVA	
N_{MP}	Statistic	β_{NMP}	η_{NMP}	β_{NMP}	η_{NMP}
10^8	**2.50%**	0.4044	127280	1.2777	285200
	median	1.033	234800	1.459	285360
	97.50%	1.3828	259130	1.5743	287310
10^9	**2.50%**	0.4382	282380	0.4154	359160
	median	0.5857	339900	0.601	402810
	97.50%	0.7028	381430	0.7463	429300
10^{10}	**2.50%**	0.0322	231080	0.062	288160
	median	0.0523	279200	0.0622	308710
	97.50%	0.0736	330430	0.0649	328500

As before, the experimentally measured release profiles were fitted in a similar non-linear regression model using the Weibull equation and the fitted plots closely match the experimental data with the standard deviation for all fits < 0.1, indicating high precision of the model. γ values for $N_{MP} = 10^8$ were the highest, γ is representative of the lag in the release evidenced for this group. The profiles for 10^{10}MPs embedded per scaffold varied vary slightly from their standalone MP counterparts and the shape in the release curve changed with every 10-fold increasing in N_{MP}, similar to the results from experimental data (Figure 5.9).

Overall, (Tables 5.3 and 5.4) β values varied from 0.3 to 2.1 while η varied from $1.7x10^6$-$5.35x10^6$. The relative differences in β and η for biotin versus OVA, similar to the standalone MPs, was not excessively correlated with biomolecule size. γ, on the other hand increased by an order of magnitude for OVA compared to biotin when $N_{MP} = 10^8$ while showing smaller differences for other values of N_{MP}. Altogether, these results corroborated with experimental data that varying N_{MP} embedded within the scaffold significantly influenced the release profile including the shape and scale parameters of the Weibull equation.

In order to establish a relationship between both C_{GA}, N_{MP} with β and η, we defined a simplistic model:

$$\eta_{embedded\text{-}MPs} = \eta_{CGA} + \eta_{NMP} \qquad \textbf{Equation 5.4}$$

$$\beta_{embedded\text{-}MPs} = \beta_{CGA} + \beta_{NMP} \qquad \textbf{Equation 5.5}$$

where, η_{CGA}, β_{CGA} are due to the effects of varying C_{GA}

and η_{NMP}, β_{NMP} are due to the effects of varying N_{MP}.

Accordingly, uncoupled values of β and η (table 5.5), associated with changing N_{MP} alone were plotted and their relationship is shown in Figure 5.14. Although, the η values were fit to a quadratic equation, since only three points of measurement were available, we cannot suggest the equation as a definite correlation η with N_{MP}. However, it is important to note that both 10^8 and 10^9 MPs per scaffold considerably altered the shape of the release curve (Figure 5.13) while $N_{MP} = 10^{10}$ maintained the curve shape similar to that of standalone MPs (Figure 5.11).

5.3.7 Predicting Rate of Release Required From Scaffold Containing MPs Loaded with Immunomodulators.

In the MI scaffold containing GM-CSF, DEX, PGN, peak release of immunomodulators was required differentially in for human DC cultures according to Table 5. Based on this, the $\eta_{required} = \eta_{embedded\text{-}MPs}$ was set to 'last day' of required release, for example, for human culture, $\eta_{required}$(GM-CSF) = (3-0) = 3 days or 259200s. Second, the shape of the release profile curve was selected, i.e., since $N_{MP} = 10^8$, 10^9 or 10^{10} each elicit a distinct shape, the N_{MP} value was set. In the case of human GM-CSF, since the release was expected with a relative burst profile to mimic human DC culture in which GM-CSF is supplied to peripheral blood mononuclear cells on day 0[9], the required N_{MP} was set to 10^{10}, and the η_{NMP} and β_{NMP} values were determined from table 5.5. Third, the η_{CGA} and β_{CGA} value were calculated using equation 5.4 and 5.5 respectively and used to interpolate the value of C_{GA} required which was 4.8335 ≈ 5mM for human GM-CSF. Thus the composition of GM-CSF required in the MI scaffold for human culture was predicted as 5mM crosslinked gelatin MPs embedded at 10^{10} per scaffold. Similarly, the recipes required for DEX for human DC culture were determined as 10mM crosslinked gelatin MPs embedded at 10^9 per scaffold. For PGN, we incorporated a slight modification is selecting $\eta_{required}$: instead of setting $\eta_{required}$, we used $\eta_{required}/2$ as the duration required for release. Since developing DCs would be extremely sensitive to TLR ligands such as PGN during the early phase of differentiation, we wanted to ensure that the fractional amount released would be < 30% within the first three days. The drawback of this approach would be that a portion of PGN would remain unused in the 6 to 8-day cultures.

Table 5.6 Configuration of MI scaffold required in Human DC cultures at different time-points. GM-CSF – granulocyte monocyte colony stimulating factor, DEX – dexamethasone, PGN – peptidoglycan

Immunomodulator	Days Required in Culture (Human)		
	Days	N_{MP}	C_{GA} (mM)
GM-CSF	0-3	10^{10}	5
DEX	3-5	10^{9}	10
PGN	5-6	10^{9}	25

Using this approach, an MI scaffold appropriate for human DC culture was prepared and its release profile of GM-CSF, DEX and PGN were determined and compared to the predicted release. (Figure 5.15). The release profile for hGM-CSF is nearly identical to that predicted by the model for up to 10 days which is longer than the DC culture itself. DEX of the other hand showed a curious, biphasic release with an initial burst phase during day 1 and then gradually settling into the predicted profile. Although, the initial burst was not originally planned, on researching several protocols [69-73] for developing DEX-DCs we realized that this type of initial burst may actually be beneficial to the early development of tolerogenic properties in DCs and hence chose not to modify the scaffold configuration for DEX release. For PGN, unlike OVA release (Figure 5.9), the fractional release lacked an initial lag period (= γ) and the shape of the curve shows a highly decreased burst right at the right beginning. Since the predicted values for η and β include $\pm$ limits, the experimental PGN release still falls with the predicted range suggesting that the model was effective. Using the lower limit of PGN

prediction as the basis for subsequent model prediction, priors for η and β were re-adjusted in the original Weibull model.

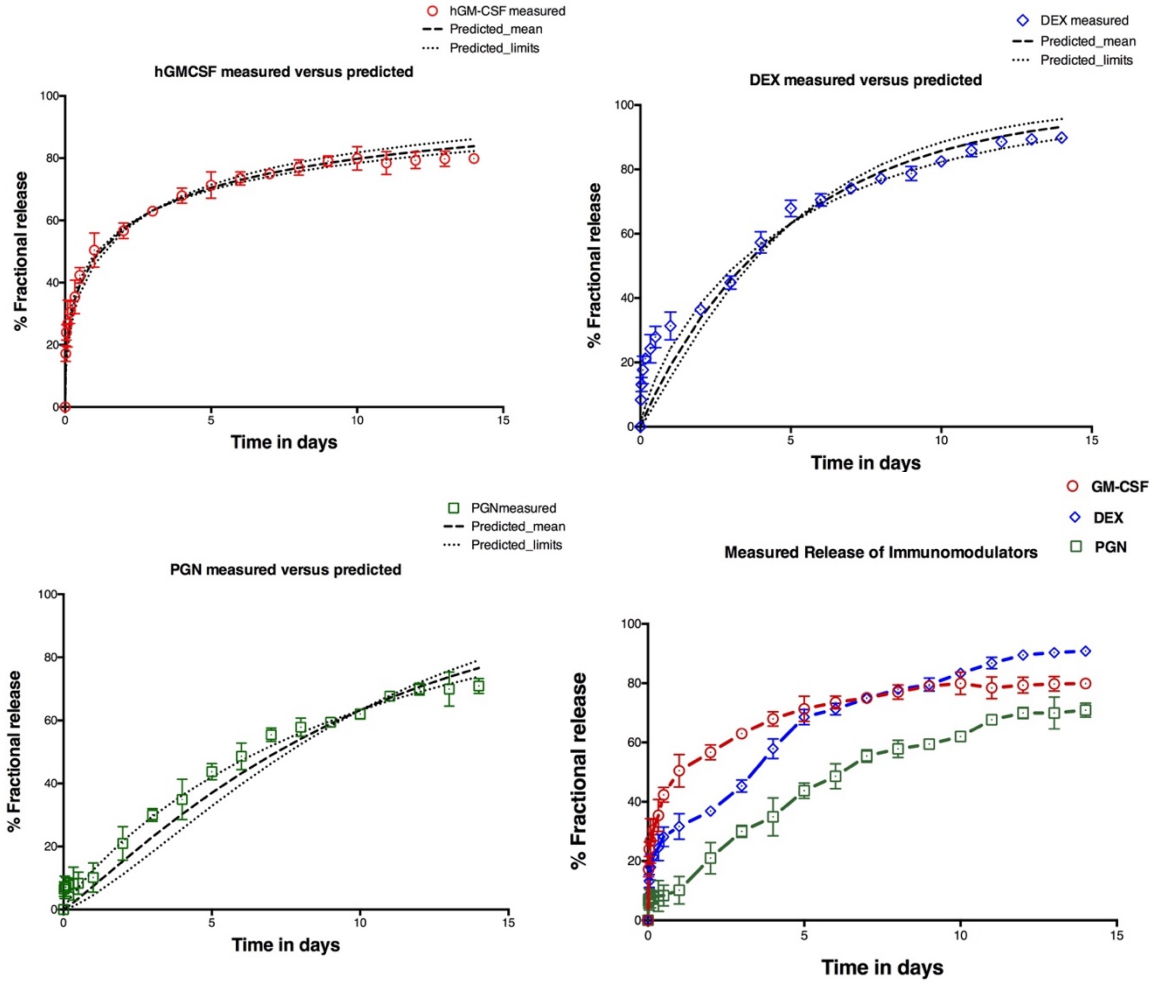

Figure 5.15 Measured vs predicted release profiles of immunomodulators from MI scaffold designed for human DC culture

Experimentally-measured release profiles of hGM-CSF (top left), DEX (top right) and PGN (bottom left) loaded onto MI scaffold correlated with those predicted by

the model. (bottom right) Combined experimentally-measured release profile of all immunomodulators from the MI scaffold.

5.4 Discussion

5.4.1 Gelatin and Agarose as Carriers

Although gelatin MPs of different material characteristics have been extensively used in research[142,152,162-164], we had not previously developed them in-house for application-specific purposes. Hence, initially, it was essential to determine the most suitable method for reproducibly preparing crosslinked gelatin MPs, characterize their size and chemical composition upon crosslinking, to ensure that chemical crosslinking would be an effective technique to manipulate the release of a loaded agent from the MPs.

The promising development and characterization of the release of model molecules in the previous section were limited only to standalone gelatin MPs. In order to create a multifunctional scaffold niche according to our proposed design, it was essential to determine optimal methods of fabricating gelatin MPs embedded within a scaffold. Agarose is a neutral polysaccharide soluble in hot water, capable of fast gelation such that the gelation temperature is a function of its concentration in aqueous solution[165]. Primarily, here, agarose was selected as the material for the scaffold base due to the its ability to maintain DCs in an immature phenotype and the induction of autologous regulatory T-cells in a mixed lymphocyte reaction[107]. Common methods of agarose scaffold preparation such inverted colloidal crystal templating[13] use strong organic

solvents that may degrade MPs within the agarose scaffold and/or denature any cytokines or growth factors that were previously loaded on the gelatin MPs; on the other hand, synthesis by cryogelation did not greatly affect the integrity of embedded crosslinked MPs nor likely affect the activity of biomolecules to be released. Cryogelation has been used more recently in research for synthesizing super-macroporous and macroporous scaffolds of hydrogels since its controlled freeze-thawing process allows the formation of a uniform porous network, suitable for biomolecule release as well as potential cell-entrapment[154,166]. Similar agarose-based cryogel scaffolds have successfully been used as structural beds for culturing insulin-producing cells[166] as well as in cartilage tissue engineering *in vivo*[167,168]. We hence expect that the MI scaffold with macroporous three-dimensional structure, when implanted into a host, would not only release factors to engender the endogenous recruitment of DCs but also enhance the time of localization of these cells at the site of the implant, thereby boosting the effectiveness of the delivered therapy.

5.4.2 IR Spectrograph

The crosslinking of peptide chains in gelatin MPs by GA is primarily due to the reaction of the primary amines groups of lysine or hydroxylysine amino acid residues with the aldehyde, producing aa aldimine, a Schiff's base with relative lability (Figure 5.16)[169]. On occasion, functional groups of gelatin such as amide, imidazoyl, carboxyl or guanidine are also involved in crosslinking (Figure 5.17)[170]. The increased stability of this type of crosslinked gelatin, may be due to the formation of stable pyridinium ions[170,171].

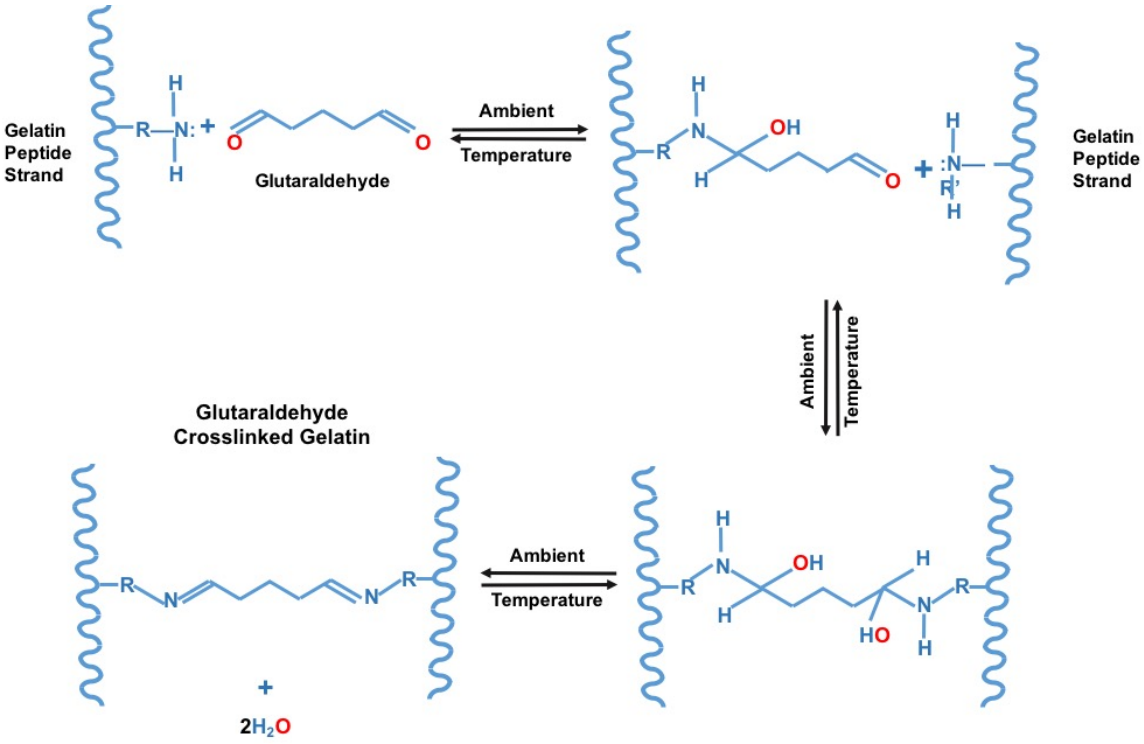

Figure 5.16 Schiff's base formation by GA crosslinking of gelatin

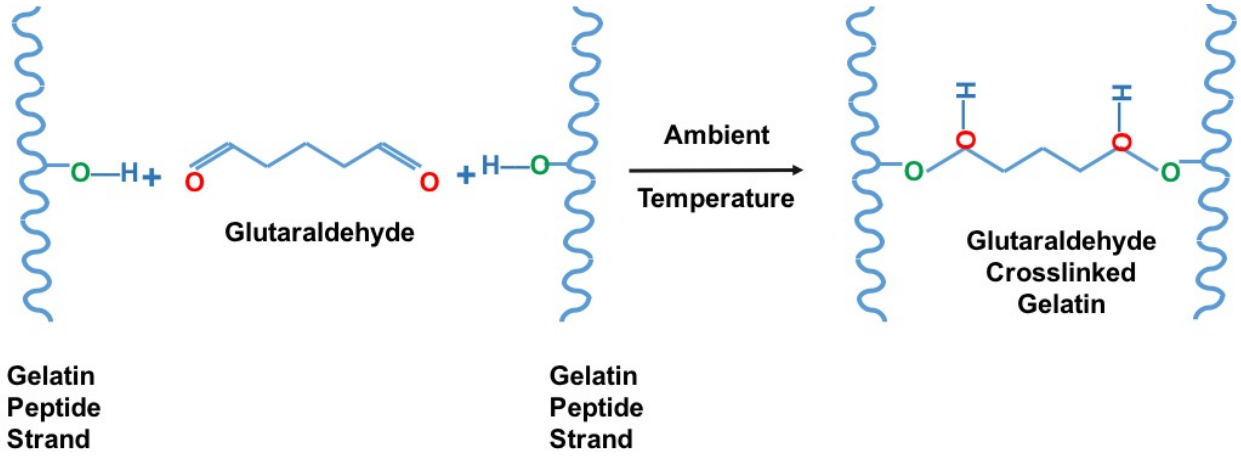

Figure 5.17 An Alternative Mechanism of GA crosslinking of gelatin (based on [172])

FTIR spectrographs (Figure 5.5) of gelatin MPs crosslinked differentially by GA of concentration from 1.25mM to 25mM showed that 3 distinct regions of the IR plots

varied gradually in heights. Region 1 indicates a relative decrease in peaks with respect to single bonds of N-H, C-H and O-H with increasing C_{GA}. Specifically, such a peak reduction indicates a loss of degrees of freedom when a single bond changes to a double, as in the change from primary to secondary amines (or imines)[158], while region 2 from indicates a decrease in C=O bond stretching that likely occurs due to a change in the absorption of in amide I band [159,160], further suggesting an alteration in the secondary structure of the peptide chains in gelatin upon increased crosslinking. Region 3 represents the amide III mode which in a simple amino acid derivative such as N-methylacetamide is the in-phase combination of the N-H bending and the C-N stretching vibration with small contributions from the C=O in plane bending and the C-C stretching vibration. In polypeptides such as gelatin, however, the composition of this mode is more complex, since it depends on side chain structure and since NH bending contributes to several modes in this region. Despite side chain contributions to the amide III mode, this mode can be used as a further indicator of change in secondary structure[158] with GA crosslinking. This absorbance, here, may also be associated with sp2/sp3 hybridization of C-O.

5.4.3 Bayesian Approach

The Bayesian approach to statistical inference considers unobservable parameters in a statistical model as random variables. When data is unavailable, a 'prior' distribution is applied to quantify knowledge that may have been obtained from theoretical considerations or previous similar experiments. However, when data is available the prior is updated to a 'posterior' distribution based on the Bayes' theorem[173]. When combined with Markov chain Monte Carlo (MCMC) simulations, Bayesian statistics allows the

evaluation of posterior distributions by simulation in complex models. Essentially, MCMC generates samples from the posterior distribution by constructing a reversible Markov-chain that has as its equilibrium distribution the target posterior distribution [155]. There is also noteworthy criticism for using Bayesian approaches to construct models with little knowledge about the inherent mechanism or parameters. Mainly, it requires users to specify prior distributions for all unknown parameters. However, for setting up models of non-linear regression fit, this issue of unknown prior distributions can be easily tackled by linearizing the regression model and obtaining initial parameter estimates that can subsequently be used to define limits for prior distribution assumptions, as done in this study.

5.4.4 Weibull Equation, Physical Significance of Parameters and Limitations

Weibull statistical distribution was originally suggested[174] and adapted[156] to fit empirical drug release data as

$$\boldsymbol{F(t) = 1 - \exp(-at^{\beta})} \qquad \textbf{Equation 5.6}$$

in which a, β are the fitting parameters and β corresponded to the mechanism of release and F(t) as noted previously indicates the fractional drug released. For early time points, Equation 5.4 would reduce to the widely-explored Peppas equation[145]:

$$\boldsymbol{F(t) = kt^{n}} \qquad \textbf{Equation 5.7}$$

in which k and n are the fitting parameters, and n corresponds to the release mechanism. Although Eq. 5.3 was frequently used to illustrate empirical drug release models, it has been criticized for (i) its lack of kinetic basis and (ii) non-physical nature of its

parameters (including 'a' having units of s^{-b}). A modification of Eq. 5.2 was suggested[175] such that the parameter 'a' was re-expressed as $(1/\eta)^{\beta}$, as shown in Eq. 5.1. As the lowest possible value for the exponential term in Eq.5.1 when t >0 is '-1', such that it reduces to F = exp (-1) = 1/e = 0.632, suggesting that 'η', the time constant, physically equals the amount of time required to release approximately 63.2% of the initially loaded biomolecule. From our observations of release from both standalone MPs and scaffold-embedded MPs (Figure 5.7 and 5.9), it was evident that η corresponded to 63.2% release when crosslinking was below 25mM GA concentration or when N_{MP} in the scaffold was nearly 10^{10}, i.e. η displayed a dependency on the crosslinking concentration and MP number density.

Furthermore, the location parameter, γ, represents the lag time before the onset of the dissolution or release process and in most cases will be zero. From our studies, it was evident that γ was indeed was between 1-2 s, which in comparison to the larger time scales of 't' (>10^4 s) was negligible or as good as zero for most cases. The only observed conditions for which γ was of the order 10^3 s was the diffusional barrier for releasing loaded biomolecules was greatly increased using ≤ 10^{10} MPs within the cryogel scaffold. This was likely due to the way were distributed within the scaffold: when in large numbers, MPs decreased the total diffusional driving force of loaded biomolecules to the external solution, lower MP number density caused sparse spatial organization or aggregation of MPs within the inner scaffold core thereby greatly increasing diffusional driving force and almost completely negating burst release. The diffusion coefficient, associated with η, may also be dependent on scaffold porosity and tortuosity, which may

collectively increase when the total MP number density is low. Additionally, lower N_{MP} may have resulted in the total loaded drug in exceeding the saturation drug concentration associated with the total gelatin content thereby causing the drug to behave "dispersed" rather than dissolved. In such cases when drugs associated with a polymer matrix are in "dispersed" phase, a lag time is required for the drug to transform from dispersed to dissolved state is necessary prior to any observable release; these systems can readily be described by the Higuchi equation[144,176]. In general, the shape parameter, β, would characterize the curve as either exponential (β=1) (Case 1), sigmoid, S-shaped, with upward curvature followed by a turning point (β>1) (Case 2), or parabolic, with a higher initial slope and after that consistent with the exponential (β<1) (Case 3). We observed that β increased gradually with the crosslinking concentration used, although displaying values <1 (Case 3) when release was characterized from standalone MPs, indicating largely exponential behavior and thereby association with Fickian diffusion. Intriguingly, the shape of the curve changed dramatically as the MP number density was decreased from 10^{10} to 10^{9}(β≈1) and 10^{8} (β≈2), indicating a deviation from Fickian diffusion to non-Fickian and other stochastic forces.

The one-dimensional steady state approximation of the Fick's law defines the fractional drug released as

$$\boldsymbol{F = \frac{M_t}{M_\infty} = 4\left(\frac{D\,t}{R^2}\right)^2} \qquad \textbf{Equation 5.8}$$

where,

M_t and M_∞ are the amounts of drug release and loaded respectively,

D is the diffusivity constant

t is the time of release

R is the characteristic length scale

Here, Eq.5.8 can be re-written in terms of a time-constant, η, such that

$$\boldsymbol{F = \frac{M_t}{M_\infty} = 4\left(\frac{t}{\eta_{Fick}}\right)^2} \qquad \textbf{Equation 5.9}$$

such that time constant $\eta_{Fick} = R^2/D$.

In a similar manner, we can define η from Equation 5.1 as η = function (R, D). Although a direct relationship of η and R or D could not be arrived at using the Weibull model, from Figures 5.11 and 5.13 we were able to obtain a relationship of η with experimentally variable parameters such as C_{GA} and N_{MP}, which can intuitively be understood as responsible for controlling the characteristic length and diffusivity of the construct.

Collectively, from this study, we can gather that although the physical association of Weibull parameters have not been previously determinable or relevant, we can qualitatively correlate their behavior with physical attributes of the scaffold/MP release system, such as crosslinking density or pore size, diffusional distance or number density of MPs. Similarly, a recent study indicates the differential nature of these parameters with changing size and porosity of capsules releasing small molecule drugs was established[177]. Although, we have made simplified assumptions (Equations 5.4 and 5.5) that can be applied to predict release only in the short time frames of 1-14 days, since the application expected for the scaffold does not require release times longer than 14 days, the limitations of the model assumptions are not of particular concern. However, in order to

completely elucidate a quantitative relationship for these parameters, a more detailed characterization of such systems perhaps resolution with a mechanistic rather than an empirical model would be required in the future.

5.4.5 Charge, Scaffold Design and Applicabiltiy

Traditionally, pure gelatin[150] or gelatin-based[142] MPs were designed to deliver protein or other charged molecules due to their inherent charged nature. The common forms of gelatin used in MP formation are type A or type B, named due to the processes industrially used to derive them Acid treatment or Alkaline (Basic) treatment respectively [178]. Gelatin type A also known as basic gelatin[143] has an isoelectric point (pI) ranging from 7.0 to 9.0 and hence possesses a net positive charge in solutions at physiological pH. Acidic gelatin or type B has a relatively narrow range of pI from 4.7 to 5.2 and generally tends to possess a net negative charge at physiological pH. MPs have been developed from both acidic and basic types of gelatin along with biodegradable capabilities to prolong the release of a loaded oppositely charged protein or growth factor[142] for over 30 days. Here we chose not to incorporate charge as a factor of controlling release by using type B or acidic gelatin. Both GM-CSF and DEX used here, are negatively charged molecules and hence would have likely been readily released from the gelatin MPs, hence charge was definitely not a release rate-determining factor. Since we were interested in delivering these molecules only within the time frame of 1 week, the charge-repelling nature of this system did not particularly concern us. Further, the properties of PGN may widely vary based on the mechanism of purification[179], and although PGN may have varied in widely in size and charge, we were unable to obtain

the relevant information from the manufacturer. Using known values of size and charge for PGN would allow improved design of the delivery system.

Alternatively, this scaffold design could be used to deliver factors other than GM-CSF, DEX and PGN. Any protein or growth factor possessing a net negative charge at physiological pH such as epidermal growth factor (EGF, pI = 4.6[180]) or could be delivered in a similar manner as the currently-used biomolecules, as it was clearly illustrated by our results that size of the loaded biomolecule played a relatively smaller effect than varying glutaraldehyde concentration on the release profile (Figures 5.6, 5.8-5.13). Molecules with pI in the relatively neutral range of 7.0-8.0 such as homologs of IL-10 cytokine family[181] may also be delivered by the current scaffold design although release times may be slightly increased due to any polyion complexations these cytokines may undergo with the crosslinked gelatin. Highly positively charged cytokines pI > 9 may require further material modification of the gelatin MPs and as such cannot be effectively delivered by the current design.

The MI scaffold designed here possesses the ability to deliver GM-CSF, DEX and PGN in temporally distinct profiles. The current scaffold design possesses ≈ 1.2 x 10^{10} MPs that are differentially crosslinked. Theoretically, the scaffold would be able to deliver more than three biomolecules as long as the total MP number per scaffold is within the saturation level for the associated agarose solution used. With respect to DC cultures, an additional cytokine such as IL-4, essential for DC development from monocytes[31] could be incorporated on to the existing scaffold. Furthermore, DCs have

long known to elicit tolerogenic responses upon capturing apoptotic cells[182]. In-situ targeting of donor-derived apoptotic cells to DCs has correlated with lowered indirect allorecognition and allograft vasculopathy in a fully-mismatched aortic allograft model[183]. Incorporating apoptotic cells can have many advantages including transference of a strong signal of immunosuppression to DCs[184], serve as a rich source of MHC molecules[185] and can be easily obtained and prepared for use. The MI scaffold can be seeded with apoptotic cells for achieving either alleviation of allograft rejection or autoimmune therapy. We speculate that endogenous DCs recruited by the MI scaffold would be able to process the additional apoptotic material and elicit improved targeting of their tolerogenic responses.

CHAPTER 6 EFFECTIVENSS OF THE MULTIFUNCTIONAL IMMUNOMODULATORY SCAFFOLD IN GENERATING FUNCTIONAL ALTERNATIVELY ACTIVATED DENDRITIC CELLS

6.1 Overview

Development of immunotherapies to direct dendritic cell (DC) phenotypes is clinically significant in the context of cancer vaccines, tissue engineering, autoimmune disorders and allogeneic transplant rejection. Particularly, for the latter two applications, involvement of tolerogenic or regulatory DCs either externally delivered or endogenously generated is critical to the reversal or reduction of disease outcomes.

Dendritic cells are professional antigen presenting cells, serving as a crucial link between innate and adaptive immune responses[33]. Dendritic cells, available in a variety of subsets within the body, either circulating or tissue-resident, in their homeostatic state have the ability to regulate auto-reactivity of T-cells to harmless and self-antigen thereby contributing to constitutive peripheral tolerance[5]. When activated by PAMPs during infections, they undergo a change in phenotype and dynamically initiate powerful, protective antigen-specific T-cell and humoral responses to eliminate the infection. When there is a loss or aberrance in DC-mediated immune regulation, the resultant T-cell or antibody response to self-antigen can cause autoimmune diseases such as Multiple Sclerosis (MS), Rheumatoid arthritis (RA), Systemic Lupus Erythematosus (SLE) [186].

and many others[187,188]. In allogeneic transplantations, however, the rejection of transplants is associated with active immunogenesis by host DCs and sometimes, by donor DCs, as in graft-versus-host-disease[189,190]. In both cases (autoimmunity and transplant rejection), an induction of tolerogenic behavior in respective DCs, preferably in an antigen-specific manner, may be sufficient in reversing disease symptoms. *In vitro*, a variety of tolerogenic DCs have been generated with the aid immunosuppressive agents such as corticosteroids[17,69-73], vitamin D3[74-77], immunosuppressive cytokines such as IL-10[78-82] and others, rapamycin[83-85], neuropeptides[86,87] and many more[88-93], either alone or in combination with others treatments. Among them, IL-10-, vitamin D3-, dexamethasone-, and rapamycin-induced tolerogenic dendritic cells are most prominent types, well-studied in mouse and/or human systems. In addition to simple tolerogenic treatments, combinations with maturation stimulators have also been explored: sometimes known as semi-mature or aaDCs[23], these are essentially DCs with tolerogenic behavior that also possess LN-migratory capability similar to steady-state, homeostatic DCs[191]. Maturation agents used typically are TLR agonists or pro-inflammatory cytokines. Many groups[23,192,193] have shown stable DC phenotypes of semi-mature features when treated with maturation stimuli after immunosuppressive treatments[17,23]. With a growing knowledge of DC biology, there is need to develop translatable methods for delivering or endogenously generating these types of DCs for effective immunotherapies.

Biomaterials can serve as excellent vehicles for delivering encapsulated cells or biomolecules for *in vivo* therapies. Considerable research done in the area of host

response to biomaterials, either singularly or as part of complex combination devices including biologics, shows that DCs are critical to the success of these materials[194-197]. Playing a unique role in the host response, DCs are also known to respond to biomaterials differentially by undergoing changes in their expressed phenotypes[13,25,106]. A synthetic material such as PLGA can give rise to a mature, activated DC phenotype whereas a naturally derived material such as agarose can maintain immature DCs in their relatively quiescent state. Additionally, agarose-treated DCs can behave similar to native regulatory DCs and can polarize a regulatory T-cell response towards associated antigen[107]. It is essential to incorporate these features into the therapeutic design of biomaterial in order to effectively develop disease-specific treatments for immunomodulation.

Herein, we describe the *in vitro* testing of a multifunctional, multicomponent immunomodulatory (MI) scaffold developed as described in Chapter 5 for the generation of functional DCs from human and murine precursors, with tolerogenic as well as migratory properties. The scaffold itself is made of porous cryogel scaffold from agarose hydrogel, a substance known to support immunomodulatory features of DCs. Embedded inside the scaffold are differentially crosslinked gelatin microparticles that will release GM-CSF (during days 0-3), DEX (days 3-5/6) and PGN (day 5/6). The hypothesis implied here is that GM-CSF would induce differentiation of iDC from human peripheral blood mononuclear cell precursors or murine bone marrow-derived dendritic cell progenitors. Subsequently, DEX, a powerful glucocorticoid, would induce tolerogenic DCs from iDCs, upon which following PGN treatment would engender late-stage maturation to give rise to aaDCs with enhanced migratory abilities. To show proof of

concept and theoretically simplify the model, we used only DEX and PGN in the MI scaffold whereas GM-CSF was added as a soluble agent during culture. The efficacy of the MI scaffold to act as an alternative for standard culture, serving as a single niche for aaDC enrichment, was also evaluated. We propose that a localized and temporally controlled delivery system of these biomolecules would be able to recapitulate the development of aaDCs *in vitro*. Furthermore, if implanted in an *in vivo* model, we expect that the MI scaffold would be capable of recruiting endogenous precursors to the implant site for aaDCs induction that and subsequently, migrate to the draining LNs, thereby promoting the presentation of any co-delivered antigen.

6.2 Methods

6.2.1 Animals:

Animal care and treatment were in compliance with the Institution Animal Care and Use Committee at Georgia Institute of Technology. Male C57BL/6 mice of 8-12 weeks old were purchased from Jackson Labs, Bar Harbor, ME. Mice were housed at 6 or less per cage and allowed to acclimate for 1 week prior to receiving experimental treatments. Male 2D2 mice were obtained from Dr. Brian Evavold, Emory University, Atlanta, GA.

6.2.1.1 Human Peripheral Blood-Derived DC Culture and MI Scaffold Treatment:

Peripheral human blood was collected from consenting healthy donors and treated with an anticoagulant, namely heparin at 333U/ml blood (Baxter Healthcare Corporation,

Deerfield, IL in accordance with protocol #H10011 of the Institutional Review Board of Georgia Institute of Technology. DCs were differentiated from peripheral blood mononuclear cells (PBMCs) as previously published [198,199] with modifications for MI scaffold treatment.

Briefly, the collected blood was diluted 1:1 in phosphate buffer saline free of Mg and Ca ions (D-PBS; Invitrogen, Carlsbad, CA), and the PBMCs were collected by differential centrifugation using lymphocyte separation medium (Cellgro MediaTech, Herndon, VA). Residual red blood cells in the suspension were lysed (155 mM NH_4CI, 10 mM $KHCO_3$, 0.1 mM EDTA) and the PBMCs were washed with D-PBS. Ten milliliters of PBMCs were plated in a Primaria 100 × 20 mm^2 tissue-culture dish (Becton Dickinson, Franklin Lakes, NJ) at a concentration of 5×10^6 cells/ml in DC media [RPMI-1640 (Invitrogen), 10% heat inactivated FBS (Cellgro MediaTech) and 100 U/ml of penicillin/streptomycin (Cellgro MediaTech)]. After 2 h of incubation at 37°C, the dishes were washed with DC media to remove non-adherent cells. The remaining adherent monocytes were hydrated with warm DC media and supplemented with cytokines [1000 U/ml human recombinant GM-CSF and 800 U/ml IL-4 (PeproTech, Rocky Hill, NJ)]. One dish was retained solely for scaffold treatment, to which one (70% ethanol-) sterilized MI scaffold to get final concentration of DEX (2×10^{-6} M) and PGN (5μg/ml) was placed in the dish-center and gently swirled twice on days 0, 1, 2, 3, 4, 5; whereas another dish was treated on day 5 with 10^{-6} M DEX (which was to later receive DEX and PGN on day 6) All remaining plates were incubated for 5 days without swirling upon which the scaffold-untreated cells developed into iDCs.

On day 5 of culture, loosely adherent and non-adherent cells were harvested from plates without the scaffold and re-suspended in DC media 10^5 cells/ml. All cells were supplemented with cytokines as before. Immature DCs were exposed to control treatments such as LPS at 1μg/ml (Sigma-Aldrich), DEX 10^{-6}M (Sigma-Aldrich) and PGN at 5μg/ml (Sigma-Aldrich) for 24 hours or left untreated.

On day 6, the MI scaffold was gently extracted from the sole remaining plate, loosely adherent and non-adherent cells were collected in conical tube (Beckton Dickinson). To remove any loosely adherent cells from the scaffold without mechanical agitation (that would likely alter the release profile for biomolecules from it as well as activate quiescent DCs), scaffold was incubated for 5 min with 5 ml of a salt-based cell dissociation solution (Gibco) and 5ml of media. Subsequently, the scaffold was washed with 10 ml of warm media on both sides and the remaining supernatant was added to the same conical tube. The conical tube thus containing 30ml of MI scaffold-treated cells were centrifuged at 1100 rpm and re-suspended media at 10^5 cells/ml. All cells were analyzed using flow cytometry (Beckton Dickinson, LSR II) by staining with fluorescently labeled antibodies against CD80 (Beckton Dickinson, Clone L307.4) CD83(Beckton Dickinson, clone HB15e), CD86 (Ancell, clone: BU63), HLA-DR (Beckton Dickinson, G46-6, HLA-DQ (Beckton Dickinson, Tu169), DC-SIGN (R&D Systems, Clone 120507) and/or ILT-3 (BioLegend, clone ZM4.1). Analysis was done using FlowJo software (TreeStar Inc.) to obtain cell numbers and/or median fluorescence intensity. A small portion of cells were retained for up to 3 days after control treatments,

to obtain supernatant from cell culture for subsequent cytokine analysis. Secreted IL-10 and IFN-γ were assessed using ELISA kits (R& D Systems) according to manufacturer's protocol.

6.2.2 Mixed Lymphocyte Reaction of Human DCs with Allogeneic Naïve T-Cells

Mixed lymphocyte reaction was performed to determine the extent of reduction in the proliferation allogeneic T-cell when co-cultured with MI scaffold-derived DCs using a method adapted from previously published research[200,201]. Briefly, on Day 6 of human DC culture, stimulator cells are prepared by suspending DONOR 1 DCs (iDCs, mDCs, tDCs, DEX+PGN-DCs and MI DCs) in MLR media (RPMI 1640 (Invitrogen) and 10% Human-AB serum, heat-inactivated). Treatment of DCs with mitomycin-c was not be necessary, as these purified DC populations are not expected to be capable of any proliferation. In addition, mitomycin may act as a "suppressive" factor for the DCs thereby interfering with the true analysis of the MI scaffold-treatment of DCs. DONOR 2 PBMC without monocyte fraction were obtained by following the procedure from Day 0 of the above mentioned human DC culture excluding the last 2h-incubation step; non-adherent cells were collected and instead the adherent monocyte population were discarded. Resulting population consist of T and B cells. The T-cell population was enriched by negative selection using a human Pan T-cell isolation kit (Miltenyi Biotec) (according to manufacturer's protocol) to obtain responder cells re-suspended in MLR media. To a 96-well plate 100 µl each of stimulator and responder cells along with 100 µl of media were added at ratios of DC to T-cell from 1:100 to 1:6.25. Each sample was run in triplicate. After 3 days of incubation at 37°C, the cells were harvested and analyzed for

proliferation using a bromodeoxyuridine (brdU) assay (Roche) according to manufacturer's protocol.

6.2.3 Murine Bone Marrow-Derived DC (BMDC) Culture and MI Scaffold Treatment:

Bone marrow-derived DC culture was performed according to a previously published protocol[202] with modifications made for MI scaffold incorporation. Briefly, femurs and tibia of male mice were isolated and their bone marrow was flushed out using a 20ml syringe (Beckton Dickinson) with a 26G needle with Hank's balanced salt solution (HBSS) (Invitrogen) compensated with 10% fetal bovine serum (FBS) (Gibco). Red blood cells were lysed with a buffer containing 155 mM NH_4CI, 10 mM $KHCO_3$, 0.1 mM EDTA for 5 min before centrifugation at 300 Xg for 5 min. Cells were washed twice and re-suspended in a media consisting of DMEM (Mediatech), 100 U/ml penicillin and streptomycin (Mediatech), 1% non-essential amino acids (Mediatech), 1% sodium pyruvate (Mediatech), 1% HEPES buffer (Mediatech), 0.1% 2-mercaptoethanol (Gibco) and 10% FBS. Cells were plated on to a 6-well plate (Corning) at 10^6 cells/ml and supplied with 20 ng/ml of murine recombinant GM-CSF (PeproTech) and murine recombinant IL-4 (PeproTech) each. Cells were gently swirled in plates every 2 days when half the media was refreshed and additional dose of cytokines was added (20ng/ml of GM-CSF and 20ng/ml of IL-4). On day 4, only one group of cells received 10^{-6} M of DEX (Sigma-Aldrich); these cells were to later receive DEX and PGN on day 6. On day 6, loosely adherent and non-adherent cells were harvested and re-plated in a 12-well plate (Corning) at 10^6cells/ml with fresh cytokines (20 ng/ml of GM-CSF and 20 ng/ml of IL-4). Cells received treatment of LPS (1μg/ml) (Sigma-Aldrich) or IL-10 (50ng/ml)

(PeproTech) or DEX (10^{-6} M) (Sigma-Aldrich) and PGN (5μg/ml) (Sigma-Aldrich) or left untreated.

For cell culture with the MI scaffold, on day 0, one scaffold was placed in a single well and hydrated with 3 ml of cell media to which bone marrow-derived cells were added along with the required cytokines to get a total concentration 10^6 cell/ml. These MI scaffold-treated cells were swirled gently in their plates twice a day at fixed times and received fresh media every 2 days with fresh cytokines similar to their scaffold untreated counterparts. On day 8, these cells were harvested by gently washing the scaffold with fresh warm media on both sides to dislodge any loosely-adherent cells; the scaffold was treated with 5 ml of a salt-based cell-dissociation solution for 5 min on both sides after which the cells washed, and pooled with the non-adherent fraction. Note: Only the scaffold was treated with the cell-dissociation solution and not the wells themselves. Any cells adherent to the wells were discarded.

On day 8, cells from all treatment groups including the MI scaffold were collected and labeled separately. Certain cells received MOG_{35-55} peptide (Dr. Brian Evavold, Emory University) at a concentration of 100 ng/ml for 4 hours, after which the cells were washed in fresh media or prepared for analysis with flow cytometry.

For flow cytometry, the cells may or may not have been pre-blocked with Fc block (BD Pharmingen) prior to staining with antibodies. Cells suspended in FACS buffer (100 ml D-PBS (Invitrogen), 1% Bovine Serum Albumin (BSA) (Sigma-Aldrich),

0.1% Sodium Azide (Sigma-Aldrich), pH 7.4) were stained with fluorescently labeled antibodies against CD80 (Clone 1610A1, BioLegend), CD86 (clone GL1, eBioscience), CD11c (Clone HL3, BD Pharmingen), MHC I-A/I-E (Clone M5/114.152, eBioscience), PirB (Clone FAB275GP, R&D), MHC H2K (Clone AF688.5, BioLegend) and/or CD54/ICAM-1 (3E2, BD Pharmingen). Stains were performed either individually or as multicolor for 40min at 4°C in the dark and re-suspended at $5x10^6$cells/ml of FACS buffer after straining cells gently through a sterile 40 μm mesh (Nalgene) to obtain a single-cell suspension. Cells were analyzed with BD LSR II. Dead cell staining with 5 μl Propidium iodide (BD Pharmingen) was done to eliminate dead cell population during gating. PirB stained in two sections in flow cytometric output (data not shown), the population for higher MFI was gated as $PirB^{Hi}$. Data was analyzed with FlowJo software (TreeStar). A small portion of cells were retained for up to day 3 days after control treatments, to obtain supernatant from cell culture for subsequent cytokine analysis. Secreted IL-10 and IFN-γ were assessed using ELISA kits (R& D Systems) according to manufacturer's protocol.

6.2.4 Murine MOG Antigen Presentation Assay:

The following procedure adapted from published literature[201] specifically for this study. From BMDC culture, on Day 8, treated DCs (MOG-DC10s, MOG-iDCs, MOG-mDCs, DC10s, MOG-MI DCs) were prepared in RPMI-10 media (RPMI 1640 – Invitrogen with 10% heat inactivated FBS – Gibco) at 5 x 10^5 cells/ml. These were the stimulator cells of the assay. CD4+ T-cells were obtained either directly from 2D2 mouse spleens using negative selection magnetic sorting (Miltenyi Biotec) using manufacturer's

protocol or from a culture of 2D2 splenocytes supplemented with MOG and stimulated subsequently with IL-12 to increase numbers prior to experimental use. Enriched T-cells, the responder cells in the assay, were re-suspended in RPMI-10 media at 4×10^6 cells/ml. To a 96-well plate 100μl each of stimulator and responder cells along with 100μl of media was added. Each sample was run in triplicate. After 3 days of incubation at 37°C, the cells were harvested and analyzed for proliferation using a bromodeoxyuridine (brdU) assay (Roche) according to manufacturer's protocol.

6.2.5 Flow Cytometry with Intracellular Cytokine Staining for BMDCs

Cells were plated on Day 8 of BMDC culture onto a 12-well plate. 10 μg per ml of cells of Brefeldin A or 1 μl per ml of cells (2 μM) Monensin solution were added 8 hours prior to antibody staining. Cells were collected and washed with FACS buffer (100 ml D-PBS(Invitrogen), 1% Bovine Serum Albumin (BSA) (Sigma-Aldrich), 0.1% Sodium Azide (Sigma-Aldrich), pH 7.4) and re-suspended at 10^6 cells/ml for staining with antibodies against IL-10 (BioLegend, clone #JES5-16E3) and IFNγ (BioLegend, clone #XMG12) in 1.7 microcentrifuge tubes (Eppendorf) in the dark. Cells were treated with 100 μl/ml (of cells) 4% paraformaldehyde solution (Sigma-Aldrich) and incubated for 15-30 min also in the dark at room temperature. The cells were washed 3 times with permeabilization buffer [5 ml 10% Saponin solution (Sigma-Aldrich), 95ml FACS buffer, pH to 7.4] and re-suspended in FACs buffer at 10^6 cells/ml or higher in preparation for analysis with a flow cytometer (BD LSR II).

6.2.6 CCR7-Induced BMDC Migration Assay

DC migration was determined with an *in vitro* chemotaxis assay performed according to a previously published method[203] with modifications. On Day 8 of the BMDC culture, a cell suspension of DCs of $1x10^6$ per ml in the migration culture medium of (filter-sterilized RPMI-1640 (Invitrogen) with 1% FBS (Gibco) at pH 7.4) was prepared. 100 μl of cells was added to the upper chamber of a trans-well cell culture chamber (Corning Costar Corp; Corning, New York), containing a 5.0 μm pore size membrane. The lower compartment contained 600 μL of medium with or without CCL19 (100 ng/mL) (R&D: Recombinant Mouse CCL19/MIP-3 beta). A monoclonal anti-CCR7 antibody (100 ng/mL) (R&D: anti-mouse CCR7 mAb (Clone 4B12), Rat IgG2A) was added to the one well in upper chamber representing the Ab-blocked control group. After incubation at 37°C for 2 h, cells that had migrated into the lower compartment were collected and counted using the Coulter counter (Beckman Coulter). Experiments were duplicated and the percentage of migrating DCs was calculated as the number of cells in the lower chamber compared with the number of cells originally added to the upper chamber. The average percentage of DCs that migrated toward CCL19 or anti-CCR7 mAb were compared with the average percentage of cells that spontaneously migrated against the medium.

6.2.7 Statistical Analysis

Two-way ANOVA with multiple comparisons was used instead of the standard method of comparing a treatment group to a control; instead, each group (treatment or control) was compared with every other group individually. While assigning an overall

significance level (α=0.05), it enables calculation of an intermediate significance level (say α*) for each comparison. (This method is also known as α-splitting.) Using a post-test such as Sidak's or Holm-Sidak's largely corrects apparent weakness (conservativeness) of α*. This was ideal for our study which had several treatment groups applied DCs across multiple donors. When two-way ANOVA could not be applied, one-way ANOVA was used followed Sidak's post-test unless otherwise specified

6.3 Results

6.3.1 Treatment of Human PBMC-Derived DCs with MI Scaffold Lowered the Expression of Maturation Markers While Increasing that of Tolerogenic Markers

To assess the ability of the MI scaffold to induce tolerogenic-like DCs, monocytes obtained from human blood were cultured with the scaffold directly from day 0 while simultaneously a parallel culture was carried out to obtain iDCs by Day5 when soluble reagents were added to the culture to obtain controls such as LPS (mDCs), TGF-β+IFN-α (tDCs) and DEX+PGN. On Day 6, cell surface marker analysis (Figure 6.1) shows that markers characteristic of DC activation such as MHC II molecules (HLA-DQ, HLA-DR) and co-stimulatory molecules (CD80, CD86)[37] were expressed at lower levels while an inhibitory DC marker, immunoglobulin-like transcript 3 (ILT-3)[204] was increased in expression for MI scaffold-treated DCs (hence called MI DCs). This feature, consistent across donors, was similar to that of tDCs and DEX+PGN DCs while being vastly distinct from mDCs, indicating that the MI scaffold exposed to monocytes on day 0 were

able to differentiate them into inhibitory DCs by releasing their payload over a course of 5-6 days.

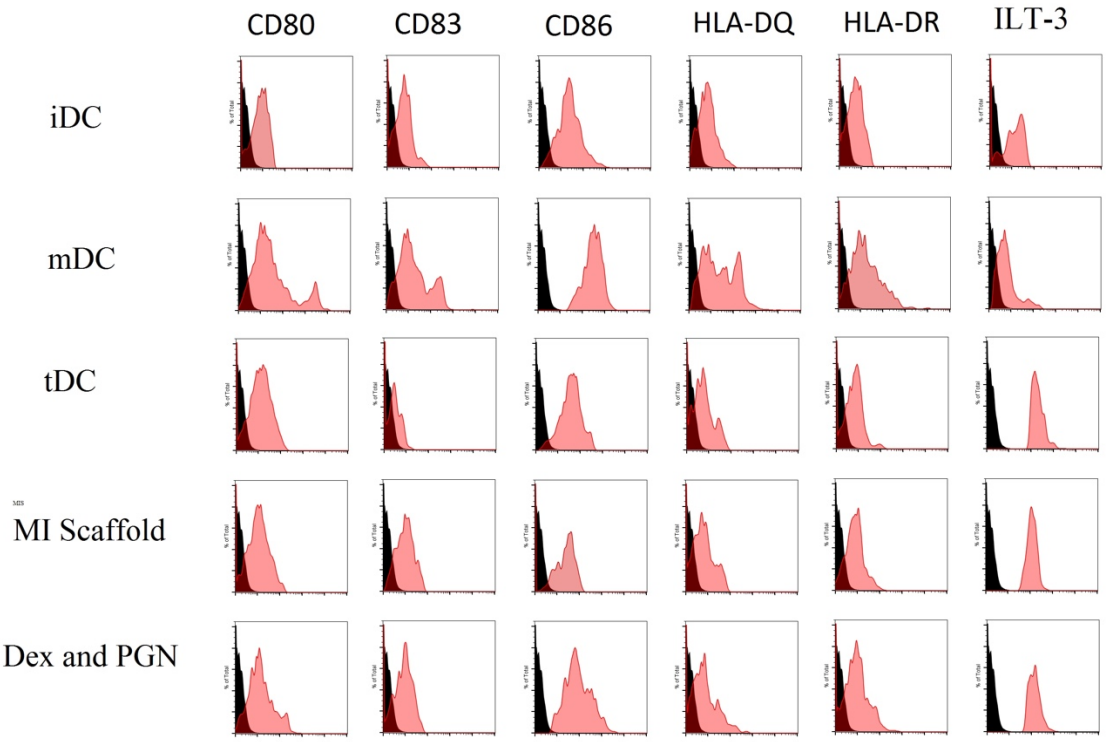

Figure 6.1 Dendritic cells cultured with MI scaffold increase expression of inhibitory marker while decreasing MHC II and co-stimulatory molecules.

MI DCs show increased expression of ILT-3 similar to tDCs and DEX+PGN DCs, and decreased expression of CD80, CD83, CD86, HLA-DQ and HLA-DR compared to mDCs. iDCs. - immature DCs, mDCs- mature DCs were treated with lipopolysaccharide(LPS), tDCs- tolerogenic DCs induced with interferon-α and interleukin-10. DEX+PGN DCs – DEX and PGN were added solubly to culture. Black peaks represent autofluorescence of unstained cells while red peaks indicate

the respective surface marker. This experiment was repeated n=6 times with similar results, and representative results are shown.

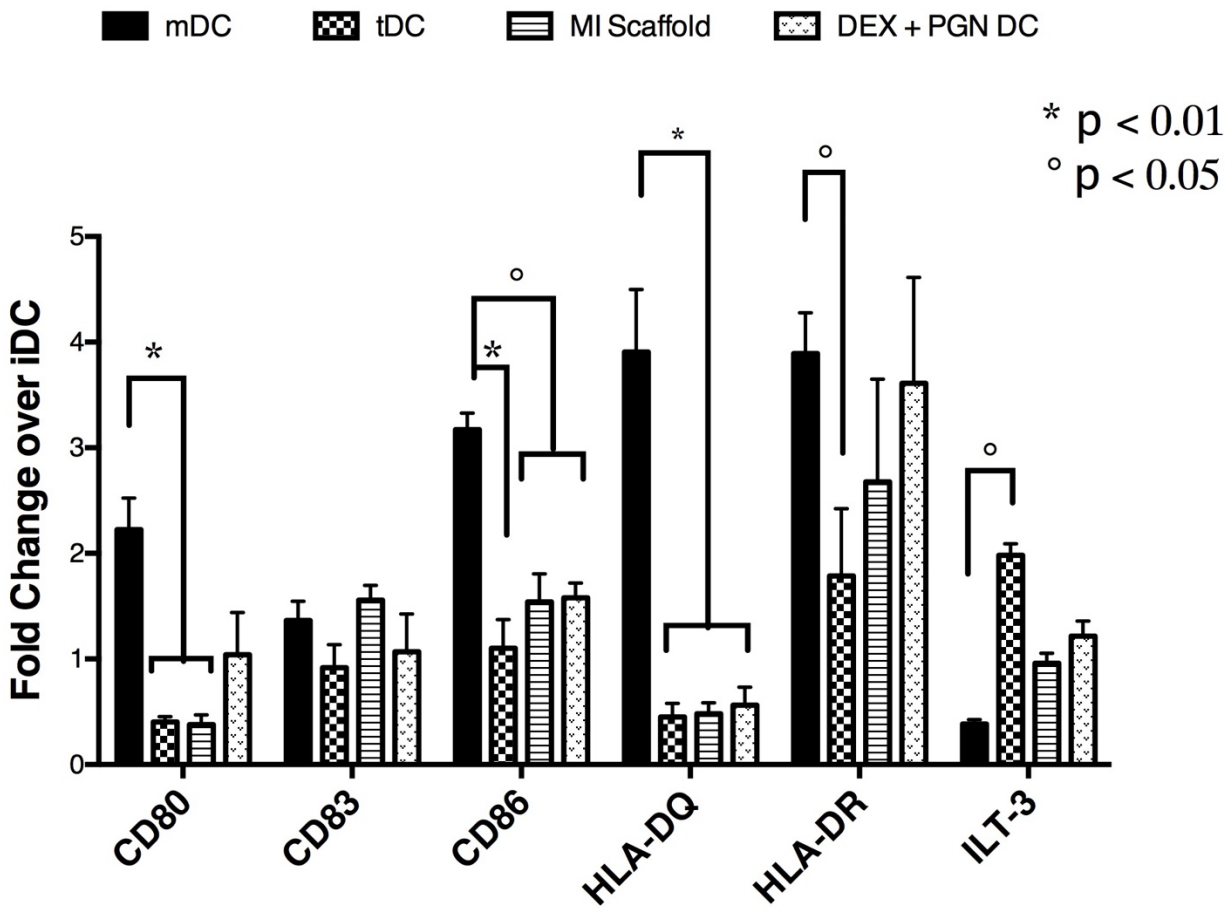

Figure 6.2 Fold change of geometric Mean Fluorescence Intensity (gMFI) of human MI scaffold-treated DCs over iDCs.

Dendritic cells cultured with MI scaffold decrease expression of MHC II and co-stimulatory molecules. MI DCs show decreased expression of CD86 and HLA-DQ compared to mDCs. iDCs. - immature DCs, mDCs- mature DCs were treated with lipopolysaccharide(LPS), tDCs- tolerogenic DCs induced with interferon-α and interleukin-10. DEX+PGN DCs – DEX and PGN were added solubly to culture.

Statistics was done using two-way ANOVA followed by multiple comparisons of treatment groups for each surface markers using Sidak's post-test and p-values < 0.05 were accepted. Adjusted p-values were calculated for individual comparisons and are as follows * $p < 0.01$ and # $p < 0.05$. Error bars represent standard errors over n=6 donors.

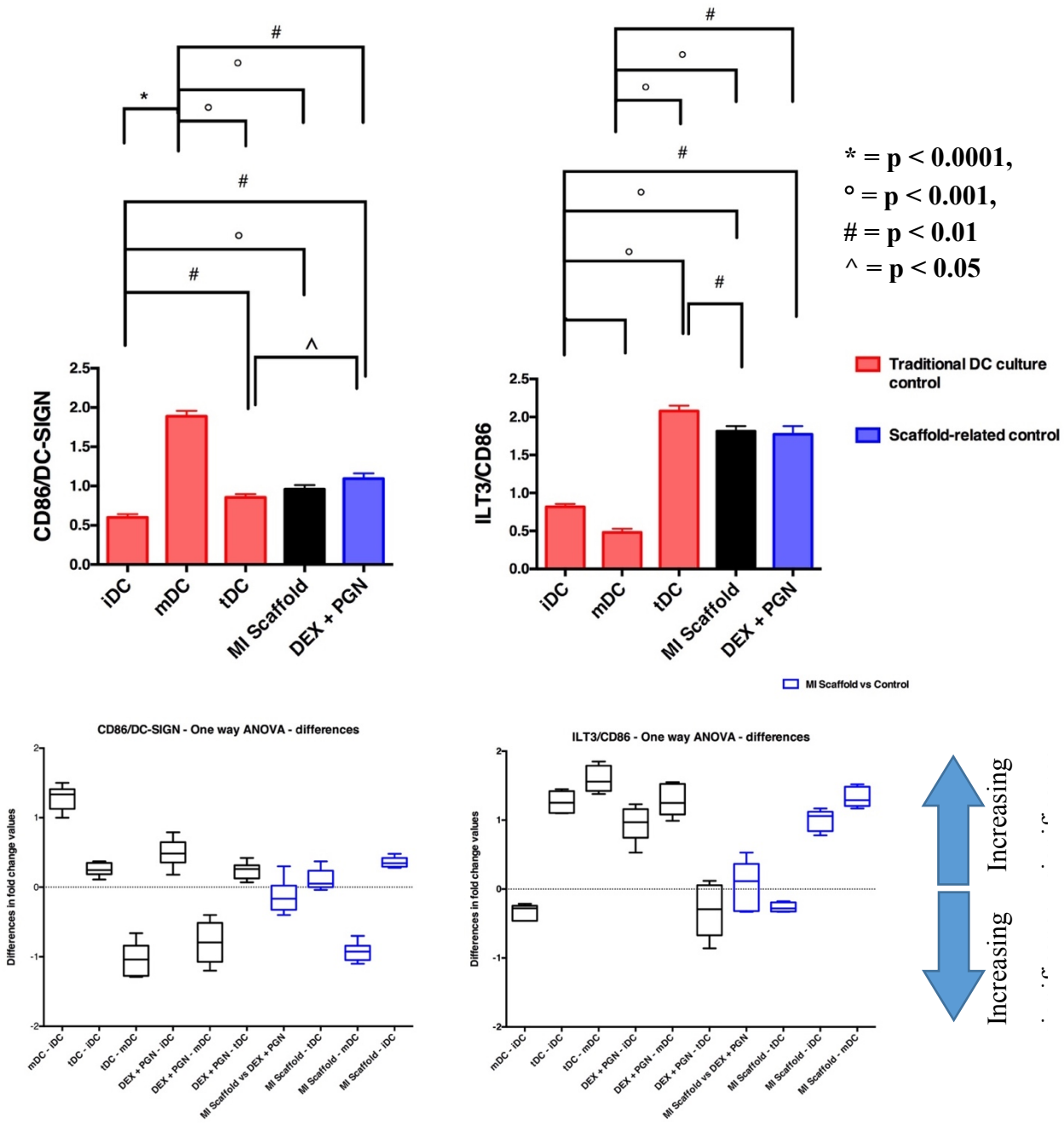

Figure 6.3 Surface marker expression on MI Scaffold-treated human DCs.

(upper left panel) Maturation marker shows fold change of GMFI of CD86/DC-SIGN, (upper right panel) tolerogenic marker show fold change of ILT-3/CD86. iDCs- immature DCs, mDCs- mature DCs were treated with lipopolysaccharide(LPS), tDCs- tolerogenic DCs induced with IFN-α and IL-10.

DEX+PGN DCs – DEX and PGN were added solubly to culture. **Statistics was done by one-way ANOVA followed by multiple comparison of paired values within each treatment group using Holm-Sidak's post-test and p-values < 0.05 were accepted. Adjusted p-values were calculated for individual comparisons and are as follows * = p < 0.0001, ° = p < 0.001, # = p < 0.01, ^ = p < 0.05. Error bars represent standard error of n=6 donors.**

In Figure 6.3 (upper panel) individual groups in all pairs of comparisons marked, were significantly different. CD86/DC-SIGN (upper left panel), maturation marker, was maximum for the LPS-treated group, i.e. mDCs while being minimum for the untreated or iDCs. The levels for the remaining groups fell in between these two extremes. Also, tDCs were more similar to iDCs than mDCs, whereas MI DCs were equally distinct from both. DEX+PGN DCs were also equally distinct from both albeit at a lower level of significance. MI DCs were not significantly different from either tDCs or DEX+PGN DCs while tDCs and DEX+PGN DCs themselves were only minimally distinct from each other. On the other hand, (upper right panel) the ILT-3/CD86 signal, tolerogenic marker, was greatest for tDCs displaying their superior tolerogenicity and clearly contrasting iDCs and mDCs.

To understand these individual comparisons better, their differences between group means within 95% confidence intervals was plotted (Figure 6.3 lower panel). The baseline at Y=0 in these plots indicates no significant differences while values not overlapping Y=0 are significantly different within any pair. Also, the degree of separation

from Y=0 translates to the extent significance. Due to the order of comparison, for example iDC vs mDC or mDC vs iDC, a plotted value may appear above or below zero; if iDC vs. mDC is negative then it indicates that of the particular marker, the value for mDC is significantly higher than iDC and vice versa. According to these guidelines, Figure 6.3 (lower left panel) shows that MI DCs are not distinct from DEX+PGN DCs or tDCs with respect to maturation marker expression while DEX+PGN DCs and tDCs themselves show significantly lower expression compared to mDCs. MI DCs, however, express CD86/DC-SIGN at significantly lower levels than mDCs and higher than iDCs. In a similar manner, from Figure 6.3 (lower right panel), plotted values of [DEX+PGN DCs vs tDCs] and [MI DCs vs DEX+PGN DCs] intersect Y=0, displaying that these pairs are nearly identical in expressing the tolerogenic marker. MI DCs exhibited slightly lowered expression of the tolerogenic marker compared tDCs while higher than that of iDCs and mDCs.

6.3.2 Treatment of Human PBMC-Derived DCs with MI Scaffold Increased the Secretion of IL-10

As cytokines secreted by cells are a strong indicator of their phenotype and functions, we assessed the cytokines in culture supernatants on days 6, 7 and 8 (day 0 being the day of introduction of MI scaffold to human blood monocytes) using ELISAs. IL-10 is an immunosuppressive cytokine known to be secreted by DCs to produce immune tolerance. In contrast, IFN-γ is produced by DCs in strongly pro-inflammatory environments[205]. Figure 6.4 (upper panel) IL-10 production by DCs receiving any form of tolerogenic factor (DEX or TGFβ) is increased in comparison to untreated (iDC) and

LPS-treated (mDC) controls. Specifically, MI DCs show significantly higher concentration of IL-10 in culture supernatants compared to iDC and mDC on days 6, 7 and 8 while exhibiting significantly lower IL-10 than tDCs and DEX+PGN DCs on day 6 and 7 only. Interestingly, the IL-10 levels in MI DC culture gradually increased over days 6, 7 and 8, such that their levels were maximal and nearly identical to DEX+PGN DCs by day 8; tDCs and DEX+PGN DCs, instead, increased in their IL-10 concentration over days 6, 7 and 8 at a lower rate. To understand this secretion data better, multiple comparisons on individual means were performed with that of every other group and the differences in means along with their 95% confidence intervals were plotted in Figure 6.4 (lower panel). Similar to section 6.3.1, plotted values of pairs overlapping the baseline at Y=0 indicate indistinct comparisons while those clearly above or below Y=0 represent significant differences within each pair. Accordingly, tDCs secreted significantly higher levels of IL-10 than iDCs, mDCs and MI DCs while being nearly identical to that of DEX+PGN DCs on all assessed days. DEX+PGN DCs, similarly, secreted high levels of IL-10 compared to iDCs, mDCs and MI DCs albeit in reducing order significance levels. However, by day 8, the IL-10 levels for MI DCs and DEX+PGN DCs were virtually identical.

Concomitantly, IFNγ levels secreted by mDCs were significantly higher than each of the other treatment groups. Figure 6.5 [Upper Panel] specifically shows the significant differences between mDCs and MI DCs, wherein MI scaffold greatly suppressed the secretion of IFNγ. [Lower Panel], in addition, shows the significant differences between each group with every other group, where, as before, any overlapping values with Y=0

indicate no difference within the respective pair. Although, with respect to IL-10, MI DCs gradually increased cytokine production over day 6, 7 and 8, the IFNγ production profile was interestingly disparate; the IFNγ produced by MI DCs increased from day 6 to day 7 however on day 8 it dropped considerably. In contrast, IFN-γ produced by DEX+PGN DCs clearly increased over the concerned days and was maximal on day 8.

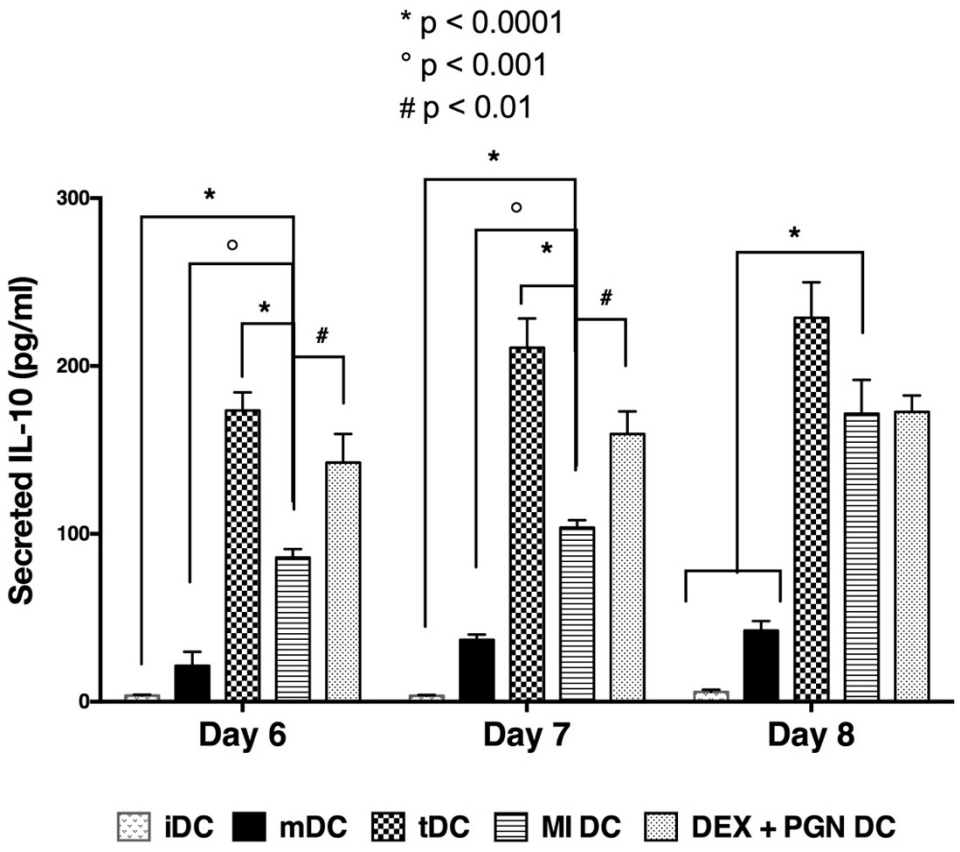
* p < 0.0001
° p < 0.001
# p < 0.01
Secreted IL-10 (pg/ml)
300
200
100
0
Day 6
Day 7
Day 8
iDC
mDC
tDC
MI DC
DEX + PGN DC

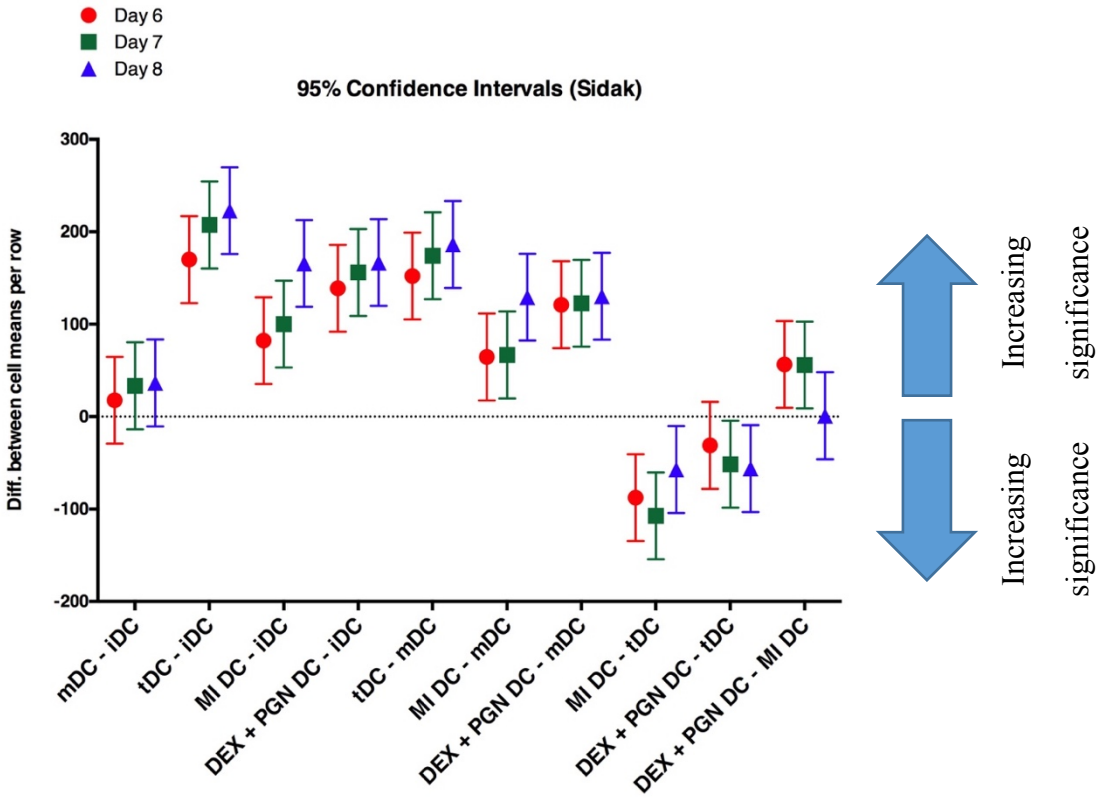
Day 6
Day 7
Day 8
95% Confidence Intervals (Sidak)
Diff. between cell means per row
300
200
100
0
-100
-200
mDC - iDC
tDC - iDC
MI DC - iDC
DEX + PGN DC - iDC
tDC - mDC
MI DC - mDC
DEX + PGN DC - mDC
MI DC - tDC
DEX + PGN DC - tDC
DEX + PGN DC - MI DC
Increasing significance
Increasing significance

Figure 6.4 MI scaffold treatment induced human PBMC-derived DCs to produce IL-10.

An ELISA of IL-10 performed on culture supernatants shows that MI DCs secreted IL-10 at higher levels than iDCs and mDCs while being lower than tDCs and (only slightly) DEX+PGN DCs. (Upper panel) shows ELISA-detected levels of IL-10 in pg/ml of supernatants obtained from DC culture on days 6, 7 and 8. iDCs- immature DCs, mDCs- mature DCs were treated with lipopolysaccharide(LPS), tDCs- tolerogenic DCs induced with IFN-α and IL-10. DEX+PGN DCs – DEX and PGN were added solubly to culture. Statistics was done using multiple comparison of paired values within each treatment group and time-points using two-way ANOVA with multiple comparisons followed by Sidak's post-test and p-values < 0.05 were accepted. Adjusted p-values were calculated and are as follows * = p < 0.0001, ° = p < 0.001 and # = p<0.01. Error bars represent standard error of n=6 donors. (Lower panel) represents differences in pair means with 95% CI obtained from statistical analysis. Note: (Upper panel) only shows comparisons made between control groups and MI DCs while actual statistics was performed on entire data set which is represented in the (lower panel).

* p<0.0001

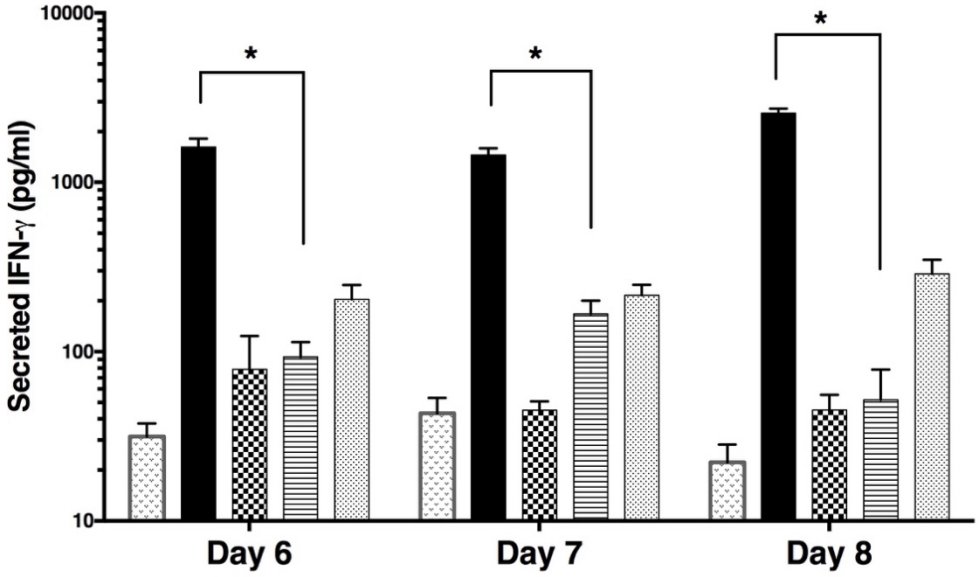
Secreted IFN-γ (pg/ml)
10000
1000
100
10
*
*
*
Day 6
Day 7
Day 8
iDC
mDC
tDC
MI DC
DEX + PGN DC

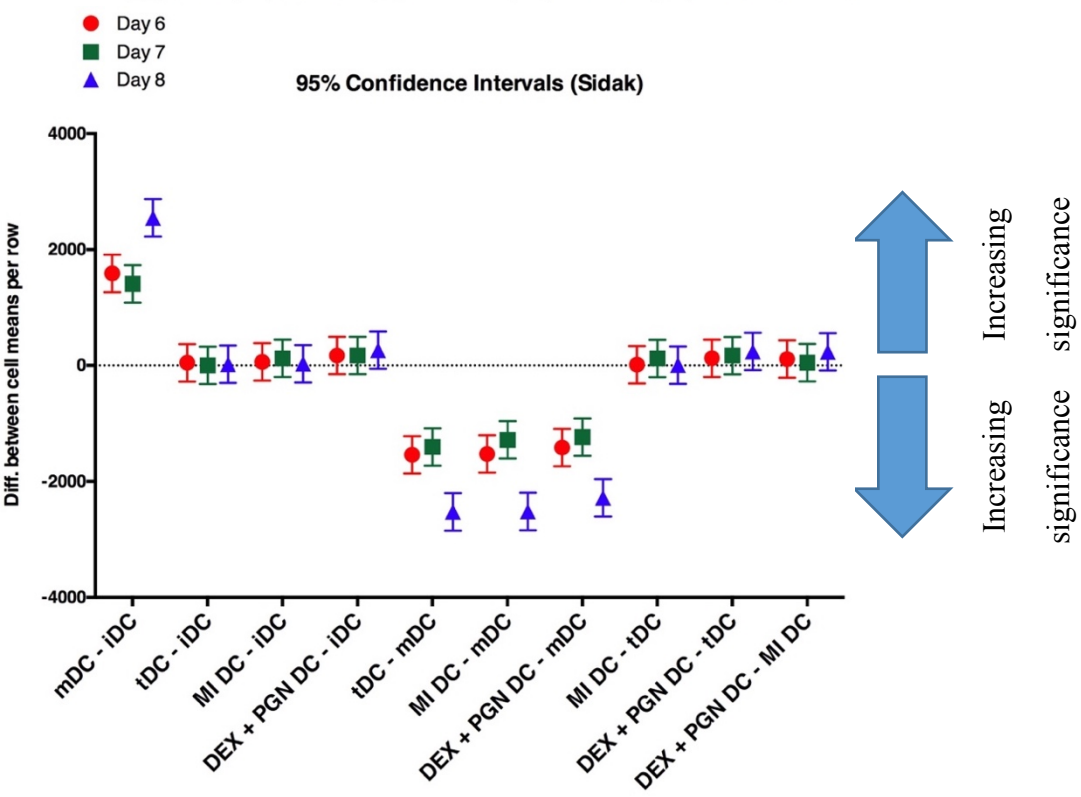
Day 6
Day 7
Day 8
95% Confidence Intervals (Sidak)
Diff. between cell means per row
4000
2000
0
-2000
-4000
mDC - iDC
tDC - iDC
MI DC - iDC
DEX + PGN DC - iDC
tDC - mDC
MI DC - mDC
DEX + PGN DC - mDC
MI DC - tDC
DEX + PGN DC - tDC
DEX + PGN DC - MI DC
Increasing significance
Increasing significance

Figure 6.5 MI scaffold treatment induced human PBMC-derived DCs to lower secretion of pro-inflammatory cytokine

IFNγ compared to mDCs. An ELISA of IFNγ performed on culture supernatants shows that MI DCs secreted IFNγ at lower levels than mDCs while being indistinct from tDCs and DEX+PGN DCs. (Upper panel) shows ELISA-detected levels of IFNγ in pg/ml of supernatants obtained from DC culture on days 6, 7 and 8. iDCs- immature DCs, mDCs- mature DCs were treated with lipopolysaccharide(LPS), tDCs- tolerogenic DCs induced with IFN-α and IL-10. DEX+PGN DCs – DEX and PGN were added solubly to culture. Statistics was done using multiple comparison of paired values within each treatment group and time-points using two-way ANOVA with multiple comparisons followed by Sidak's post-test and p-values < 0.05 were accepted. Adjusted p-values were calculated and * = p < 0.0001. Error bars represent standard error of n=6 donors. (Lower panel) represents differences in pair means with 95% CI obtained from statistical analysis. Note: (Upper panel) only shows comparisons made between control groups and MI DCs while actual statistics was performed on entire data set which is represented in the (lower panel).

6.3.3 Treatment of Human PBMC-Derived DCs with MI Scaffold Suppressed Proliferation of Allogeneic T-cells in a Mixed Lymphocyte Reaction (MLR)

To establish whether the DCs generated by the MI scaffold were functional in addition to possessing tolerogenic-like surface markers and secreted cytokines, these DCs were co-cultured with naïve T-cells obtained from an allogeneic donor at different DC to

T-cell ratios from 1:100 to 1:6.25 over the course of 3 days (Figure 6.6 Top panel). T-cells co-cultured with DCs at the highest ratio of 1:6.25 (DC:T-cell) exhibited the highest extent of proliferation after being normalized over the total number of (untreated) T-cells used on the first day prior to co-culturing. On analyzing the only this group (1:6.25) further, (Figure 6.6 middle panel) we noticed that T-cell proliferations levels induced by MI DCs significantly lower than that of immunogenic mDCs, higher than iDCs and also tDCs, and nearly indistinct from DEX+PGN DCs. Furthermore, comparing each group (not only MI DCs) to every other group among all treatments, (Figure 6.6. Bottom panel) shows that mDCs are the most potent at initiating allogeneic T-cell responses. Although containing a TLR-agonist such as PGN both MI DCs and DEX+PGN DCs induced significantly lower levels of allogeneic T-cell responses. iDCs, on the other side of the spectrum were the least capable of any allogeneic proliferative T cell responses while, interestingly, even tDCs elicited slightly (i.e. lower significance level) better responses.

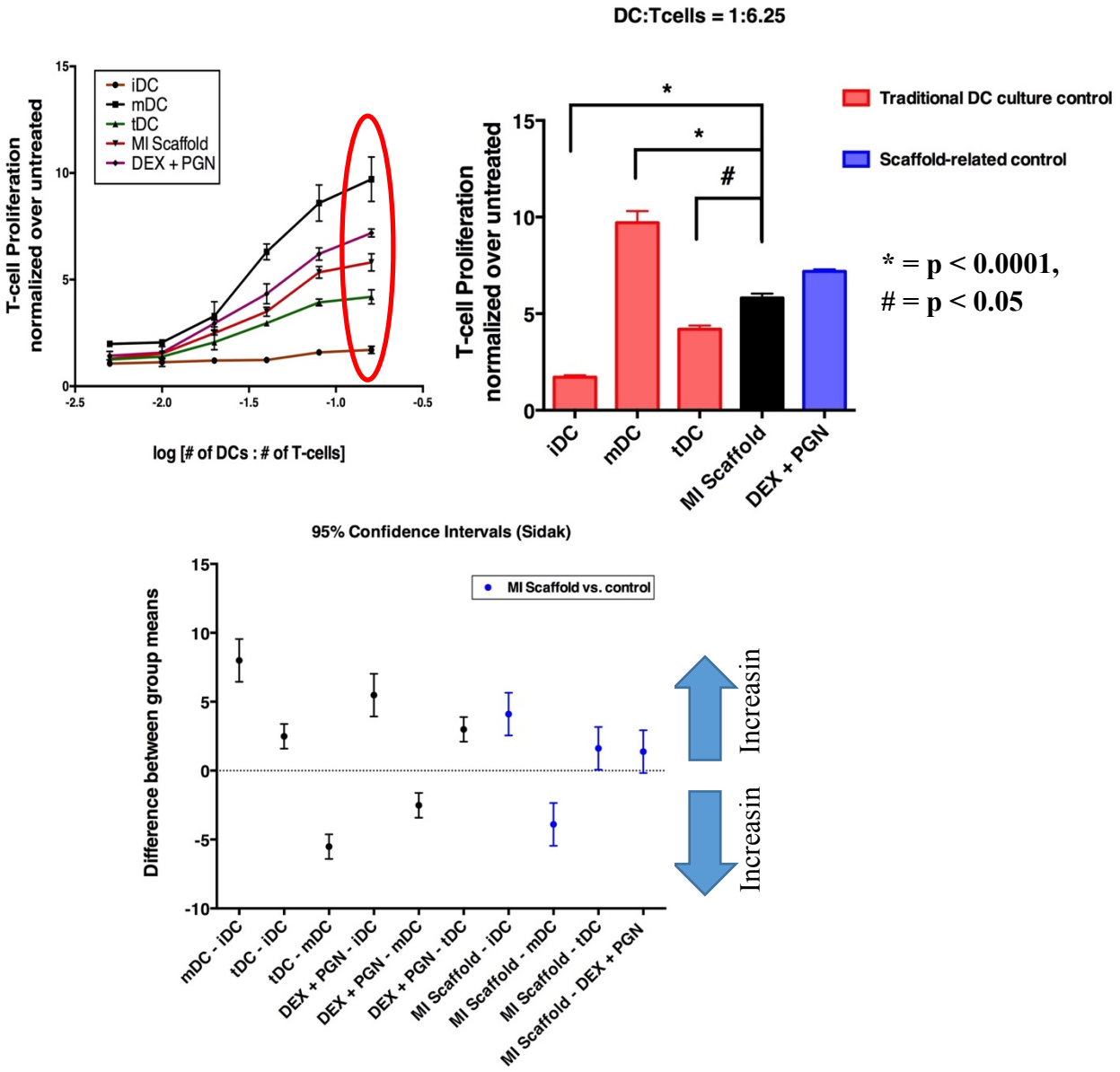

Figure 6.6 Mixed lymphocyte reaction with allogeneic T-cells: MI-scaffold treated human PBMC-derived DCs lowered T-cell proliferation compared to mDC control, in a dose-dependent manne.

(upper panel) Red ellipse represents the DC-T-cell ratio of 1:6.25. (lower panel) T-cell proliferation for DC:T-cell of 1:6.25 only are shown normalized to untreated T-cells. iDCs- immature DCs, mDCs- mature DCs were treated with

lipopolysaccharide(LPS), tDCs- tolerogenic DCs induced with interferon-α and interleukin-10. DEX+PGN – DCs – DEX and PGN were added solubly to culture. Figure is representative of n=1 donor analyzed by doing multiple comparison of unpaired values within each treatment group using one-way ANOVA followed by Dunnett's post-test to correct for multiple comparisons and p-values < 0.05 were accepted. Adjusted p-values were calculated and are as follows * = p < 0.05 and # = p<0.0001. Error bars represent standard error of n=6 readings of same sample.

6.3.4 Treatment of Murine BMDCs with MI Scaffold Lowered the Expression of Maturation Markers While Increasing that of Tolerogenic Markers

Based on our work of developing MI scaffold for human DC culture (see Chapter 5), our proposed optimized MI scaffold formulation (Figure 6.7) for mouse DC cultures contained gelatin MPs at incorporated numbers of 10^{10} MPs, 10^9 MPs and 10^9 MPs and GA crosslinking levels of 6mM, 10mM or 16mM for desired release profiles of mGM-CSF, DEX and PGN, respectively. The MI scaffold was customized for use with mice/ murine cells by altering the loaded molecules and marginally changing the formulation the scaffold (see chapter 5). To evaluate the capability of this MI scaffold system to function in a murine environment (as originally designed for this purpose), we treated bone marrow-derived murine progenitors on day 0 of BMDC culture with the MI scaffold for 8 days. Figure 6.8 shows the fold change of surface GMFIs of all DC treatments over that of iDCs. Maturation-associated surface molecules such as I-A (MHC II) and co-stimulatory molecules (CD86) were lowered in expression for MI DCs and DC10s. Curiously, I-A was highly increased in DEX+PGN DCs, significantly higher than even

mDCs. Secondary co-stimulatory molecule, namely, ICAM-I, known to synergize with B7 family molecules to stimulate CD8+ T-cells rather than CD4+[206], showed increased levels surface expression in MI DCs, DEX+PGN DCs and mDCs in comparison to tDCs. An inhibitory marker of the same class of molecules as ILT-3 (human), PirB surface expression, on the other hand, showed significantly higher levels for DC10s and MI DCs with respect to mDCs and DEX+PGN DCs (lower significance level).

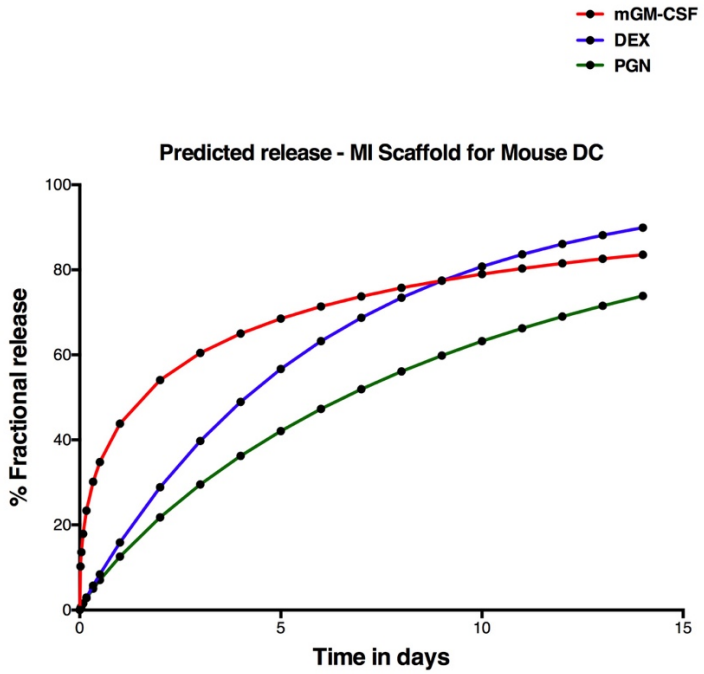

Figure 6.7 Predicted release profiles of mGM-CSF, DEX and PGN loaded into the optimized MI scaffold designed for mouse DC culture.

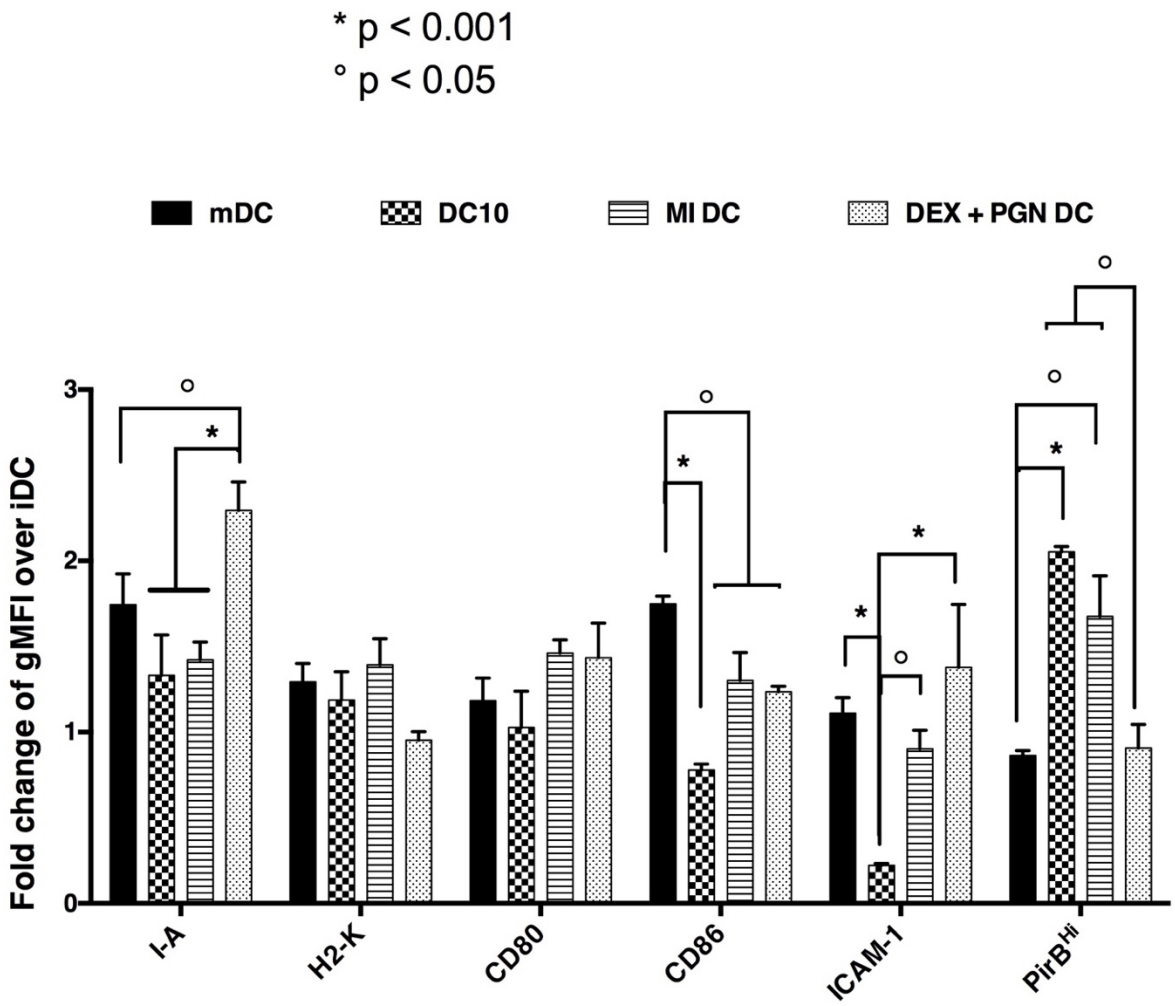

Figure 6.8 Surface marker expression of MI scaffold-treated murine DCs.

Bar graph indicates the fold change of GMFI over iDC on cells obtained on Day 8 of BMDC culture. iDCs- immature DCs, mDCs- mature DCs were treated with lipopolysaccharide(LPS), DC10s- tolerogenic DCs induced with IL-10. DEX+PGN DCs – DEX and PGN were added solubly to culture. Statistics was done by using multiple comparison of paired values within each treatment group using one-way ANOVA followed by Newman-Kaul's post-test and p-values < 0.05 were accepted. Adjusted p-values were calculated and are as follows * = p < 0.0001 and ° = p < 0.05 Error bars represent standard error of n=6

6.3.5 Treatment of Murine BMDCs with MI Scaffold induces Increased Intracellular Expression of Interleukin (IL-10)

In addition to surface markers the intracellular staining for IL-10 and IFNγ was done to determine whether MI DCs derived from murine BMDC progenitors produce suppressive cytokines similar to human MI DCs. Figure 6.9 shows GMFI fold change of intracellular cytokines over iDCs; IL-10 shows significantly higher expression for MI DCs and DC10s compared to mDCs and DEX+PGN DCs. Interestingly, DEX+PGN DCs displayed lowest levels of expression although indistinct from mDCs. Alternatively, the IFNγ expression was lowered in both DC10s and MI DCs distinct from mDCs while only DC10s were also different from DEX+PGN DCs.

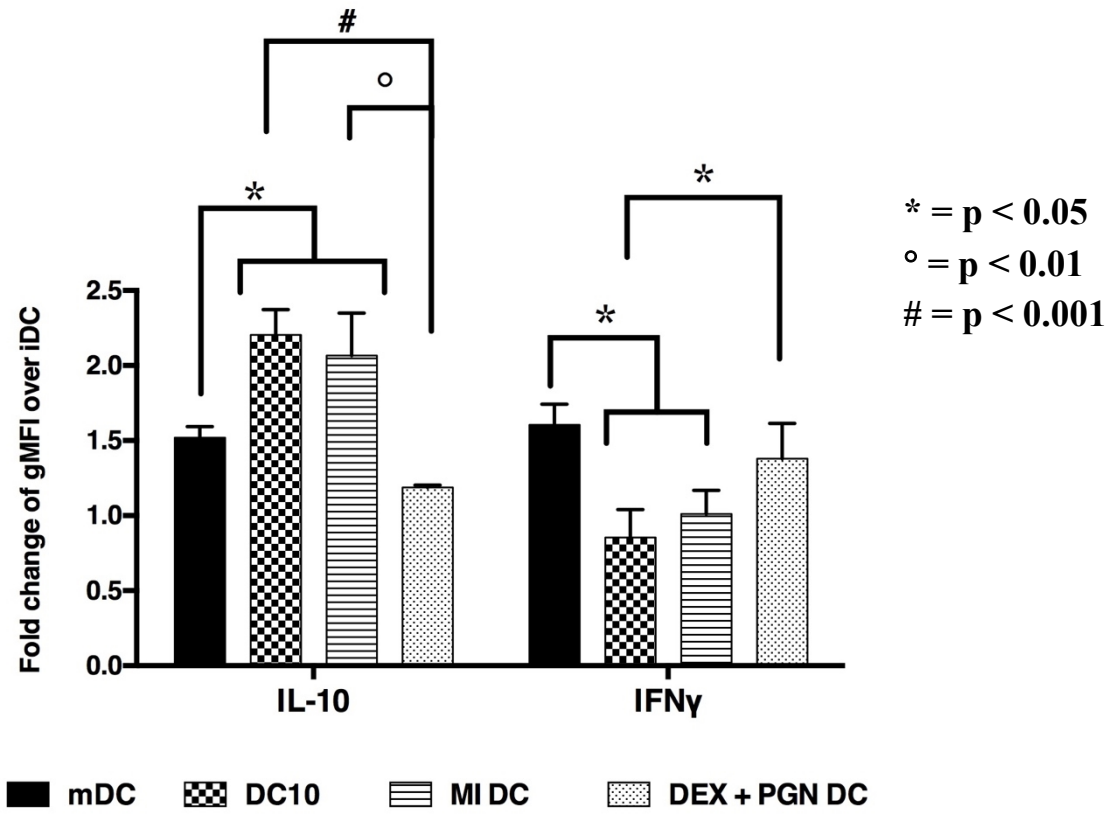

Figure 6.9 Intracellular cytokine expression of MI scaffold-treated murine DCs. Bar graph indicates the fold change of GMFI over iDC on cells obtained on Day 8 of BMDC culture. iDCs- immature DCs, mDCs- mature DCs were treated with lipopolysaccharide(LPS), DC10s- tolerogenic DCs induced with IL-10. DEX+PGN DCs – DEX and PGN were added solubly to culture. Statistics was done by using multiple comparison of paired values within each treatment group and cytokine group using two-way ANOVA and p-values < 0.05 were accepted. Adjusted p-values were calculated and are as follows * = p < 0.05, # = p<0.01 and ° = p < 0.001 Error bars represent standard error of n=4

6.3.6 Treatment of Murine BMDCs with MI Scaffold MI Scaffold Increased their Secretion of IL-10

To establish the effectiveness of the MI scaffold in rendering tolerogenic-like phenotype to DCs derived from murine BM progenitors analogous to the MI scaffold experimentation with human cells, the supernatants from the cell culture were analyzed with ELISAs specific for IL-10 and IFN-γ. Previously, for human DCs, the first sampled supernatant was from Day 6 approximately 24 h after introduction of control treatments such as LPS etc. Here however, since the time typically for analyzing controls and treatment with cytometry is 48 h, we use day 8 as the first day of supernatant analysis. To avoid confusion with human data, the days are named as 'day 1', 'day 2' and 'day 3' (corresponding to day 8, day 9 and day 10 from start of culture). From Figure 6.10 (Upper Panel), it is evident that IL-10 secreted by all groups of cells gradually increased from day 1 to day 3; at day, secreted IL-10 levels for MI DCs were greater than iDCs only (at low significance level), at day 2, MI DC IL-10 levels further increased over iDC and slightly over mDCs, (mid significance level) and by day 3, it was maximally higher than both iDCs and mDCs. Similar to human cytokine secretion data for MI scaffold, the levels on IFNγ for MI DCs stayed similar for days 1 and 2 but dropped to a lower level by day 3. Additionally, Figure 6.10 [Lower Panel] gives us a more detailed picture of the types of changes happening between pairs of individual comparisons across groups. IL-10 level secreted by iDCs and mDCs was virtually indistinct, while that by all other groups was significantly higher than iDCs. DC10s and DEX+PGN DCs also showed increased IL-10 levels over mDCs. MI DC IL-10 levels over mDCs was initially indistinct but gradually turned out to be significantly different by days 2 and 3. Moreover,

MI DCs, DEX+PGN DCs and DC10 were nearly identical in the IL-10 secretions. Conversely, Figure 6.11 (upper Panel) shows a significant decrease in IFNγ secreted by MI DCs compared to mDCs on all days while less than DEX+PGN DCs only on day1 (lower significance). Maximal IFNγ production was evident from mDCs while iDCs secreted the least. [lower panel] All other groups MI DCs, DEX+PGNs and DC10s fall in between these two extremes; wherein they are significantly lower in IFNγ levels than mDCs on all days. iDCs, DC10s, MI DCs and DEX+PGN DCs were nearly indistinct amongst each other for IFNγ secretion levels.

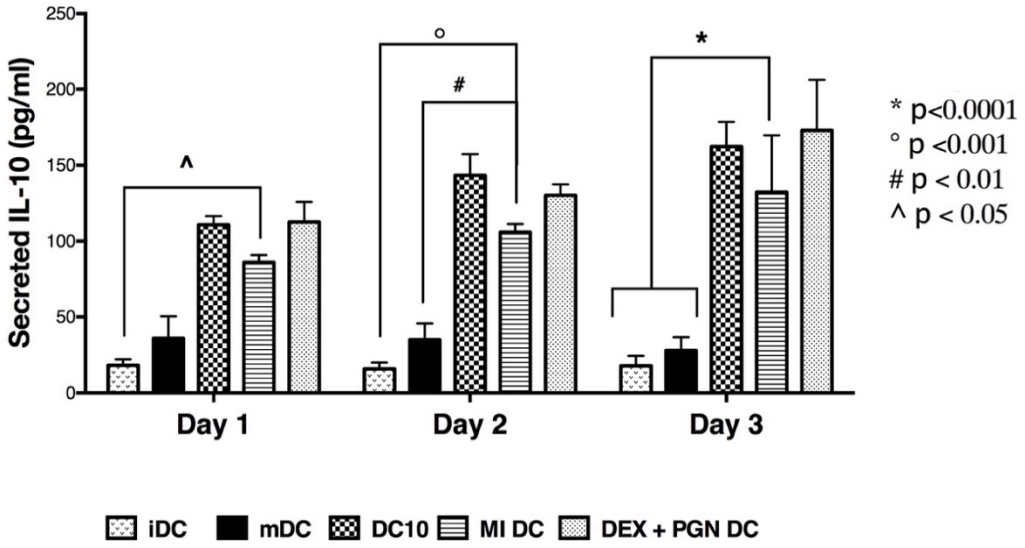

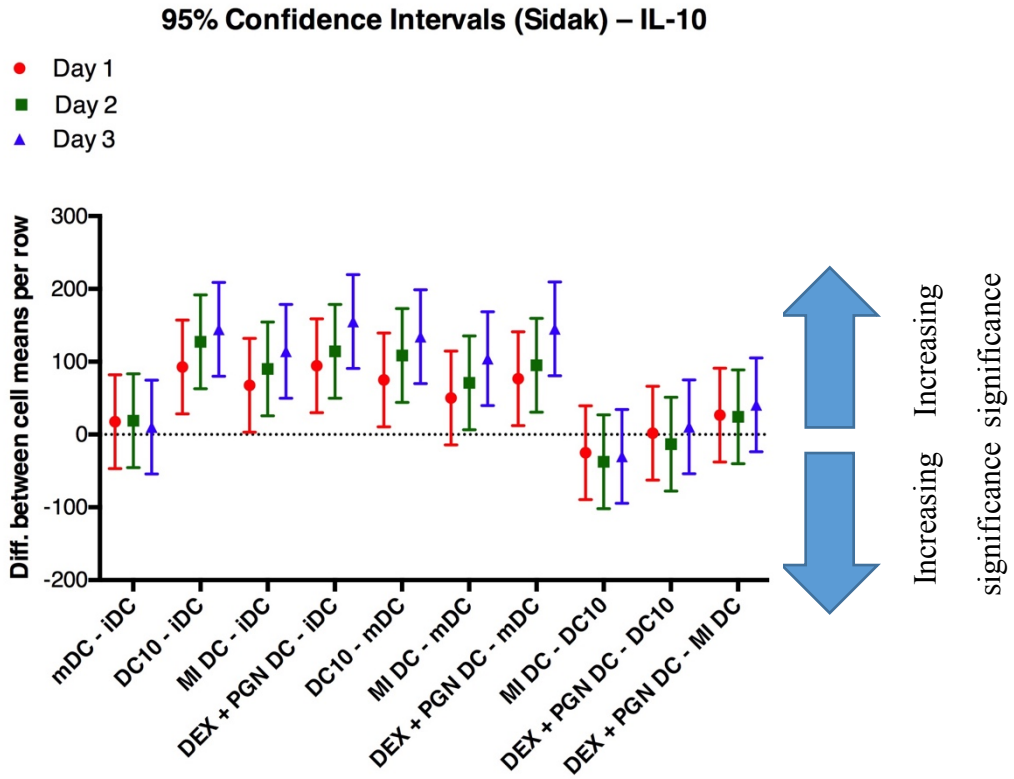

Figure 6.10 Secreted IL-10 Quantification of MI scaffold-treated murine DCs.

An ELISA of either IL-10 was performed on supernatants collected on Days 1, 2 and 3 after the end of BMDC culture. iDCs- immature DCs, mDCs- mature DCs

were treated with lipopolysaccharide(LPS), DC10s- tolerogenic DCs induced IL-10. DEX+PGN DCs – DEX and PGN were added solubly to culture. Statistics was done using multiple comparison of paired values within each treatment group and time-points using two-way ANOVA followed by Sidak's post-test to correct for multiple comparisons and p-values < 0.05 were accepted. Adjusted p-values were calculated and are as follows * = $p < 0.0001$, ° = $p < 0.001$ and # = $p<0.01$. Error bars represent standard error of n=6 mice

* p<0.0001
^ p<0.05 n=6

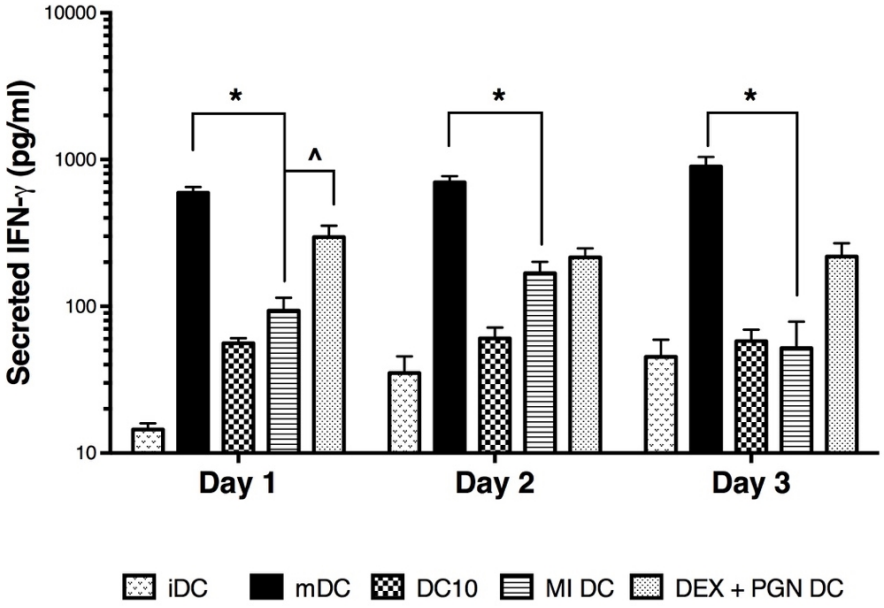

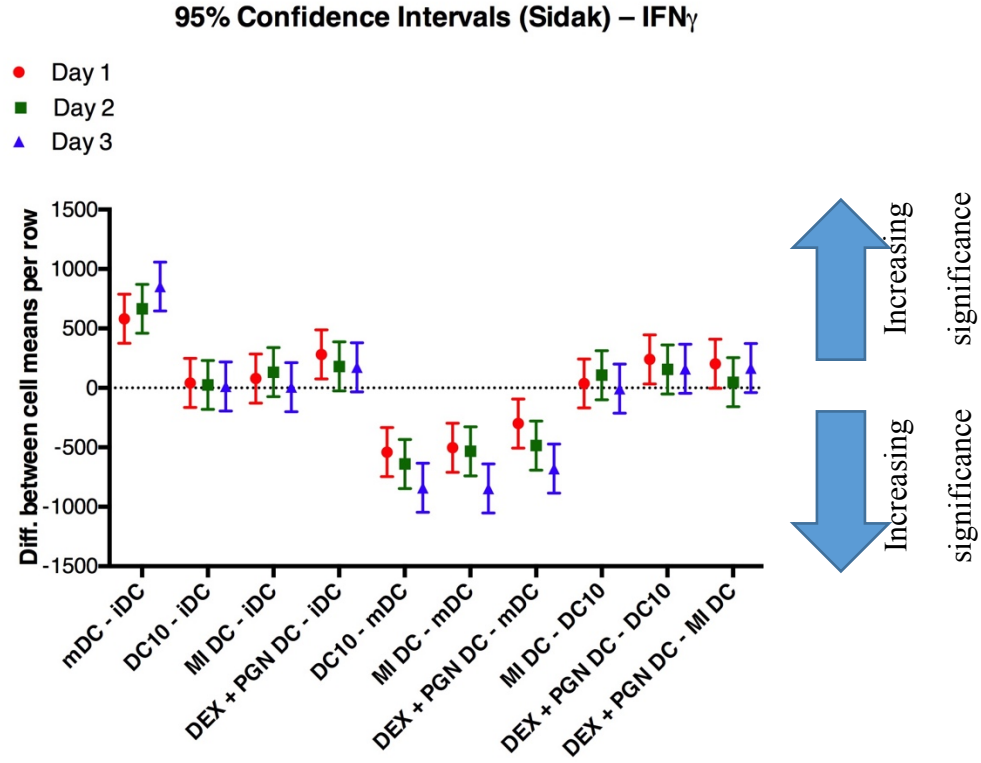

Figure 6.11 Secreted IFN-γ Quantification of MI scaffold-treated murine DCs.

An ELISA of IFN-γ was performed on supernatants collected on Days 1, 2 and 3 after the end of BMDC culture. iDCs- immature DCs, mDCs- mature DCs were treated with lipopolysaccharide(LPS), DC10s- tolerogenic DCs induced IL-10. DEX+PGN DCs – DEX and PGN were added solubly to culture. Statistics was done using multiple comparison of paired values within each treatment group and time-points using two-way ANOVA followed by Sidak's post-test to correct for multiple comparisons and p-values < 0.05 were accepted. Adjusted p-values were calculated and are as follows * = p < 0.0001, ° = p < 0.001 and # = p<0.01. Error bars represent standard error of n=6 mice.

6.3.7 Multiple Sclerosis Antigen-Loaded Murine BMDCs Cultured in the Presence of MI Scaffold Lowered Antigen-Specific T-Cell Responses – Lowering T-Cell Autoimmune Response in an Antigen-Presentation Assay

To further explore the potential of using the MI scaffold in a disease-specific autoimmune model, to show proof of concept, we co-cultured MI DCs pretreated with multiple sclerosis-specific antigen, myelin oligodendrocyte glycoprotein (MOG_{35-55}) peptide, with MOG-specific T-cells obtained from 2D2 mice spleens for three days. T-cell proliferation was assessed by computing normalizing absorbance values (obtained via BrdU assay) for all groups over that of iDCs at the end of the third day of co-culture. Figure 6.12 shows that MI DCs suppressed antigen-specific T-cell proliferation compared to mDC and phorbol-12-myristate-13-acetate + Ionomycin (P+I) positive controls.

Although, DC10s and DEX+PGN DCs also lowered T-cell proliferation, they were indistinct with MI DCs.

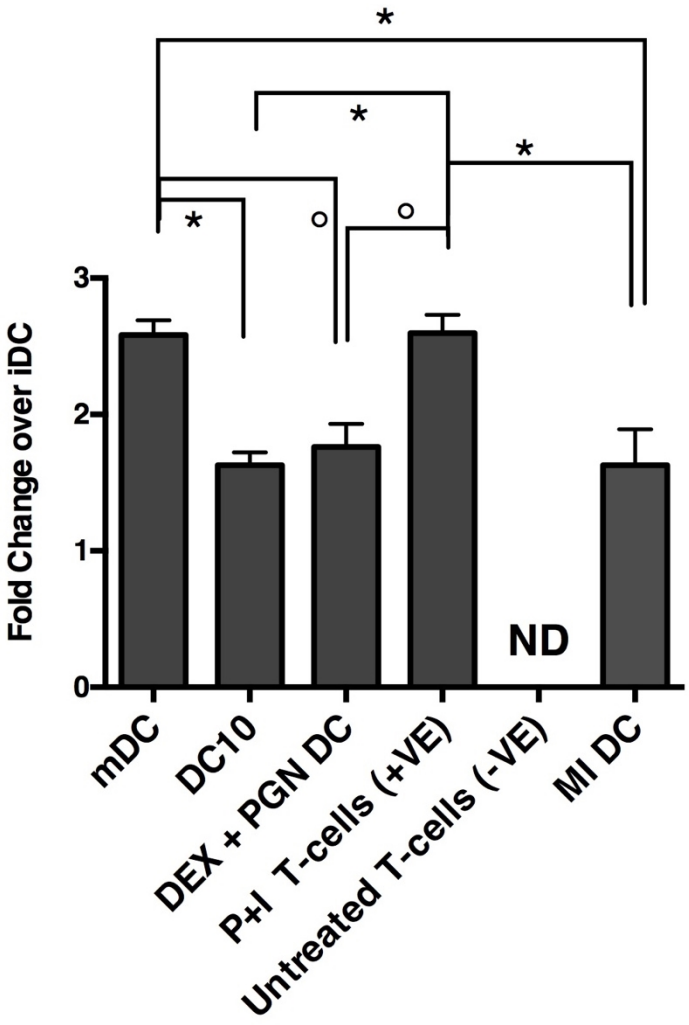

Figure 6.12 Antigen presentation assay – MOG-treated murine DCs were co-cultured with MOG-specific 2D2 T-cells and the extent of T-cell proliferation was determined.

Bar graph represents the fold change of total absorbance intensity of BrdU over that of iDC. iDCs- immature DCs, mDCs- mature DCs were treated with lipopolysaccharide(LPS), DC10s- tolerogenic DCs induced IL-10. DEX+PGN DCs –

DEX and PGN were added solubly to culture. **Statistics was done by using multiple comparison of paired values within each DC group using one-way ANOVA followed by Sidak's post-test to correct for multiple comparisons and p-values < 0.05 were accepted. Adjusted p-values were calculated and are as follows * = p < 0.0001 and ° = p < 0.05. Error bars represent standard error of n=6 mice.**

6.3.8 Murine BMDCs Treated with MI Scaffold Were More Migratory Towards CCL-19 Gradient Due to Their Surface Expression of CCR7..

The addition of the maturation stimulus, PGN was originally incorporated into the MI scaffold to allow a late-stage maturation of scaffold-induced tolerogenic DCs with the potential of improving their LN-bound migratory abilities similar to *in vitro* generated semi-mature DCs. To determine if addition of PGN to the MI scaffold was actually effective in giving rise to functional CCR7 expression on the scaffold-induced DCs, we performed a CCR7-specific chemotactic migration assay with CCL-19 as the chemoattractant. As shown in Figure 6.13, only DCs that were not pre-blocked with anti-CCR7 monoclonal antibody or CCL-19 in the top compartment of the trans-well assay plate moved across the 5μm mesh towards the CCL-19 gradient in the bottom plate. Among these cells, mDCs responded with the highest extent of movement; significantly higher than iDCs, DC10s, MI DCs and DEX+PGN DCs. MI DCs also migrated significantly. Further analysis (lower panel) showed that MI DCs migrated towards CCL-19 gradient more than iDCs at higher level of significance while not being different from DEX+PGN DCs.

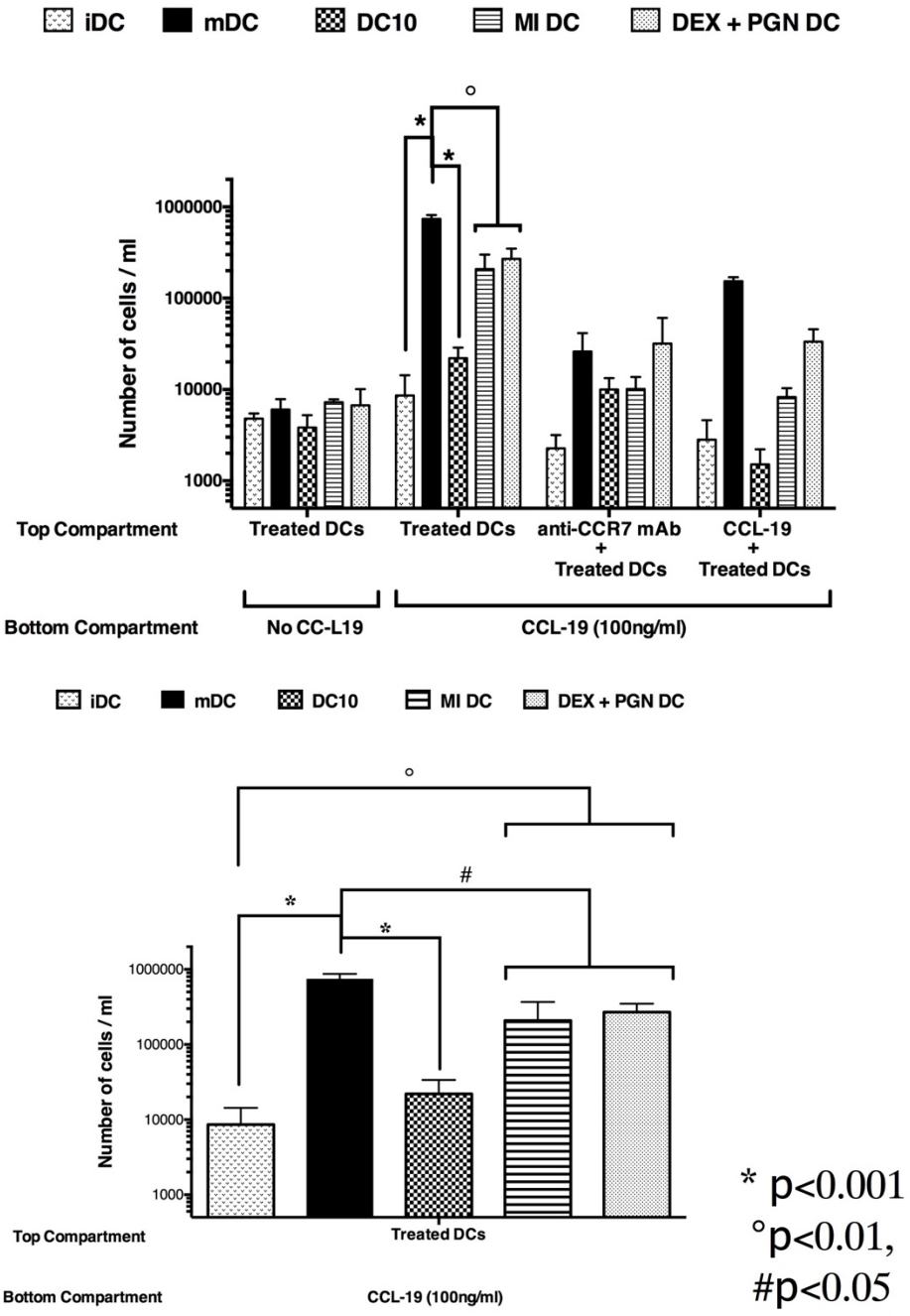

Figure 6.13 Migration assay – Extent of CCR7 expressed on murine DCs after treatment with the MI scaffold.

DCs were obtained after the completion of the BMDC culture and were setup against a gradient of CCL-19 in a transwell assay plate. (upper) DCs migrated towards the chemoattractant were counted and compared against controls such as blank (no CCL-19 in bottom chamber), anti-CCR7 mAb-blocked DCs (top chamber), CCL-19 supplemented DCs (top chamber). Lower panel is a subset of the above clearly showing only the sample group of DCs. iDCs- immature DCs, mDCs- mature DCs were treated with lipopolysaccharide(LPS), DC10s- tolerogenic DCs induced IL-10. DEX+PGN DCs – DEX and PGN were added solubly to culture. Statistics was done for whole data set (upper panel) with two-way ANOVA or (lower panel) for only main unblocked group with one-way ANOVA. Multiple comparison of paired values within each DC group by Sidak's post-test (upper panel) or Fisher's LSD (lower panel) respectively, and p-values < 0.05 were accepted. Adjusted p-values were calculated and are as follows * = $p < 0.001$ and ° = $p < 0.01$, # = $p < 0.05$. Error bars represent standard error of n=3 mice.

6.4 Discussion

Tolerogenic DCs can direct regulation or suppression of self-reactive adaptive immune responses[5]. These DCs have been induced in *in vitro* cultures using a variety of immunomodulators[207]. Biomaterials can serve ideal vehicles for the delivery of encapsulated cells (DCs) or controlled release of a combination of biomolecules to DCs. It is necessary to select biomaterials according to their influence on DCs and host responses; particularly, for DC-associated applications, the effect of the material on the phenotype of DCs must be considered. Here we describe the efficacy of a multifunctional

immunomodulatory scaffold (see chapter 5 for scaffold development) made of macroporous agarose in generating DCs with tolerogenic properties from both human and mouse DC precursors. In addition to assessing surface marker expression of these MI DCs, we tested their ability in inducing active suppression of co-cultured human allogeneic T-cells (clinically relevant in allogeneic transplantation immunotherapies) and antigen-specific murine T-cell suppression in an *in vitro* model of an autoimmune disease. Further, we demonstrated the necessity of incorporating late-stage maturation of immunosuppressant-treated DCs for eliciting DCs with LN-associated migratory features with the MI scaffold. The success of MI DCs in comparison to respectively used controls was assessed, in generating functional tolerogenic-like DCs or aaDCs with migratory capabilities suggest that they could be used subsequent immunotherapeutic models against autoimmune diseases or to treat rejection in allo-transplantations.

6.4.1 Induction of Tolerogenic Human PBMC-Derived DCs Upon MI Scaffold Treatment Based on Surface Marker Expression and Cytokine Secretion.

To determine the effectiveness of the in-house developed MI scaffold (see Chapter 5) in inducing tolerogenic properties in DCs, peripheral blood monocytes were treated with the MI scaffold on day 0 of the typically used human DC culture method (see Methods section). The MI scaffold was initially designed with the goal of being able to recruit endogenous DCs when implanted *in vivo*. Hence it was introduced to monocytes (day 0) to differentiate into DCs with tolerogenic features rather than beginning from iDCs (day 5) as in several previous studies[7,107,199]. Accordingly, the release profiles of loaded biomolecules in the scaffold were tailored to release over a period of 5-7 days.

Later introduction to cells (on day 5) would have also increased the total culture duration (from 6 to 12 days), during which the iDCs may not have survived without growth factors. Further, the comparison of late-introduced MI scaffold to standard DC culture treatments to derive mDCs and tDCs would have been inconsistent. To show proof of concept via this *in vitro* study, the MI scaffold used here contained only DEX and PGN while cytokines crucial for DC differentiation such as GM-CSF and IL-4[31] were added solubly to the culture. On the contrary, all other control treatments such as LPS, TGF-β, DEX + PGN followed the previously established DC culture method and were introduced to iDCs on day 5.

The DC precursors cultured in the presence of the MI scaffold through the course of 5-7 days (human or mouse) exhibited a tendency to mildly adhere to the scaffold. (Images not available). Cells had to be gently dissociated using a salt-based dissociation solution while cells directly cultured on tissue culture polystyrene dishes were largely non-adherent or loosely-adherent. This tendency of cells to adhere to the scaffold may be a consequence of the external scaffold surface or due to its macroporous internal bulk that could have acted as a bed for cell attachment. However conclusive judgment on the nature of cell interactions with the scaffold must be reserved until further investigation is done.

From Figures 6.1 and 6.2, it is evident that maturation-associated markers CD80, CD86 and MHC-II were expressed at lower levels while the inhibitory marker, ILT-3, was expressed at higher levels by all DC groups containing an immunosuppressant

(iDCs, tDCs, MI DCs and DEX+PGN DCs) contrary to LPS-treated mDCs. Also, the addition of PGN in both soluble form (DEX+PGN DCs) as well as scaffold-delivered form (MI DCs) did not reverse the immunosuppressive effect of DEX (indicated by the clear shift in ILT-3 compared to mDCs) while not particularly activating the DCs (the left shift for CD86 is distinct for MI DCs and tDCs only and for CD80 is distinct for all compared to mDCs).

Although, it is perfectly acceptable to represent DC maturation using extent of CD86 expression alone[37,208], a previous work shows that expressing the maturation marker as a fold change of CD86 over DC-SIGN can help eliminate noise in data due to uneven cell numbers in sample treatments and varying immune cellular profile across donors[199,209]. In general, DC-SIGN expression level is known decrease upon maturation, a facet that was, in part, evidenced in this study as well (not shown). The ratio of geometric mean fluorescent intensities (GMFI) of CD86 to DC-SIGN are shown to be cell number-independent[199]. Hence, CD86/DC-SIGN was used as a maturation marker in this work as well. Similarly, ILT-3 expression varied reciprocally with that of CD86 but in the opposite direction. Since the ILT-3 signal was cumulatively low (<10% of the total cells), dividing by value of CD86 data quality can be improved. Thus, ILT-3/CD86 was used to represent tolerogenicity rather than only ILT-3[209].

MI DCs also showed high levels of the tolerogenic marker albeit at a slightly different extent than tDCs (lower significance level). (Figure 6.3) This may be due to the inherent difference in tolerogenicity of the immunomodulators used in each of them.

TGF-β (used in tDC stimulation) is likely a strong inducer of the particular tolerance marker than DEX. This could also be due the gradual addition of DEX from the MI scaffold rather than a fixed input of cytokines for tDCs. A third explanation for this behavior could be due to the presence PGN along with DEX in the MI scaffold that may be causing a background level of resistance to the increased expression of the tolerogenic marker. On the other hand, DEX+PGN DCs were not distinct from either tDCs or MI DCs. Furthermore, all groups were significantly disparate from mDCs while only DEX+PGN DCs among them expressed a lower significance level. This could be due to the fixed addition (causing a larger diffusional driving force in cell microenvironment rather than gradual addition from MI scaffold) of PGN, a TLR-agonist, that may be remotely inhibitory to the development of tolerogenic characteristics of their respective DCs.

Collectively, these results corroborate with qualitative FI plots (Figure 6.1) and suggest that DEX treatment resulted in the general lowering of expression of the maturation marker while PGN did not necessarily act as a DC stimulatory agent. Additionally, PGN addition from either the scaffold or as a soluble factor did not reverse the immunosuppressive effects of DEX while not quite behaving immunostimulatory to DCs. Most importantly, the MI scaffold was able to efficiently deliver its biomolecules while capturing the essential features of its solubly added relative (DEX+PGN treatment). Also using CD86/DC-SIGN instead of only CD86 and similarly ILT-3/CD86 instead of only ILT-3, resulted in lowering the standard errors (very small error bars) across donors

and aided in meaningful calculations of individual (α^*) and overall (α) significance levels for multiple comparisons.

Several cytokines may be associated with induced DC phenotypes. Immunogenic DCs may be accompanied with pro-inflammatory cytokines such as IL-12, TNF-α, IL-17, IFN-γ and many others[37,210] while induced tolerogenic DCs may be associated with secretion of immunosuppressive cytokines such as IL-10 and TGF-β[207]. However, we restricted our analysis to only two representative cytokines, IFN-γ[211] to show immunogenicity and IL-10[79] to show tolerogenicity, mainly because these cytokines been shown to be accurate indicators of respective DC phenotypic states. Cytokine production by MI DCs and associated controls were assessed over 3 days after the completion of DC culture. The levels of secreted IL-10 by these cells (Figure 6.4) increased gradually in three days while positive controls showed a more rapid increase. Interestingly, mDCs also produced gradually increasing levels of IL-10 although not as high as the immunosuppressive groups, a behavior consistent with literature[81]. This is explained as a built-in regulatory mechanism of pro-inflammatory or immunogenic DCs : IL-10 is secreted to regulate the adverse reactions of concomitantly secreted pro-inflammatory cytokines. [212]IFN-γ secretion (Figure 6.5), on the other hand, by MI DCs was decreased in comparison to mDCs. Curiously however, IFN-γ produced by MI DCs increased gradually on days 1 and day 2 after the end of DC culture while plunging on day 3; this may be due to active simultaneous immunosuppressive signals from these DCs. As before, in both these cases (IL-10 and IFN-γ), the levels of significance from controls groups can be quantitatively understood from the plots of differences in Cis (lower panels

of both Figure 6.4 and 6.5) suggesting a potential value for using these types of plots in future analyses.

6.4.2 Suppression of Allogeneic T-Cell Responses by Human DCs Treated with MI Scaffold

The clinical significance of the measured outcomes is a universal concern for all *in vitro* studies. *In vitro* experiments with allogeneic human DCs and T-cells demonstrate provide an important piece of information in understanding clinical outcomes of transplant-associated immune rejection. Common treatments of immunosuppression in transplant patients involve the systemic (oral or intravenous) delivery of small-molecule immunosuppressants. More recently, a T-cell-targeted approach was approved by FDA for therapeutic use in human kidney transplants[213]. This drug, named belatacept (trade name Nulojix) is a fusion protein composed of the Fc fragment of a human IgG1 immunoglobulin linked to the extracellular domain of CTLA-4, which is a molecule crucial in the regulation of T-cell co-stimulation (via APCs), selectively blocking the process of T-cell activation. Using functional DC strategies to promote T-cell regulation would serve as constitutive treatments and thereby have long-lasting effects from a few doses. In this context we studied the co-culture of human MI-DCs with allogeneic T-cells.

Human PBMC-derived DCs and co-cultured allogeneic T-cells showed an increase in T-cell proliferation across all treatment groups that was dose-dependent, i.e. higher the DC: T-cell ratio, the higher the T-cell proliferation (Figure 6.6). Presence of

immunomodulators in DC treatments, expectedly, suppressed the T-cell response. MI DCs engendered a T-cell proliferation similar to DEX+PGN DCs, (slightly) significantly greater than tDCs but very significantly lower than mDCs. These results suggest that tolerogenic properties were imparted to MI DCs by the incorporated immunomodulators while not being significantly different from their soluble-delivered treatment counterparts (DEX+PGN DCs), i.e. MI scaffold was able to mimic the effects of solubly added immunomodulators in culture albeit from a single niche.

6.4.3 Induction of Tolerogenic Murine BMDCs Upon MI Scaffold Treatment Based on Surface Marker Expression and Cytokine Secretion

As with human studies, the expression of maturation markers such CD80, CD86 and MHC-II were lowered for MI DCs. In addition, the expression of ICAM-1 on DCs was similarly lowered on MI DCs. ICAM-1 or CD54 is a molecule associated with secondary co-stimulation with the ability to bind lymphocyte function-associated antigen 1 (LFA-1) expressed on naive T-cells and other leukocytes[214]. Both intracellularly stained and secreted cytokines (Figures 6.9-6.11) give evidence of a tolerogenic behavior for MI DCs similar too soluble control-generated DCs, suggesting its efficacy in serving as a single niche alternative of generating tolerogenic-like DCs. Taken together, this study also validated the optimized design proposed for MI scaffold in mouse cultures.

6.4.4 Murine BMDC Multiple Sclerosis-Specific in vitro Antigen Presentation Assay

Antigen presentation assays are used to quantify the ability of APCs such as DCs or B-cells in triggering antigen-specific T-cell responses in a controlled *in vitro* co-culture of these cells[215]. In situations where transplantation tolerance or induced tolerance in autoimmune disorders is expected, a similar setup is employed wherein a reduction in associated T-cell expansion is indicative of a tolerogenic properties of the respective APCs. This is a controlled *in vitro* representation of APC performance in an *in vivo* disease model, where only one disease-antigen is used.

In MS, several central nervous system-antigens including myelin basic protein (MBP), proteolipid protein (PLP), myelin associated glycoprotein (MAG), 2′,3′-cyclic nucleotide 3′-phosphodiesterase (CNPase) and many others have been described as targets for auto-antibodies, however their individual roles in disease progression is still ambiguous. Interestingly, myelin oligodendrocyte glycoprotein (MOG), induced by CNS tissue homogenates[216], was recognized as a major target antigen for demyelinating antibodies in experimental autoimmune encephalomyelitis (EAE). MOG is a minor type I transmembrane protein, which is exclusively expressed in the CNS on the surface of myelin sheaths and oligodendrocytes. As only one Ig-domain is exposed in its extracellular space[217] and therefore easily accessible for autoantibodies. This extracellular domain is the only antigen known to induce both an encephalitogenic T-cell response and a pathogenic demyelinating antibody response in EAE which is mediated by complement and antibody-dependent cell cytotoxicity (ADCC)-dependent effector mechanisms[218]. Bettelli et. al., developed a novel TCR transgenic mouse model specific

for MOG, names 2D2 mice[219] in which constitutively expressed MOG-specific T-cells were functionally competent and not tolerized. These mice, however, spontaneously developed optic neuritis but not EAE. 2D2 T cells obtained from these mice were dominantly CD4 restricted.

In this study, DCs (iDCs, mDCs, MI DCs or DEX+PGN DCs) were pulsed with MOG_{35-55} prior to their co-culture with 2D2 T-cells that lasted three days. MI DCs were capable of significantly suppressing the extent of 2D2 T-cell proliferation compared to positive controls such as mDCs or PMA + Ionomycin-treated T-cells (Figure 6.12). Similarly, DC10s and DEX+PGN DCs were able to lower the T-cell response, suggesting that MI DCs were not necessarily distinct from either of these groups in terms of their MOG-specific tolerance induction. Together, these results suggest that our MI scaffold could potentially serve as an alternative for IL-10-treated DCs[15] in an *in vivo* model of EAE to lower disease severity.

6.4.5 Murine BMDC CCR7-Specific Chemotactic Migration

Pro-inflammatory cytokines such as TNF-α, as well as TLR agonists such as LPS[220] or PGN [221] are known to increase DC migration to LNs primarily by increasing expression of surface CCR7[222]; whereas certain immunosuppressive cytokines such as TGF-β have been shown to inhibit DC migration to LNs by lowering CCR7 expression[223]. To achieve a therapeutic response irrespective of the disease model used in, it is absolutely imperative that antigen uptaken by DCs are presented to naïve T-cells,

an interaction that occurs in secondary lymphoid organs[22]. Without the sufficient and irreversible expression of surface CCR7 expression, such migration to LNs would be impaired. This has been a key reason to introduce a late-stage maturation in several studies done previously[23,224] as well as in this study. As CCR7 presence on DCs is generally better quantified by mRNA expression and migration assay rather than flow cytometric surface expression[225], we chose to perform the chemotactic assay with CCL-19 as the chemoattractant that also reveals functionality of the chemokine receptor. Alternatively, we could have used CCL-21 or a combination of CCL-19 and CCL-21 as the chemokine gradient in this assay.

The chemokines CCL19 and CCL21 are expressed by stromal cells in the T-cell zone of secondary lymphoid tissues. [226,227] Additionally, in the T-cell zone, a DC subset has also is known to produce CCL19.[228]. CCL19 and CCL21 attract cells expressing their common receptor CCR7[203,229,230] and it is still unclear as to which chemokine signal is dominant during disease progression, although one study[231] shows that CCL21 may be the more critical one. Regardless, these two chemokines mobilize naive or central memory T cells and mature DCs to the T-cell zone[232-235] and thus can potentially affect T-cell responses.

In this study, we employed three sets of control groups, i.e. treated DCs (top compartment) without a chemokine gradient (bottom compartment), treated DCs pre-blocked with anti-CCR7 mAb (top) and CCl-19 (bottom), and lastly, treated DCs pre-blocked with CCL-19 (top) and CCl-19 (bottom). Interestingly, DCs pre-blocked with an

anti-CCR7 antibody also migrated towards the CCL-19 gradient likely due to insufficient CCR7 blocking. Some background level of top to bottom compartment migration was observed of the control group without the chemoattractant. Also, DC groups with CCL-19 added to both compartments at equal concentrations displayed a migratory trend similar to the sample group (discussed below) suggesting that some CCL-19 from the top compartment sifted through the 5μm pore into the bottom one likely due to gravity. In comparison to these groups, (Figure 6.13) treated DCs (top) with CCL-19 gradient (bottom) migrated most efficiently – among which, mDCs displayed the highest numbers, MI DC and DEX+PGN DC numbers came in second, followed by DC10s and iDCs. The migration of MI DCs was significantly more than iDCs and DC10s, significantly less than mDCs and indistinct from DEX+PGN DCs. Collectively, these results indicate that PGN-based DC stimulation in both MI DCs and DEX+PGN DCs had engendered functional CCR7 ability that was lacking in iDCs and DC10s. Also, this expression was lower than LPS-stimulated mDCs likely due to the presence of DEX in both MI scaffold and DEX+PGN soluble treatments or perhaps due to LPS being a stronger activator of DCs than other TLR agonists[236]. We suspect that the addition of PGN to DCs likely induced CCR7-based migration however additional controls consisting of DCs solubly treated only with DEX or DCs treated with the MI scaffold containing only DEX without PGN would be required to conclusively determine the involvement of PGN is endowing these DCs with migratory capabilities. Nevertheless, our results suggest that the MI scaffold would likely be successful in inducing DC migration to LNs in therapeutic *in vivo* models.

6.4.6 Future Directions:

Although we were able to exhibit the ability of the MI scaffold to induce tolerogenic surface markers and functional T-cell tolerance in cultured human and mouse DCs while simultaneously ensuring their migratory capabilities (in the mouse model) were not suppressed, it is greatly necessary to test its efficacy in an *in vivo* mouse disease model such as EAE. Although the originally designed MI scaffold contained three immunomodulators (GM-CSF, DEX and PGN), in order to show proof of concept, the experiments done here involved the use of only DEX + PGN. Hence, it would be important to revisit its functionalities along with incorporated GM-CSF.

The predictive model developed in Chapter 5 is solely empirical and is relevant for *in vitro* release of the immunomodulators at 37°C and pH 7.4. However, it does not address how the release profiles of these agents would vary in an implanted model. Early events expected in the host response to such an implantation are local blood-material interactions and protein adsorption resulting in local cell attachment in turn signaling the recruitment of a variety of innate immune cells[6,237,238]. The type of cellular population recruited *in situ* would strongly dictate the characteristic of host response to enhance or mitigate the success of the implant. Tissue reactions such as acute inflammation or fibrous encapsulation often accompanied with the formation of foreign body giant cells[237] from macrophages could cause material contraction or degradation and impose mass transfer limitations[196] that could in turn greatly affect the release characteristics of immunomodulators from the MI scaffold and dilute it efficacy *in vivo*. Assuming that the MI scaffold implanted in a mouse model would cause at least a low level of

inflammation, this could result in a depressed acidic pH in extracellular fluids[239]. A change in local pH would considerably alter the apparent charges on the immunomodulators as well as the gelatin MPs within the scaffold thereby creating an opportunity for the release to vary drastically than that predicted by the model. Also, the possible presence of circulating collagenase in subjects afflicted with an autoimmune disorder[240] can alter the release of loaded agents by degrading the scaffold-embedded gelatin MPs. In addition to these issues, implantation of the MI scaffold in an *in vivo* mouse model comes with the added difficulty of scale and flow characteristics: whereas in the *in vitro* study, all released agents ended up in the unmoving sink of the well or petri-dish, in the mouse all release agents are likely to be cleared continuously thereby altering their local diffusion gradient; the overall dosage of the immunomodulators may have to be accordingly scaled to bring about an efficient treatment scheme. We believe with additional *in vivo* data our empirical model can be modified to account for these issues. Moreover, due to its modular nature (see Chapter 5), the MI scaffold could be modified to incorporate MOG or perhaps another autoimmune disease-specific antigen along with existing treatments and applied directly to *in vivo* disease models, in both autoimmunity as well as allogeneic transplantations. These antigen treatments may be either adsorbed onto the scaffold for early non-specific release in vivo; alternatively, they could be loaded on scaffold-embedded gelatin MPs similar to other treatments in order to delay release. From what is known of the antigen presentation biology of DCs, early introduction of antigen without inflammatory agents or with local immunosuppressants may sufficiently generate antigen-specific regulatory DC responses. However, when mild to extreme inflammation is known to occur in either due to the procedure or location of

the implant, introducing antigen early on may simultaneously generate immunogenic antigen-specific DCs that would be undesirable or even detrimental to the success of the tolerogenic treatment– in these cases the delayed antigen exposure may be required. While mild inflammation may be favorable for recruiting monocytes to the implant site, it is yet to be determined how is would affect antigen exposure to DCs during the course of immunomodulator release. Identifying the inherent differences in the timing of antigen exposure to DCs along with a known microenvironment may help us better understand the process of induction of aberrant DCs in autoimmune diseases and in turn design suitable treatments.

The release of immunomodulators *in vivo* from the MI scaffold would likely recruit endogenous cells primarily monocytes and differentiate them into DCs. It would be interesting to examine what other cell types would be migrating either to the site of the implant or attaching to the scaffold itself upon 1-2 weeks post implantation. Using additional cytokines an enrichment of desired cell populations could be achieved to enhance the success of the MI scaffold as a treatment.

Furthermore, the incorporation of immunomodulator-releasing gelatin MPs into an agarose scaffold was done keeping in mind the non-stimulatory nature of agarose towards DCs *in vitro*[107], possibly nudging the DCs towards a tolerogenic phenotype. The agarose scaffold used here was developed using a cryogelation technique (see Chapter 5) that provides these scaffolds with macropores.[154] These scaffolds can be used not only to deliver immunomodulators but also adapted to deliver cells such as pre-conditioned DCs

or T-cells. The advantages of having an endogenous DC recruitment system versus a pre-conditioned cell delivery system can be explored within the confines of using the same scaffold. The possibility of developing combinatorial treatments of *ex vivo*-treated cell-delivery with *in vivo* endogenous cell enrichment may also be investigated. In conclusion, the MI scaffold has been tested as a proof-of-concept in this work in *in vitro* human and murine studies and offers a myriad of exploratory avenues to improve understanding of DC biology as well as in clinical applications to treatment aberrant immune disorders.

CHAPTER 7 CONCLUSIONS AND FUTURE DIRECTIONS

7.1 Conclusions

Dendritic cell phenotype is a strong indicator of its downstream effector response. Since biomaterials can influence DC phenotype, they can be used as a tool for modulating effector adaptive immune responses. Poly(lactic-co-glycolic acid) (PLGA), has been shown to induced a DC phenotype similar to mDCs (induced by bacterial LPS) and has also been associated with an adjuvant response *in vivo* when co-delivered with a model antigen (e.g.(OVA). The research study described herein elucidated the missing link between PLGA's effect of DC phenotype *in vitro* and its adjuvant effect *in vivo* by addressing whether PLGA would influences the co-delivered antigen-specific T cell proliferation if DCs were absent from the animal model. CD11c+ DCs were conditionally ablated *in vivo* by delivering DT to CD11c-DTR transgenic mice while simultaneously implanting PLGA scaffolds with incorporated OVA for its controlled release. As a read-out of induced OVA-specific T cell proliferation, CFSE-labeled OVA-reactive OT-II or OT-I cells were adoptively transferred and loss of fluorescence determined. Upon adoptive transfer of OT-II, CD4+ T-cells into DC-depleted mice failed to undergo complete proliferation in contrast to those in DC control mice possessing intact DCs. The lower proliferation of these adoptively transferred T-cells *in vivo* was likely due to the lack PLGA-dependent antigen presentation via mature DCs . Moreover, the CD8+ T-cell response was also affected by DC depletion, indicating that PLGA may be important for boosting the antigen cross-presentation response of DCs as well. Thus, the work described in Chapter 4 conclusively established that the effect of PLGA *in vivo*

on the antigen-specific proliferative T-cell response, a likely early precursor to antibody response, was indeed due to its effects on DC phenotype.

The next objective of this doctoral work was to address the feasibility of designing an agarose-based controlled delivery system that can deliver small-molecule as well as protein-based drugs at distinct times (likely mimicking culture doses and times) to condition DCs to acquire a tolerogenic phenotype that can subsequently be applied in immunotherapies for autoimmunity or to alleviate allograft rejection. In order to effectively design a single niche that could enrich tolerogenic DCs by differentially releasing multiple factors to DC precursors in a manner similar to an *in vitro* culture, we aimed to study the release profiles of control small (~ 1000 Da, Biotin-AF647) or large (~ 45,000 Da, OVA-AF647) from crosslinked gelatin MPs embedded in a macroporous cryogel scaffold made of agarose. Here, agarose was selected due to its ability to maintain DCs in an immature phenotype and while gelatin was selected due to its customizability with crosslinking and compatibility with agarose scaffold formulation protocol. These control molecule release profiles were fitted by non-linear regression to a stretched exponential function namely, the Weibull equation, based on which a simplified empirical model was defined to predict experimentally variable parameters (such as crosslinker concentration and number density of MPs per scaffold) and thereby predict the scaffold configuration to delivery immunomodulators such as GM-CSF, DEX and PGN in a differential manner. The model predictions were validated by experimental measurements of release of these immunomodulators and any differences between predicted and measured values were incorporated into the model as a method of

optimizing the model for future predictions. Thus, in Chapter 5, we were successfully able to design a model of controlled release to deliver multiple factors, both small and large in size, within the desired time-frame of around one week that would standard DC culture to generate tolerogenic DCs *in vitro*. Also, as the model is capable of determining the release profiles of other molecules with physical properties such as size and charge similar to Biotin or OVA, we believe it is possible to apply the same model in designing release profiles of drugs or proteins for different applications that will be discussed in the next section (Future Directions).

In Chapter 6, the effectiveness of the multifunctional immunomodulatory (MI) scaffold (delivering DEX and PGN only) design suggested by the model in Chapter 5, in inducing tolerogenic properties in human and murine DCs. First, the cellular surface markers of DCs generated from human blood monocytes upon treatment with the MI scaffold revealed a lower levels of expression of the maturation marker CD86/DC-SIGN cotemporaneous with an increase of the tolerogenic marker ILT-3/CD86. Second, the secreted cytokines from these MI DCs showed an increase in the immunosuppressive cytokine IL-10 along with a decrease in the pro-inflammatory cytokine IFN-γ compared to mDCs (DCs matured using LPS). Third, MI DCs were able to diminish the allostimulatory T-cell response when co-cultures with allogeneic naïve T-cells. Collectively, these results indicated that the MI scaffold was able to induce a functional tolerogenic phenotype in DCs derived from human blood monocytes. Importantly, the ability of human MI DCs to lower the allostimulatory T-cell response is highly relevant in clinical scenarios of alleviating allograft rejection. The antigen-specificity of the MI

DC-mediated T-cell response may be necessary to determine in specific disease models such as Multiple Sclerosis or autoimmune diabetes in a way that is relevant for subsequent immunotherapies. This will be discussed in more detail in the next section. (Future Directions).

Similar to the human studies, when the optimized MI scaffold was tested with murine bone marrow-derived DCs to establish a tolerogenic phenotype, the cell surface marker expression profile showed a lowering of maturation markers such as MHC II, primary co-stimulatory marker CD86 and secondary costimulatory molecule ICAM-1 along with an elevation in tolerogenic marker PirB (analogous to human ILT-3). Additionally, murine MI DCs increased secreted IL-10 while decreasing IFN-γ, results that we corroborated by the intracellular expression profile of the same cytokines. Furthermore, these murine MI DCs, when pre-treated with a Multiple Sclerosis-specific antigen, namely MOG_{35-55}, were co-cultured with MOG-reactive T-cells, were able to alleviate the MOG-reactive T-cell response. The addition of PGN to the MI scaffold was done to ensure that immunosuppressants it released would not render the treated DCs incapable of migrating to lymph nodes, a response that is essential in determining the successful outcome of using these DCs in immunotherapies. A late-stage release of a TLR ligand, such as PGN, to DEX-treated DCs would likely endow the DCs with migratory properties similar to endogenous populations of circulating tolerogenic DCs[60] by upregulating lymph node-homing related chemokine receptor, CCR7. In order to determine the efficacy of PGN release by the MI scaffold in inducing functional CCR7 expression in murine DCs, the ability of murine MI DCs to migrate towards a CCR7-

specific ligand, namely CCL19, was analyzed in a CCR7-chemotactic assay. The results from this assay showed that MI DCs as well as DCs treated with soluble DEX and PGN, were able to migrate towards CCL19, separated by a 5μm mesh barrier, at a significantly higher rate than untreated iDCs suggesting the importance of incorporating PGN along with immunosuppressive treatments in the future. Taken together, from Chapter 6, we can surmise that the MI scaffold design proposed based on an empirical model from Chapter 5 for human studies and optimized for murine studies was successfully able to induce tolerogenic properties in treated DCs. In addition, the MI scaffold was able to render CCR7-dependent migratory properties to murine DCs and hence can be considered 'alternatively activated' or aaDCs.

Overall, in this thesis, the importance of DC phenotype in determining is functional downstream outcome while using biomaterials to condition the response has been reiterated, first in the context of using PLGA (known to induce a mature phenotype in DCs) in the absence of DCs to diminish the immunogenicity of OVA *in vivo* and second, by delivering temporally differential immunomodulators from a DC-non-stimulatory biomaterial such as agarose, to induce functional DCs with tolerogenic and migratory properties that are highly relevant in designing future immunotherapies targeting autoimmune diseases as well as in alleviating allograft rejection.

7.2 Significance of Findings

Dendritic cells had long been hypothesized to be associated in the ability of PLGA to enhance a humoral immune response to co-delivered antigen. By establishing

that antigen-specific T-cell proliferation in response to antigen-loaded PLGA – an early step necessary for downstream humoral T-cell responses – used here as a substitute to measuring antigen-specific antibody titers – was diminished *in vivo* in the absence of DCs, we can infer that DCs play a major role in bringing about early antigen presentation in the context of PLGA. Similarly, DC phenotype with non-stimulatory materials such as agarose has been correlated with lower levels of induced antigen-specific antibodies or a negative adjuvant effect. Based on our results we can reasonably assert that the differential effect of biomaterials on the adaptive immune response is mediated *in vivo* primarily due the presence of DCs and biomaterial effects on the DC phenotype.

Further, proof-of-concept studies with the MI scaffold have shown that it possesses untapped potential and in a number of ways can further research in immune-associated biomaterials devices. For example, batch synthesis of MI scaffold may offer a unique advantage over manual addition of soluble treatments in standard culture. MI scaffold may thereby offer scalability along with reproducibility of cell culture, ideal for a larger scale of development of *ex vivo* therapies. Although development of novel in vivo therapies are more sought after, there is a market for developing *ex vivo* such as Sipuleucel-T as they require shorter clinical trials and are likely to be approved by the FDA faster than in vivo therapies for human use. MI scaffolds could aid in establishing such clinical applications.

Of course, the larger goal of designing these scaffold will always be for in vivo applications. Implantation of these scaffolds may be associated with some inflammation that could be favorable used to recruit endogenous cells. By incorporating growth factors such as GM-CSF in the scaffold would act as an additional recruitment factor for locally enriching DC populations. In recent years, combinatorial immunotherapies are being widely investigated primarily due to their higher potential of clinical efficacy. In this

context, using an MI scaffold with multicomponent temporally distinct treatments could be crucial to fine-tuning immune outcomes that may be not be possible with singular, non-synergistic approaches. With the MI scaffold, we could achieve several levels of combinatorial therapy – i) local implantation proximal to target draining LN (depending on the disease situation), ii) surgery-induced local inflammation to recruit a host of innate immune cells such as neutrophils, monocytes and macrophages, iii) locally deliver multicomponent timed treatments thereby achieving spatiotemporal conditioning of homing in cell iv) macroporous scaffold base could deliver *ex vivo* cultured cells such as DCs to enhance host T-cell responses or even serve as a bed for endogenously recruitment cell attachment v) prolonged localization of cells and signals could produce long-lasting immunotherapies. Thus the innovation in this work of designing and developing an MI scaffold with modular biomolecular delivery that can be differential timed using the mathematical model, can have exciting far-reaching applications in immunoengineering.

7.3 Future Directions

The experiments done in this thesis uncovered specific phenomena with respect to designing biomaterial-based immunotherpeutics targeted towards DCs: 1) The in vivo PLGA adjuvant effect ascertained by previous members of the Babensee laboratory is correlated to the role PLGA plays in altering immature DCs to exhibit a mature phenotype. This is further responsible for initiating an immunogenic downstream response to co-delivered antigen, highly relevant in designing vaccines against infectious disease as well as for cancer, 2) Differentially crosslinked gelatin microparticles embedded in a layer of macroporous agarose (a material known to maintain DCs in an immature phenotype) can be used to temporally control the release of multiple immunomodulators both small and large to induce alternatively activated DC phenotype

in vitro 3) the model developed in Chapter 5 is amenable to designing multi-component temporally distinct release profiles of molecules other than the ones currently used as long as they meet the criteria of similar charge and size to the tested control molecules and the limited time-frame of 1-2 weeks 4) since the agarose cryogel scaffold is macroporous and traditionally used to deliver cells, we can explore the possibilities of delivering immunomodulator and cells as therapy 5) human blood-derived MI DCs were able to diminish the allostimulatory T-cell response, their effectiveness in functioning in an antigen-specific manner can be easily tested in autoimmune patients 6) Since murine bone marrow-derived MI DCs were successfully established as tolerogenic and CCR7-dependent migratory, the efficacy of the MI scaffold containing GM-CSF in addition of the existing treatments of DEX and PGN, in bringing about functional immunotherapy can be determined by implanting it in a mouse EAE model either prophylactically or therapeutically.

To this effect, the immediate future directions of this project can be divided into three tracks, 1) *in vitro* clinical studies with blood from human or mice with multiple sclerosis 2) *in vivo* studies in mice or rodent model that mimics an autoimmune disease condition 3) using the tunable properties of the scaffold design to deliver different components either immunomodulators or cells in the context of immunotherapy.

7.3.1 Efficacy of MI Scaffold in Re-Educating Multiple Sclerosis Patient-Derived DCs to Obtain an Antigen-Specific Alternatively Activated Phenotype.

This dissertation established the ability of inducing tolerogenic and migratory properties in DCs derived from human blood or murine bone barrow. To establish the

clinical significance of the results from this work, it is necessary to test the scaffold in the context of an autoimmune disease.

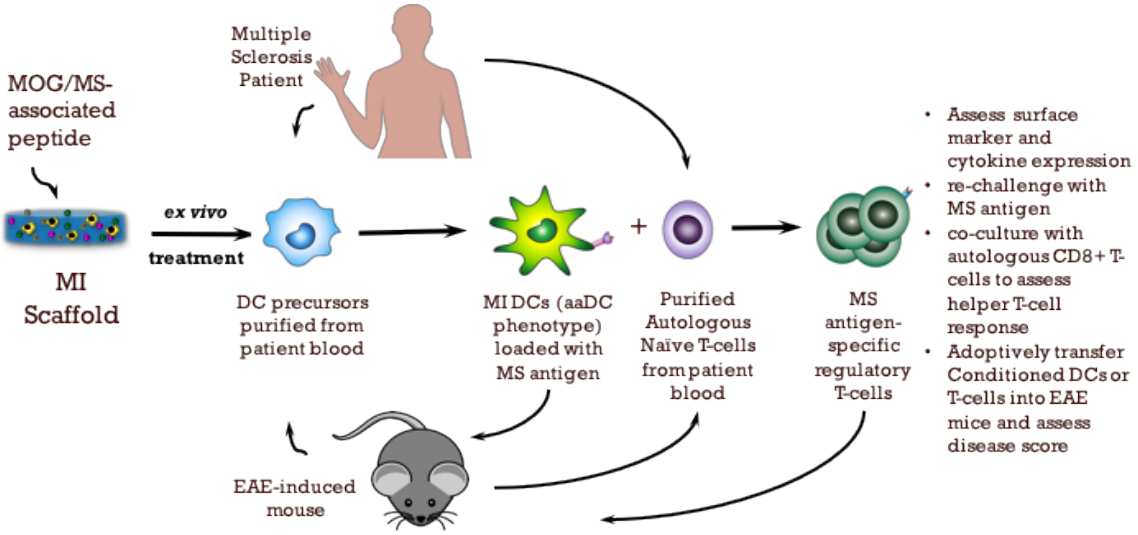

Figure 7.1 Schematic of assessing the efficacy of MI scaffold as an *ex vivo* treatment in reconditioning DCs from MS patients (human or mice)

Blood derived from human patients or mice with EAE can be purified and cultured in the presence of the MI scaffold either with GM-CSF incorporated in MPs embedded in the scaffold or as a soluble factor according the methods described in Chapter 6. These MI DCs can be treated with MS-related antigen such as MOG, myeline basic protein (MBP), proteolipid protein (PLP) and/or myelin associated glycoprotein (MAG), 2′,3′-cyclic nucleotide 3′-phosphodiesterase (CNPase), known to be targeted by autoantibodies, after the final day of culture for 4-8 hours and purified. These DCs may be co-cultured with naïve T-cells obtained from the same patients or similar EAE mice, and the severity of the ensuing T-cell response can be determined in an MLR-like or antigen presentation assay. T-cells specific for the respectively used antigen, if available, may replace naïve T-cells in the above co-culture. To determine the antigen-specificity of the T-cell response when naïve T-cells are used, T-cells can be assessed by flow cytometry by multiple staining with CD3 (a T-cell marker), fluorescently-tagged antigen peptide and other surface markers such as FoxP3, CD4, CD25, CD8, PD-1 and PD-2.

Additionally, intracellular cytokine staining may be done for IL-10, IL-2, IFN-γ and IL-17. Autoreactive T-cells in several autoimmune diseases have been shown to produce elevated levels of IL-17 and reduced levels of IL-10[241-243]. Additionally, T-cells conditioned by the co-culture with MI DCs can be purified using flow cytometric or magnetic separation and re-challenged with the antigen and the ensuing T-cell proliferation response can be determined. Furthermore, these T-cells could also be co-cultured with naïve CD8+ T-cells obtained from the same MS patient or similar EAE mice to determine the effector T-cell helper response of T-cells primed with the MI DCs. As an additional measure, murine T-cells conditioned by MI DCs can be adoptively transferred into mice with established EAE to determine if the treatment is able to reduce the MS disease score. The caveat for this experiment would be that large total number of conditioned T-cells would be required (>10^8) which may be not be possible to obtain from the *in vitro* co-culture experiments. To circumvent this issue, conditioned T-cell can be artificially expanded in vitro either using IL-2 or the antigen itself to obtain T-cell numbers suitable for adoptive transfer in to EAE mice. We expect the MI scaffold-treated patient-derived DCs (either human or mouse) to diminish the severity of the antigen-specific T-cell response.

7.3.2 Therapeutic Application of the MI Scaffold in Alleviating Disease Severity in an Experimental Autoimmune Encephalitis (EAE) Model in Mice

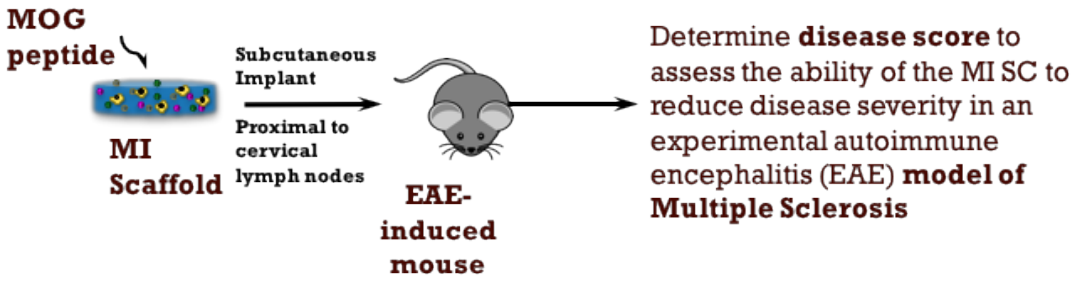

Figure 7.2 Schematic of assessing efficacy of MI scaffold in alleviating disease in EAE mouse model

As next step it would be very important to show the efficiency of the MI scaffold to perform in the context of a simulated disease condition thereby providing a justification for future human *in vivo* therapeutic use. The MI scaffold, previously used for generating murine bone marrow-derived aaDCs, will be used here with additional GM-CSF loaded onto crosslinked gelatin MPs incorporated into the scaffold. Two types of treatment models can be defined in this respect. 1) Prophylactic treatment – Mice can be implanted with the MI scaffold with adsorbed MOG peptide and eight days later (keeping consistent in time with the mouse culture of DCs) EAE can be induced with MOG peptide emulsified in CFA or pertussis toxin. These mice would be monitored for 21 days (typical for EAE model) during or after which a disease score evaluation will be done as described previously[244]. 2) Therapeutic treatment – Mice can be induced with EAE using MOG peptide with CFA or pertussis toxin. After a minimum numbers of days required for EAE establishment, typically 8 days, the MI scaffold will be implanted in these mice. There a couple of things to keep in mind while designing these experiments, first is the site of implantation and its effects on the efficacy of the MI scaffold and second is the establishment of relevant controls. With respect to the site of implantation: brain antigen in functionally distinct APCs are shown to drain into the cervical lymph nodes in MS and EAE[245], hence it may be important to deliver our immunotherapy in a region proximal to these LNs. Hence dorsal subcutaneous implantation can be performed on these mice near the neck, a surgery that is feasible and not as extremely invasive as intraperitoneal implantation. Unpublished work (Aline Thomas et al.) from our laboratory has shown that IL-10 treated MOG-primed DCs when delivered in a self-assembling polyethylene glycol (PEG)-based hydrogel[246] injected near the cervical lymph nodes were viable for up to three days with the hydrogel visible for explanation for up to 14

days and the hydrogel-delivered DCs were able to alleviate EAE disease score significantly compared to bank hydrogel delivered control mice versus hydrogel encapsulated IL-10 DCs injected into the flank region in mice that showed no significant improvement is disease over blank controls. These studies reinforce a need to pay close attention to the site of in vivo delivery of the treatment. Respective controls for the experiments described here should include a group of mice in whom EAE is induced without any treatment, another group receiving IL-10 DCs in hydrogel to make this study comparable to previous work, MI scaffold with only GM-CSF and DEX (i.e. without PGN) to validate the incorporation of PGN in the scaffold design in *in vivo* studies and perhaps another group with the immunomodulators injected directly near the cervical LNs. As an alternate strategy propose testing the ability of the MI scaffold seeded with IL-10 DCs similar to previous work (Aline Thomas et al.) to in the context of EAE. Here, we would expect that dual treatment – 1) *ex vivo* conditioned tolerogenic DCs and 2) *in situ* conditioning of endogenous DCs , would boost the level of efficacy of these types of treatments in the EAE mouse model. Overall, we expect the MI scaffold when implanted near cervical LNs in EAE mice to show benefit over untreated EAE mice in alleviating disease severity.

7.3.3 Therapeutic Application of the MI Scaffold in Alleviating Disease Severity in an a Spontaneous Type 1 Autoimmune Diabetes Model in Mice

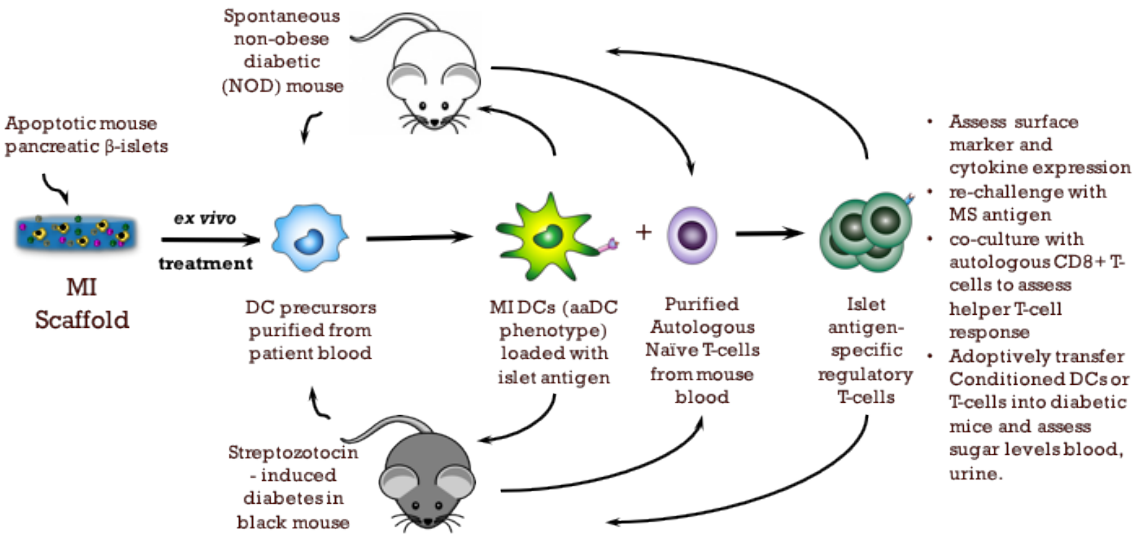

Figure 7.3 Schematic of testing MI scaffold in an autoimmune diabetes model

Non obese diabetic (NOD) mouse is an excellent model of type 1 autoimmune diabetes spontaneously undergoes the disease[247] whereas, in different mouse model, streptozotocin (STZ)[248] can be used to type I diabetes in wild-type mice The efficacy of the MI scaffold in reversing the loss of insulin-producing β-islet cells can be determined in a manner similar to the experiments described in the previous sub-section. Briefly, MI scaffold containing GM-CSF, DEX and PGN along with apoptotic β-islet cells from NOD mice or wild type mice to be induced with STZ, adsorbed onto the scaffold can be administered to NOD mice or STZ mice, after a minimum period of 8 days (consistent with in vitro culture time point) the blood and insulin levels of these mice can be compared with that of untreated NOD mice. Additionally, splenic T-cells can be isolated from MI scaffold-treated mice and challenged externally with β-islet cells to determine if the antigen-specific T-cell response has be modified by use of the MI scaffold. Moreover, assessing autoantibodies against β-islet cells in blood titers before and after implantation of the MI scaffold would evaluate its effect on the humoral immune response involved in

type-1 diabetes. As before, we need to determine the most suitable site of immunotherapy delivery; here, we expect that a site proximal to the peri-pancreatic LNs[249] would better target the immunomodulator delivery from the MI scaffold in autoimmune diabetes. Alternatively, *ex vivo* conditioned DCs or T-cells can be adoptively transferred into these disease-inflicted mice could be used as a treatment instead of directly implanting the MI scaffold. Understanding how the MI scaffold functions in these diabetic mice will help us design improved treatments for human patients with autoimmune type-1 diabetes.

APPENDIX A.

A.1. Supplemental to Aim 1

A.1.1. Confirmation of in vitro OT-II T-Cell proliferation

To confirm that the OT-II T-cells were responsive to OVA, we setup an in vitro assay using OVA peptide (323-339). T-cells were purified from splenocytes of OT-II mice using a negative selection T-cell enrichment kit. T-cells were labeled with CFSE and treated with OVA peptide and cells obtained from the positive fraction at a ratio of 100:1.[131]. Despite using an OVA peptide, for effective antigen recognition by the T-cells, the peptide must be presented along with MHC molecules – this is easily achieved by adding a small portion of T-cell depleted splenocytes that contain a cocktail of antigen presenting cells[250].

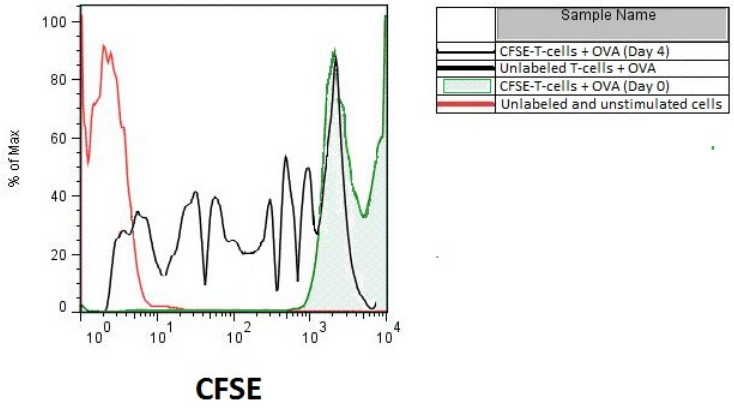

Figure A 1 OT-II T-cells proliferated in vitro in response to OVA peptide (323-339).

Flow cytometric histogram shows a decrease in CFSE fluorescence with each stage of cell division. (red) unstained and unstimulated T-cells, (green) CFSE-labeled T-cells before OVA treatment, (black) CFSE-labeled T-cells treated with OVA peptide after 3 days.

CFSE-labeled T-cells (Figure A 1) exhibited proliferation assessed by the reduced in the CFSE fluorescence intensity. Each successive peak is an indication of cell division that causes the reduction in fluorescence intensity. This results served as a confirmation of OT-II T-cell reactivity to OVA, a necessary preliminary step prior to *in vivo* OVA treatment to OT-II T-cells.

A.1.2. Confirmation of Adoptive Transfer via intravenous injection

Successful adoptive transfer of T-cells was confirmed by injecting CFSE labeled T-cells into either via the tail or penile vein of wild type mice. These mice were sacrificed at 24h and the infiltration of T-cells was analyzed in circulating blood and splenocytes using flow cytometry.

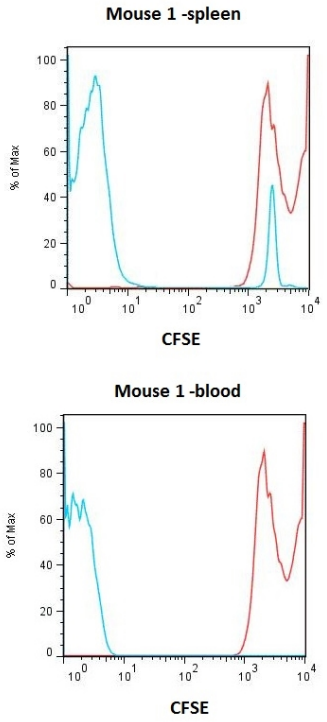

Figure A 2 Confirmation of adoptive transfer of T-cells

The T-cells adoptively transferred in this experiment were naïve or non-specific for OVA. Figure A 2 shows that fluorescence was detected in splenocytes but not in the circulating blood possibly due to T-cell enrichment at the spleen along with a simultaneous dilution in the blood. Nevertheless these results suggested that the adoptive transfer procedure was successful in delivering labeled T-cells *in vivo*.

A.1.3.Assessing in vivo OT-II T-Cell Proliferation in Response to Intraperitoneally Delivered Model Antigen OVA

After confirming that the OT-II T-cells were reactive to OVA in an *in vitro* setting, we assessed their sensitivity to intraperitoneally delivered OVA. OVA was injected either dissolved in PBS or emulsified in CFA. CFSE-labeled OT-II T-cells were

adoptively transferred as before and splenocytes were analyzed from CFSE fluorescence after 2 days.

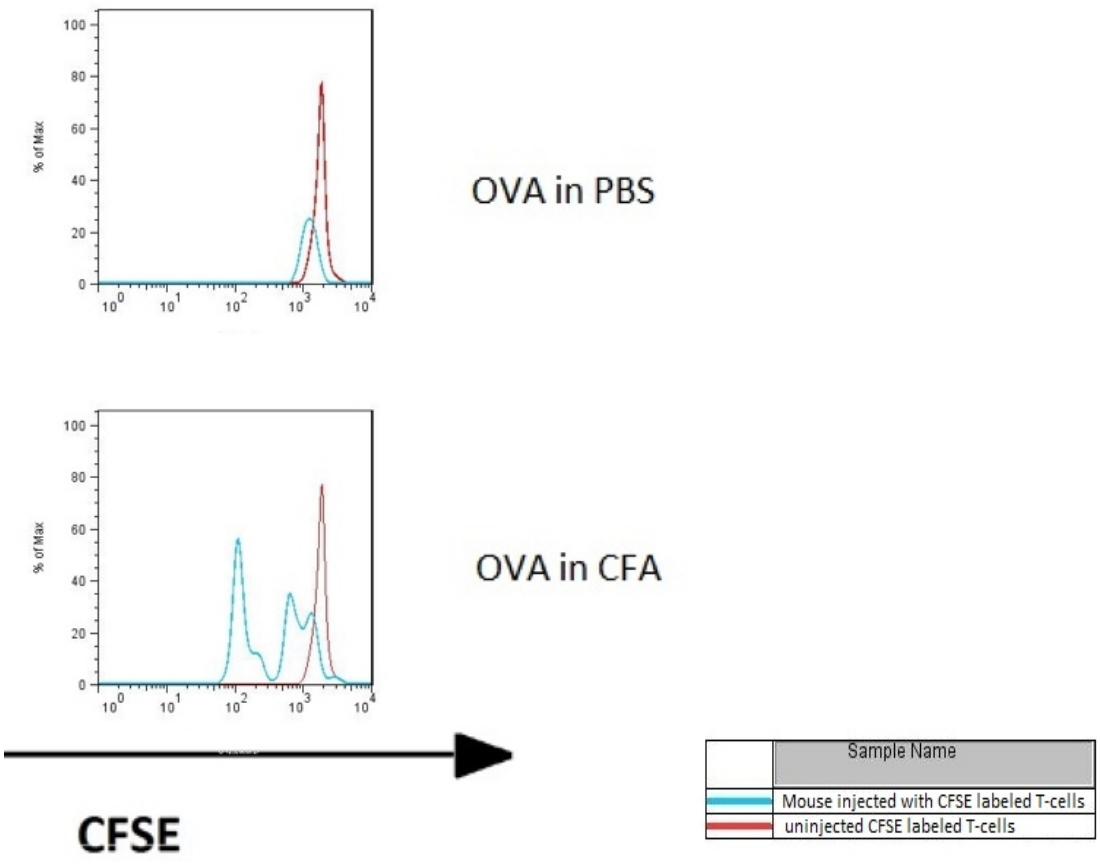

Figure A 3 OT-II T-cells proliferated *in vivo* in response to OVA in PBS (top) or CFA(bottom).

Flow cytometric histogram shows a decrease in CFSE fluorescence with each stage of cell division. (red) uninjected CFSE-labeled T-cells, (blue) CD3+ cells from mouse spleen 2 days after OT-II T-cell adoptive transfer. Image shown is representative of n=2 mice.

CFSE fluorescence detected after 2 days revealed that injected OVA in PBS was not able to induce OT-II T-cell proliferation. However, OVA when combined with an

adjuvant such as CFA, was able to induce T-cell proliferation as indicated by the successive reduction in fluorescence intensity of peaks in Figure A 3.

A.2. Supplemental to Aim 2

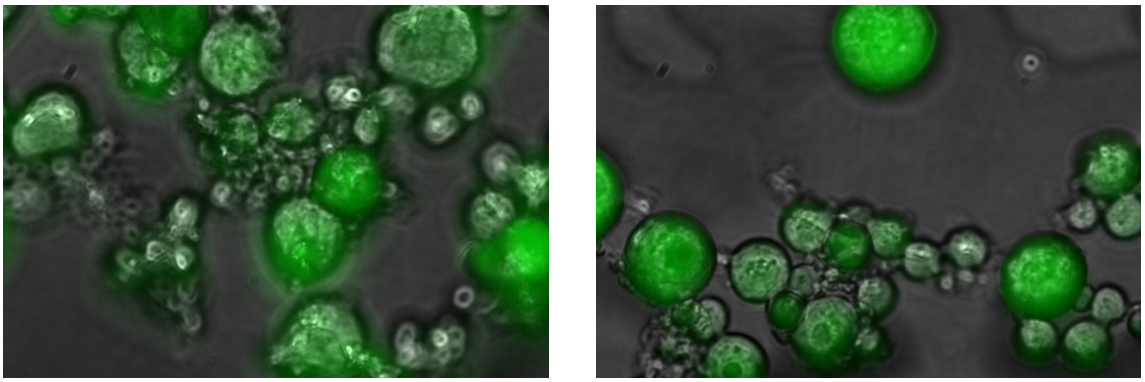

Figure A 4 Light microscopic images of crosslinked gelatin MPs (left)10mM, (right) 25mM of glutaraldehyde crosslinker

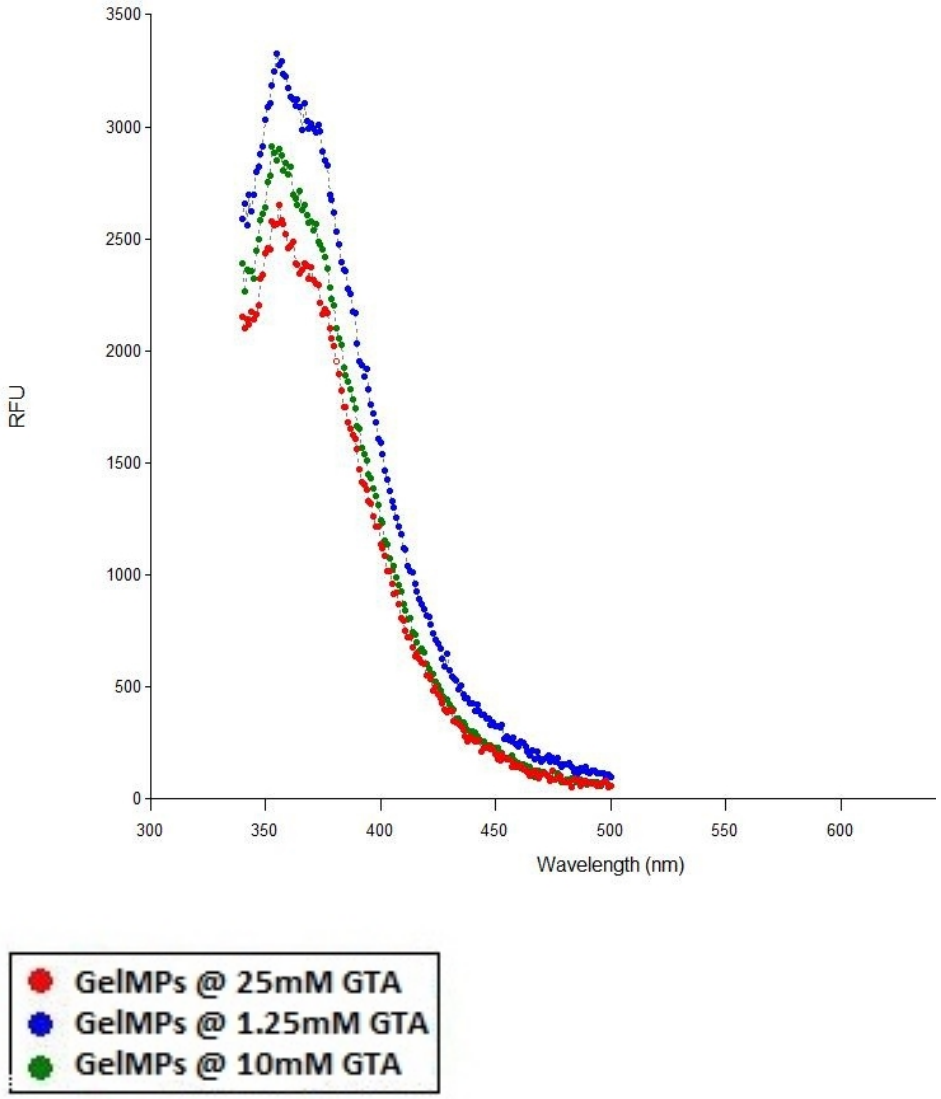

Figure A 5 Gelatin MP exhibit autofluorescence at 360nm that increases with crosslinking density

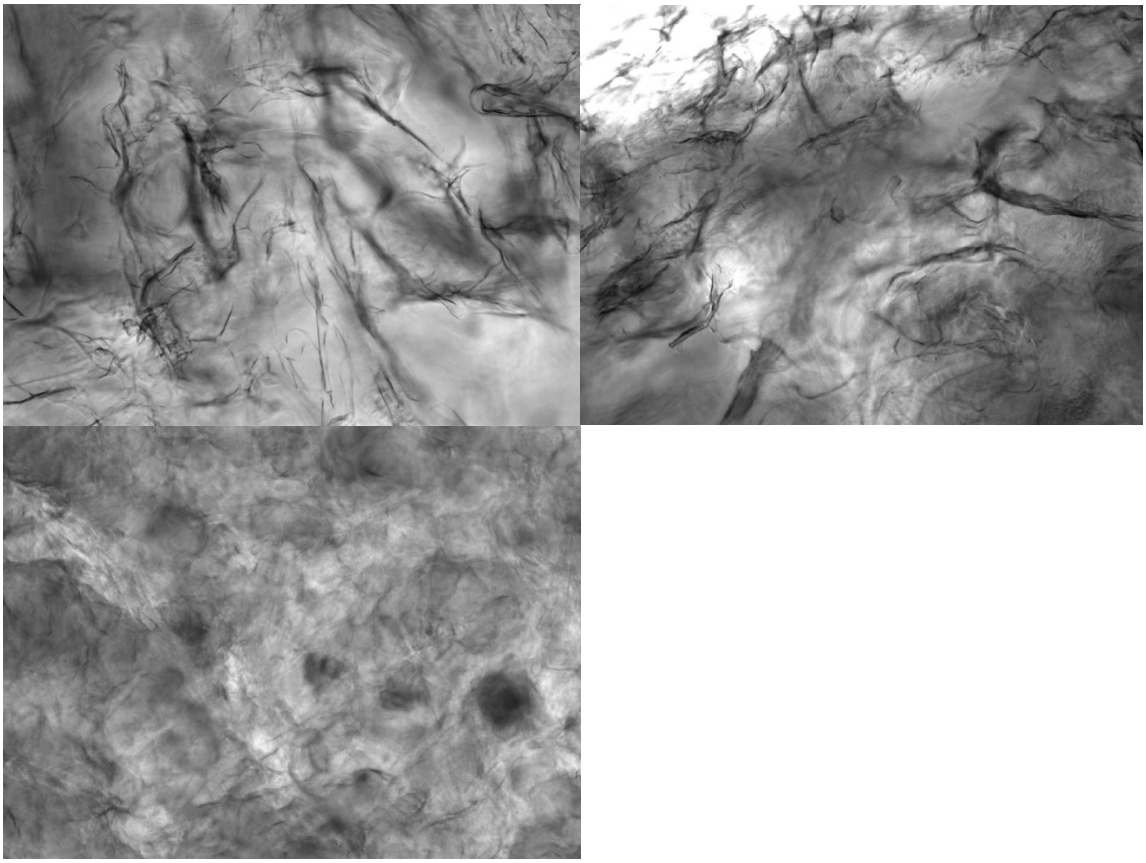

Figure A 6 Light microscopic images of swollen agarose cryogel scaffold at 4x magnification.

Cryogels were made from (top left) 1%, (top right) 1.5% or (bottom) 3% w/w solution of low melting temperature ultrapure agarose. Images reveal interconnected network that gets denser with increasing agarose concentration.

A.3. Supplemental to Aim 3

A.3.1. Optimizing Bone Marrow-Derived DC Culture

In order to optimize culture parameters such as timing, cell adherence and treatment groups, we experimented with a wide range of variables and determined their effects on the cell surface markers at the end of culture. Culture period was extended to 8

days allowing 2 days of exposure to maturation or tolerogenic treatments. Cytokine addition particular that of IL-4 was increased from 4ng to 20ng (see Methods section in Chapter 6). The figures shown below are those of cell surface markers associated with DC cell phenotype under 2 variables – i) different maturation stimuli to generate mDCs namely LPS or TNF-α, ii) extent of cellular adhesion to tissue culture plates – non-adherent and loosely adherent versus adherent

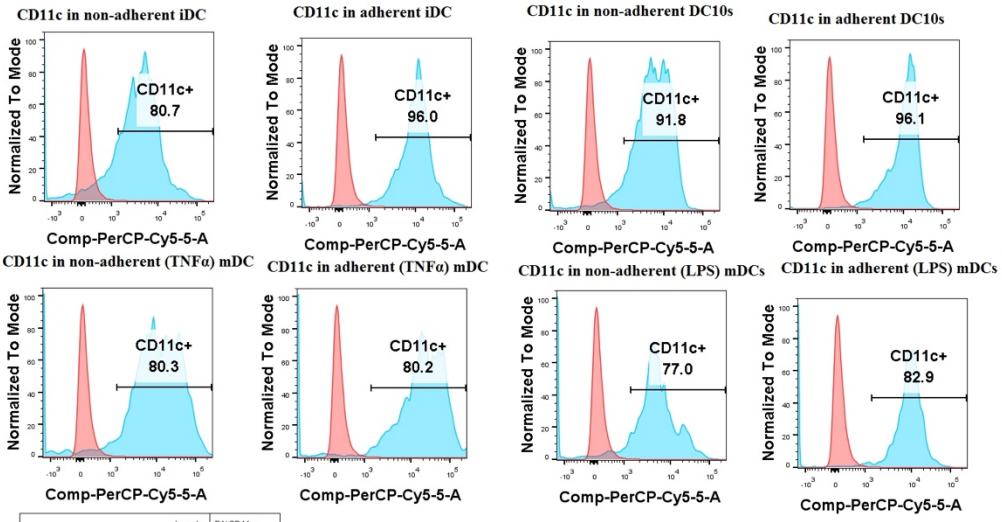

Ancestry Subset Statistic For	P1/CD11c+ Geometric Mean
DC10_IL-10_CD11c-IA_Percp_PE.fcs	6527
DC10s with IL-10_cell_stripper_CD11c-IA_Percp_PE.fcs	10637
iDC_CD11c-IA_Percp_PE.fcs	4904
iDC_CD11c_Percp.fcs	8604
iDC_IA_PE.fcs	1935
iDC_Unstained.fcs	2468
iDC_cell_stripper_CD11c-IA_Percp_PE.fcs	10681
mDC with LPS_CD11c-IA_Percp_PE.fcs	5786
mDC with LPS_cellstripper_CD11c-IA_Percp_PE.fcs	9576
mDC with TNFalpha_CD11c-IA_Percp_PE.fcs	12893
mDC with TNFalpha_cell_stripper_CD11c-IA_Percp_PE.fcs	21041
Mean	8640
SD	5389

Figure A 7 CD11c surface expression on BMDCs derived with GM-CSF (20ng/ml) and IL-4 (20ng/ml) added every other day over an 8 day period. TNF-α (5ng/ml) or LPS (1μg/ml) was added on day 6 and cells were assessed with flow cytometry on day 8. shown

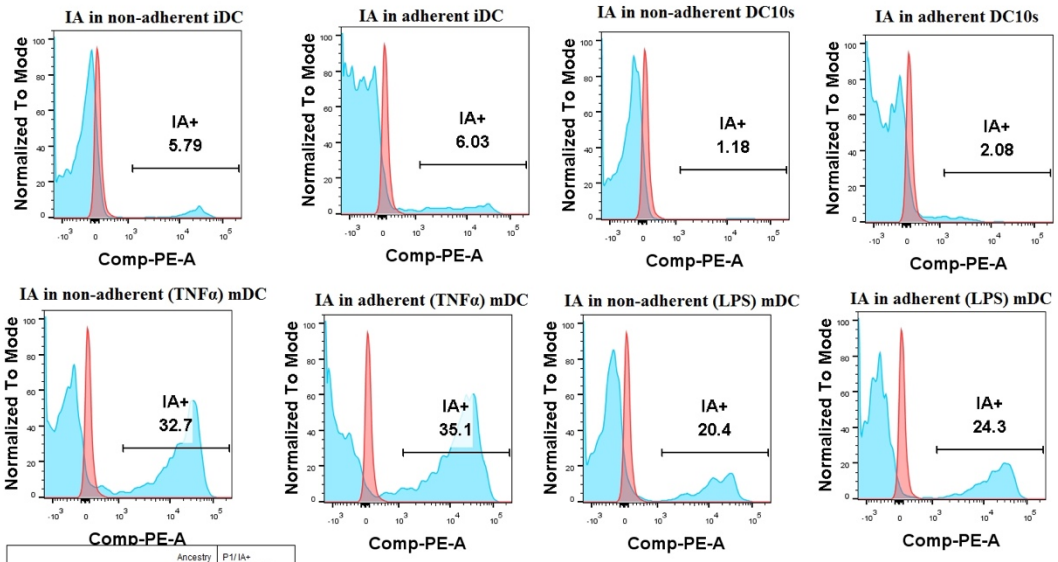

Ancestry Subset Statistic For	P1/IA+ Geometric Mean
DC10_IL-10_CD11c-IA_Percp_PE.fcs	11555
DC10s with IL-10_cell_stripper_CD11c-IA_Percp_PE.fcs	2079
iDC_CD11c-IA_Percp_PE.fcs	17838
iDC_CD11c_Percp.fcs	n/a
iDC_IA_PE.fcs	16269
iDC_Unstained.fcs	1396
iDC_cell_stripper_CD11c-IA_Percp_PE.fcs	7956
mDC with LPS_CD11c-IA_Percp_PE.fcs	13659
mDC with LPS_cellstripper_CD11c-IA_Percp_PE.fcs	16543
mDC with TNFalpha_CD11c-IA_Percp_PE.fcs	17282
mDC with TNFalpha_cell_stripper_CD11c-IA_Percp_PE.fcs	15297
Mean	
SD	

Figure A 8 I-A (MHC-II) surface expression on BMDCs stimulated with a maturation agent

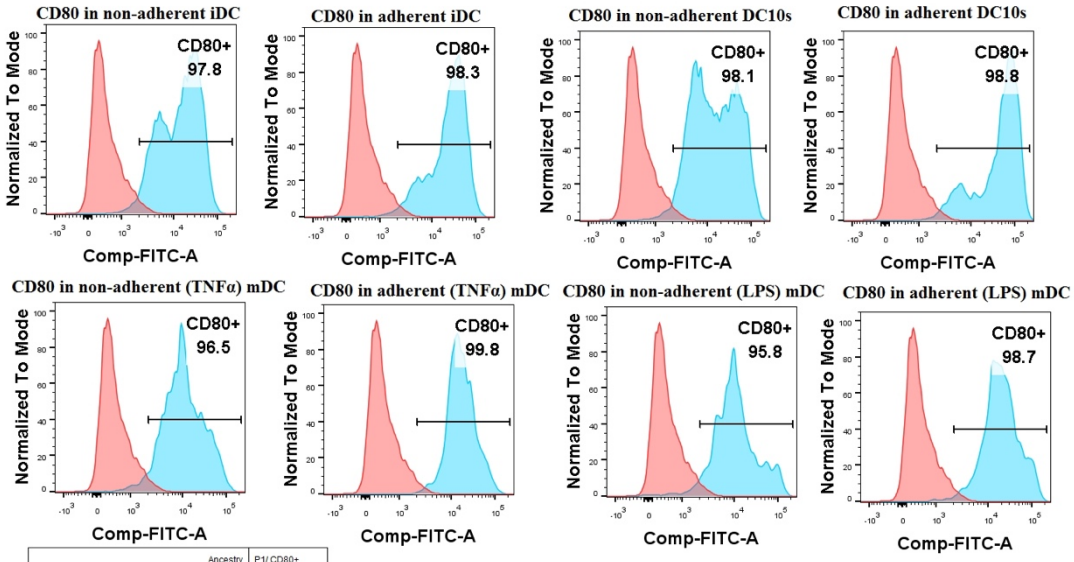

Ancestry Subset Statistic For	P1/ CD80+ Geometric Mean
DC10_IL-10_CD80-CD86_FITC-APC.fcs	15487
DC10s with IL-10_cell_stripper_CD80-CD86_FITC-APC.fcs	39995
iDC_CD80-CD86_FITC-APC.fcs	14275
iDC_CD80_FITC.fcs	14404
iDC_CD86-APC.fcs	3144
iDC_Unstained.fcs	2810
iDC_cell_stripper_CD80-CD86_FITC-APC.fcs	23057
mDC with LPS_CD80-CD86_FITC-APC.fcs	11855
mDC with LPS_cellstripper_CD80-CD86_FITC-APC.fcs	20329
mDC with TNFalpha_CD80-CD86_FITC-APC.fcs	11825
mDC with TNFalpha_cell_stripper_CD80-CD86_FITC-APC.fcs	17263
Mean	*15856*
SD	*10191*

Figure A 9 CD80 surface expression on BMDCs stimulated with a maturation agent

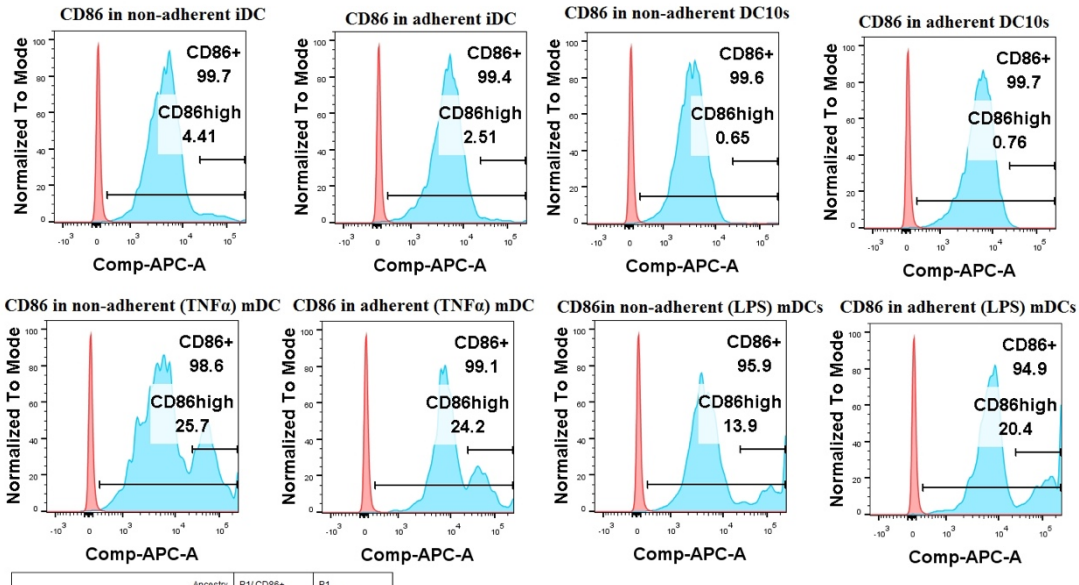

Ancestry Subset Statistic For	P1/ CD86+ Geometric Mean	P1 CD86high Geometric Mean
DC10_IL-10_CD80-CD86_FITC-APC.fcs	3424	71029
DC10s with IL-10_cell_stripper_CD80-CD86_FITC-APC.fcs	5404	37599
iDC_CD80-CD86_FITC-APC.fcs	4600	55446
iDC_CD80_FITC.fcs	652	n/a
iDC_CD86-APC.fcs	3332	56398
iDC_Unstained.fcs	619	n/a
iDC_cell_stripper_CD80-CD86_FITC-APC.fcs	4879	54820
mDC with LPS_CD80-CD86_FITC-APC.fcs	6188	99014
mDC with LPS_cellstripper_CD80-CD86_FITC-APC.fcs	10875	98118
mDC with TNFalpha_CD80-CD86_FITC-APC.fcs	8076	57659
mDC with TNFalpha_cell_stripper_CD80-CD86_FITC-APC.fcs	11605	52945
Mean	*5423*	
SD	*3616*	

Figure A 10 CD86 surface expression on BMDCs stimulated with a maturation agent

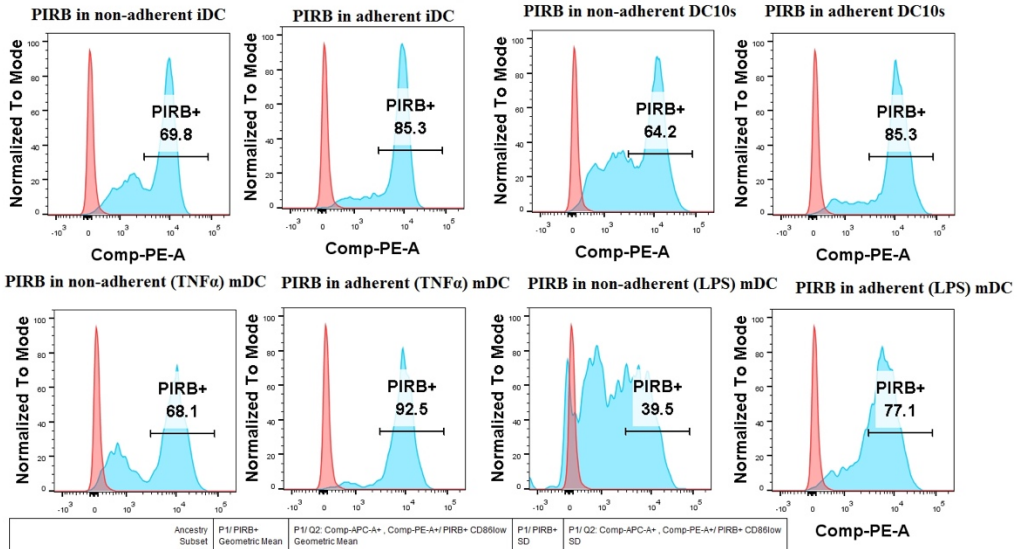

Ancestry Subset Statistic For	P1/ PIRB+ Geometric Mean	P1/ Q2: Comp-APC-A+ , Comp-PE-A+/ PIRB+ CD86low Geometric Mean	P1/ PIRB+ SD	P1/ Q2: Comp-APC-A+ , Comp-PE-A+/ PIRB+ CD86low SD
DC10_IL-10_CD86-PIRB_APC-PE.fcs	10039	3240	7574	2305
DC10s with IL-10_cell_stripper_CD86-PIRB_APC-PE.fcs	12133	3941	7986	2867
iDC_CD86-APC.fcs	n/a	4711	n/a	n/a
iDC_CD86-PIRB_APC-PE.fcs	9714	3634	3975	2823
iDC_PIRB_PE.fcs	8204	1316	3718	549
iDC_Unstained.fcs	n/a	n/a	n/a	n/a
iDC_cell_stripper_CD86-PIRB_APC-PE.fcs	8949	4334	3444	3190
mDC with LPS_CD86-PIRB_APC-PE.fcs	6771	5080	5877	3309
mDC with LPS_cellstripper_CD86-PIRB_APC-PE.fcs	7075	4672	5238	2839
mDC with TNFalpha_CD86-PIRB_APC-PE.fcs	9855	5506	6395	4232
mDC with TNFalpha_cell_stripper_CD86-PIRB_APC-PE.fcs	9379	7916	5214	3891
Mean				
SD				

Figure A 11 PirB surface expression on BMDCs stimulated with a maturation agent

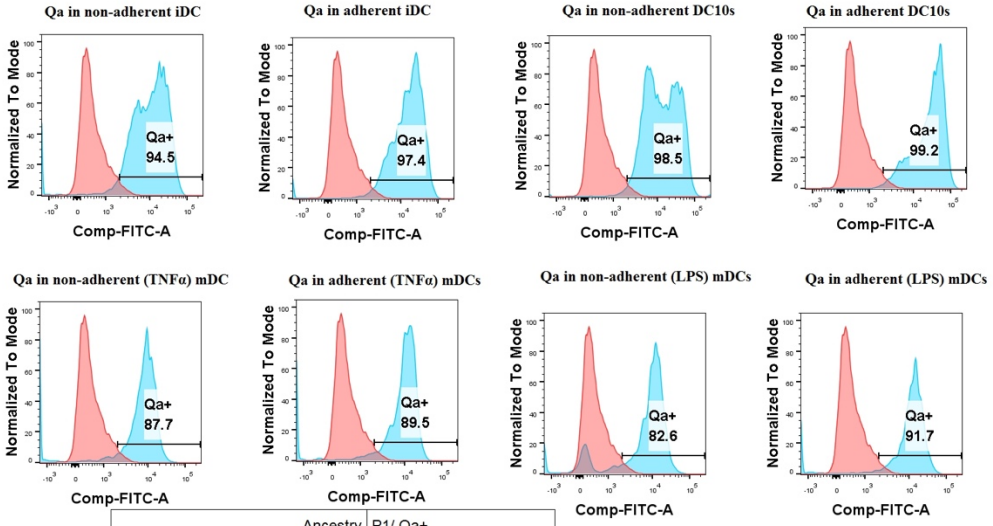

Ancestry Subset Statistic For	P1/ Qa+ Geometric Mean
DC10_IL-10_Qa-IA_FITC-PE.fcs	13575
DC10s with IL-10_cell_stripper_Qa-IA_FITC-PE.fcs	25233
iDC_IA_PE.fcs	2563
iDC_Qa-IA_FITC-PE.fcs	11195
iDC_Qa_FITC.fcs	12401
iDC_Unstained.fcs	2642
iDC_cell_stripper_Qa-IA_FITC-PE.fcs	15715
mDC with LPS_Qa-IA_FITC-PE.fcs	10618
mDC with LPS_cellstripper_Qa-IA_FITC-PE.fcs	12659
mDC with TNFalpha_Qa-IA_FITC-PE.fcs	8810
mDC with TNFalpha_cell_stripper_Qa-IA_FITC-PE.fcs	10734
Mean	11468
SD	6163

Figure A 12 Qa-1 (MHC-I) surface expression on BMDCs stimulated with a maturation agent

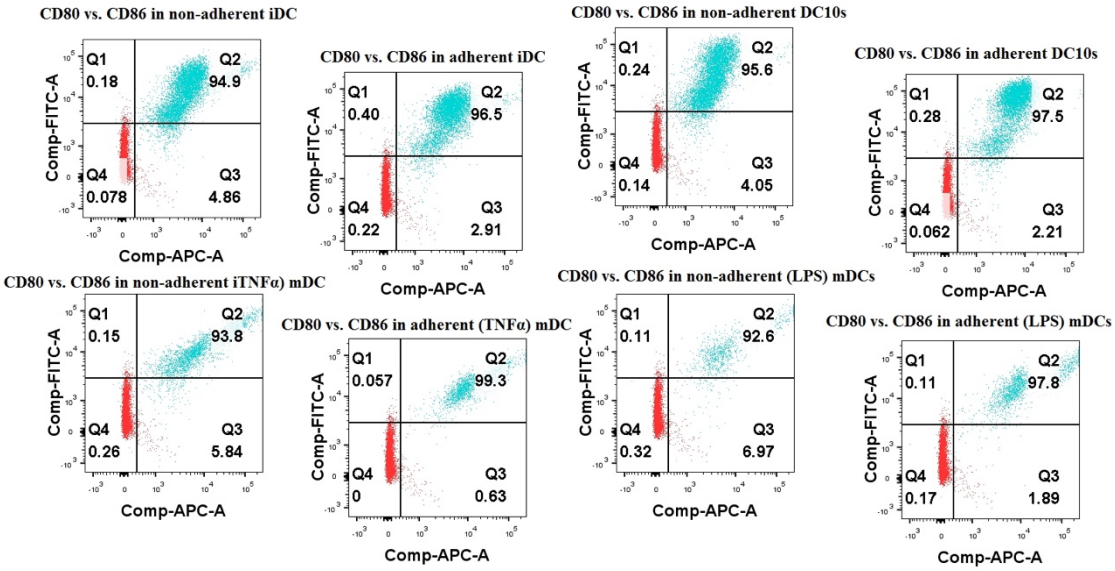

Figure A 13 CD80 vs. CD86 surface expression on BMDCs stimulated with a maturation agent

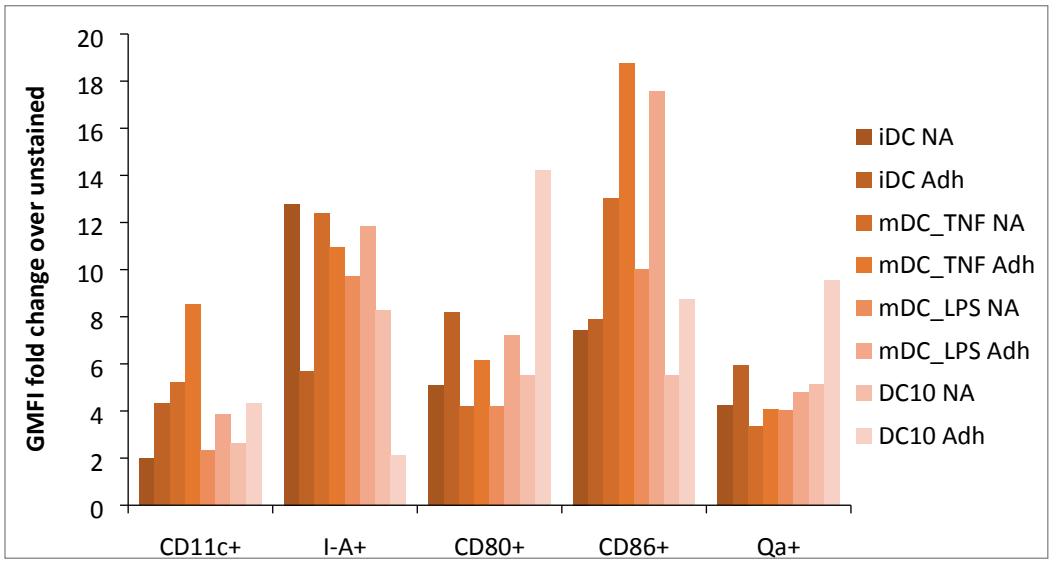

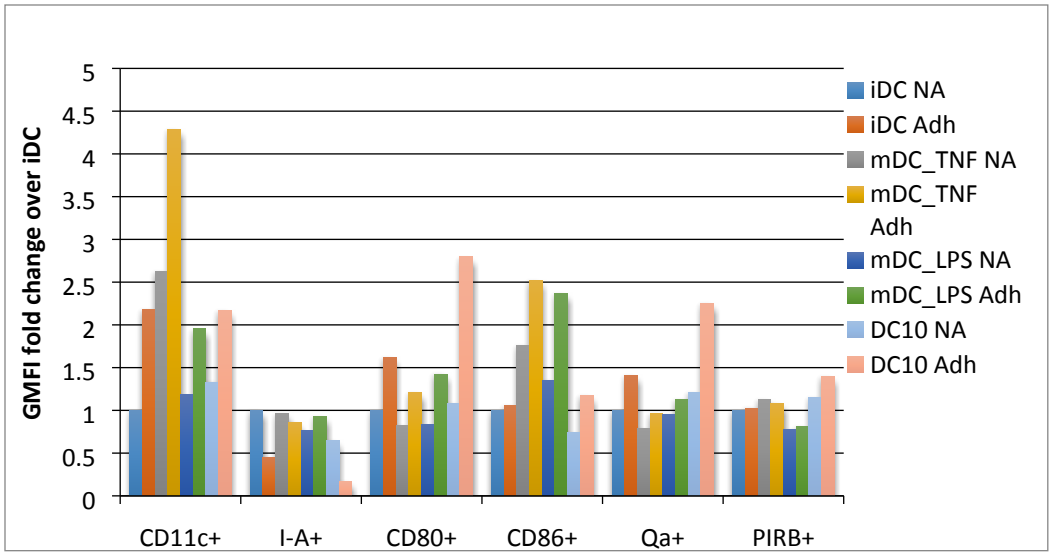

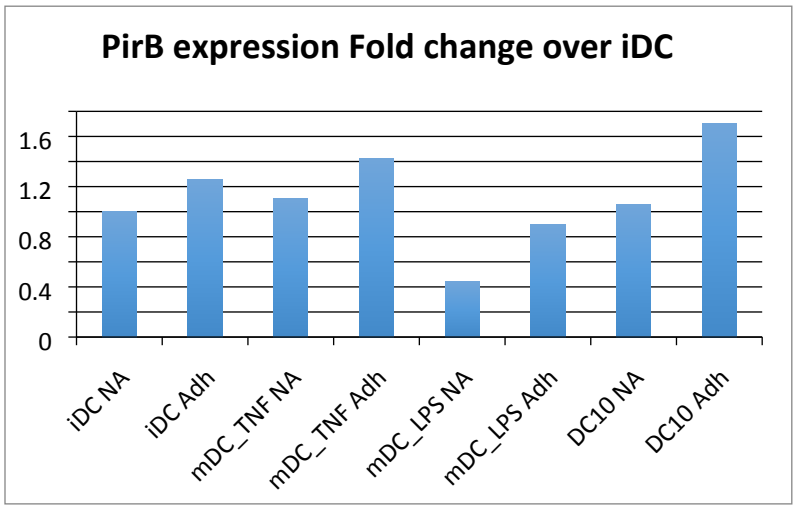

Figure A 14 Comparison of non-adherent and adherent murine BM-derived DCs displayed strong DC characteristics in terms of surface marker expression. iDC – immature or untreated DC, mDC – mature DCs stimulated by LPS or TNF-α, DC10s – IL-10-treated DCs. NA –non- oe loosely adherent, Adh – adherent. (top) GMFI fold change of unstained or (middle) iDCs. (Bottom) Expression of PirB, a tolerogenic marker. (For specific concentrations of treatments and timings please refer to the Methods section on BMDC culture in Chapter 6). Data is averaged over n=2 mice.

A.4. Determine the differential effects of biomaterials co-delivering a model cellular antigen on the humoral immune response in an *in vivo* mouse model

A.4.1. Overview

The Babensee laboratory has previously shown that PLGA elicits an adjuvant effect towards model antigen ovalbumin (OVA) in mice[13]. Additionally, other materials such as agarose produce differential adjuvant response than PLGA[13]. Further, it would be interesting to explore if the observed differential effects of biomaterials are also rendered by the delivery of cells in biomaterials with potential significance in applications designed to treat pathogenic or autoimmune diseases. OVA-producing cells namely E.G7-OVA[251], a murine lymphoma cell line transfected to secrete OVA in culture, will be delivered in PLGA or agarose in the model. We *hypothesize* that the differential effect caused by PLGA and agarose on the recipient's immune system will be consistent even when the antigen is delivered in cellular form; the non-activating effect of agarose would allow the tolerization of the recipient's immune system in the context of the co-delivered cellular if the agarose scaffold is implanted prior to that of PLGA such that the adjuvant effect of PLGA to the co-delivered cellular antigen would be reduced, highlighting that such material-based techniques can be further exploited to conditionally re-educate the immune system towards specific antigen.

A.4.2.Methods

A.4.2.1.1. EG7.OVA culture

E.G7-OVA cells (ATCC, Manassas, VA) were maintained according to manufacturer's protocol. Briefly, the cells were kept at 37°C and 5% CO_2 atmosphere in RPMI culture medium along with fetal bovine serum, necessary cell nutrients and 1%pennicillin/streptomycin. The culture medium was renewed every 3 days. Cells were collected and centrifuged at 300x g for 5 minutes and the supernatants were collected, frozen or used for experiments. Supernatants were diluted at 1:100, 1:1000, 1:10000 ratios in sterile PBS and analyzed for the presence of OVA using a sandwich ELISA and the concentration of secreted OVA was quantified and normalized against the cell numbers.

A.4.2.1.2. Preparation of PLGA/Agarose scaffolds w/OVA or w/E.G7-OVA-cells

PLGA and agarose scaffolds were prepared according to methods described in Chapter 4 and 5. OVA was added directly to the PLGA (see Chapter 4) or agarose solution during casting when required, based on previous studies from our lab. Cell-carrying scaffolds were prepared by placing sterilized, lyophilized biomaterial scaffolds in wells consisting of 1-10 x 10^6 cells/ml for 4 hours at 37°C. Scaffolds were coated in a 0.5% solution of filter-sterilized agarose and dried in the tissue culture hood for 30 minutes allowing the external coat to partially solidify to contain the cells within the scaffold. Scaffolds were later withdrawn and washed with media. Cells eluted in the washes were counted to determine the number of adsorbed cells in the scaffolds

A.4.2.1.3. Assessment of viability and functionality of cell-carrying scaffold

Cell-carrying scaffolds were prepared at varying cell concentrations – 10^6 -10^8 cells per 8mm diameter scaffold and maintained in culture in 12-well plates. Media was refreshed every 3 days. These scaffolds were analyzed with 3-(4,5-dimethylthiazol-2-yl)-2,5-diphenyltetrazolium bromide (MTT) assay to assess cell viability at 2,4,6,8,10 days and compared against cells in suspension at similar concentrations (i.e. without scaffold). Supernatants collected every 3 days during medium replacement, and were analyzed with ELISA to determine production of OVA. Additional set of cell-carrying scaffolds were fixed at days 2,3,4,6,8,10 in 1% formalin and prepared for histology.

A.4.2.1.4. Implantation of OVA-PLGA scaffolds and serum cytokine analyses

OVA was co-delivered in PLGA scaffold implanted in the dorsal subcutaneous region of the mice or as soluble OVA in CFA or in PBS. Blood was withdrawn from mice via retro-orbital method every 2 weeks for up to 12 weeks post implantation. Serum was isolated from blood and ELISA for IgG, IgG1, IgG2a specific for OVA was done to determine antibody production over time as previously described[13].

A.4.3.Results

A.4.3.1.1. Functionality OVA-secreting cells

To determine the effectiveness of OVA secretion from these cells, a sandwich ELISA was performed against OVA protein indicating the presence of OVA in the E.G7-OVA culture supernatants and concentration of OVA (214.32 ± 25.76 ng/ml at 10^6 cells/ml cultured for 3 days) was determined based on a standard curve (Figure A)

derived from a set of serially diluted OVA in PBS solutions of known concentrations.

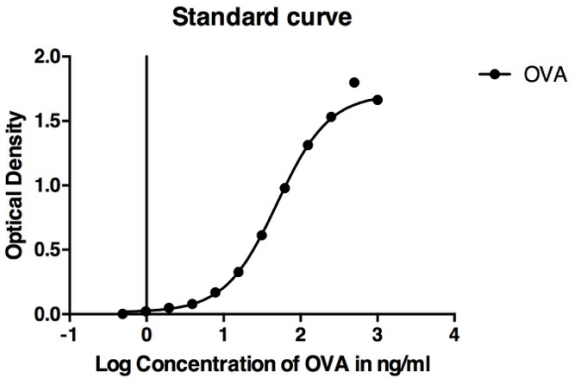

Figure A 15 Standard curve of serially diluted OVA for anti-OVA ELISA

A.4.3.1.2. Encapsulation of OVA-secreting cells in agarose gels

Scaffolds of PLGA or agarose were prepared with or without E.G7-OVA cells by diffusional loading of cells. Since the pore sizes were an order of magnitude higher than the cells, it was expected that diffusional loading would be effective strategy for cell incorporation. However, based on the extent of eluted cells, it was observed that only a ~ 20-30% of the total cells were loaded, which improved to 40% in agarose scaffolds that were coated with agarose solution. This suggested a necessity for increasing the concentration of cells available for loading, thereby increasing the diffusional driver of the loading event

A.4.3.1.3. Viability of encapsulated OVA-secreting cells

Modification in the MTT assay was required in order to allow the reagents to penetrate through the scaffold before reaching the cells Supernatants from the samples showed OVA production up to ten days when in scaffold (not shown). To enable better

penetration of MTT, slices of the scaffold prepared under sterile conditions resulting in sustained viability of cells for up to 4 days after which there was a significant drop in viability by day 6.These results were however not corroborated by the findings of the histological analysis, which showed increased dead cells in all samples older than 2 days. This may have been due to an experimental deficiency during histological processing, as repeat MTT assays were consistent with the original results

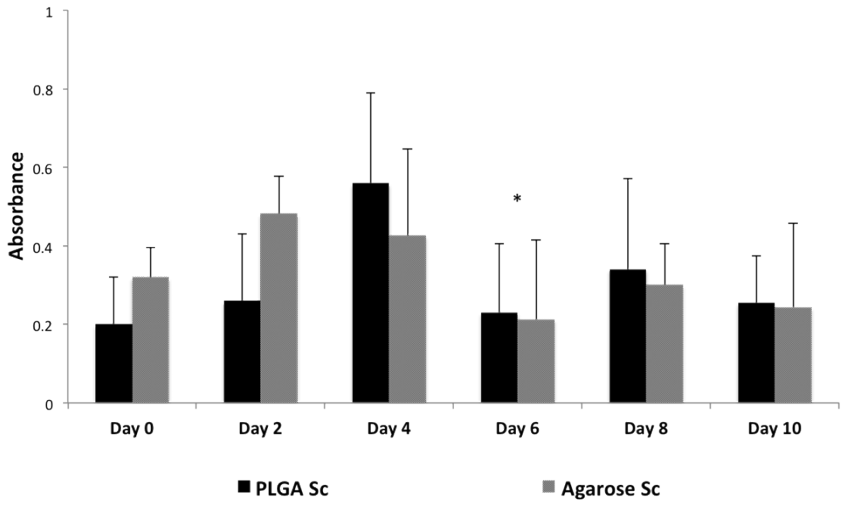

Figure A 16 Viability of scaffold-encapsulated OVA.

MTT assay was done on slices of PLGA or agarose scaffolds containing 10^8 cells per scaffold, over a 10-day period where there was a significant drop in viability on day 6 compared to the previous time point (* $p < 0.05$). Absorbance shown is the direct measured value not normalized for the total number of cells measured at each time point, however, thickness of sliced scaffold was maintained uniform

A.4.3.1.4. Humoral Immune Response of OVA-loaded PLGA scaffold in vivo

Mice that received OVA in PLGA scaffold showed a gradual increase in the assessed OVA-specific antibodies over the 12-week period in a manner comparable to the OVA/CFA treated mice controls signifying that PLGA was indeed eliciting an adjuvant effect, also confirming the previous results from our lab[13].

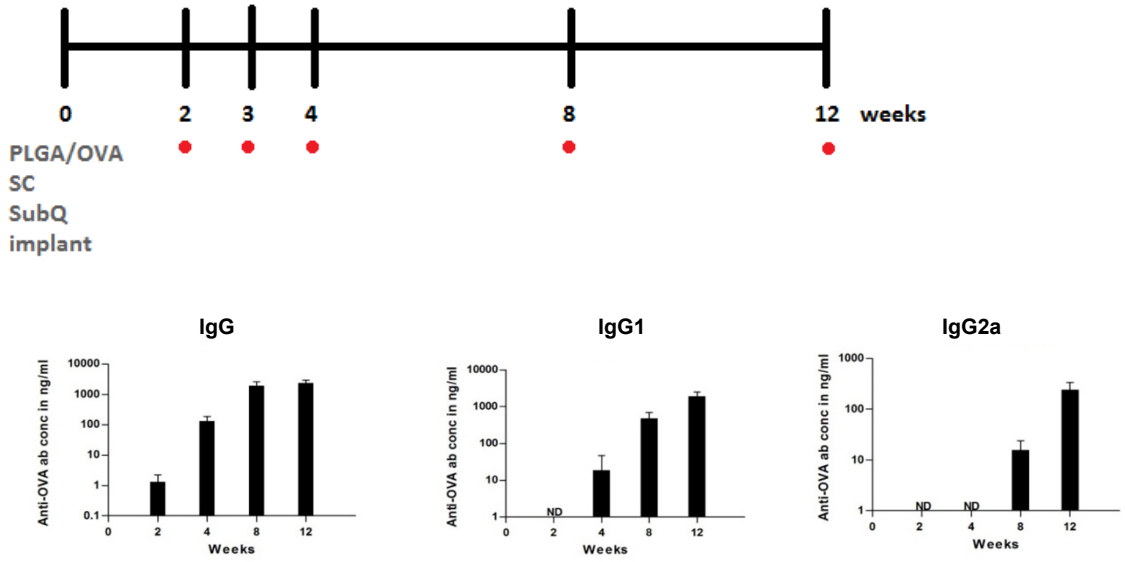

Figure A 17 PLGA adjuvant effect *in vivo*. OVA/PLGA Scaffold-implanted mice were monitored over a 12-week period (top – timeline) during which orbital blood was collected and assessed with an ELISA against OVA-specific antibodies such as IgG, IgG1, IgG2a

A.4.4.Discussion

The primary objective of this section was to determine whether the differential biomaterial adjuvant effect – observed in vivo for PLGA and agarose delivering model

antigen OVA – would occur if the soluble model antigen was replaced by live cells secreting OVA. Although here we were unable to testing the biomaterial cell-delivery model in vivo, we were able to successfully establish the groundwork by testing individual components. Subsequent work would require combining these individual parts in a model shown in Figure A 17. As agarose is known to maintain DCs in a rather immature phenotype, we expect that the agarose scaffold-primed sample group would exhibit a reduced humoral response to PLGA-cell scaffold. To determine the humoral immune response *in vivo*, C57Bl/6 wild type mice would receive subcutaneous implants of OVA-producing cells or OVA in PLGA or agarose and the production of Th2 antibodies such as IgG, IgG1, IgG2a specific for OVA in the serum would be measured to that of controls groups treated with OVA in CFA and OVA in PBS. Serum samples are isolated every 2 weeks for up to 12 weeks after implantations. A minimum of 2 weeks would be required to generate detectable levels of antibodies in the blood.

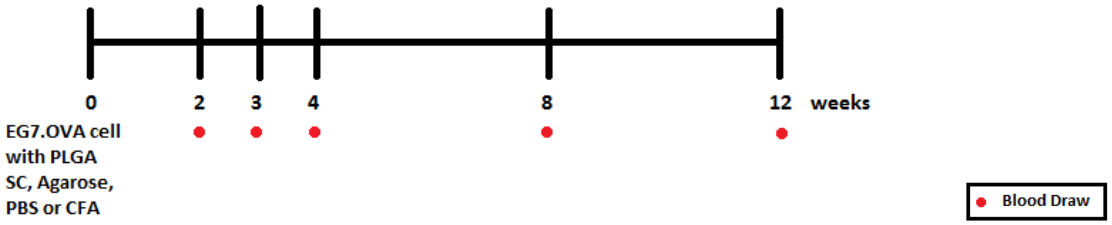

Figure A 18 Timeline for determining biomaterial adjuvant effect to encapsulated OVA-secreting cells

Countless strategies in tissue engineering and regenerative medicine currently being explored involve the use of a cell delivery schemes[252]. In *in vivo* applications of these strategies would elicit an immune response to the cellular antigen as well as an

inflammatory or other host response to the material. From our knowledge of biomaterial and host interaction, it is straightforward to suggest that the nature of the biomaterial in these applications can strongly influence their outcome. By establishing a methodology of cell encapsulation and delivery with our existing models of biomaterial and host interaction, we believe there is plenty to learn from the role of host response in regeneration in designing successful clinical therapies.

In the context of immunotherapies, several approaches involving cell-loaded are being investigated as treatments for cancer and other immune-related disorders. Scaffolds can deliver DCs or T-cells in these therapies to re-condition host immune systems. Combining biomaterial-based approaches with cell delivery especially in a way that can synergistically effect the immune response – for example, using a DC maturation-inducing material such as PLGA to deliver DCs with cancer-associated antigen to ramp up endogenous immune attack on tumors, or using a DC maturation non-stimulating material such as agarose to deliver DCs or T-cells to influence a regulatory behavior in the native immune system in the case of autoimmune diseases – serve an a attractive opportunity to develop clinical immunotherapies.

REFERENCES

1. Weinhold, B. Examining Assumptions about Female Dominance in Autoimmune Disease. *Environmental Health Perspectives* **120,** a107 (2012).
2. Jacobson, D. L., Gange, S. J., Rose, N. R. & Graham, N. M. H. Epidemiology and Estimated Population Burden of Selected Autoimmune Diseases in the United States. *Clinical Immunology and Immunopathology* **84,** 223–243 (1997).
3. Shoenfeld, Y. & Isenberg, D. A. The mosaic of autoimmunity. *Immunol. Today* **10,** 123–126 (1989).
4. Atassi, M. Z. & Casali, P. Molecular mechanisms of autoimmunity. *Autoimmunity* **41,** 123–132 (2008).
5. Steinman, R. M., Hawiger, D. & Nussenzweig, M. C. Tolerogenic Dendritic Cells. *Annu. Rev. Immunol.* **21,** 685–711 (2003).
6. Ratner, B. D. *Biomaterials science: an introduction to materials in medicine*. (Academic Press, 2004).
7. Yoshida, M. & Babensee, J. E. Differential effects of agarose and poly(lactic-co-glycolic acid) on dendritic cell maturation. *J. Biomed. Mater. Res.* **79A,** 393–408 (2006).
8. Fischer, S., Uetz-von Allmen, E., Waeckerle-Men, Y., Groettrup, M., Merkle, H. P. & Gander, B. The preservation of phenotype and functionality of dendritic cells upon phagocytosis of polyelectrolyte-coated PLGA microparticles. *Biomaterials* **28,** 994–1004 (2007).
9. Kou, P. M., Schwartz, Z., Boyan, B. D. & Babensee, J. E. Acta Biomaterialia. *Acta BIOMATERIALIA* **7,** 1–10 (2010).
10. Babensee, J. E. Interaction of dendritic cells with biomaterials. *Innate and Adaptive Immune Responses in Tissue Engineering* **20,** 101–108 (2008).
11. Yoshida, M., Mata, J. & Babensee, J. E. Effect of poly(lactic-co-glycolic acid) contact on maturation of murine bone marrow-derived dendritic cells. *J. Biomed. Mater. Res.* **80A,** 7–12 (2007).
12. Bennewitz, N. L. & Babensee, J. E. The effect of the physical form of poly(lactic-co-glycolic acid) carriers on the humoral immune response to co-delivered antigen. *Biomaterials* **26,** 2991–2999 (2005).
13. Norton, L. W., Park, J. & Babensee, J. E. Journal of Controlled Release. *Journal of Controlled Release* **146,** 341–348 (2010).
14. Boks, M. A., Kager-Groenland, J. R., Haasjes, M. S. P., Zwaginga, J. J., van Ham, S. M. & Brinke, ten, A. IL-10-generated tolerogenic dendritic cells are optimal for functional regulatory T cell induction — A comparative study of human clinical-applicable DC. *Clinical Immunology* **142,** 332–342 (2012).
15. Perona-Wright, G., Anderton, S. M., Howie, S. E. M. & Gray, D. IL-10 permits transient activation of dendritic cells to tolerize T cells and protect from central nervous system autoimmune disease. *International Immunology* **19,** 1123–1134 (2007).
16. Yamazaki, S., Bonito, A. J., Spisek, R., Dhodapkar, M., Inaba, K. & Steinman, R. M. Dendritic cells are specialized accessory cells along with TGF-β for the differentiation of Foxp3+ CD4+ regulatory T cells from peripheral Foxp3− precursors. *Blood* **110,**

4293–4302 (2007).

17. Rozkova, D., Horvath, R., Bartunkova, J. & Spisek, R. Glucocorticoids severely impair differentiation and antigen presenting function of dendritic cells despite upregulation of Toll-like receptors. *Clinical Immunology* **120,** 260–271 (2006).

18. Matzelle, M. M. & Babensee, J. E. Humoral immune responses to model antigen co-delivered with biomaterials used in tissue engineering. *Biomaterials* **25,** 295–304 (2004).

19. Yoshida, M. & Babensee, J. E. Poly(lactic-co-glycolic acid) enhances maturation of human monocyte-derived dendritic cells. *J. Biomed. Mater. Res.* **{71A},** 45–54 (2004).

20. Jung, S., Unutmaz, D., Wong, P., Sano, G.-I., De los Santos, K., Sparwasser, T., Wu, S., Vuthoori, S., Ko, K. & Zavala, F. In Vivo Depletion of CD11c+ Dendritic Cells Abrogates Priming of CD8+ T Cells by Exogenous Cell-Associated Antigens. *Immunity* **17,** 211–220 (2002).

21. Bar-On, L. & Jung, S. Defining in vivo dendritic cell functions using CD11c-DTR transgenic mice. 429–442 (2010). doi:10.1007/978-1-60761-421-0

22. Murphy, K. P., Travers, P., Walport, M. & Janeway, C. *Immunobiology - NCBI Bookshelf*. (Garland Science, 2008). at <http://www.ncbi.nlm.nih.gov/books/NBK10757/>

23. Lan, Y. Y., Wang, Z., Raimondi, G., Wu, W., Colvin, B. L., de Creus, A. & Thomson, A. W. 'Alternatively activated' dendritic cells preferentially secrete IL-10, expand Foxp3+ CD4+ T cells, and induce long-term organ allograft survival in combination with CTLA4-Ig. *The Journal of Immunology* **177,** 5868–5877 (2006).

24. Debierre-Grockiego, F., Campos, M. A., Azzouz, N., Schmidt, J., Bieker, U., Resende, M. G., Mansur, D. S., Weingart, R., Schmidt, R. R. & Golenbock, D. T. Activation of TLR2 and TLR4 by glycosylphosphatidylinositols derived from Toxoplasma gondii. *J Immunol* **179,** 1129–1137 (2007).

25. Park, J. & Babensee, J. E. Differential functional effects of biomaterials on dendritic cell maturation. *Acta BIOMATERIALIA* **8,** 3606–3617 (2012).

26. Janeway, C. A. & Medzhitov, R. INNATE IMMUNE RECOGNITION. *Annu. Rev. Immunol.* **20,** 197–216 (2002).

27. Ishii, K. J., Coban, C. & Akira, S. Manifold Mechanisms of Toll-Like Receptor-Ligand Recognition. *J. Clin. Immunol.* **25,** 511–521 (2005).

28. Chaplin, D. D. Overview of the immune response. *Journal of Allergy and Clinical Immunology* **125,** S3–S23 (2010).

29. Murphy, K. P., Travers, P., Walport, M. & Janeway, C. *Janeway's immunobiology*. (Garland Science, 2008).

30. Finlay, B. B. & McFadden, G. Anti-Immunology: Evasion of the Host Immune System by Bacterial and Viral Pathogens. *Cell* **124,** 767–782 (2006).

31. Steinman, R. M. & Cohn, Z. A. IDENTIFICATION OF A NOVEL CELL TYPE IN PERIPHERAL LYMPHOID ORGANS OF MICE : I. MORPHOLOGY, QUANTITATION, TISSUE DISTRIBUTION. *J. Exp. Med.* **137,** 1142–1162 (1973).

32. Steinman, R. M. & Cohn, Z. A. IDENTIFICATION OF A NOVEL CELL TYPE IN PERIPHERAL LYMPHOID ORGANS OF MICE : II. FUNCTIONAL PROPERTIES IN VITRO. *J. Exp. Med.* **139,** 380–397 (1974).

33. Steinman, R. M. The dendritic cell system and its role in immunogenicity. *Annu. Rev. Immunol.* **9,** 271–296 (1991).

34. Steinman, R. M., Kaplan, G., Witmer, M. D. & Cohn, Z. A. Identification of a novel cell type in peripheral lymphoid organs of mice. V. Purification of spleen dendritic cells, new surface markers, and maintenance in vitro. *J. Exp. Med.* **149,** 1–16 (1979).

35. Steinman, R. M. & Witmer, M. D. Lymphoid dendritic cells are potent stimulators of the primary mixed leukocyte reaction in mice. *Proc. Natl. Acad. Sci. U.S.A.* **75,** 5132–5136 (1978).

36. Bamboat, Z. M., Stableford, J. A., Plitas, G., Burt, B. M., Nguyen, H. M., Welles, A. P., Gonen, M., Young, J. W. & DeMatteo, R. P. Human Liver Dendritic Cells Promote T Cell Hyporesponsiveness. *J Immunol* **182,** 1901–1911 (2009).

37. Banchereau, J. & Steinman, R. M. Dendritic cells and the control of immunity. *Nature* **392,** 245–252 (1998).

38. Lipscomb, M. F. & Masten, B. J. Dendritic Cells: Immune Regulators in Health and Disease. *Physiol Rev* **82,** 97–130 (2002).

39. Banchereau, J., Briere, F., Caux, C., Davoust, J., Lebecque, S., Liu, Y.-J., Pulendran, B. & Palucka, K. Immunobiology of dendritic cells. *Annu. Rev. Immunol.* **18,** 767–811 (2000).

40. Merad, M., Sathe, P., Helft, J., Miller, J. & Mortha, A. The dendritic cell lineage: ontogeny and function of dendritic cells and their subsets in the steady state and the inflamed setting. *Annu. Rev. Immunol.* **31,** 563–604 (2013).

41. Caux, C., Ait-Yahia, S., Chemin, K., de Bouteiller, O., Dieu-Nosjean, M. C., Homey, B., Massacrier, C., Vanbervliet, B., Zlotnik, A. & Vicari, A. Dendritic cell biology and regulation of dendritic cell trafficking by chemokines. *Springer Semin. Immunopathol.* **22,** 345–369 (2000).

42. Kawai, T. & Akira, S. The roles of TLRs, RLRs and NLRs in pathogen recognition. - PubMed - NCBI. *International Immunology* **21,** 317–337 (2009).

43. Cravens, P. D. & Lipsky, P. E. Dendritic cells, chemokine receptors and autoimmune inflammatory diseases. *Immunol Cell Biol* **80,** 497–505 (2002).

44. Mellman, I. & Steinman, R. M. Dendritic cells: specialized and regulated antigen processing machines. *Cell* (2001). doi:10.1016/S0092-8674(01)00449-4

45. Lanzavecchia, A. Mechanisms of antigen uptake for presentation. **8,** 348–354 (1996).

46. Kamphorst, A. O., Guermonprez, P., Dudziak, D. & Nussenzweig, M. C. Route of Antigen Uptake Differentially Impacts Presentation by Dendritic Cells and Activated Monocytes. *J Immunol* **185,** 3426–3435 (2010).

47. Mantegazza, A. R., Magalhaes, J. G., Amigorena, S. & Marks, M. S. Presentation of Phagocytosed Antigens by MHC Class I and II. *Traffic* **14,** 135–152 (2012).

48. Saeki, H., Moore, A. M., Brown, M. J. & Hwang, S. T. Cutting edge: secondary lymphoid-tissue chemokine (SLC) and CC chemokine receptor 7 (CCR7) participate in the emigration pathway of mature dendritic cells from the skin to regional lymph nodes. *J Immunol* **162,** 2472–2475 (1999).

49. Harris, N. L. & Ronchese, F. The role of B7 costimulation in T-cell immunity. *Immunol Cell Biol* **77,** 304–311 (1999).

50. Sittig, S. P., Bakdash, G., Weiden, J., Sköld, A. E., Tel, J., Figdor, C. G., de Vries, I. J. M. & Schreibelt, G. A Comparative Study of the T Cell Stimulatory and Polarizing Capacity of Human Primary Blood Dendritic Cell Subsets. *Mediators of Inflammation* **2016,** 1–11 (2016).

51. Tanaka, H., Demeure, C. E., Rubio, M., Delespesse, G. & Sarfati, M. Human monocyte-derived dendritic cells induce naive T cell differentiation into T helper cell type 2 (Th2) or Th1/Th2 effectors. Role of stimulator/responder ratio. *J Exp Med* **192,** 405–412 (2000).

52. Dustin, M. L., Tseng, S. Y., Varma, R. & Campi, G. T cell–dendritic cell immunological synapses. *Current Opinion in Immunology* (2006). doi:10.1016/j.coi.2006.05.017

53. Joffre, O. P., Segura, E., Savina, A. & Amigorena, S. Cross-presentation by dendritic cells. *Nat Rev Immunol* **12,** 557–569 (2012).

54. Weiner, H. L., da Cunha, A. P., Quintana, F. & Wu, H. Oral tolerance. - PubMed - NCBI. *Immunological Reviews* **241,** 241–259 (2011).

55. Sigmundsdottir, H., Pan, J., Debes, G. F., Alt, C., Habtezion, A., Soler, D. & Butcher, E. C. DCs metabolize sunlight-induced vitamin D3 to 'program' T cell attraction to the epidermal chemokine CCL27. - PubMed - NCBI. *Nat Immunol* **8,** 285–293 (2007).

56. Karman, J., Ling, C., Sandor, M. & Fabry, Z. Initiation of immune responses in brain is promoted by local dendritic cells. *J Immunol* **173,** 2353–2361 (2004).

57. Ben Clarkson, Rayasam, A., Walker, A., Harris, M., Sandor, M. & Fabry, Z. Migration of i.c. injected BMDCs from brain to deep cervical lymph nodes is CCR7 dependent but does not promote EAE disease progression (CCR1P.244). *J Immunol* **192,** 48.4–48.4 (2014).

58. Sun, C.-M., Hall, J. A., Blank, R. B., Bouladoux, N., Oukka, M., Mora, J. R. & Belkaid, Y. Small intestine lamina propria dendritic cells promote de novo generation of Foxp3 T reg cells via retinoic acid. *J. Exp. Med.* **204,** 1775–1785 (2007).

59. Akbari, O., DeKruyff, R. H. & Umetsu, D. T. Pulmonary dendritic cells producing IL-10 mediate tolerance induced by respiratory exposure to antigen. *Nat Immunol* **2,** 725–731 (2001).

60. Lutz, M. B. & Schuler, G. Immature, semi-mature and fully mature dendritic cells: which signals induce tolerance or immunity? *Trends in Immunology* **23,** 445–449 (2002).

61. Dzionek, A., Fuchs, A., Schmidt, P., Cremer, S., Zysk, M., Miltenyi, S., Buck, D. W. & Schmitz, J. BDCA-2, BDCA-3, and BDCA-4: three markers for distinct subsets of dendritic cells in human peripheral blood. *J Immunol* **165,** 6037–6046 (2000).

62. Huysamen, C., Willment, J. A., Dennehy, K. M. & Brown, G. D. CLEC9A is a novel activation C-type lectin-like receptor expressed on BDCA3+ dendritic cells and a subset of monocytes. *J. Biol. Chem.* **283,** 16693–16701 (2008).

63. Schäkel, K., Kannagi, R., Kniep, B., Goto, Y., Mitsuoka, C., Zwirner, J., Soruri, A., Kietzell, von, M. & Rieber, E. P. 6-Sulfo LacNAc, a novel carbohydrate modification of PSGL-1, defines an inflammatory type of human dendritic cells. *Immunity* **17,** 289–301 (2002).

64. MacDonald, K. P. A., Munster, D. J., Clark, G. J., Dzionek, A., Schmitz, J. & Hart, D. N. J. Characterization of human blood dendritic cell subsets. *Blood* **100,** 4512–4520

(2002).

65. Gregori, S., Tomasoni, D., Pacciani, V., Scirpoli, M., Battaglia, M., Magnani, C. F., Hauben, E. & Roncarolo, M.-G. Differentiation of type 1 T regulatory cells (Tr1) by tolerogenic DC-10 requires the IL-10–dependent ILT4/HLA-G pathway. *Blood* **116,** 935–944 (2010).

66. Schulz, O., Jaensson, E., Persson, E. K., Liu, X., Worbs, T., Agace, W. W. & Pabst, O. Intestinal CD103+, but not CX3CR1+, antigen sampling cells migrate in lymph and serve classical dendritic cell functions. *J. Exp. Med.* **206,** 3101–3114 (2009).

67. Mucida, D., Pino-Lagos, K., Kim, G., Nowak, E., Benson, M. J., Kronenberg, M., Noelle, R. J. & Cheroutre, H. Retinoic Acid Can Directly Promote TGF-β-Mediated Foxp3+ Treg Cell Conversion of Naive T Cells. *Immunity* **30,** 471–472 (2009).

68. Sharma, M. D., Baban, B., Chandler, P., Hou, D.-Y., Singh, N., Yagita, H., Azuma, M., Blazar, B. R., Mellor, A. L. & Munn, D. H. Plasmacytoid dendritic cells from mouse tumor-draining lymph nodes directly activate mature Tregs via indoleamine 2,3-dioxygenase. *J. Clin. Invest.* **117,** 2570–2582 (2007).

69. Mainali, E. S., Kikuchi, T. & Tew, J. G. Dexamethasone Inhibits Maturation and Alters Function of Monocyte-Derived Dendritic Cells from Cord Blood. *Pediatric Research* **58,** 125–131 (2005).

70. Roca, L., Di Paolo, S., Petruzzelli, V., Grandaliano, G., Ranieri, E., Schena, F. P. & Gesualdo, L. Dexamethasone modulates interleukin-12 production by inducing monocyte chemoattractant protein-1 in human dendritic cells. *Immunol Cell Biol* **85,** 610–616 (2007).

71. Bosma, B. M., Metselaar, H. J., Nagtzaam, N. M. A., de Haan, R., Mancham, S., van der Laan, L. J. W., Kuipers, E. J. & Kwekkeboom, J. Dexamethasone transforms lipopolysaccharide-stimulated human blood myeloid dendritic cells into myeloid dendritic cells that prime interleukin-10 production in T cells. *Immunology* **125,** 91–100 (2008).

72. Piemonti, L., Monti, P., Allavena, P., Sironi, M., Soldini, L., Leone, B. E., Socci, C. & Di Carlo, V. Glucocorticoids affect human dendritic cell differentiation and maturation. *J Immunol* **162,** 6473–6481 (1999).

73. Gong, Y.-B., Huang, Y.-F., Li, Y., Han, G.-C., Li, Y.-R., Wang, D.-J., Du, G.-P., Yu, J.-F. & Song, J. Experimental study of the mechanism of tolerance induction in dexamethasone-treated dendritic cells. *Medical Science Monitor : International Medical Journal of Experimental and Clinical Research* **17,** BR125–BR131 (2011).

74. Olliver, M., Spelmink, L., Hiew, J., Meyer-Hoffert, U., Henriques-Normark, B. & Bergman, P. Immunomodulatory Effects of Vitamin D on Innate and Adaptive Immune Responses to Streptococcus pneumoniae. *Journal of Infectious Diseases* **208,** 1474–1481 (2013).

75. Sigmundsdottir, H., Pan, J., Debes, G. F., Alt, C., Habtezion, A., Soler, D. & Butcher, E. C. DCs metabolize sunlight-induced vitamin D3 to 'program' T cell attraction to the epidermal chemokine CCL27. *Nat Immunol* **8,** 285–293 (2007).

76. Sayers, B., Haniffa, M., Diboll, J., Isaacs, J. & Hilkens, C. Generation of dexamethasone and vitamin D3-treated human monocyte-derived dendritic cells with tolerogenic properties. *Arthritis Res Ther* **9,** P11 (2007).

77. Unger, W. W. J., Laban, S., Kleijwegt, F. S., van der Slik, A. R. & Roep, B. O.

Induction of Treg by monocyte-derived DC modulated by vitamin D3 or dexamethasone: differential role for PD-L1. - PubMed - NCBI. *Eur. J. Immunol.* **39,** 3147–3159 (2009).

78. Simon, J. C., Tigelaar, R. E., Bergstresser, P. R., Edelbaum, D. & Cruz, P. D. Ultraviolet B radiation converts Langerhans cells from immunogenic to tolerogenic antigen-presenting cells. Induction of specific clonal anergy in CD4+ T helper 1 cells. *J Immunol* **146,** 485–491 (1991).

79. Enk, A. H., Angeloni, V. L., Udey, M. C. & Katz, S. I. Inhibition of Langerhans cell antigen-presenting function by IL-10. A role for IL-10 in induction of tolerance. *J Immunol* **151,** 2390–2398 (1993).

80. Hubo, M., Trinschek, B., Kryczanowsky, F., Tuettenberg, A., Steinbrink, K. & Jonuleit, H. Costimulatory molecules on immunogenic versus tolerogenic human dendritic cells. - PubMed - NCBI. *Frontiers in Immunology* **4,** 82 (2013).

81. Zhou, H., Wang, Y., Lian, Q., Yang, B., Ma, Y., Wu, X., Sun, S., Liu, Y. & Sun, B. Differential IL-10 production by DCs determines the distinct adjuvant effects of LPS and PTX in EAE induction. - PubMed - NCBI. *Eur. J. Immunol.* **44,** 1352–1362 (2014).

82. Cook, P. C., Jones, L. H., Jenkins, S. J., Wynn, T. A., Allen, J. E. & MacDonald, A. S. Alternatively activated dendritic cells regulate CD4+ T-cell polarization in vitro and in vivo. *Proceedings of the National Academy of Sciences* **109,** 9977–9982 (2012).

83. Battaglia, M. Rapamycin selectively expands CD4+CD25+FoxP3+ regulatory T cells. *Blood* **105,** 4743–4748 (2005).

84. Macedo, C., Turquist, H., Metes, D. & Thomson, A. W. Immunoregulatory properties of rapamycin-conditioned monocyte-derived dendritic cells and their role in transplantation. *Transplantation Research 2012 1:1* **1,** 16 (2012).

85. Li, X., Li, J.-J., Yang, J.-Y., Wang, D.-S., Zhao, W., Song, W.-J., Li, W.-M., Wang, J.-F., Han, W., Zhang, Z.-C., Yu, Y., Cao, D.-Y. & Dou, K.-F. Tolerance induction by exosomes from immature dendritic cells and rapamycin in a mouse cardiac allograft model. *PLoS ONE* **7,** e44045 (2012).

86. Gonzalez-Rey, E. Vasoactive intestinal peptide generates human tolerogenic dendritic cells that induce CD4 and CD8 regulatory T cells. - PubMed - NCBI. *Blood* **107,** 3632–3638 (2006).

87. Toscano, M. G., Delgado, M., Kong, W., Martin, F., Skarica, M. & Ganea, D. Dendritic Cells Transduced With Lentiviral Vectors Expressing VIP Differentiate Into VIP-secreting Tolerogenic-like DCs. *Mol Ther* **18,** 1035–1045 (2010).

88. Watanabe, N., Wang, Y.-H., Lee, H. K., Ito, T., Wang, Y.-H., Cao, W. & Liu, Y.-J. Hassall's corpuscles instruct dendritic cells to induce CD4+CD25+ regulatory T cells in human thymus. - Google Search. *Nature* **436,** 1181–1185 (2005).

89. Chang, J., Thangamani, S., Kim, M. H., Ulrich, B., Morris, S. M., Jr. & Kim, C. H. Retinoic acid promotes the development of Arg1-expressing dendritic cells for the regulation of T-cell differentiation. *Eur. J. Immunol.* **43,** 967–978 (2013).

90. Coombes, J. L., Siddiqui, K. R. R., Arancibia-Cárcamo, C. V., Hall, J., Sun, C.-M., Belkaid, Y. & Powrie, F. A functionally specialized population of mucosal CD103 +DCs induces Foxp3 +regulatory T cells via a TGF-β– and retinoic acid–dependent mechanism. *J Exp Med* **204,** 1757–1764 (2007).

91. Cassani, B., Villablanca, E. J., De Calisto, J., Wang, S. & Mora, J. R. Vitamin A and immune regulation: role of retinoic acid in gut-associated dendritic cell education, immune protection and tolerance. - PubMed - NCBI. *Molecular Aspects of Medicine* **33,** 63–76 (2012).

92. Hackstein, H., Morelli, A. E., Larregina, A. T., Ganster, R. W., Papworth, G. D., Logar, A. J., Watkins, S. C., Falo, L. D. & Thomson, A. W. Aspirin inhibits in vitro maturation and in vivo immunostimulatory function of murine myeloid dendritic cells. *J Immunol* **166,** 7053–7062 (2001).

93. Wu, H. Y., Quintana, F. J., da Cunha, A. P., Dake, B. T., Koeglsperger, T., Starossom, S. C. & Weiner, H. L. In Vivo Induction of Tr1 Cells via Mucosal Dendritic Cells and AHR Signaling. *PLoS ONE* **6,** e23618 (2011).

94. Li, X., Yang, A., Huang, H., Zhang, X., Town, J., Davis, B., Cockcroft, D. W. & Gordon, J. R. Induction of Type 2 T Helper Cell Allergen Tolerance by IL-10–Differentiated Regulatory Dendritic Cells. *American Journal of Respiratory Cell and Molecular Biology* **42,** 190–199 (2012).

95. Boks, M. A., Zwaginga, J. J., Van Ham, S. M. & Brinke, Ten, A. An optimized CFSE-based T-cell suppression assay to evaluate the suppressive capacity of regulatory T-cells induced by human tolerogenic dendritic ... - PubMed - NCBI. *Scandinavian Journal of Immunology* **72,** 158–168 (2010).

96. Cohen, N. GILZ expression in human dendritic cells redirects their maturation and prevents antigen-specific T lymphocyte response. - PubMed - NCBI. *Blood* **107,** 2037–2044 (2006).

97. Zimmer, A., Bouley, J., Le Mignon, M., Pliquet, E., Horiot, S., Turfkruyer, M., Baron-Bodo, V., Horak, F., Nony, E., Louise, A., Moussu, H., Mascarell, L. & Moingeon, P. A regulatory dendritic cell signature correlates with the clinical efficacy of allergen-specific sublingual immunotherapy. *Journal of Allergy and Clinical Immunology* **129,** 1020–1030 (2012).

98. Coenen, J. J. A., Koenen, H. J. P. M., van Rijssen, E., Hilbrands, L. B. & Joosten, I. Rapamycin, and not cyclosporin A, preserves the highly suppressive CD27+ subset of human CD4+CD25+ regulatory T cells. *Blood* **107,** 1018–1023 (2006).

99. Haidinger, M., Poglitsch, M., Geyeregger, R., Kasturi, S., Zeyda, M., Zlabinger, G. J., Pulendran, B., Horl, W. H., Saemann, M. D. & Weichhart, T. A Versatile Role of Mammalian Target of Rapamycin in Human Dendritic Cell Function and Differentiation. *J Immunol* **185,** 3919–3931 (2010).

100. Mahé, E., Morelon, E., Lechaton, S., Sang, K.-H. L. Q., Mansouri, R., Ducasse, M.-F., Mamzer-Bruneel, M.-F., de Prost, Y., Kreis, H. & Bodemer, C. Cutaneous adverse events in renal transplant recipients receiving sirolimus-based therapy. *Transplantation* **79,** 476–482 (2005).

101. Turnquist, H. R., Raimondi, G., Zahorchak, A. F., Fischer, R. T., Wang, Z. & Thomson, A. W. Rapamycin-conditioned dendritic cells are poor stimulators of allogeneic CD4+ T cells, but enrich for antigen-specific Foxp3+ T regulatory cells and promote organ transplant tolerance. *J Immunol* **178,** 7018–7031 (2007).

102. Pan, J., Ju, D., Wang, Q., Zhang, M., Xia, D., Zhang, L., Yu, H. & Cao, X. Dexamethasone inhibits the antigen presentation of dendritic cells in MHC class II pathway. *Immunology Letters* **76,** 153–161 (2001).

103. Chamorro, S., Garcia-Vallejo, J. J., Unger, W. W. J., Fernandes, R. J., Bruijns, S. C. M., Laban, S., Roep, B. O., 't Hart, B. A. & van Kooyk, Y. TLR Triggering on Tolerogenic Dendritic Cells Results in TLR2 Up-Regulation and a Reduced Proinflammatory Immune Program. *The Journal of Immunology* **183,** 2984–2994 (2009).

104. O'Flynn, L., Treacy, O., Ryan, A. E., Morcos, M., Cregg, M., Gerlach, J., Joshi, L., Nosov, M. & Ritter, T. Donor Bone Marrow–derived Dendritic Cells Prolong Corneal Allograft Survival and Promote an Intragraft Immunoregulatory Milieu. *Mol Ther* **21,** 2102–2112 (2013).

105. Lutz, M. B., Suri, R. M., Niimi, M., Ogilvie, A. L., Kukutsch, N. A., Rossner, S., Schuler, G. & Austyn, J. M. Immature dendritic cells generated with low doses of GM-CSF in the absence of IL-4 are maturation resistant and prolong allograft survival in vivo. *Eur. J. Immunol.* **30,** 1813–1822 (2000).

106. Babensee, J. E. & Paranjpe, A. Differential levels of dendritic cell maturation on different biomaterials used in combination products. *J. Biomed. Mater. Res.* **{74A},** 503–510 (2005).

107. Park, J., Gerber, M. H. & Babensee, J. E. Phenotype and polarization of autologous T cells by biomaterial-treated dendritic cells. *J. Biomed. Mater. Res.* **103,** 170–184 (2014).

108. Alegre, M.-L., Frauwirth, K. A. & Thompson, C. B. T-cell regulation by CD28 and CTLA-4. - PubMed - NCBI. *Nat Rev Immunol* **1,** 220–228 (2001).

109. Keir, M. E., Butte, M. J., Freeman, G. J. & Sharpe, A. H. PD-1 and Its Ligands in Tolerance and Immunity. *Annu. Rev. Immunol.* **26,** 677–704 (2008).

110. Bluestone, J. A. & Abbas, A. K. Opinion-Regulatory Lymphocytes: Natural versus adaptive regulatory T cells. *Nat Rev Immunol* **3,** 253–257 (2003).

111. Gagliani, N., Magnani, C. F., Huber, S., Gianolini, M. E., Pala, M., Licona-Limon, P., Guo, B., Herbert, D. R., Bulfone, A., Trentini, F., Di Serio, C., Bacchetta, R., Andreani, M., Brockmann, L., Gregori, S., Flavell, R. A. & Roncarolo, M.-G. Coexpression of CD49b and LAG-3 identifies human and mouse T regulatory type 1 cells - Google Search. *Nat Med* **19,** 739–746 (2013).

112. Wang, Y. M. & Alexander, S. I. CD8 regulatory T cells: What's old is now new. *Immunol Cell Biol* **87,** 192–193 (2009).

113. Churlaud, G., Pitoiset, F., Jebbawi, F., Lorenzon, R., Bellier, B., Rosenzwajg, M. & Klatzmann, D. Human and Mouse CD8+CD25+FOXP3+ Regulatory T Cells at Steady State and during Interleukin-2 Therapy. *Frontiers in Immunology* **6,** 775 (2015).

114. Rosser, E. C. & Mauri, C. Regulatory B cells: origin, phenotype, and function. - PubMed - NCBI. *Immunity* **42,** 607–612 (2015).

115. Turley, S. J. Dendritic cells: inciting and inhibiting autoimmunity. *Current Opinion in Immunology* **14,** 765–770 (2002).

116. Ludewig, B., Odermatt, B., Landmann, S., Hengartner, H. & Zinkernagel, R. M. Dendritic cells induce autoimmune diabetes and maintain disease via de novo formation of local lymphoid tissue. *J Exp Med* **188,** 1493–1501 (1998).

117. Dittel, B. N., Visintin, I., Merchant, R. M. & Janeway, C. A. Presentation of the self antigen myelin basic protein by dendritic cells leads to experimental autoimmune encephalomyelitis. *J Immunol* **163,** 32–39 (1999).

118. Green, E. A., Eynon, E. E. & Flavell, R. A. Local expression of TNFalpha in neonatal

NOD mice promotes diabetes by enhancing presentation of islet antigens. *Immunity* **9,** 733–743 (1998).

119. Dantal, J., Hourmant, M., Cantarovich, D., Giral, M., Blancho, G., Dreno, B. & Soulillou, J.-P. Effect of long-term immunosuppression in kidney-graft recipients on cancer incidence: randomised comparison of two cyclosporin regimens. *The Lancet* **351,** 623–628 (1998).

120. Verbeke, C. S. & Mooney, D. J. Injectable, Pore-Forming Hydrogels for In Vivo Enrichment of Immature Dendritic Cells. *Adv. Healthcare Mater.* **4,** 2677–2687 (2015).

121. Palucka, K. & Banchereau, J. Cancer immunotherapy via dendritic cells. *Nat Rev Cancer* **12,** 265–277 (2012).

122. Kastenmüller, W., Kastenmüller, K., Kurts, C. & Seder, R. A. Dendritic cell-targeted vaccines — hope or hype? *Nat Rev Immunol* **14,** 705–711 (2014).

123. Anassi, E. & Ndefo, U. A. Sipuleucel-T (provenge) injection: the first immunotherapy agent (vaccine) for hormone-refractory prostate cancer. *P T* **36,** 197–202 (2011).

124. Search of: plga - List Results - ClinicalTrials.gov.

125. Menei, P., Capelle, L., Guyotat, J., Fuentes, S., Assaker, R., Bataille, B., François, P., Dorwling-Carter, D., Paquis, P., Bauchet, L., Parker, F., Sabatier, J., Faisant, N. & Benoit, J.-P. Local and sustained delivery of 5-fluorouracil from biodegradable microspheres for the radiosensitization of malignant glioma: a randomized phase II trial. *Neurosurgery* **56,** 242–8– discussion 242–8 (2005).

126. Hu, F., Zeng, X.-Y., Xie, Z.-L., Liu, L.-L. & Huang, L. Clinical outcomes of amniotic membrane loaded with 5-FU PLGA nanoparticles in experimental trabeculectomy. *International Journal of Ophthalmology* **8,** 29–34 (2015).

127. Clarke, S. R., Barnden, M., Kurts, C., Carbone, F. R., Miller, J. F. & Heath, W. R. Characterization of the ovalbumin-specific TCR transgenic line OT-I: MHC elements for positive and negative selection. *Immunol Cell Biol* **78,** 110–117 (2000).

128. BARNDEN, M. J., ALLISON, J., Heath, W. R. & Carbone, F. R. Defective TCR expression in transgenic mice constructed using cDNA-based alpha- and beta-chain genes under the control of heterologous regulatory elements. *Immunol Cell Biol* **76,** 34–40 (1998).

129. Miltenyi Biotec. Pan T Cell Isolation Kit II, mouse - Miltenyi Biotec. *miltenyibiotec.com* at <http://www.miltenyibiotec.com/en/products-and-services/macs-cell-separation/cell-separation-reagents/t-cells/pan-t-cell-isolation-kit-ii-mouse.aspx>

130. Parish, C. R., Glidden, M. H., Quah, B. J. C. & Warren, H. S. *Use of the Intracellular Fluorescent Dye CFSE to Monitor Lymphocyte Migration and Proliferation*. (John Wiley & Sons, Inc., 2001). doi:10.1002/0471142735.im0409s84

131. Quah, B. J. C., Warren, H. S. & Parish, C. R. Monitoring lymphocyte proliferation in vitro and in vivo with the intracellular fluorescent dye carboxyfluorescein diacetate succinimidyl ester. *Nat Protoc* **2,** 2049–2056 (2007).

132. Blair, D. A., Turner, D. L., Bose, T. O., Pham, Q.-M., Bouchard, K. R., Gumpenberger, K., McAleer, J. P., Cauley, L. S., Vella, A. T. & Lefrançois, L. Duration of antigen availability influences the expansion and memory differentiation of T cells. *Journal of immunology (Baltimore, Md. : 1950)* **187,** 2310–2321 (2011).

133. Serre, K., Mohr, E., Gaspal, F., Lane, P. J. L., Bird, R., Cunningham, A. F. &

MacLennan, I. C. M. IL-4 directs both CD4 and CD8 T cells to produce Th2 cytokines in vitro, but only CD4 T cells produce these cytokines in response to alum-precipitated protein in vivo. *Molecular Immunology* **47,** 1914–1922 (2010).

134. Ullman-Culleré, M. H. & Foltz, C. J. Body condition scoring: a rapid and accurate method for assessing health status in mice. *Comparative Medicine* **256,** 1392–1394 (1999).

135. Crowley, M., Inaba, K., Witmer-Pack, M. & Steinman, R. M. The cell surface of mouse dendritic cells: FACS analyses of dendritic cells from different tissues including thymus. *Cell. Immunol.* **118,** 108–125 (1989).

136. Dudziak, D., Kamphorst, A. O., Heidkamp, G. F., Buchholz, V. R., Trumpfheller, C., Yamazaki, S., Cheong, C., Liu, K., Lee, H. W., Park, C. G., Steinman, R. M. & Nussenzweig, M. C. Differential Antigen Processing by Dendritic Cell Subsets in Vivo. *Science* **315,** 107–111 (2007).

137. Jiang, W., Swiggard, W. J., Heufler, C., Peng, M., Mirza, A., Steinman, R. M. & Nussenzweig, M. C. The receptor DEC-205 expressed by dendritic cells and thymic epithelial cells is involved in antigen processing. *Nature* **375,** 151–155 (1995).

138. Probst, H. C., Tschannen, K., Odermatt, B., Schwendener, R., Zinkernagel, R. M. & Van Den Broek, M. Histological analysis of CD11c-DTR/GFP mice after in vivo depletion of dendritic cells. *Clin Exp Immunol* **141,** 398–404 (2005).

139. Hey, Y. Y. & O'Neill, H. C. Murine spleen contains a diversity of myeloid and dendritic cells distinct in antigen presenting function. *J. Cell. Mol. Med.* **16,** 2611–2619 (2012).

140. Zeisberger, S. M., Odermatt, B., Marty, C., Zehnder-Fjällman, A. H. M., Ballmer-Hofer, K. & Schwendener, R. A. Clodronate-liposome-mediated depletion of tumour-associated macrophages: a new and highly effective antiangiogenic therapy approach. *Br J Cancer* **95,** 272–281 (2006).

141. Progatzky, F., Dallman, M. J. & Celso, Lo, C. From seeing to believing: labelling strategies for in vivo cell-tracking experiments. *Interface Focus* **3,** 20130001–20130001 (2013).

142. Patel, Z. S., Yamamoto, M., Ueda, H., Tabata, Y. & Mikos, A. G. Biodegradable gelatin microparticles as delivery systems for the controlled release of bone morphogenetic protein-2. *Acta BIOMATERIALIA* **4,** 1126–1138 (2008).

143. Yamamoto, M., Ikada, Y. & Tabata, Y. Controlled release of growth factors based on biodegradation of gelatin hydrogel. *J Biomater Sci Polym Ed* **12,** 77–88 (2001).

144. Higuchi, T. Mechanism of sustained-action medication. Theoretical analysis of rate of release of solid drugs dispersed in solid matrices. *J. Pharm. Sci.* **52,** 1145–1149 (1963).

145. Siepmann, J. & Peppas, N. A. Modeling of drug release from delivery systems based on hydroxypropyl methylcellulose (HPMC). *Adv. Drug Deliv. Rev.* **48,** 139–157 (2001).

146. Dash, S., Murthy, P. N., Nath, L. & Chowdhury, P. Kinetic modeling on drug release from controlled drug delivery systems. *Acta Pol Pharm* **67,** 217–223 (2010).

147. Hadjitheodorou, A. & Kalosakas, G. Analytical and numerical study of diffusion-controlled drug release from composite spherical matrices. *Mater Sci Eng C Mater Biol Appl* **42,** 681–690 (2014).

148. Nagatsuka, H., Kamakura, T. & Balakrishnan, N. A consistent method of estimation for the three-parameter Weibull distribution. *Computational Statistics & Data Analysis* **58,**

210–226 (2013).

149. Bartkut, V. & Sakalauskas, L. The method of three-parameter Weibull distribution estimation. *Acta et commentationes Universitatis Tartuensis de mathematica* **12,** 65–78. (2008).

150. Tabata, Y., Hijikata, S., Muniruzzaman, M. & Ikada, Y. Neovascularization effect of biodegradable gelatin microspheres incorporating basic fibroblast growth factor. *J Biomater Sci Polym Ed* **10,** 79–94 (1999).

151. Garza-Licudine, E., Deo, D., Yu, S., Uz-Zaman, A. & Dunbar, W. B. Portable nanoparticle quantization using a resizable nanopore instrument - The IZON qNano&#x2122. in *2010 32nd Annual International Conference of the IEEE Engineering in Medicine and Biology Society (EMBC 2010)* 5736–5739 (IEEE). doi:10.1109/IEMBS.2010.5627861

152. Tabata, Y., Ikada, Y. & Morimoto, K. Surfactant-free preparation of biodegradable hydrogel microspheres for protein release. *Journal of bioactive ...* (1999).

153. Copeland, J. R., Santillan, I. A., Schimming, S. M., Ewbank, J. L. & Sievers, C. Surface Interactions of Glycerol with Acidic and Basic Metal Oxides. *J. Phys. Chem. C* **117,** 21413–21425 (2013).

154. Lozinsky, V. I., Damshkaln, L. G., Bloch, K. O., Vardi, P., Grinberg, N. V., Burova, T. V. & Grinberg, V. Y. Cryostructuring of polymer systems. XXIX. Preparation and characterization of supermacroporous (spongy) agarose-based cryogels used as three-dimensional scaffolds for culturing insulin-producing cell aggregates. *J. Appl. Polym. Sci.* **108,** 3046–3062 (2008).

155. Lunn, D., Jackson, C., Best, N., Thomas, A. & Spiegelhalter, D. *The BUGS Book*. (CRC Press, 2012).

156. Langenbucher, F. Letters to the Editor: Linearization of dissolution rate curves by the Weibull distribution. *Journal of Pharmacy and Pharmacology* **24,** 979–981 (2011).

157. Öner, L. & GROVES, M. J. Optimization of Conditions for Preparing 2- to 5-Micron-Range Gelatin Microparticles by Using Chilled Dehydration Agents. *Pharm Res* **10,** 621–626 (1993).

158. Barth, A. Infrared spectroscopy of proteins. *Biochimica et Biophysica Acta (BBA) - Bioenergetics* **1767,** 1073–1101 (2007).

159. Byler, D. M. & Susi, H. Examination of the secondary structure of proteins by deconvolved FTIR spectra. *Biopolymers* **25,** 469–487 (1986).

160. Yang, H., Yang, S., Kong, J., Dong, A. & Yu, S. Obtaining information about protein secondary structures in aqueous solution using Fourier transform IR spectroscopy. *Nat Protoc* **10,** 382–396 (2015).

161. Papadopoulou, V., Kosmidis, K., Vlachou, M. & Macheras, P. On the use of the Weibull function for the discernment of drug release mechanisms. *International Journal of Pharmaceutics* **309,** 44–50 (2006).

162. Young, S., Wong, M., Tabata, Y. & Mikos, A. G. Gelatin as a delivery vehicle for the controlled release of bioactive molecules. *Journal of Controlled Release* **109,** 256–274 (2005).

163. Solorio, L., Zwolinski, C., Lund, A. W., Farrell, M. J. & Stegemann, J. P. Gelatin microspheres crosslinked with genipin for local delivery of growth factors. *J Tissue Eng*

Regen Med **4,** 514–523 (2010).

164. Esposito, E., Cortesi, R. & Nastruzzi, C. Gelatin microspheres: influence of preparation parameters and thermal treatment on chemico-physical and biopharmaceutical properties. *Biomaterials* **17,** 2009–2020 (1996).

165. Letherby, M. R. & Young, D. A. The gelation of agarose. *J. Chem. Soc., Faraday Trans. 1* **77,** 1953–1966 (1981).

166. Lozinsky, V. I. Cryogels on the basis of natural and synthetic polymers: preparation, properties and application. *Russ. Chem. Rev.* **71,** 489–511 (2007).

167. Bhat, S., Tripathi, A. & Kumar, A. Supermacroprous chitosan–agarose–gelatin cryogels: in vitro characterization and in vivo assessment for cartilage tissue engineering. *Journal of the Royal Society Interface* **8,** 540–554 (2011).

168. Tripathi, A. & Kumar, A. Multi-Featured Macroporous Agarose-Alginate Cryogel: Synthesis and Characterization for Bioengineering Applications. *Macromol. Biosci.* **11,** 22–35 (2010).

169. Schacht, E., Nobels, M., Vansteenkiste, S., Demeester, J., Franssen, J. & Lemahieu, A. Some aspects of the crosslinking of gelatin by dextran dialdehydes. *Polymer Gels and Networks* **1,** 213–224 (1993).

170. Tabor, B. E. Crosslinking efficiency of gelatin hardeners. *J. Appl. Polym. Sci.* **12,** 1967–1979 (1968).

171. Davis, N. R. & Anwar, R. A. Mechanism of formation of desmosine and isodesmosine cross-links of elastin. *J. Am. Chem. Soc.* **92,** 3778–3782 (1970).

172. Phromsopha, T., Baimark, Y., Phromsopha, T. & Baimark, Y. Preparation of Starch/Gelatin Blend Microparticles by a Water-in-Oil Emulsion Method for Controlled Release Drug Delivery. *International Journal of Biomaterials* **2014,** 1–6 (2014).

173. Vidakovic, B. *Statistics for Bioengineering Sciences*. (Springer Science & Business Media, 2011).

174. Weibull, W. *A Statistical Distribution Function of Wide Applicability, journal of applied mechanics*. (1951).

175. Casault, S. & Slater, G. W. Comments concerning: Monte Carlo simulations for the study of drug release from matrices with high and low diffusivity areas. *International Journal of Pharmaceutics* **365,** 214–215 (2009).

176. Koizumi, T. & Panomsuk, S. P. Release of medicaments from spherical matrices containing drug in suspension: Theoretical aspects. *International Journal of Pharmaceutics* **116,** 45–49 (1995).

177. Gomes Filho, M. S., Oliveira, F. A. & Barbosa, M. A. A. A statistical mechanical model for drug release: Investigations on size and porosity dependence. *Physica A: Statistical Mechanics and its Applications* **460,** 29–37 (2016).

178. Gelatin Handbook. *gelatin-gmia.com* at <http://www.gelatin-gmia.com/images/GMIA_Gelatin_Manual_2012.pdf>

179. Fukuhara, H., Umemoto, T., Sagawa, H., Kato, K. & Kotani, S. Purification and quantitative chemical analysis of cell wall peptidoglycans of Leptotrichia buccalis. *Infect. Immun.* **39,** 132–136 (1983).

180. Taylor, J. M., Mitchell, W. M. & Cohen, S. Epidermal growth factor. Physical and

chemical properties. *J. Biol. Chem.* **247,** 5928–5934 (1972).

181. Zdanov, A. Structural features of the interleukin-10 family of cytokines. *Current Pharmaceutical Design* **10,** 3873–3884 (2004).

182. Steinman, R. M., Turley, S., Mellman, I. & Inaba, K. The Induction of Tolerance by Dendritic Cells That Have Captured Apoptotic Cells. *J Exp Med* **191,** 411–416 (2000).

183. Wang, Z., Shufesky, W. J., Montecalvo, A., Divito, S. J., Larregina, A. T. & Morelli, A. E. In Situ-Targeting of Dendritic Cells with Donor-Derived Apoptotic Cells Restrains Indirect Allorecognition and Ameliorates Allograft Vasculopathy. *PLoS ONE* **4,** e4940 (2009).

184. Gleisner, M. A., Rosemblatt, M., Fierro, J. A. & Bono, M. R. Delivery of Alloantigens via Apoptotic Cells Generates Dendritic Cells With an Immature Tolerogenic Phenotype. *Transplantation Proceedings* **43,** 2325–2333 (2011).

185. Stuart, L. M., Lucas, M., Simpson, C., Lamb, J., Savill, J. & Lacy-Hulbert, A. Inhibitory effects of apoptotic cell ingestion upon endotoxin-driven myeloid dendritic cell maturation. *J Immunol* **168,** 1627–1635 (2002).

186. Ding, D., Mehta, H., McCune, W. J. & Kaplan, M. J. Aberrant phenotype and function of myeloid dendritic cells in systemic lupus erythematosus. *J Immunol* **177,** 5878–5889 (2006).

187. Ganguly, D., Haak, S., Sisirak, V. & Reizis, B. The role of dendritic cells in autoimmunity. *Nat Rev Immunol* **13,** 566–577 (2013).

188. Liu, J. & Cao, X. Regulatory dendritic cells in autoimmunity: A comprehensive review. *Journal of Autoimmunity* **63,** 1–12 (2015).

189. Zhuang, Q., Liu, Q., Divito, S. J., Zeng, Q., Yatim, K. M., Hughes, A. D., Rojas-Canales, D. M., Nakao, A., Shufesky, W. J., Williams, A. L., Humar, R., Hoffman, R. A., Shlomchik, W. D., Oberbarnscheidt, M. H., Lakkis, F. G. & Morelli, A. E. Graft-infiltrating host dendritic cells play a key role in organ transplant rejection. *Nature Communications* **7,** 12623 (2016).

190. Benichou, G., Yamada, Y., Yun, S.-H., Lin, C., Fray, M. & Tocco, G. Immune recognition and rejection of allogeneic skin grafts. *Immunotherapy* **3,** 757–770 (2011).

191. Lutz, M. B. & Schuler, G. Immature, semi-mature and fully mature dendritic cells: which signals induce tolerance or immunity? *Trends in Immunology* **23,** 445–449 (2002).

192. Dudek, A. M., Martin, S., Garg, A. D. & Agostinis, P. Immature, Semi-Mature, and Fully Mature Dendritic Cells: Toward a DC-Cancer Cells Interface That Augments Anticancer Immunity. *Frontiers in Immunology* **4,** (2013).

193. Xin, H.-M., Peng, Y.-Z., Yuan, Z.-Q. & Guo, H. In vitro maturation and migration of immature dendritic cells after chemokine receptor 7 transfection. *Can. J. Microbiol.* **55,** 859–866 (2009).

194. Rogers, T. H. & Babensee, J. E. Biomaterials. *Biomaterials* **32,** 1–10 (2010).

195. Kou, P. M. & Babensee, J. E. Macrophage and dendritic cell phenotypic diversity in the context of biomaterials. *J. Biomed. Mater. Res.* **96,** 239–260 (2011).

196. Srinivasan, S. & Babensee, J. E. in *Scaffolds for Tissue Engineering: Biological Design, Materials, and Fabrication* 115–171–171 (Pan Stanford Publishing, 2014).

doi:10.1201/b15649-6

197. Lewis, J. S. & Keselowsky, B. G. in *Host Response to Biomaterials* 131–150 (Elsevier, 2015). doi:10.1016/B978-0-12-800196-7.00007-4

198. Romani, N., Gruner, S., Brang, D., Kämpgen, E., Lenz, A., Trockenbacher, B., Konwalinka, G., Fritsch, P. O., Steinman, R. M. & Schuler, G. Proliferating dendritic cell progenitors in human blood. *J. Exp. Med.* **180,** 83–93 (1994).

199. Kou, P. M. & Babensee, J. E. Validation of a high-throughput methodology to assess the effects of biomaterials on dendritic cell phenotype. *Acta BIOMATERIALIA* **6,** 2621–2630 (2010).

200. Davies, J. K., Barbon, C. M., Voskertchian, A. R., Nadler, L. M. & Guinan, E. C. Induction of Alloantigen-specific Anergy in Human Peripheral Blood Mononuclear Cells by Alloantigen Stimulation with Co-stimulatory Signal Blockade. *JoVE* e2673–e2673 (2011). doi:10.3791/2673

201. Kruisbeek, A. M., Shevach, E. & Thornton, A. M. Proliferative assays for T cell function. *Curr Protoc Immunol* **Chapter 3,** Unit 3.12 (2004).

202. Wells, J. W., Darling, D., Farzaneh, F. & Galea Lauri, J. Influence of Interleukin-4 on the Phenotype and Function of Bone Marrow-Derived Murine Dendritic Cells Generated Under Serum-Free Conditions. *Scandinavian Journal of Immunology* **61,** 251–259 (2005).

203. Hansson, M., Lundgren, A., Elgbratt, K., Quiding-Järbrink, M., Svennerholm, A.-M. & Johansson, E.-L. Dendritic cells express CCR7 and migrate in response to CCL19 (MIP-3β) after exposure to Helicobacter pylori. *Microbes and Infection* **8,** 841–850 (2006).

204. Cella, M., Döhring, C., Samaridis, J., Dessing, M., Brockhaus, M., Lanzavecchia, A. & Colonna, M. A Novel Inhibitory Receptor (ILT3) Expressed on Monocytes, Macrophages, and Dendritic Cells Involved in Antigen Processing. *Journal of Experimental Medicine* **185,** 1743–1751 (1997).

205. Morelli, A. E., Zahorchak, A. F., Larregina, A. T., Colvin, B. L., Logar, A. J., Takayama, T., Falo, L. D. & Thomson, A. W. Cytokine production by mouse myeloid dendritic cells in relation to differentiation and terminal maturation induced by lipopolysaccharide or CD40 ligation. *Blood* **98,** 1512–1523 (2001).

206. Deeths, M. J. & Mescher, M. F. ICAM-1 and B7-1 provide similar but distinct costimulation for CD8+ T cells, while CD4+ T cells are poorly costimulated by ICAM-1. *Eur. J. Immunol.* **29,** 45–53 (1999).

207. Gordon, J. R., Ma, Y., Churchman, L., Gordon, S. A. & Dawicki, W. Regulatory Dendritic Cells for Immunotherapy in Immunologic Diseases. *Frontiers in Immunology* **5,** 7 (2014).

208. Ali, O. A. & Mooney, D. J. Sustained GM-CSF and PEI condensed pDNA presentation increases the level and duration of gene expression in dendritic cells. *Journal of Controlled Release* **132,** 273–278 (2008).

209. Hotaling, N. A., Ratner, D. M., Cummings, R. D. & Babensee, J. E. Presentation Modality of Glycoconjugates Modulates Dendritic Cell Phenotype. *Biomaterials science* **2,** 1426–1439 (2014).

210. Bayry, J., Thirion, M., Delignat, S., Misra, N., Lacroix-Desmazes, S., Kazatchkine, M. D. & Kaveri, S. V. Dendritic cells and autoimmunity. - PubMed - NCBI. *Autoimmunity*

Reviews **3,** 183–187 (2004).

211. Vremec, D., O'Keeffe, M., Hochrein, H., Fuchsberger, M., Caminschi, I., Lahoud, M. & Shortman, K. Production of interferons by dendritic cells, plasmacytoid cells, natural killer cells, and interferon-producing killer dendritic cells. *Blood* **109,** 1165–1173 (2007).

212. Jiang, H.-R., Muckersie, E., Robertson, M., Xu, H., Liversidge, J. & Forrester, J. V. Secretion of interleukin-10 or interleukin-12 by LPS-activated dendritic cells is critically dependent on time of stimulus relative to initiation of purified DC culture. *Journal of Leukocyte Biology* **72,** 978–985 (2002).

213. Vincenti, F., Rostaing, L., Grinyo, J., Rice, K., Steinberg, S., Gaite, L., Moal, M.-C., Mondragon-Ramirez, G. A., Kothari, J., Polinsky, M. S., Meier-Kriesche, H.-U., Munier, S. & Larsen, C. P. Belatacept and Long-Term Outcomes in Kidney Transplantation. *http://dx.doi.org/10.1056/NEJMoa1506027* **374,** 333–343 (2016).

214. Dustin, M. L. & Springer, T. A. Lymphocyte function-associated antigen-1 (LFA-1) interaction with intercellular adhesion molecule-1 (ICAM-1) is one of at least three mechanisms for lymphocyte adhesion to cultured endothelial cells. *The Journal of Cell Biology* **107,** 321–331 (1988).

215. Delamarre, L., Holcombe, H. & Mellman, I. Presentation of exogenous antigens on major histocompatibility complex (MHC) class I and MHC class II molecules is differentially regulated during dendritic cell maturation. *J Exp Med* **198,** 111–122 (2003).

216. Lebar, R., Lubetzki, C., Vincent, C., Lombrail, P. & Boutry, J. M. The M2 autoantigen of central nervous system myelin, a glycoprotein present in oligodendrocyte membrane. *Clin Exp Immunol* **66,** 423–434 (1986).

217. Kroepfl, J. F., Viise, L. R., Charron, A. J., Linington, C. & Gardinier, M. V. Investigation of myelin/oligodendrocyte glycoprotein membrane topology. *J. Neurochem.* **67,** 2219–2222 (1996).

218. Iglesias, A., Bauer, J., Litzenburger, T., Schubart, A. & Linington, C. T- and B-cell responses to myelin oligodendrocyte glycoprotein in experimental autoimmune encephalomyelitis and multiple sclerosis. *Glia* **36,** 220–234 (2001).

219. Bettelli, E., Pagany, M., Weiner, H. L., Linington, C., Sobel, R. A. & Kuchroo, V. K. Myelin Oligodendrocyte Glycoprotein–specific T Cell Receptor Transgenic Mice Develop Spontaneous Autoimmune Optic Neuritis. *J. Exp. Med.* **197,** 1073–1081 (2003).

220. Martín-Fontecha, A., Sebastiani, S., Höpken, U. E., Uguccioni, M., Lipp, M., Lanzavecchia, A. & Sallusto, F. Regulation of Dendritic Cell Migration to the Draining Lymph Node. *J Exp Med* **198,** 615–621 (2003).

221. Tripp, C. H., Ebner, S., Ratzinger, G., Romani, N. & Stoitzner, P. Conditioning of the Injection Site With CpG Enhances the Migration of Adoptively Transferred Dendritic Cells and Endogenous CD8+ T-cell Responses. *Journal of Immunotherapy* **33,** 115–125 (2010).

222. Sallusto, F., Schaerli, P., Loetscher, P., Schaniel, C., Lenig, D., Mackay, C. R., Qin, S. & Lanzavecchia, A. Rapid and coordinated switch in chemokine receptor expression during dendritic cell maturation. *Eur. J. Immunol.* **28,** 2760–2769 (1998).

223. Ogata, M., Zhang, Y., Wang, Y., Itakura, M., Zhang, Y. Y., Harada, A., Hashimoto, S.

& Matsushima, K. Chemotactic response toward chemokines and its regulation by transforming growth factor-beta1 of murine bone marrow hematopoietic progenitor cell-derived different subset of dendritic cells. *Blood* **93,** 3225–3232 (1999).

224. Lutz, M. B. Therapeutic Potential of Semi-Mature Dendritic Cells for Tolerance Induction. *Frontiers in Immunology* **3,** 123 (2012).

225. Le Nouën, C., Hillyer, P., Winter, C. C., McCarty, T., Rabin, R. L., Collins, P. L. & Buchholz, U. J. Low CCR7-Mediated Migration of Human Monocyte Derived Dendritic Cells in Response to Human Respiratory Syncytial Virus and Human Metapneumovirus. *PLOS Pathog* **7,** e1002105 (2011).

226. Gunn, M. D., Tangemann, K., Tam, C., Cyster, J. G., Rosen, S. D. & Williams, L. T. A chemokine expressed in lymphoid high endothelial venules promotes the adhesion and chemotaxis of naive T lymphocytes. *Proceedings of the National Academy of Sciences* **95,** 258–263 (1998).

227. Luther, S. A., Tang, H. L., Hyman, P. L., Farr, A. G. & Cyster, J. G. Coexpression of the chemokines ELC and SLC by T zone stromal cells and deletion of the ELC gene in the plt/plt mouse. - PubMed - NCBI. *Proceedings of the National Academy of Sciences* **97,** 12694–12699 (2000).

228. Ngo, V. N., Tang, H. L. & Cyster, J. G. Epstein-Barr virus-induced molecule 1 ligand chemokine is expressed by dendritic cells in lymphoid tissues and strongly attracts naive T cells and activated B cells. *J Exp Med* **188,** 181–191 (1998).

229. Yoshida, R., Nagira, M., Imai, T., BABA, M., Takagi, S., Tabira, Y., Akagi, J., Nomiyama, H. & Yoshie, O. EBI1-ligand chemokine (ELC) attracts a broad spectrum of lymphocytes: activated T cells strongly up-regulate CCR7 and efficiently migrate toward ELC. *International Immunology* **10,** 901–910 (1998).

230. Förster, R., Davalos-Misslitz, A. C. & Rot, A. CCR7 and its ligands: balancing immunity and tolerance. *Nat Rev Immunol* **8,** 362–371 (2008).

231. Britschgi, M. R., Favre, S. & Luther, S. A. CCL21 is sufficient to mediate DC migration, maturation and function in the absence of CCL19. - PubMed - NCBI. *Eur. J. Immunol.* **40,** 1266–1271 (2010).

232. Nakano, H., Mori, S., Yonekawa, H., Nariuchi, H., Matsuzawa, A. & Kakiuchi, T. A Novel Mutant Gene Involved in T-Lymphocyte–Specific Homing Into Peripheral Lymphoid Organs on Mouse Chromosome 4. *Blood* **91,** 2886–2895 (1998).

233. Stein, J. V., Rot, A., Luo, Y., Narasimhaswamy, M., Nakano, H., Gunn, M. D., Matsuzawa, A., Quackenbush, E. J., Dorf, M. E. & Andrian, von, U. H. The CC chemokine thymus-derived chemotactic agent 4 (TCA-4, secondary lymphoid tissue chemokine, 6Ckine, exodus-2) triggers lymphocyte function-associated antigen 1-mediated arrest of rolling T lymphocytes in peripheral lymph node high endothelial venules. *J Exp Med* **191,** 61–76 (2000).

234. Sallusto, F., Lenig, D., Förster, R., Lipp, M. & Lanzavecchia, A. Two subsets of memory T lymphocytes with distinct homing potentials and effector functions. - PubMed - NCBI. *Nature* **401,** 708–712 (1999).

235. Sallusto, F., Mackay, C. R. & Lanzavecchia, A. The Role of Chemokine Receptors in Primary, Effector, and Memory Immune Responses. *Annu. Rev. Immunol.* **18,** 593–620 (2000).

236. Dearman, R. J., Cumberbatch, M., Maxwell, G., Basketter, D. A. & Kimber, I. Toll-like

receptor ligand activation of murine bone marrow-derived dendritic cells. *Immunology* **126,** 475–484 (2009).

237. Anderson, J. M. BIOLOGICAL RESPONSES TO MATERIALS. *Annu. Rev. Mater. Res.* **31,** 81–110 (2001).

238. Anderson, J. M., Rodriguez, A. & Chang, D. T. Foreign body reaction to biomaterials. *Innate and Adaptive Immune Responses in Tissue Engineering* **20,** 86–100 (2008).

239. Simmen, H. P., Battaglia, H., Giovanoli, P. & Blaser, J. Analysis of pH, pO2 and pCO2 in drainage fluid allows for rapid detection of infectious complications during the follow-up period after abdominal surgery. *Infection* **22,** 386–389 (1994).

240. Keyszer, G., Lambiri, I., Nagel, R., Keysser, C., Keysser, M., Gromnica-Ihle, E., Franz, J., Burmester, G. R. & Jung, K. Circulating levels of matrix metalloproteinases MMP-3 and MMP-1, tissue inhibitor of metalloproteinases 1 (TIMP-1), and MMP-1/TIMP-1 complex in rheumatic disease. Correlation with clinical activity of rheumatoid arthritis versus other surrogate markers. *J. Rheumatol.* **26,** 251–258 (1999).

241. Kattah, N. H., Newell, E. W., Jarrell, J. A., Chu, A. D., Xie, J., Kattah, M. G., Goldberger, O., Ye, J., Chakravarty, E. F., Davis, M. M. & Utz, P. J. Tetramers reveal IL-17–secreting CD4+ T cells that are specific for U1-70 in lupus and mixed connective tissue disease. *Proc. Natl. Acad. Sci. U.S.A.* **112,** 3044–3049 (2015).

242. Cao, Y., Amezquita, R. A., Kleinstein, S. H., Stathopoulos, P., Nowak, R. J. & O'Connor, K. C. Autoreactive T Cells from Patients with Myasthenia Gravis Are Characterized by Elevated IL-17, IFN-γ, and GM-CSF and Diminished IL-10 Production. *The Journal of Immunology* **196,** 2075–2084 (2016).

243. Fletcher, J. M., Lalor, S. J., Sweeney, C. M., Tubridy, N. & Mills, K. H. G. T cells in multiple sclerosis and experimental autoimmune encephalomyelitis. *Clin Exp Immunol* **162,** 1–11 (2010).

244. Miller, S. D. & Karpus, W. J. *Experimental Autoimmune Encephalomyelitis in the Mouse*. (John Wiley & Sons, Inc., 2001). doi:10.1002/0471142735.im1501s77

245. van Zwam, M., Huizinga, R., Melief, M.-J., Wierenga-Wolf, A. F., van Meurs, M., Voerman, J. S., Biber, K. P. H., Boddeke, H. W. G. M., Höpken, U. E., Meisel, C., Meisel, A., Bechmann, I., Hintzen, R. Q., Hart, B. A. T., Amor, S., Laman, J. D. & Boven, L. A. Brain antigens in functionally distinct antigen-presenting cell populations in cervical lymph nodes in MS and EAE. *Journal of Molecular Medicine* **87,** 273–286 (2008).

246. Phelps, E. A., Enemchukwu, N. O., Fiore, V. F., Sy, J. C., Murthy, N., Sulchek, T. A., Barker, T. H. & García, A. J. Maleimide Cross-Linked Bioactive PEG Hydrogel Exhibits Improved Reaction Kinetics and Cross-Linking for Cell Encapsulation and In Situ Delivery. *Adv. Mater.* **24,** 64–70 (2011).

247. Pearson, J. A., Wong, F. S. & Wen, L. The importance of the Non Obese Diabetic (NOD) mouse model in autoimmune diabetes. *Journal of Autoimmunity* **66,** 76–88 (2016).

248. King, A. J. The use of animal models in diabetes research. *British Journal of Pharmacology* **166,** 877–894 (2012).

249. Aspord, C., Rome, S. & Thivolet, C. Early events in islets and pancreatic lymph nodes in autoimmune diabetes. *Journal of Autoimmunity* **23,** 27–35 (2004).

250. Winzler, C., Rovere, P., Rescigno, M., Granucci, F., Penna, G., Adorini, L., Zimmermann, V. S., Davoust, J. & Ricciardi-Castagnoli, P. Maturation stages of mouse dendritic cells in growth factor-dependent long-term cultures. *J Exp Med* **185,** 317–328 (1997).

251. Moore, M. W., Carbone, F. R. & Bevan, M. J. Introduction of soluble protein into the class I pathway of antigen processing and presentation. *Cell* **54,** 777–785 (1988).

252. Qi, C., Yan, X., Huang, C., Melerzanov, A. & Du, Y. Biomaterials as carrier, barrier and reactor for cell-based regenerative medicine. *Protein Cell* **6,** 638–653 (2015)